# Characterization of Controlled Salinity Waterflooding in Carbonate Using Streaming Potential Measurements

**Dawoud Al-Mahrouqi**

Imperial College London

Department of Earth Engineering and Science

**Supervised by**

**Prof. Matthew D. Jackson**

**Dr. Jan Vinogradov**

A dissertation submitted in fulfilment of the requirements for the degree of Doctor of Philosophy in Earth Science and Engineering of Imperial College London and the Diploma of Imperial College London

December 2016

# Declaration of Originality

I declare that this thesis, **Characterization of Controlled Salinity Waterflooding in Carbonate Using Streaming Potential Measurements**, is entirely my own work under the supervision of Prof. Matthew D. Jackson and the co-supervision of Dr. Jan Vinogradov. The work was performed in the Department of Earth Science and Engineering at Imperial College London. All published and unpublished material used in this thesis has been given full acknowledgement. This work has not been previously submitted, in whole or in part, to any other academic institution for a degree, diploma, or any other qualification.

Dawoud Al-Mahrouqi
Department of Earth Science and Engineering
Imperial College London

**© 2016 by Dawoud Al-Mahrouqi.**

**The copyright of this thesis rests with the author and is made available under a Creative Commons Attribution Non-Commercial No Derivatives licence. Researchers are free to copy, distribute or transmit the thesis on the condition that they attribute it, that they do not use it for commercial purposes and that they do not alter, transform or build upon it. For any reuse or redistribution, researchers must make clear to others the licence terms of this work**

# Abstract

The impact of brine composition on rock wettability and oil recovery in carbonates has been an area of active research in recent years. Many studies have reported contradictory results and the underling mechanism(s) are actively debated. The zeta potential, which is a measure of the electrical charge at the mineral surface, is highly variable in carbonates, depending on the ionic composition of the pore water. The zeta potential controls the magnitude and polarity of the electrostatic interactions between the mineral surface and polar species in the brine and oil; it also controls the magnitude and polarity of the streaming potential, an electrical potential which arises in response to pressure gradients across saturated rocks. Here we report the use of streaming potential measurements to determine key controls on zeta potential at mineral-brine and oil-brine interfaces, and characterise wettability and optimise injection brine composition during controlled salinity waterflooding in carbonates at reservoir conditions of salinity and temperature.

The zeta potential is controlled by the concentration-dependent adsorption of the lattice ions $Ca^{2+}$, $Mg^{2+}$ and $CO_3^{2-}$ within the Stern layer. A Nernstian relationship between zeta potential and pCa or pMg (where p represents the negative logarithm of concentration in M; 1 M = 1 mol $L^{-1}$) is observed over the range of typical natural brines. Addition of $SO_4^{2-}$ can affect zeta potential by moderating $Ca^{2+}$ in solution. The temperature dependence of the zeta potential can be correlated with the temperature dependence of pCa and shows a Nernstian linear relationship. The zeta potential in intact carbonate samples decreases with temperature at low ionic strength and independent of temperature at high ionic strength irrespective of brine composition. Thus, for a given carbonate type, zeta potential measurements in natural brines (e.g. saline aquifers, formation waters or seawater; ionic strength ≥0.5M) at laboratory conditions may be applied in situ.

The zeta potential at both the mineral-water and oil-water interfaces must be determined when characterising wettability and designing the optimum brine

composition for controlled salinity waterflooding in carbonates. The experimental method presented here allows this to be done using intact core samples saturated with the crude oil and brine of interest.

We find a monotonic relationship between zeta potential and wettability expressed in terms of the Amott water index ($I_w$). Thus, measurements of streaming potential can be used to characterise wettability more quickly and cheaply than existing laboratory methods. Results reported here demonstrate that the oil-water interface can be positively charged at the high pH and ionic strength relevant to the formation brines found in many carbonate reservoirs. It is usually assumed that the oil-brine interface is negatively charged.

Improved recovery during controlled salinity waterflooding in carbonates is observed if the change in brine composition yields a zeta potential at each interface that has the same polarity, such that a repulsive electrostatic force acts between the interfaces and stabilizes a water film on the mineral surface. These results have broad application and significance in allowing oil companies to design water injection strategies that yield improved oil recovery from carbonate reservoirs.

# Acknowledgements

First, I would like to raise all type of thankfulness to almighty ALLAH who gave me the strength and the passion throughout my study journey in the field that I love the best. Then to my country (Oman) and sponsor (Petroleum Development Oman-PDO) for their full financial support of my PhD study. TOTAL are thanked for funding the Reservoir Physics Laboratory where the SPM and coreflooding experiments reported here were undertaken.

My special thanks are extended to my supervisor Prof. Matthew D. Jackson for his great support and enthusiasm for the research project and confidence instilled in me throughout my academic studies. Big thanks to my co-supervisor Dr. Jan Vinogradov for his endless support in the laboratory and scientific interpretation of the results. I am grateful to Graham Nash for the continued technical support in the laboratory throughout the research process. TOTAL, Daleel Petroleum Oman, Nayef Alyafei and Ali Al-Menhali are thanked for providing crude oil samples. I would like to thank Prof. Martin Blunt and Prof. Aksel Hiorth for being my examiners and taking the time and effort to evaluate this thesis.

Thanks to all members of Smart well and Reservoir Monitoring group at Imperial College for sharing their expertise and valuable discussion during group meetings, in particular; Abdulkareem Alroudhan, Donald John and Dr. Shuai for their experimental experience and knowledge in the laboratory. I thank Dr. Emma Humphreys-Williams for helping in the ICP-AES analysis and Jens Najorka for helping in the XRD analysis in their laboratories at National History Museum.

Finally, a huge thank to my beautiful wife (Wafa), my beloved daughter (Wajd) and my little angel son (Bishr) for being part of me during this journey; and for their support, assurance and love, which without this thesis would simply not have been possible. I also thank my family in Oman for their continuous prayers for me and my little beloved family in UK during our studies.

﴿O my Lord! Open for me my chest. And ease my task for me. And make loose the knot from my tongue, that they understand my speech﴾ Quran Kareem versus 20/25-chapter 28

# Publications

## Peer-Reviewed Journal Articles

Al Mahrouqi. D, Vinogradov. J, Jackson M. D (2016). “Zeta Potential of Artificial and Natural Calcite in Aqueous Solution”. Advances in Colloid and Interface Science. doi: 10.1016/j.cis.2016.12.006.

Al Mahrouqi. D, Vinogradov. J, Jackson M. D (2016). Temperature-dependence of the Zeta Potential in Intact Natural Carbonates. Geophysical Research Letters. *43*. doi: 10.1002/2016GL071151.

Jackson M. D, Al Mahrouqi. D, Vinogradov. J (2016). Zeta Potential in Oil-water-carbonate Systems and Its Impact on Oil Recovery During Controlled Salinity Water-flooding. Scientific Reports. *6*. 37363. doi: 10.1038/srep37363

Al Mahrouqi. D, Vinogradov. J, Jackson M. D. “Quantification of Carbonate Rock Wettability Using Streaming Potential Measurements”. Energy & Fuels (Ready to be submitted).

## Conference Papers

Al Mahrouqi, D., Vinogradov, J. & Jackson, M. (2015). Understanding controlled salinity waterflooding in carbonates using streaming potential measurements. *Proceedings of the SPE Latin American and Caribbean Petroleum Engineering Conference, 18-20 November, Quito, Ecuador*. SPE-177242-MS. doi: 10.2118/177242-MS.

Al Mahrouqi, D., Vinogradov, J. & Jackson, M (2016). Optimization of Controlled Salinity Waterflooding in Carbonates. *Proceedings of the SPE Annual Technical Conference and Exhibition, 26-28 December, Dubai, UAE*. SPE-181390-MS. doi: 10.2118/181390-MS

## Conference Presentations

Al Mahrouqi, D., Vinogradov, J. & Jackson, M. “Zeta potential of carbonates in saline brines as a function of NaCl salinity and potential determining ions: Ca, Mg and $SO_4$”. AGU Fall Meeting, 15 - 19 December 2014, San Francisco, USA.

Al Mahrouqi, D., Vinogradov, J. & Jackson, M. “Zeta Potential in Intact Natural Carbonates at Elevated Temperatures”. AGU Fall Meeting, 14-18 December 2015, San Francisco, USA.

Al Mahrouqi, D., Vinogradov, J. & Jackson, M. “New Method to Characterise Wettability and Predict Successful Controlled Salinity Waterflooding in Carbonate Rocks”. DEVEX 2016, 18-19 May 2016, Aberdeen, UK.

# Table of Contents


Declaration of Originality ..... 2
Abstract ..... 3
Acknowledgements ..... 5
Publications ..... 6
Table of Contents ..... 7
List of Tables ..... 11
List of Figures ..... 12
Nomenclature ..... 16
**Chapter 1. Introduction ..... 20**
1.1. Overview ..... 20
1.2. Aim and Objectives ..... 23
1.3. Thesis Outline ..... 25
**Chapter 2. Impact of Brine Composition on Rock Wettability and Oil Recovery ..... 27**
2.1. Introduction ..... 27
2.2. Low Salinity Waterflooding in Sandstones ..... 28
2.3. Controlled Salinity Waterflooding in Carbonates ..... 30
2.3.1. Spontaneous Imbibition (SI) Experiments ..... 31
2.3.2. Forced Displacement (Coreflood) Experiments ..... 33
2.4. Proposed Mechanisms for CSW in Carbonates ..... 34
2.5. Interaction of Crude Oil, Rock and Brine ..... 37
2.6. Measurements of Wettability and Wettability Alteration ..... 41
2.6.1. Contact Angle ..... 41
2.6.2. Amott and USBM Tests ..... 42
2.6.3. Spontaneous Imbibition (SI) Rate ..... 44
2.6.4. Zeta Potential Measurements ..... 45
2.7. Summary ..... 47
**Chapter 3. Zeta Potential of Artificial and Natural Calcite in Aqueous Solutions - Overview ..... 48**
3.1. Introduction ..... 48
3.2. Zeta Potential and the Electrical Double Layer ..... 49
3.2.1. The Electrical Double Layer ..... 49
3.2.2. Electrokinetic Phenomena ..... 50
3.2.2.1 Electrophoretic Mobility Method ..... 52
3.2.2.2 Streaming Potential Method ..... 53
3.3. Development of Surface Charge on Calcite in Aqueous Solution ..... 59
3.3.1. Effect of pH ..... 59
3.3.2. Potential Determining Ions ..... 61
3.4. Experimental Measurements of Zeta Potential ..... 63
3.4.1. Electrolyte Concentration and Composition ..... 64
3.4.1.1 Effect of pH ..... 64
3.4.1.2 Effect of Ca and $CO_3$ ..... 69
3.4.1.3 Effect of pMg and $pSO_4$ ..... 71

3.4.1.4 Indifferent Ions and Total Ionic Strength ..... 73
3.4.2. Partial Pressure of $CO_2$ ..... 74
3.4.3. Natural versus Synthetic Calcite ..... 75
3.4.4. Measurement Technique ..... 77
3.4.5. Establishment of Equilibrium Between Sample and Electrolyte ..... 78
3.5. Summary ..... 80
**Chapter 4. Measurements of Zeta Potential on Natural Limestone Rock Samples: Impact of Rock Type, PDI concentration and Ionic Strength ..... 81**
4.1. Introduction ..... 81
4.2. Methodology ..... 82
4.2.1. Materials and Sample Preparation ..... 82
4.2.2. Measurements of Streaming Potential Coupling Coefficient Using the Streaming Potential Method (SPM) ..... 86
4.2.3. Measurements of Brine Conductivity, Brine Viscosity and Brine Permittivity ..... 89
4.2.4. Measurements of Saturated Rock Conductivity ..... 90
4.2.5. Measurements of the Intrinsic Formation Factor ..... 92
4.2.6. Interpretation of the Zeta Potential ..... 94
4.2.7. Measurements of Electrolyte Composition ..... 94
4.2.8. Design of Experiments ..... 95
4.3. Results ..... 96
4.3.1. Impact of $Na^+$ Concentration on Zeta Potential ..... 97
4.3.2. Impact of $Ca^{2+}$, $Mg^{2+}$ and $SO_4^{2-}$ Concentration on Zeta Potential ..... 98
4.3.3. Relationship Between pH and pCa or pMg ..... 101
4.3.4. Impact of Varying Multiple PDIs ..... 102
4.4. Discussion ..... 103
4.4.1. Impact of Indifferent Ions ..... 103
4.4.2. Impact of Carbonate Type ..... 104
4.4.3. $SO_4$ as a PDI for Calcite ..... 106
4.4.4. Implications for Wettability Alteration and Hydrocarbon Recovery in Carbonate Reservoirs ..... 107
4.5. Conclusions ..... 109
**Chapter 5. Temperature-Dependence of the Zeta Potential in Intact Natural Carbonates ..... 111**
5.1. Introduction ..... 111
5.2. Methodology ..... 111
5.2.1. Materials and Sample Preparation ..... 111
5.2.2. Measurements of Zeta Potential using the SPM at Elevated Temperature ..... 112
5.2.2.1 Brine Conductivity as a Function of Temperate and Salinity ..... 114
5.2.2.2 Brine Viscosity as a Function of Temperate ..... 114
5.2.2.3 Brine Permittivity as a Function of Temperate ..... 115
5.3. Results ..... 117
5.3.1. Impact of NaCl Ionic Strength ..... 117

5.3.2. Effect of SW Dilution and Addition of $SO_4$ to SW on Zeta Potential at 80°C ..... 120
5.4. Discussion ..... 121
5.4.1. Effect of Varying NaCl Concentration on Temperature Dependence of Zeta Potential ..... 121
5.4.2. Implications for Controlled Salinity Waterflooding (CSW) ..... 126
5.5. Conclusion ..... 127
**Chapter 6. Quantification of Carbonate Rock Wettability Using Streaming Potential Measurements ..... 128**
6.1. Introduction ..... 128
6.2. Methodology ..... 129
6.2.1. Materials and Sample Preparation ..... 129
6.2.2. Aging to Alter Wettability ..... 130
6.2.3. Spontaneous Imbibition (SI) and Coreflood Tests ..... 131
6.2.4. Measurement of Amott Water Index ($I_w$) ..... 132
6.2.5. Measurement of Zeta Potential at $S_w$ =1 and $S_w$=1-$S_{or}$ ..... 132
6.2.6. Design of Experiments ..... 133
6.3. Results ..... 135
6.3.1. Impact of Water Saturation ($S_w$ = 1-$S_{or}$) and Rock Conductivity on Zeta Potential ..... 135
6.3.2. Impact of Wettability on Zeta Potential ..... 139
6.3.3. Impact of Varying Oil Composition on Zeta Potential ..... 141
6.4. Discussion ..... 142
6.4.1. The Relationship Between Wettability and Zeta Potential ..... 142
6.4.2. Controls on Zeta Potential of Mineral-Brine and Oil-Brine Interfaces ..... 145
6.4.3. Crude Oil Composition and Polarity of Oil-Brine Interface ..... 147
6.4.4. Successful Wettability Alteration with Charged Interfaces of the Same Polarity at High Ionic Strength ..... 148
6.4.5. Practical Application of Wettability Characterisation using the SPM Method ..... 149
6.5. Conclusions ..... 149
**Chapter 7. Designing the Brine Composition: Improved Oil Recovery from Carbonate During Controlled Salinity Waterflooding ..... 151**
7.1. Introduction ..... 151
7.2. Methodology ..... 152
7.3. Results ..... 154
7.3.1. Brine Composition and the Zeta Potential of Water-Wet Carbonate Samples ..... 154
7.3.2. Controlled Salinity Waterflooding with Varying Ionic Strength ..... 155
7.3.3. Controlled Salinity Waterflooding with Varying Ca Concentration ..... 157
7.3.4. Correlation Between Zeta Potential and Improved Oil Recovery ..... 159
7.4. Discussion ..... 161

7.5. Conclusions ..... 166
**Chapter 8. Summary, Conclusions and Future Work ..... 167**
8.1. Summary and Conclusion ..... 167
8.2. Implications ..... 169
8.3. Future Work ..... 170
**References…. ..... 173**
**Appendices ..... 187**
Appendix A: Streaming Potential Measurements: Application to Porous Media ..... 187
Appendix B: XRD Data for Ketton, Estaillades and Portland ..... 193
Appendix C: Determination of Rock Permeability and Porosity and Fluid Saturation ..... 196
C.1 Rock Permeability ..... 196
C.2 Rock Porosity ..... 197
C.3 Fluid Saturations ..... 197
Appendix D: n-decane SPM experiments ..... 198
Appendix E: Compilation of SPM and Coreflooding Results ..... 200

# List of Tables

Table 3-1: Summary of published zeta potential of calcite and natural carbonates with varying pH and pCa. ..... 66
Table 4-1: Properties and mineralogy of rock samples used in this study ..... 83
Table 4-2: Properties and composition of brines used in chapter 4 ..... 83
Table 6-1: Properties and composition of brines used in chapter 6 ..... 130
Table 6-2: Properties of the oils used in chapters 6 and 7 ..... 130
Table 6-3: Summary of the experiments conducted in chapter 6 ..... 135
Table 7-1: Properties and composition of brines used in chapter 7 ..... 153

# List of Figures

Figure 2-1: The multi-ion exchange (MIE) mechanism during low salinity waterflooding in sandstones. ..... 29

Figure 2-2: Examples of spontaneous imbibition (SI) experiments in carbonate during controlled salinity waterflooding. ..... 32

Figure 2-3: Examples of coreflood experiments in carbonate during controlled salinity waterflooding at room and elevated temperatures. ..... 34

Figure 2-4: Surface ion exchange (SIE) mechanism for the wettability alteration induced by seawater (SW) injection in Stevns Klint chalk. ..... 35

Figure 2-5: Mineral dissolution-precipitation mechanism during seawater injection in carbonate at high temperature. ..... 36

Figure 2-6: Disjoining pressure as a function of double layer thickness for the solution compositions and conditions used in Karoussi and Hamouda, 2007 (reported in Figure 2-2c). After Hiorth et al., (2010). ..... 39

Figure 2-7: Oil droplet contact angle alteration on limestone surface under formation brine (FMB) and seawater (SW). After Mahani et al., (2015). ..... 42

Figure 2-8: Relationship between wettability index and total oil recovery for formation brine (FMB), seawater (SW) and single-components brine solutions in secondary mode. After Gandomkar and Rahimpour, (2015). ..... 44

Figure 2-9: Oil recovery vs. scaled imbibition rate ($t_D$) for three imbibing fluids (low, medium and high salinity). After Morrow and Buckley, (2011). ..... 45

Figure 2-10: Zeta potential measurements and wettability alteration at mineral surfaces after aging in formation brine (FMB) and oil proposed by Jackson and Vinogradov, (2012). ..... 46

Figure 3-1: Schematic representation of (a) the electrical double layer at the calcite-water interface and (b) the variation in the electrical potential with distance from the mineral surface. ..... 51

Figure 3-2: The theory of streaming potential. A schematic showing a separation of charge in the electrical double layer (EDL) occurs due to a pressure gradient and at equilibrium streaming potential arises to maintain electrical neutrality. Adapted from Jackson et al., (2012). ..... 54

Figure 3-3: Zeta potential of Iceland spar and synthetic calcite in indifferent electrolytes as a function of pH. ..... 64

Figure 3-4: Zeta potential of natural calcite and carbonate rocks in indifferent electrolytes as a function of pH. ..... 65

Figure 3-5: Zeta potential and electrophoretic mobility of synthetic calcite and Iceland spar as a function of pH in experiments with constant pCa. ..... 68

Figure 3-6: Zeta potential of synthetic calcite and natural carbonate in indifferent electrolytes as a function of pCa at low Ca concentration only. ..... 70

Figure 3-7: Zeta potential of synthetic calcite and natural carbonate in indifferent electrolytes as a function of pCa at low and high Ca concentration. ..... 71

Figure 3-8: Zeta potential of synthetic calcite and natural carbonate as a function of pMg. ..... 72

Figure 3-9: Zeta potential of synthetic calcite and natural carbonate as a function of $pSO_4$. ..... 73

Figure 3-10: Zeta potential of Iceland spar in deionized water with various $pCO_2$ as a function of pH. ..... 76

Figure 3-11: Calcite-water-$CO_2$ equilibrium of natural Portland rock samples with deionised water. ..... 79

Figure 4-1: A flowchart showing all steps conducted during streaming potential experiments on natural carbonates samples including brine and sample preparation, streaming potential measurements technique and brine composition measurements. ..... 85

Figure 4-2: Experimental apparatus for measuring streaming potential coupling coefficient. ..... 87

Figure 4-3: The relationship between brine salinity and brine conductivity (a and b) and between brine viscosity and brine salinity (c). ..... 90

Figure 4-4: The measured impedance and electrical resistance of 2M NaCl saturated sample of the Estaillades limestone as a function of the frequency range 10 Hz-2 MHz. ..... 91

Figure 4-5: The calculated reactance (X) as a function of the meausred electrical resistance of 2M NaCl saturated sample of the Estaillades limestone. The minimum reactance corresponds to resistance (R) of 69.15 ohm. ..... 92

Figure 4-6: Saturated sample conductivity of (a) Ketton and (b) Estaillades samples versus NaCl-EQ brine conductivity. One linear regression can be fitted through all points and the reciprocal of the slope yields the intrinsic formation factor, which is used in equation (3.13)..... 93

Figure 4-7: Typical results from streaming potential measurements (SPM) experiments on natural carbonate samples. ..... 96

Figure 4-8: Effect of NaCl concentration on zeta potential on the Ketton (squares) and Estaillades (triangles) samples. ..... 97

Figure 4-9: Zeta potential versus (a) pCa and pMg, and (b) $pSO_4$ for the Ketton and Estaillades samples at different NaCl concentrations. ..... 99

Figure 4-10: Relationship between pH, pCa (or pMg) and zeta potential from the SPM experiments reported in this study. ..... 101

Figure 4-11: Impact of formation brine (FMB), seawater (SW) and derived compositions from SW on zeta potential of Ketton and Estaillades ..... 103

Figure 4-12: Equilibrium pCa (a) and $pSO_4$ (b) versus NaCl concentration for the Ketton (squares) and Estaillades (triangles) samples. ..... 105

Figure 4-13: Impact of $pSO_4$ on $Ca^{2+}$ concentration and zeta potential measured on the Estaillades sample. ..... 107

Figure 5-1: Experimental apparatus in measuring streaming potential coupling coefficient at elevated temperature. ..... 116

Figure 5-2: Experimental results of NaCl electrolytes at elevated temperatures. ..... 118

Figure 5-3: Zeta potential and equilibrium pCa, pMg and $pSO_4$ as a function of temperature. ..... 119

Figure 5-4: Effect of seawater dilution and addition of $SO_4$ to seawater on zeta potential of natural carbonates at 80ºC. ..... 121

Figure 5-5: Relationship between zeta potential and PDI concentration. (a) Zeta potential plotted against pCa. (b) Zeta potential plotted against $p(Ca+Mg–SO_4)$. ..... 124

Figure 6-1: Zeta potential as a function of water saturation ($S_w=1-S_{or}$) for the Portland samples aged with oil A in (a) 2M NaCl and (b) formation brine (FMB1). ..... 136

Figure 6-2: Zeta potential as a function of water saturation ($S_w=1-S_{or}$) for the Estaillades samples aged with oil B in (a) formation brine (FMB2), (b) seawater (SW) and (c) diluted SW (20dSW). ..... 138

Figure 6-3: Impact of rock conductivity on zeta potential and wettability for the Estaillades samples aged with oil B in formation brine (FMB2). ..... 139

Figure 6-4: Zeta potential as a function of water wetting index for oil A using the Portland samples saturated with 2M NaCl (NaB) or formation brine (FMB1) and residual oil saturation. ..... 141

Figure 6-5: Zeta potential as a function of water wetting index for oil B using the Estaillades samples saturated with formation brine (FMB2), seawater (SW) and 20dSW and residual oil saturation. ..... 141

Figure 6-6: Zeta potential as a function of water wetting index for each of the four oils tested (B-E) using the Estaillades samples saturated with formation brine (FMB2) and residual oil saturation. ..... 142

Figure 6-7: Schematics showing postulated wettability of mineral- and oil-brine interfaces in carbonate samples using oils (A-E) in formation brines. ..... 145

Figure 7-1: Impact of brine composition on the zeta potential of water-wet carbonate samples in formation brine (FMB), seawater (SW), diluted seawater (20dSW) and varying Ca in FMB and 2M NaCl. ..... 155

Figure 7-2: Effect of conventional low salinity waterflooding LSW (FMB -> SW - > 20dSW) and inverted LSW (20dSW -> SW - > FMB) on oil recovery and zeta potential change. ..... 157

Figure 7-3: Effect of decreasing/increasing Ca concentration on oil recovery and zeta potential change. ..... 159

Figure 7-4: Summary of results showing cumulative incremental oil recovery against cumulative normalised zeta potential ..... 160

Figure 7-5: Impact of disjoining pressure on water film thickness and wettability. ..... 162

# Nomenclature

| Abbreviation | Description |
|---|---|
| 10dSW | Ten times diluted seawater |
| 20dSW | Twenty times diluted seawater |
| 2dSW | Two times diluted seawater |
| AN | Acid number |
| BN | Base number |
| COZPI | Crude Oil Zeta Potential Indicator |
| CSE | Controlled salinity effect |
| CSW | Controlled salinity waterflooding |
| DIW | De-ionized water |
| DLE | Double layer expansion |
| DLVO | Derjaguin-Landau-Verwey-Overbeek |
| EDL | Electrical double layer |
| EPM | Electrophilic mobility |
| FaCa | Brine of the same ionic strength as formation brine (FMB) but varying $Ca^{2+}$ concentrations |
| FMB | Formation brine |
| IC | Ion chromatography |
| ICP-AES | Inductively coupled plasma atomic emission spectroscopy |
| IEP | Iso-electric point |
| IFT | Interfacial tension |
| IHP | Inner Helmholtz plane (1-plane) |
| IR | Infrared spectroscopic |
| IS | Ionic strength |
| LSE | Low salinity effect |
| LSW | Low salinity waterflooding |
| MIE | Multi-component ions exchange |
| NaB | 2M NaCl equilibrated brine with natural carbonate and $CO_2$ |
| NaCa | Brine of the same ionic strength as 2M NaCl brine (NaB) but varying $Ca^{2+}$ concentrations |

| | |
|---|---|
| NaCl-EQ | NaCl equilibrated brine with carbonate and $CO_2$ |
| NMR | Nuclear magnetic resonance |
| OHP | Outer Helmholtz plane (2-plane) |
| P | Pressure |
| pCa | Negative logarithm of calcium concentration in mol/l |
| PDI | Potential determining ion |
| pMg | Negative logarithm of magnesium concentration in mol/l |
| PS | Paired stabilization |
| $pSO_4$ | Negative logarithm of sulfate concentration in mol/l |
| PVI | Pore volume injected |
| PZC | Point of zero charge |
| RF | Recovery factor |
| SCM | Surface complexation model |
| SI | Spontaneous imbibition |
| SIE | Surface ions exchange |
| SPM | Streaming potential measurements |
| SW | Seawater |
| SW2S | Seawater with two times sulfate concentration |
| SW3S | Seawater with three times sulfate concentration |
| SW4S | Seawater with four times sulfate concentration |
| T | Temperature |
| TDS | Total dissolved solids |
| USBM | US Bureau of Mines |
| V | Voltage |
| WF | Waterflooding |
| XPS | X-ray photoelectron spectroscopic |
| XRD | X-ray diffraction |

| Symbols | Description | SI Unit |
|---|---|---|
| $\varepsilon$ | Brine permittivity | $F \cdot m^{-1}$ |
| $\Pi$ | Disjoining pressure | Pa |
| $\zeta$ | Zeta potential | V |
| $z$ | Valance on ion | N/A |
| $r$ | Local radius of curvature | m |
| $P_w$ | Pressure on water | Pa |
| $P_o$ | Pressure on oil | Pa |
| $P_c$ | Oil-water capillary pressure | Pa |
| $L_c$ | Core length | m |
| $k$ | Boltzmann constant | $kg\ m^2\ s^{-2}\ K^{-1}$ |
| $F_0$ | Intrinsic Formation Factor | N/A |
| $F_a$ | Apparent Formation Factor | N/A |
| $e$ | Electron charge | C |
| $D$ | Thickness of water film | m |
| $C_s$ | Stern layer Capacitance | $F\ m^{-2}$ |
| $C_d$ | Diffuse layer Capacitance | $F\ m^{-2}$ |
| $C_{sp}$ | Streaming potential coupling coefficient | V/Pa |
| $A_{wo}$ | Area under the imbibition curve in the capillary pressure plot (water displacing oil) | $m^2$ |
| $A_{ow}$ | Area under the drainage curve in the capillary pressure plot (oil displacing water) | $m^2$ |
| $A$ | Hamaker constant | $kg\ m^2\ s^{-2}$ |
| $t_D$ . | Scaled rate of imbibition (dimensionless time) | N/A |
| $V_{wsp}$ | Volume of water spontaneously imbibed | $m^3$ |
| $V_{osp}$ | Volume of oil spontaneously imbibed | $m^3$ |
| $V_{wt}$ | Total volume of water produced by both spontaneous imbibition and waterflooding | $m^3$ |
| $V_{ot}$ | Total volume of oil produced by both spontaneous imbibition and waterflooding | $m^3$ |

| | | |
|---|---|---|
| $S_{spw}$ | Water saturation after the imbibition process | N/A |
| $S_{spo}$ | Oil saturation after the imbibition process | N/A |
| $S_{cw}$ | Connate (irreducible) water saturation | N/A |
| $S_{or}$ | Residual oil saturation | N/A |
| $I_w$ | Amott wettability index to water | N/A |
| $I_o$ | Amott wettability index to oil | N/A |
| $I_{o-w}$ | Amott-Harvey wettability index | N/A |
| $I_u$ | USBM wettability index | N/A |
| $t$ | Time | s |
| $k$ | Core permeability | $m^2$ (Darcy in field unit) |
| $\phi$ | Fractional porosity | N/A |
| $\sigma$ | Interfacial tension | N $m^{-1}$ |
| $\mu_w$ | Brine viscosity | Pa·s |
| $\sigma_f$ | Brine conductivity | S·$m^{-1}$ |
| $\sigma_{rf}$ | Brine saturated rock conductivity | S·$m^{-1}$ |
| $\sigma_s$ | Surface conductivity | S·$m^{-1}$ |
| $IS$ | Ionic strength | M (mol $l^{-1}$) |
| $T$ | Temperature | K |
| $\psi_{oil}$ | Surface potential at oil-brine interface | V |
| $\psi_{water}$ | Surface potential at mineral-brine interface | V |
| $\kappa$ | Debye-Huckel reciprocal length | $nm^{-1}$ |

# Chapter 1.

# Introduction

## 1.1. Overview

Carbonates are the group of rocks composed primarily of the minerals calcite ($CaCO_3$) and dolomite ($CaMg(CO_3)_2$) along with impurities such as quartz, anhydrite, clay minerals, organic matter and apatite (*Tucker and Wright*, 1990). Carbonate rocks host most of the world's oil reserves (>60%; *Klemme and Ulmishek*, 1991). However, the proportion of oil recovered from carbonate reservoirs is low (typically <40%; *Downs and Hoover*, 1989). Methods for improved oil recovery (IOR) from carbonate reservoirs are therefore of broad scientific and engineering interest.

The first (primary) recovery from an oil reservoir results from pressure depletion and is usually modest (5 – 10%; *Bradley*, 1987). In many reservoirs, water is injected to increase (secondary) recovery by maintaining the reservoir pressure and displacing oil towards the production wells. This process is termed waterflooding (*Willhite*, 1986). The water injected may be formation brine produced from the oil reservoir or an underlying aquifer, seawater, or water from some other convenient source. Formation brine (FMB) is typically highly saline (total ionic strength >2M) and rich in monovalent and divalent ions such as Na, Cl, Ca and Mg (*Romanuka et al.*, 2012; *Shehata et al.*, 2014). Seawater (SW) is less saline than typical FMB (total ionic strength 0.55-0.69M) but is still rich in a range of monovalent and divalent ions

Laboratory experiments and field trials have shown that oil recovery from carbonate reservoirs can be increased by modifying the composition of the brine

injected during waterflooding in a process termed ‘controlled salinity waterflooding’ (CSW; e.g. *Zhang and Austad*, 2006; *Karoussi and Hamouda*, 2007; *Zhang et al.*, 2007; *Strand et al.*, 2008; *Rezaeidoust et al.*, 2009; *Fathi et al.*, 2010; *Hiorth et al.*, 2010). In laboratory coreflooding experiments, oil is displaced from cylindrical rock samples (‘cores’) by injecting water of the desired composition over one face and producing oil (and water) from the opposing face to model the reservoir waterflooding process. In spontaneous imbibition (SI) experiments, core samples are immersed in water and the volume of oil spontaneously displaced by water is measured. These laboratory experiments are slow and expensive to undertake, as are field trials (e.g. *Yousef et al.*, 2012b). A reliable method for identifying the optimum composition for CSW is therefore essential.

The most typical CSW approach in carbonates is to switch from formation brine to seawater (*Fathi et al.*, 2010; *Shariatpanahi et al.*, 2010; *Rashid et al.*, 2015) and/or to dilute formation brine or seawater (*Austad et al.*, 2011; *Yousef et al.*, 2011). Other studies have adjusted the concentration of one or more of the divalent ions $Ca^{2+}$, $Mg^{2+}$ or $SO_4^{2-}$ (*Strand et al.*, 2006; *Zhang and Austad*, 2006; *Zhang et al.*, 2007; *Strand et al.*, 2008). The problem is that improved recovery is not observed in all cases (*Austad et al.*, 2011). Despite numerous studies, CSW in carbonates remains controversial. Many studies have reported the successful application of CSW, but many others (and more unpublished) observed no benefit, and the available data are often inconsistent and contradictory. More fundamentally, the pore- to mineral-surface-scale mechanisms responsible for improved oil recovery during CSW are actively debated.

Improved recovery during CSW in carbonates appears to be observed when the initial wetting state is mixed- or oil-wet, and the wettability changes to become more water-wet after injecting water with modified composition (e.g. *Austad and Standnes*, 2003; *Strand et al.*, 2006; *Zhang and Austad*, 2006; *Karoussi and Hamouda*, 2007; *Zhang et al.*, 2007; *Fathi et al.*, 2010; *Alotaibi and Nasr-El-Din*, 2011; *Gandomkar and Rahimpour*, 2015). As the reservoir first fills with oil, polar functional groups on the molecules in the oil adsorb onto mineral surfaces,

rendering them oil-wet. During CSW, some of these molecules desorb, the surfaces become more water-wet and oil is released. Several adsorption/desorption processes at the calcite surface have been proposed (e.g. *Strand et al.,* 2006; *Austad et al.,* 2007; *Karoussi and Hamouda,* 2007; *Puntervold et al.,* 2007; *Hiorth et al.,* 2010). Many of these cause changes in the zeta potential of the mineral surface, which modifies the electrostatic forces acting between the surface and the polar functional groups in the oil, consistent with the Derjaguin-Landau-Verwey-Overbeek (DLVO) theory (e.g. *Evans and Wennerström*, 1999).

In carbonates, there are several ions (e.g. $Ca^{2+}$, $Mg^{2+}$, $HCO_3^-$, $CO_3^{2-}$, $SO_4^{2-}$, $H^+$, $OH^-$) that can interact with the surface and control the density of the electrical surface charge. However, studies revealed that the zeta potential is controlled by the concentration-dependent adsorption of the divalent ions (e.g. $Ca^{2+}$, $Mg^{2+}$, $CO_3^{2-}$, $SO_4^{2-}$) within the Stern layer, primarily at the Outer Helmholtz Plane (OHP) (e.g. *Douglas and Walker*, 1950; *Thompson and Pownall*, 1989; *Pierre et al.*, 1990; *Somasundaran*, 2006; see chapter 3). In this thesis, we refer to those ions whose concentration in aqueous solution controls the magnitude and polarity of zeta potential of the mineral surface as potential determining ions (PDIs). The key studied PDIs in the literature of zeta potential of carbonates and its relation to the wetting sate and oil recovery are $Ca^{2+}$, $Mg^{2+}$ and $SO_4^{2-}$ because of their presence in the formation and controlled injection (e.g. SW) brines. In the experiments reported here, we investigate the relationship between these PDIs, zeta potential, wettability and oil recovery using systems that are more realistic and representative of reservoir conditions.

Measurements of zeta potential on intact carbonate rock samples, obtained using the streaming potential method (SPM; e.g. *Jaafar et al.*, 2009; *Vinogradov et al.*, 2010; *Vinogradov and Jackson*, 2011) has been utilized to identify the wetting state of carbonate mineral surfaces. Existing experimental evidence suggested that the wetting behaviour of carbonate mineral surfaces can be affected by their surface electrical properties (*Jackson and Vinogradov*, 2012). These measurements may also be used during controlled salinity waterflooding

experiments to determine if and how changes in zeta potential and wetting state are responsible for improved oil recovery from carbonate samples.

Given this, the importance of understanding the development of zeta potential of carbonates for reservoir characterization and various enhanced oil recovery processes such as CSW, $CO_2$ flooding and surfactant flooding needs measurements in natural conditions of salinity and temperature and in the presence of carbonate rock, brine and oil in the same system. The main advantage of the SPM over other zeta potential measurements (e.g. electrophoretic mobility) is that the SPM can be conducted on a porous medium where the full description of the reservoir system can be represented in the laboratory in terms of brine salinity and composition, temperature and wetting state.

## 1.2. Aim and Objectives

The aim of this research is to characterise wettability and predict successful controlled salinity waterflooding in carbonates rocks using measurements of streaming potential on intact carbonate core samples. Zeta potential obtained from the SPM method is used to quantify the relationship between water chemistry, carbonate rock type, temperature, wettability and oil recovery during CSW using an integrated experimental approach. The main objective is to determine changes in zeta potential and brine composition during CSW experiments at reservoir conditions of salinity and temperature, complemented with measurements of main ions such as $Na^+$, $Ca^{2+}$, $Mg^{2+}$ and $SO_4^{2-}$ from effluent brines. In outline, the scope of this project investigates the following:

- Changes in zeta potential of intact carbonate core samples fully saturated with water when the chemistry of injected brine is varied at ambient temperature. The specific objectives are to investigate how the zeta potential is affected by the following:

I. NaCl equilibrated brine concentrations: we cover a wide range of salinity from fresh (0.01M NaCl) to very saline (5M NaCl). M is molar per litre concentration (mol/l).

II. Carbonate rock type: we use two apparently identical limestone named Estaillades and Ketton and compared results to a third previously studied carbonate rock type named Portland (*Alroudhan*, 2015).

III. Potential determining ions (PDIs; $Ca^{2+}$, $Mg^{2+}$ and $SO_4^{2-}$). We vary the concentration of these ions in NaCl solutions over a range typical to natural brines.

IV. Brine compositions represent natural brines including typical formation brine found in hydrocarbon reservoirs (FMB), typical seawater composition (SW) and modified seawater compositions used in controlled salinity waterflooding.

- The impact of elevated temperatures on zeta potential of natural carbonate. In these experiments, we use variation of hydrocarbon reservoir temperatures (40 to 120 $^oC$) to investigate the change of zeta potential of the three investigated carbonate rock types in various brine compositions. We examine the following:

  I. Effect of indifferent ions: we use two different NaCl electrolytes: 0.01M (ionic strength comparable to potable water) and 0.5M (ionic strength comparable to seawater).

  II. Effect of simple dilution of SW and addition of $SO_4^{2-}$ to SW at one typical reservoir temperature (80$^oC$).

- Extension of streaming potential experiments in the intact carbonate core samples to account for the presence of two fluids in the pore-space. We start by investigating the relationship between brine composition, zeta potential and wettability at room temperature using one carbonate rock type (Estaillades) saturated with various brine and oil compositions. The results are compared to previously studied Portland sample studied by *Alroudhan,* (2015) using the same experimental approach.

- Finally, we address the relationship between brine composition, zeta potential and oil recovery during CSW at ambient conditions using the same oils and the carbonate rock type investigated in the wettability characterisation phase. In this section, we use conventional typical low salinity waterflooding (LSW) and unconventional methods where the brine composition is modified so as to maximize the electrostatic repulsion between the mineral-brine and oil-brine interfaces.

## 1.3. Thesis Outline

Chapter 2 starts by reviewing the experimental evidence that address the impact of brine composition on wettability alteration and oil recovery in sandstones and carbonates. Then, the chapter reviews the main mechanisms proposed for CSW in carbonates and finishes by briefly reviewing the key methods used to characterise wettability and wettability alteration, including zeta potential measurements.

Chapter 3 reviews previous measurements of zeta potential on natural and artificial calcite and carbonate as a resource for measurements obtained in this project and future studies, and addresses the key controls on zeta potential and where uncertainties remain. The chapter also addresses the main differences between the most typical two method used to interpret zeta potential; the electrophoretic mobility and the streaming potential. Also, the limitations of zeta potential measurements using the SPM approach in carbonates are addressed; and the derivation and assumptions behind the relationship between zeta potential and streaming potential coupling coefficient are clearly explained.

Chapter 4 reports new data of zeta potential on natural carbonates in aqueous solutions typical to natural brines. The chapter describes the methodology and apparatus used for streaming potential measurements and coreflooding experiments, including brine and sample preparation and brine

composition measurements. The implications of the results for wettability alteration and oil recovery in carbonate reservoirs are briefly discussed.

Chapter 5 presents first zeta potential measurements in intact carbonates at elevated temperature in simple NaCl solutions and artificial brines typical to SW and modified versions of SW. The chapter aims to understand the zeta potential of natural carbonates at elevated temperatures typical to hydrocarbon systems.

Chapter 6 examines the relationship between zeta potential and wettability using natural carbonates, brines and crude oils. The key controls on zeta potential at mineral-brines and oil brine interfaces, along with the implication on the stability of wetting films are also presented.

In chapter 7, results presented in chapter 6 are used to design brine compositions that lead improved oil recovery during CSW in carbonates. The chapter finishes by giving a practical approach for the demonstrated experimental method.

Finally, in chapter 8, results are summarized and key conclusions are drawn, along with contributions and implication of the results to the subject of improved/enhanced oil recovery from carbonate reservoirs during CSW. The chapter finishes with suggested future work.

# Chapter 2.

# Impact of Brine Composition on Rock Wettability and Oil Recovery

## 2.1. Introduction

There are several controls on rock wettability. These controls involve crude oil, rock mineralogy, temperature and brine composition, which can be split into two main categories. The first category includes wettability determining properties that are not changeable such as crude oil properties, rock mineralogy, formation brine composition and temperature (e.g. *Buckley et al.*, 1989; *Buckley et al.*, 1998; *Romanuka et al.*, 2012).

The second category involves injection brine composition. As will be discussed in more details below, the impact of brine composition on rock wettability is noticeable for both sandstones and carbonates. Unlike the first category, injection brine composition is easy to change and can be controlled. Extensive experimental studies have been conducted to link between brine composition and change in rock wettability (e.g. *Strand et al.*, 2006; *Zhang and Austad*, 2006; *Karoussi and Hamouda*, 2007; *Zhang et al.*, 2007; *Fathi et al.*, 2010; *Mahani et al.*, 2015; *Yousef et al.*, 2011). It is widely agreed that wettability alteration towards more water-wet during LSW or CSW is the main cause for the observed improved oil recovery from sandstone and carbonate rocks (e.g. *Morrow*, 1990; *Jadhunandan and Morrow*, 1995; *Hiorth et al.*, 2010; *Morrow and Buckley*, 2011; *Gandomkar and Rahimpour*, 2015; *Mohammed and Babadagli*, 2015). The following sections review LSW in sandstones and CSW in carbonates, and the main methods used to characterise wettability and wettability alteration.

## 2.2. Low Salinity Waterflooding in Sandstones

For sandstone, the improvement of oil recovery has been achieved by lowering the total salinity of the injected brine, preferably below 5000 ppm total dissolved solids (TDS) (e.g. *Tang and Morrow*, 1997, 1999; *Webb et al.*, 2003; *Lager et al.*, 2008). Evidence from experimental data and field trials have been gathered indicating a successful LSW in the oil recovery from sandstone rocks (e.g. *Webb et al.*, 2003; *McGuire et al.*, 2005; *Webb et al.*, 2005). For example, 25-50% reduction in residual oil saturation was observed from log analysis when injecting with low salinity brine, similar to previous laboratory experimental tests (*Webb et al.*, 2003).

The low salinity effect (LSE) observed in sandstone during LSW has been linked to the presence of clay (e.g. *Bernard*, 1967; *McGuire et al.*, 2005; *Ligthelm et al.*, 2009; *Soraya et al.*, 2009; *Austad et al.*, 2010; *Berg et al.*, 2010; *Vledder et al.*, 2010; *Hassenkam et al.*, 2011; *Morrow and Buckley*, 2011; *Nasralla et al.*, 2013). *Tang and Morrow,* (1999) observed that adsorption of polar compounds of crude oil on clay particles at pore walls gives mixed-wet fines. Therefore, the removal of these fines, with oil drops adhered to it, during LSW yields improved oil recovery. Recently, *Morrow and Buckley,* (2011) also noted that LSW and LSE are accompanied with the mixed wet clay particles (e.g. kaolinites) migration.

Despite the strong link between clay minerals and the LSE in sandstones, the underpinning pore- to mineral-surface-scale processes of wettability alteration remains uncertain and a consistent agreed mechanism has not yet emerged (*Morrow and Buckley*, 2011). The key mechanisms that have been reported for the LSE in sandstones include (i) double layer expansion (DLE; *Vledder et al.*, 2010), (ii) migration of mixed-wet fine particles (*Tang and Morrow*, 1999), (iii) pH-induced interfacial tension reduction (IFT; *McGuire et al.*, 2005) and (iv) multi-component ion exchange (MIE; *Lager et al.*, 2008). The latter posited that the negatively charged carboxylic oil compounds are bound to the surface of oil-wet clay constituents by cation bridging (e.g. RCOO-Ca-surface). During LSW, the electrical double layer (EDL) at the clay surface expands and the bound multivalent

cations (e.g. $Ca^{2+}$) become accessible for the monovalent cations (e.g. $Na^{+}$) dissolved in the injected water. This MIE process leads to detachment of carboxylic oil compounds from the mineral surface, causing an increase in the water-wetness of the rock surface and therefore improves oil recovery (Figure 2-1; *Lager et al.*, 2008).

Likewise, double layer expansion (DLE) states that the transition from high salinity formation brine that rich in multivalent cations (e.g. $Ca^{2+}$ and $Mg^{2+}$) to low salinity brine causes the electrical double layer to expand; thus, enhancing the repulsive forces between the negatively charged clay particles and the crude oil materials. This allows the crude oil polar components to detach from the clay particles and therefore more oil to be produced during LSW (e.g. *Berg et al.*, 2010; *Vledder et al.*, 2010; *Morrow and Buckley*, 2011; *Nasralla et al.*, 2013).

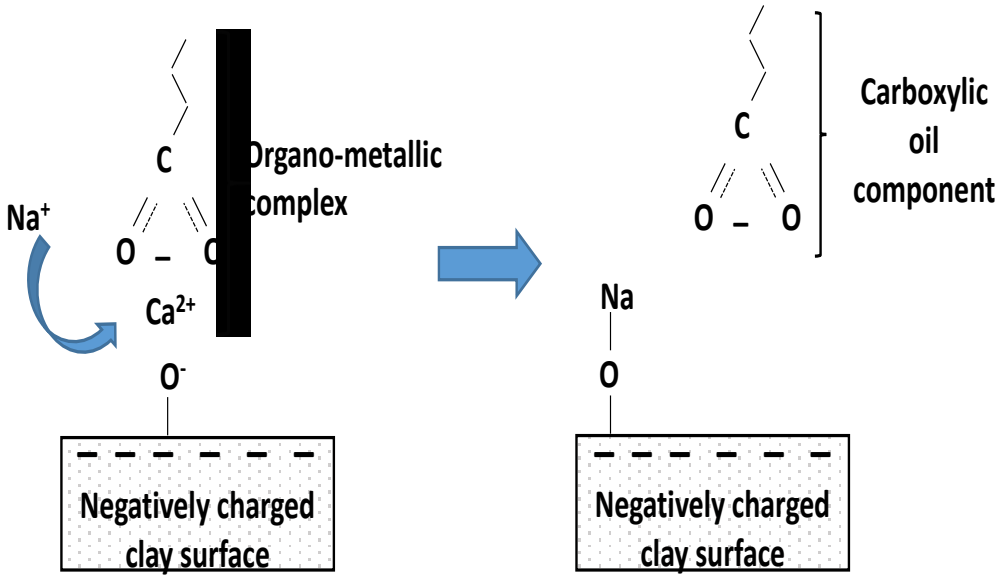



**Figure 2-1: The multi-ion exchange (MIE) mechanism during low salinity waterflooding in sandstones.A schematic showing negatively charged carboxylic oil compounds are bound to the surface of oil-wet clay constituents by cation bridging. During LSW, the bound multivalent cations, e.g. $Ca^{2+}$, become accessible for the monovalent cations, e.g. $Na^{+}$, dissolved in injected water. Modified from *Lager et al.,* (2008).**

A common relationship between these mechanisms is zeta potential, which will change as a response of MIE, local pH change and DLE processes. However, this relationship is still poorly addressed; owing to lack of data acquired at relevant natural conditions. Most of zeta potential measurements have been obtained in

powdered samples with relatively low ionic strengths, limiting temperature range and presence of one phase (e.g. *Alotaibi et al.*, 2011b; *Nasralla and Nasr-El-Din*, 2012; *Nasralla and Nasr-El-Din*, 2014). Recently, some of these issues have been addressed by Jackson and co-authors using the SPM on intact natural sandstone samples at high salinities (*Jaafar et al.*, 2009; *Vinogradov et al.*, 2010), during multiphase (*Vinogradov and Jackson*, 2011) and at elevated temperature (*Vinogradov and Jackson*, 2015) relevant to natural petroleum systems.

## 2.3. Controlled Salinity Waterflooding in Carbonates

In carbonate, chemical compositions of the brine seem to play an important role in the oil/brine/rock interactions even if the total ionic strength is above the reported threshold salinity (< 5000 ppm) in sandstone. Seawater composition, with a total salinity of 30,000 to 45,000 ppm, is widely accepted to alter the wettability of carbonate rocks from preferentially oil-wet to preferentially water-wet, and thus trigger more oil recovery (e.g. *Strand et al.*, 2006; *Austad et al.*, 2007; *Karoussi and Hamouda*, 2007; *Puntervold et al.*, 2007; *Hiorth et al.*, 2010). Moreover, improvement of oil recovery was observed from carbonate rocks by LSW using diluted brines with salinities ranges 21,000 to 220 ppm compared to 220,000 ppm formation brines (e.g. *Austad et al.*, 2011; *Yousef et al.*, 2011; *Romanuka et al.*, 2012). Given this, LSW seems to work in carbonates but not necessarily in the same exact way as in sandstones.

In the last decade, a wide range of laboratory experiments have been conducted to understand the chemical effects behind SW injection, specifically in chalk, and CSW in carbonates. Chalk and carbonate reservoirs can be highly fractured; thus oil displacement by waterflooding is a combination of viscous forces through matrix and capillary forces at the matrix-fracture interface (*Blunt*, 2001). Therefore, evidence supporting the CSE in carbonate is taken from spontaneous imbibition (SI) or forced displacement coreflood experiments.

### 2.3.1. Spontaneous Imbibition (SI) Experiments

Following the great success of SW injection in the highly fractured Ekofisk chalk reservoir, the impact of brine composition on wettability alteration and improved oil recovery (IOR) during CSW was extensively studied by Austad and co-workers (e.g. *Standnes and Austad*, 2000; *Strand et al.*, 2006; *Zhang and Austad*, 2006; *Austad et al.*, 2007; *Zhang et al.*, 2007; *Karoussi and Hamouda*, 2007, 2008). These studies have shown that IOR from chalk samples can be successfully achieved by altering the concentration of the key potential determining ions (PDIs; $Ca^{2+}$, $Mg^{2+}$ and $SO_4^{2-}$). The proposed conditions for the observed CSE in these studies are:

- *Presence of $SO_4^{2-}$* (*Strand et al.*, 2006; Figure 2-2a) and *either $Ca^{2+}$ or $Mg^{2+}$* (*Zhang et al.*, 2007; Figure 2-2b) in the imbibing fluid. The latter study argued that $Mg^{2+}$ becomes more active at higher temperatures (>60$^o$C) and its presence with $SO_4$ in the imbibing brine can lead to higher recovery compared to lower temperature range (40$^o$C; Figure 2-2b). These authors demonstrated that the presence of potential determining anions and cations are essential for the wettability alteration of chalk core samples. They argued that $SO_4^{2-}$ alone was not active as wettability modifier in the chalk; moreover, $Ca^{2+}$ and $Mg^{2+}$ were not able to increase the imbibition rate in the absence of $SO_4^{2-}$. On contrary, several studies showed that the CSE has not observed in different types of chalk (*Fernø et al.*, 2011), or in carbonates (*Romanuka et al.*, 2012) when $SO_4^{2-}$ was added to the imbibing brine (e.g. Figure 2-3d).
- *Wettability alteration*. SI experiments showed that wettability alteration towards more water-wet conditions is accompanied by a higher imbibition rate and improved oil recovery as controlled salinity brine is induced. For example, *Karoussi and Hamouda,* (2007) showed that $Mg^{2+}$ was able to alter chalk wettability towards higher water-wet conditions compared to $SO_4^{2-}$ at different temperature ranges (40, 70 and 90$^o$C; Figure 2-2c).
- *Higher temperature*: most SI experiments that observed the CSE in chalk were obtained at temperatures > 90$^o$C (e.g. *Zhang et al.*, 2007; *Strand et al.*, 2006;

*Zhang and Austad*, 2006). However, some studies observed CSE with brines contain various concentrations of $SO_4^{2-}$, $Ca^{2+}$ and $Mg^{2+}$ at temperature as low as 40°C (e.g. Figure 2-2c; *Karoussi and Hamouda*, 2007). Indeed, as the temperature increases, oil recovery improves significantly (e.g. *Karoussi and Hamouda*, 2007; *Zhang et al.*, 2007; *Fernø et al.*, 2011; *Gupta et al.*, 2011) due to enhanced desorption/adsorption processes at rock surface between relative multivalent ions ($SO_4^{2-}$, $Ca^{2+}$ and $Mg^{2+}$) in the brine and polar oil molecules (*Strand et al.*, 2006; *Hiorth et al.*, 2010).

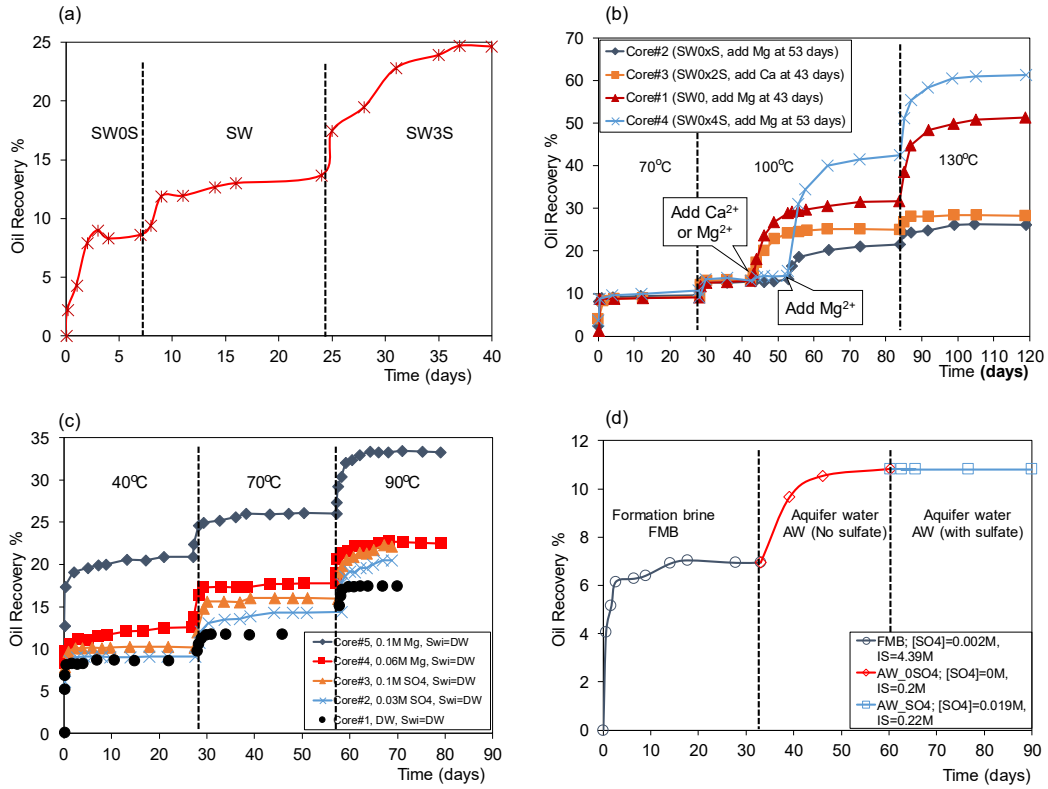



**Figure 2-2: Examples of spontaneous imbibition (SI) experiments in carbonate during controlled salinity waterflooding. (a,b,c) show examples from Stevns Klint chalk and (d) show an example from carbonate core samples during CSW. (a) shows results of varying $SO_4$ in SW on oil recovery from core sample initially saturated with Ekofisk FMB at 110°C (data from *Strand et al.*, 2006). (b) shows results on core samples initially saturated with modified Ekofisk FMB (zero $Ca^{2+}$ and $Mg^{2+}$) at 70, 100 and 130°C. Modified SW (zero $Ca^{2+}$ and $Mg^{2+}$) with varying $SO_4^{2-}$ in the order; SW0x0S→SW0→SW0x2S→ SW0x4S used as imbibition brine. $Ca^{2+}$ and $Mg^{2+}$ are added after 43 and 53 days to analyse their effect on the oil recovery (data from *Zhang et al.*, 2007). (c) shows results of varying either $SO_4$ or Mg in distilled water (DIW) on oil recovery from core samples initially saturated with DIW at 40, 70 and 90°C (data from *Karoussi and Hamouda*, 2007). (d) shows results of varying $SO_4$ and ionic strength (IS) in FMB brine on oil recovery from limestone sample at 70 °C (data from *Romanuka et al.*, 2012).**

### 2.3.2. Forced Displacement (Coreflood) Experiments

Despite the numerous successful SI experiments that observed CSE using brines containing different concentrations of $SO_4^{2-}$, $Ca^{2+}$ and $Mg^{2+}$, several corefloods still observed CSE when these ions (e.g. $SO_4^{2-}$) were removed from the injection brine (e.g. *Austad et al.*, 2011; *Gupta et al.*, 2011). In these coreflood experiments, the CSE was observed during secondary mode (*Al-Attar et al.*, 2013) using DIW compared to FMB (e.g. Figure 2-3a); and tertiary mode (*Austad et al.*, 2011) when injection brine was switched from FMB to 100 times diluted FMB (e.g. Figure 2-3b). Others started with SW as the first injection brine and showed that several dilution of SW provided substantial incremental oil recovery during coreflood experiments compared to injecting SW (Figure 2-3c; *Yousef et al.*, 2011).

In contrast, *Fathi et al.,* (2010) reported a modest incremental oil recovery from Stevns Klint chalk during coreflood experiments. They used four different brines; (1) artificial FMB, similar to Valhall Stevns Klint chalk field, (2) SW, (3) SW with removed NaCl (SW0NaCl) and (4) diluted SW to salinity of 10000ppm (equivalent to 5 times dilution; 5dSW). They reported a small increase in oil recovery from SW injection, whilst no additional oil recovery was observed during injection of either SW0NaCl or 5dSW (Figure 2-3d). Furthermore, it has been reported in the same study that SW0NaCl brine increased the imbibition rate compared to SW whilst no improvement in imbibition rate was observed when 5dSW was used.

Thus, coreflood oil recoveries have a mixed response towards modification of brine salinity and compositions. Most of reported experiments observed the CSE in carbonate in response of lowering the ionic strength (e.g. *Austad et al.*, 2011; *Gupta et al.*, 2011; *Yousef et al.*, 2011; *Al-Attar et al.*, 2013) rather than increasing concentrations of multivalent ions ($SO_4^{2-}$, $Ca^{2+}$, $Mg^{2+}$) in the injection brine. Moreover, the temperature effect on coreflood recoveries has no clear trend; some secondary flooding of chalk core plugs showed no change in oil recovery with temperature, with the exception of Stevn Klint chalk (*Zahid et al.*, 2012), while tertiary flooding showed a slight increase in oil recovery with temperature (*Zahid*

*et al.*, 2010). Others observed an improved oil recovery during secondary flooding with low salinity brine (e.g. DIW) compared to high salinity brine (e.g. FMB) at room temperature (*Al-Attar et al.*, 2013).

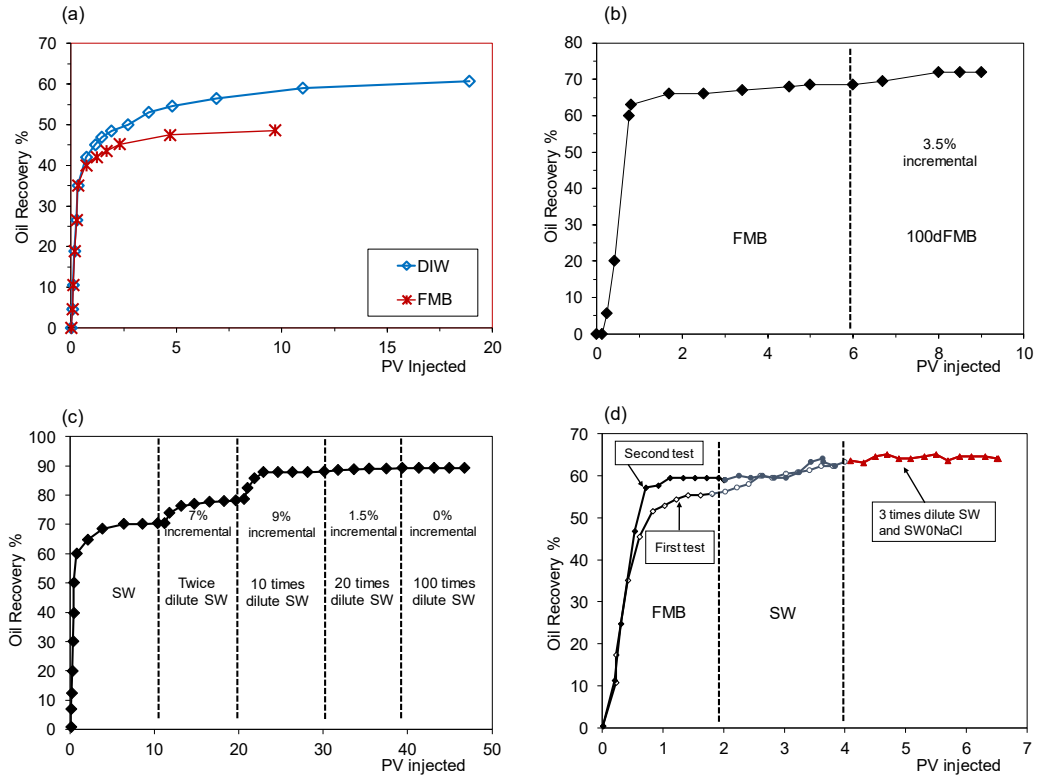



**Figure 2-3: Examples of coreflood experiments in carbonate during controlled salinity waterflooding at room and elevated temperatures. (a, d) show examples from Stevns Klint chalk and (b, c) show examples from natural carbonate core samples in (a) secondary mode and in (b, c, d) tertiary flooding mode. (a) shows results of DIW and FMB at 25°C; DIW yields an additional 17% oil recovery compared to FMB (data from *Al-Attar et al.*, 2013). (b) shows switch from FMB to 100 diluted FMB at 110°C (data from *Austad et al.*, 2011). (c) shows switch from SW to diluted SW up to 100 times at 100°C (data from *Yousef et al.*, 2011). (d) shows switch from FMB to SW and modified SW composition at 120°C (data from *Fathi et al.*, 2010).**

## Proposed Mechanisms for CSW in Carbonates

The main documented mechanisms for the CSW in carbonates include (1) *surface ion exchange* (*SIE*; *Strand et al.*, 2006; *Zhang and Austad*, 2006) and (2) *mineral dissolution-precipitation* (*Hiorth et al.*, 2010).

The surface ions exchange (SIE) theory refers to adsorption of PDI's, changing the rock surface charge, and desorption of carboxylic oil components from the rock surface, which alters rock wettability and improves oil recovery (*Strand et al.*, 2006). It has been proposed that increasing the concentration of

negative PDI's (e.g. $SO_4^{2-}$), which have higher affinity to the rock surface than the negatively charged oil components, will result in adsorption on the positively charged chalk surface. Adsorption of $SO_4^{2-}$ facilitates de-sorption of carboxylic oil components by reducing the positive surface charge, and therefore improved oil recovery. Moreover, reducing the positive charge on the surface will facilitate the reaction between the excess $Ca^{2+}$ (in EDL and at the mineral surface) and carboxylic oil components (Figure 2-4a). At high temperature, $Mg^{2+}$ can replace $Ca^{2+}$ in the carboxylate complex at the chalk surface and result in more oil recovery (Figure 2-4b; *Zhang et al.*, 2007).

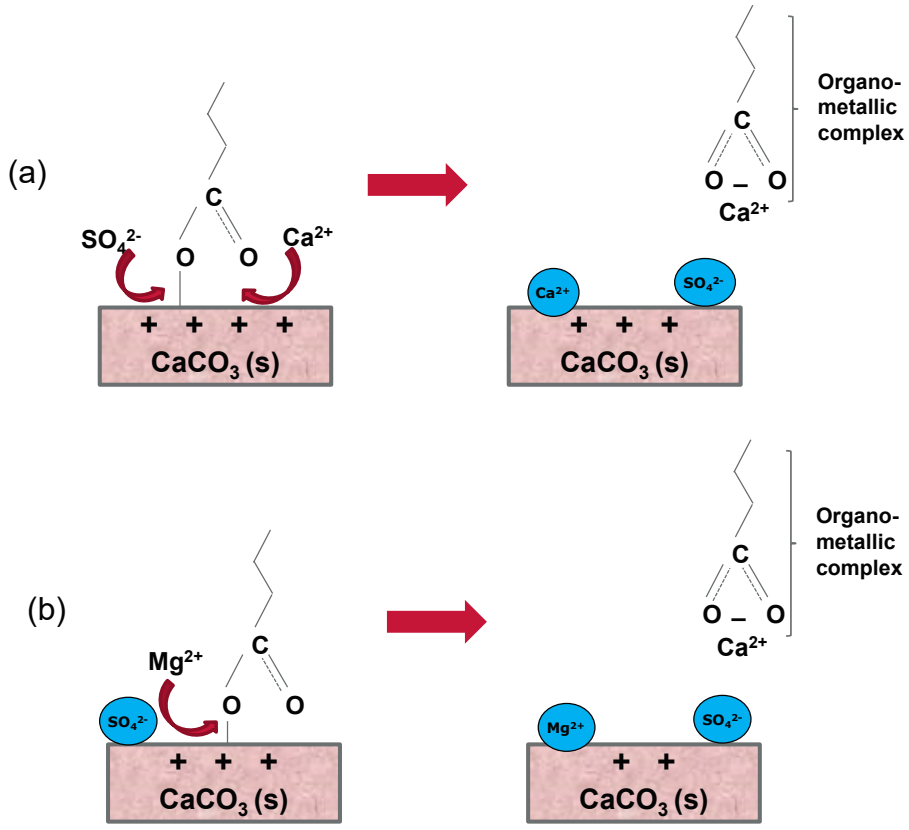



**Figure 2-4: Surface ion exchange (SIE) mechanism for the wettability alteration induced by seawater (SW) injection in Stevns Klint chalk. Schematics showing (a) proposed mechanism when $Ca^{2+}$ and $SO_4^{2-}$ are active at lower temperature. (b) Proposed mechanism when $Mg^{2+}$ and $SO_4^{2-}$ are active at higher temperatures. Modified from *Zhang et al.,* (2007).**

Alternatively, mineral dissolution-precipitation process states that minerals such as huntite ($MgCa(CO_3)_4$), magnesite ($MgCO_3$), and anhydrite ($CaSO_4$) precipitate when magnesium- and/or sulfate-rich brine (e.g. SW) not equilibrated with carbonate is injected and calcite mineral dissolves to balance the decreased

aqueous concentrations of calcium and carbonate ions (*Hiorth et al.*, 2010; *Madland et al.*, 2011). Any polar oil compounds adsorbed on the dissolved mineral surface is released and exposing a water-wet surface (Figure 2-5). Oil recovery improves as dissolution increases pore system connectivity between macro- and micro-pores (*Yousef et al.*, 2011).

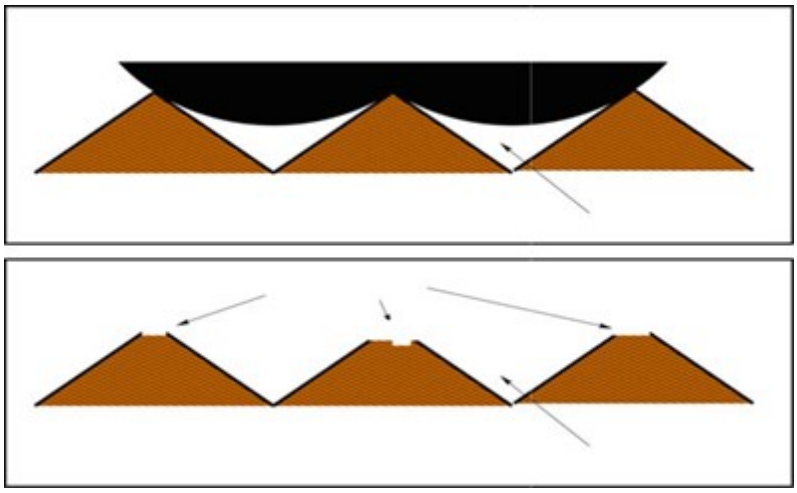


**Figure 2-5: Mineral dissolution-precipitation mechanism during seawater injection in carbonate at high temperature. A schematic showing a section of the pore space, before any dissolution reaction (top). The surface is rough and oil is attached where there is a large curvature and the water film is broken. Bottom: Dissolution of the chalk surface has taken place where the oil was attached, and new water wet rock surface has been created. From *Hiorth et al.,* (2010).**

In addition, *Rezaeidoust et al.,* (2009) proposed a *salting-in* effect, which is the increased solubility of organic materials as a result of removing salts from the water, as part of LSW mechanisms in both sandstone and carbonate. According to these authors, cations such as $Na^+$, $Ca^{2+}$, $Mg^{2+}$ act as an organic-water structure breaker, allowing organic materials to adhere to the rock surface. Lowering the concentration of these cations in water increases the solubility of organic material in the aqueous phase, and thus more oil can be produced during LSW. They claimed that the *salting-in* effect is more effective in clays than in carbonates due to the strong adhesion force between organic material and carbonate. In clays, this adhesion force is relatively weak, which allows organic materials to be released easily from the clay surfaces by LSW. In carbonates, the organic materials can be removed from the carbonate surface by enhancing the surface reactivity of the PDIs at high temperature by a mechanism similar to the *MIE* proposed by *Lager*

*et al.,* (2008). Thus, wettability alteration can be observed at high salinity such as SW salinity, unlike in sandstone (*Rezaeidoust et al.*, 2009). Other published hypotheses considered DLE (*Yi and Sarma*, 2012) and mineral fine migration (*AlShaikh and Mahadevan*, 2016), similar to sandstones, as potential mechanisms for observed CSW effect in carbonates.

## 2.5. Interaction of Crude Oil, Rock and Brine

It is generally accepted that petroleum reservoirs were initially filled with water before oil migrates into the pore spaces, pushing water out of them and leaving non-mobile water behind (*Abdallah et al.*, 1986). This creates a water film or layer at the pore walls, which separates oil from contacting the rock surfaces and maintains the pristine water wetness of the reservoir minerals. When the crude oil has the ability to break this water film, and adsorb on the pore walls, then the wettability will reverse causing some areas to be oil-wet. This reversal process is dependent on the oil properties such as acid and base active groups, asphaltene and resin materials (*Buckley et al.*, 1989; *Hirasaki*, 1991). The stability of the water film acts as a determinant for wettability alteration as suggested by *Kovscek et al.,* (1993). In other words, wettability alteration is the process where the wetting status reverses back to the pristine status, which is water-wet. The instability of water film is a result of oil/brine/rock interaction; and its stability is controlled by the pressure force in oil relative to the pressure force in water (so-called disjoining pressure; *Israelachvili*, 1985; *Kovscek et al.*, 1993; *Bergeron and Radke*, 1995).

Disjoining pressure is described by the three type of forces: the repulsive structural force, the attractive van del Waal force and the electrostatic double layer force. The last is strongly dependent on the surface potential at mineral-water and oil-water interfaces and ionic strength of the aqueous phase (*Israelachvili*, 1985; *Hirasaki*, 1991). The water film will collapse if the attraction electrostatic force between the interfaces exceeds the repulsion force. Then, oil polar components contact the rock surface and can adsorb on the calcium and carbonate sites,

causing a change in wettability. This phenomenon occurs when both interfaces have opposite surface potential/zeta potential (*Buckley et al.*, 1989). The simple approximation of disjoining pressure ($\Pi$) is (*Israelachvili*, 1985; *Hiorth et al.*, 2010)

$$\Pi(D) = -\left(\frac{A}{10^{-20}}\right)\cdot\frac{10^{7}}{6\pi D^{3}} + 1.12\cdot 10^{6}\,\frac{IS}{T}\psi_{oil}\cdot\psi_{water}\cdot\exp(-\kappa D),$$
$$\kappa = 56.2\sqrt{\frac{IS}{T}}, \qquad (2.1)$$

where *D* is the thickness of water film (m), *A* is Hamaker constant (5x10$^{-9}$ J), $IS$ is the ionic strength (M), $T$ is temperature in Kelvin, $\psi_{oil}$ is surface potential at oil-brine interface (V), $\psi_{water}$ is surface potential at mineral-brine interface (V) and $\kappa$ is the Debye-Huckel reciprocal length (nm$^{-1}$).

*Hiorth et al.,* (2010) combined the disjoining pressure and the chemical model to explain the SI results obtained by *Karoussi and Hamouda,* (2007), described above. They calculated surface potential for water and oil at different aging fluids used in *Karoussi and Hamouda,* (2007) study (DIW and DIW with addition of $Na_2SO_4$ and $MgCl_2$). In the case of $MgCl_2$, the chalk surface is positively charged and assumed oil-brine interface is negatively charged; thus the water film is collapsed, making the rock oil-wet. When the chalk is aged with $Na_2SO_4$ fluid, the surface becomes negatively charged and the water film is stabilised making the rock more water-wet. The calculation of disjoining pressure showed that oil pressure needs to exceed the water pressure by around 10 bar for 0.1M $Na_2SO_4$ and 5 bar for 0.03M $Na_2SO_4$ (Figure 2-6) to collapse the water film and reverse wettability to oil-wet. However, this is not the case when the aging fluid is $MgCl_2$ since the two interface have an opposing charge. This explains why aging with $Na_2SO_4$ makes the rock more water-wet and thus more water spontaneously imbibed into the core plug than aging with $MgCl_2$ fluid.

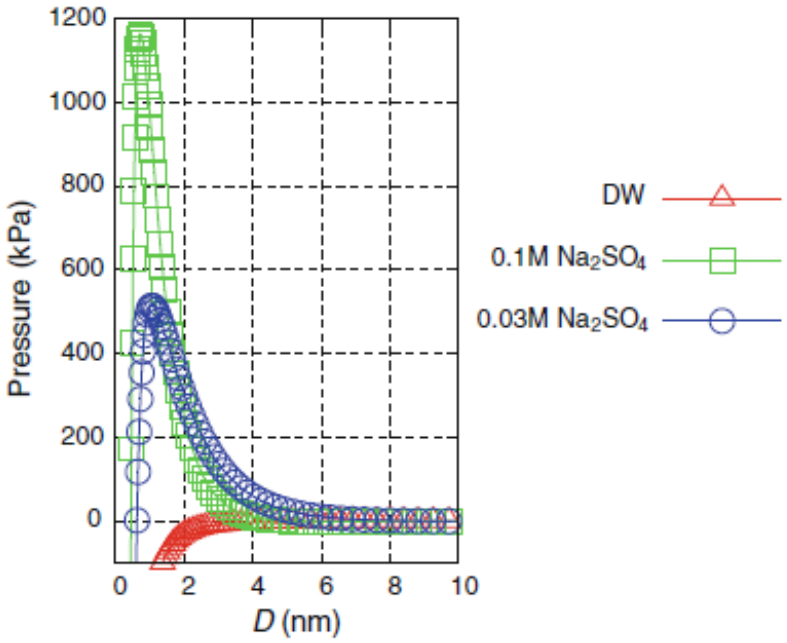



**Figure 2-6: Disjoining pressure as a function of double layer thickness for the solution compositions and conditions used in *Karoussi and Hamouda*, 2007 (reported in Figure 2-2c). After *Hiorth et al.,* (2010). Disjoining pressure is calculated using equation 2.1.**

Additionally, oil composition could play a major role in the rock/brine/oil interaction, and hence a wettability alteration. It is mostly agreed that fatty acids (e.g. carboxylic acids) adsorbs more on positively charged carbonate surfaces (e.g. *Morrow et al.*, 1973; *Anderson*, 1986a). On the other hand, basic surface groups can adsorb easily on the negatively charged clay surfaces (e.g. *Anderson*, 1986a; *Buckley et al.*, 1989) at reservoir conditions of temperature and salinity. Moreover, asphaltene content in the crude oil can play a big role in reversing the rock wettability from water-wet to oil-wet (*Wagner and Leach*, 1959). *Buckley and Morrow,* (1990) investigated the interaction between oil and brine of various NaCl composition (0.01 – 0.1M) using adhesion test on glass mica. They showed that removal of heavy asphaltene components results in no change in wettability and adhesion test no longer observed. Moreover, they argued that the adhesion test is a pH dependent, which above a characteristic value (around 5 to 7, depending on brine concentration) no adhesion was observed. However, no quantitative link has been observed between asphaltene and change in wettability. Some studies indicated that change in wettability is correlated with the amount of acid components in crude oil (e.g. *Buckley et al.*, 1989; *Standnes and Austad*, 2000).

Others claimed that none of these oil parameters is significant alone to alter the rock wettability. Rather, it is in combination of asphaltene precipitation, acid and base number and oil density that they can give a qualitative indication to an extent of which oil can alter the wettability (*Buckley and Liu*, 1998). The proposed possible mechanisms of oil/brine/rock interactions are as follows (*Buckley et al.*, 1998):

- *Polar interactions*, which is the main mechanism of asphaltene adsorption on the rock surface at the absence of initial water saturation. Measurements of surface forces between two mica surfaces interacted with crude oil, viscosity and interfacial tension measurements between oil and water indicated that this polar components adsorption (more likely high molecular weight polymeric or asphaltene component) plays a major role in the interaction of oil/brine/rock (*Christenson and Israelachvili*, 1987). However, this process is very slow.
- *Acid/Base interaction*, which becomes important in the presence of water phase where both rock surface and oil become electrically charged. Active polar surface groups in the mineral and oil can either donate or gain protons when immersed in water. The net electrical charge at both interfaces is pH and ionic strength dependent (e.g. *Buckley et al.*, 1989), which in turn affects the stability of the water film and hence wettability alteration process as discussed above.
- *Surface precipitation*, which indicates the ability of crude oil to act as a solvent. Some crude oils are good solvents for their asphaltene and, therefore, a poor wettability modifier of the rock surface. Poor solvent crude oils can enhance the wettability alteration (*Al-Maamari and Buckley*, 2003).
- *Ion binding/bridging*. This mechanism becomes important in brine rich in multivalent cation such as $Ca^{2+}$. Several binding interactions are proposed (oil-Ca-oil, oil-Ca-mineral or mineral-Ca-mineral). When $Ca^{2+}$ acts as a bridge between oil and mineral, it enhances the change in wettability towards more oil-wet (*Buckley et al.*, 1998).

## 2.6. Measurements of Wettability and Wettability Alteration

Wettability is widely defined as the ability of a fluid to adhere to the solid surface in the presence of another fluid (*Anderson*, 1986a). In petroleum systems, the reservoir rocks are classified as neutral, where the rock has similar affinity to oil and water, preferentially water-wet when the rock has higher affinity to water than oil or preferentially oil-wet when the rock has higher affinity to oil than water. If the reservoir rock has some areas wetted by water and other areas wetted by oil then it is called mixed-wet (*Sakuma et al.*, 2014).

There have been several methods reported in literature to measure and characterise wettability and wettability alteration in sandstone and carbonate (*Anderson*, 1986b). Each of these methods has advantages and disadvantages in measuring wettability in conditions similar to natural reservoirs. In this section, we summarize the most common methods used to quantify wettability and wettability alteration.

### 2.6.1. Contact Angle

Contact angle measurement is the most quantitative direct method to measure wettability in a specified pure surface either in a static or dynamic condition (*Anderson*, 1986b). Contact angle measurements basically defines how water interact with the rock surface in the presence of another fluid (e.g. oil), and it is defined at the point of interaction between the two fluids (e.g. oil and water). The main difficulties associated with this method include (i) long equilibration time, (ii) hysteresis effect between advancing (oil droplet pulled over a surface) and receding (oil droplet pushed back to surface) measurements (*Andersen et al.*, 1988), (iii) contamination effect (*Treiber and Owens*, 1972) and (iv) representation of rock heterogeneity (*Morrow*, 1975). Thus it might not be a good representative of porous media and natural conditions. Hysteresis effect can be as big as 60$^{o}$ (*Johnson and Dettre*, 1969). Surface roughness and heterogeneities present in the

porous media are reported to be the main causes for the hysteresis effect (*Johnson and Dettre*, 1969; *Adamson*, 1976).

Moreover, contact angle is used to characterise wettability alteration. Change in contact angle towards higher values indicates a change in wettability towards more oil-wet. Wettability alteration during SI and coreflood experiments from oil-wet to water-wet is indicated by the reduction in contact angle (e.g. *Yousef et al.*, 2011; *Mahani et al.*, 2015). These studies illustrated that switching to SW and diluted SW reduce the contact angle compared to FMB. The reduction could be as high as 17º (Figure 2-7; *Mahani et al.*, 2015). *Yousef et al.,* (2011) showed that significant reduction in contact angle can be achieved by further dilution of SW up to 20 times, which is correlated with substantial incremental oil recovery obtained during CSW (as illustrated in Figure 2-3c).

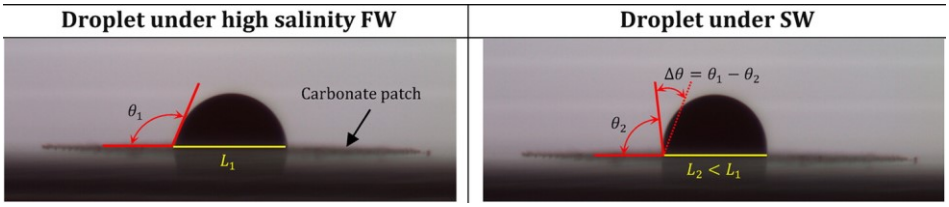



**Figure 2-7: Oil droplet contact angle alteration on limestone surface under formation brine (FMB) and seawater (SW). After *Mahani et al.,* (2015).**

### 2.6.2. Amott and USBM Tests

Amott (*Amott*, 1959) and US Bureau of Mines (USBM; *Donaldson et al.*, 1969) methods involve a full displacement cycle and highly depend on the capillary pressure and microscopic displacement efficiency. They have been mostly used to quantify wettability and wettability alteration based on SI and forced displacement of oil and water (e.g. *Jadhunandan and Morrow*, 1995; *Buckley et al.*, 1996; *Ma et al.*, 1999; *Morrow and Buckley*, 2011; *Gandomkar and Rahimpour*, 2015). Amott test uses the ratio of displacements by water and oil during SI to the total volume displaced during SI and forced displacement tests; and expresses them as displacement by water-ratio ($I_w$; equation 2.2) and displacement by oil-ratio ($I_o$; equation 2.3).

$$I_w = \frac{V_{wsp}}{V_{wt}} = \frac{S_{spw} - S_{cw}}{1 - S_{cw} - S_{or}} \tag{2.2}$$

$$I_o = \frac{V_{osp}}{V_{ot}} = \frac{S_{spo} - S_{or}}{1 - S_{cw} - S_{or}}, \tag{2.3}$$

where $V_{wsp}$ and $V_{osp}$ are the volumes of water and oil spontaneously imbibed, $V_{wt}$ and $V_{ot}$ are the total volumes of water and oil produced by both spontaneous imbibition and waterflooding. $S_{spw}$ is the water saturation after the imbibition process, $S_{spo}$ is the oil saturation after the imbibition process, $S_{cw}$ is the connate water saturation and $S_{or}$ is the residual oil saturation after waterflooding. Strongest oil-wet cases have $I_w = 0$ and $I_o = 1$, neutral wetting systems have the same affinity to water and oil with $I_w = I_o = 0$. Strongest water-wet case has $I_o = 0$ and $I_w = 1$.

The USBM method uses the ratio of areas under the drainage (oil displacing water; $A_{ow}$) and imbibition (water displacing oil; $A_{wo}$) capillary curves (equation 2.4; *Donaldson et al.*, 1969). These areas represent the degree of wettability; i.e. strongly water-wet system has lower $A_{wo}$ and higher $A_{ow}$ and *vice versa*. Thus $I_u$ is increasing towards more positive as water-wetness increases

$$I_u = \log \frac{A_{ow}}{A_{wo}} \tag{2.4}$$

The advantage of the Amott and USBM tests over contact angle measurements are their ability to capture the surface roughness and heterogeneity. However, the main limitation for Amott method is its insensitivity near a neutral wetting state (i.e. contact angle 60 – 120; *Morrow and McCaffery*, 1978; *Ma et al.*, 1999). At this state, neither fluid will spontaneously imbibe and displace the other in significant quantities. In this case, USBM method can help ($I_u$=0); however, it cannot cover a wide range of wettability.

Recent work of *Gandomkar and Rahimpour,* (2015) investigated the relationship between Amott-Harvey wettability index ($I_{w\text{-}o} = I_w - I_o$) and oil recovery for different brine compositions in secondary mode injection. They found that as the wettability alters from oil-wet ($I_{w\text{-}o} \rightarrow -1$) to neutral-wet ($I_{w\text{-}o} = 0$) conditions the

oil recovery increases, reaching a maximum value near a neutral-wet system and then decreases as the wettability decreases to water-wet ($I_{w\text{-}o} \rightarrow 1$; Figure 2-8). They related the decrease in oil recovery in strongly water-wet cases to the snap-off effect. During the transition from neutral-wet to water-wet conditions, the water film thickness increases and water layers become more connected in larger pores, causing some oil to be trapped in narrower pore throats behind the water front.

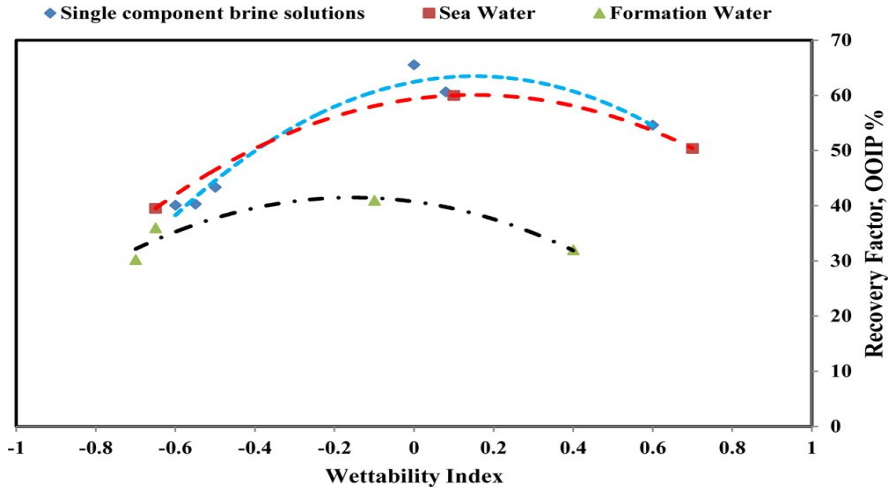



**Figure 2-8: Relationship between wettability index and total oil recovery for formation brine (FMB), seawater (SW) and single-components brine solutions in secondary mode. After *Gandomkar and Rahimpour,* (2015). Single components solutions include NaCl, KCl, $MgSO_4$, $MgCl_2$, $CaCl_2$ and $Na_2SO_4$.**

### 2.6.3. Spontaneous Imbibition (SI) Rate

The spontaneous imbibition (SI) rate has been used in many studies to assess qualitatively wettability and characterise wettability alteration in reservoir core samples (e.g. *Morrow et al.*, 1994; *Ma et al.*, 1999; *Morrow and Buckley*, 2011; *Gandomkar and Rahimpour*, 2015). The SI test indicates the ability of wetting phase to displace non-wetting phase and highly dependent on the capillary pressure. Water can easily imbibe into water-wet core sample as a result of positive capillary pressure. In oil-wet systems, negative capillary pressure prevents water from spontaneously imbibe into the core sample (e.g. *Jadhunandan and Morrow*, 1995). *Morrow et al.,* (1994) showed the effect of aging on the SI time. They demonstrated a decrease trend in SI rate as the aging time increases of two sets of crude oils in Berea sandstone cores. They used scaled rate (dimensionless

time) that account for fluid and rock properties to measure the rate of change in wettability. Dimensionless time is expressed as (equation 2.5):

$$t_D = 1.8849\text{x}10^{-2} t \sqrt{\frac{k}{\phi}} \frac{\sigma}{\mu_w} \frac{1}{L_c^2}, \qquad (2.5)$$

where $t_D$ is dimensionless time, $t$ is imbibition time (minutes), $k$ is the core permeability (mD), $\phi$ is fractional porosity, $\sigma$ is interfacial tension (dynes/cm), $\mu_w$ is brine viscosity (cP) and $L_c$ is a characteristic length (cm).

*Morrow and Buckley,* (2011) assessed the relationship between oil recovery during HSW and LSW, and scaled rate of imbibition ($t_D$). They illustrated that the extent of imbibition increases significantly in low salinity brine compared to high and medium salinity brines (Figure 2-9), indicating a significant improvement on microscopic displacement efficiency.

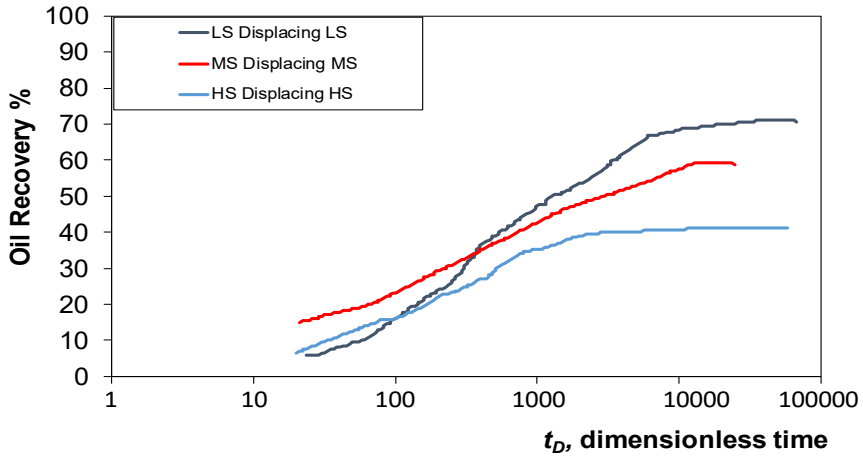



**Figure 2-9: Oil recovery vs. scaled imbibition rate ($t_D$) for three imbibing fluids (low, medium and high salinity). After *Morrow and Buckley,* (2011). Connate and imbibed water have identical ionic concentrations.**

### 2.6.4. Zeta Potential Measurements

Zeta potential is used as a measure of the electrostatic forces between the mineral-brine and oil-brine interfaces, which have been argued to have a major control on the interaction of crude oil/rock/brine, hence wettability (*Buckley and Morrow*, 1990; *Hirasaki*, 1991). Several studies have used zeta potential measurements to explain wettability alteration and oil recovery measurements

(e.g. *Hirasaki and Zhang*, 2004; *Strand et al.*, 2006; *Zhang and Austad*, 2006; *Zhang et al.*, 2007; *Hiorth et al.*, 2010; *Alotaibi and Nasr-El-Din*, 2011; *Alotaibi et al.*, 2011a; *Yousef et al.*, 2012a). However, these measurements were obtained separately and not during corefloods or SI experiments. Moreover, these studies used zeta potential measurements on powdered samples suspended in low salinity brines to explain oil recovery from SI or coreflooding tests on intact rocks where brine and oil present in the pore space.

The relationship between zeta potential and wettability has been given more attention by Jackson and co-workers (e.g. *Jackson and Vinogradov*, 2012; *Alroudhan*, 2015). These authors addressed this relationship using the SPM on intact carbonate core sample saturated in brines relevant to natural condition. *Jackson and Vinogradov,* (2012) found that mixed-wet (aged) sample yields zero zeta potential within experimental error compared to (non-aged) sample (Figure 2-10a). They argued that aging causes some areas of the mineral surfaces to become oil-wet; large pores are wetted by oil after drainage (Figure 2-10b) whilst small pores are not invaded by oil, and remain water-wet (Figure 2-10c).

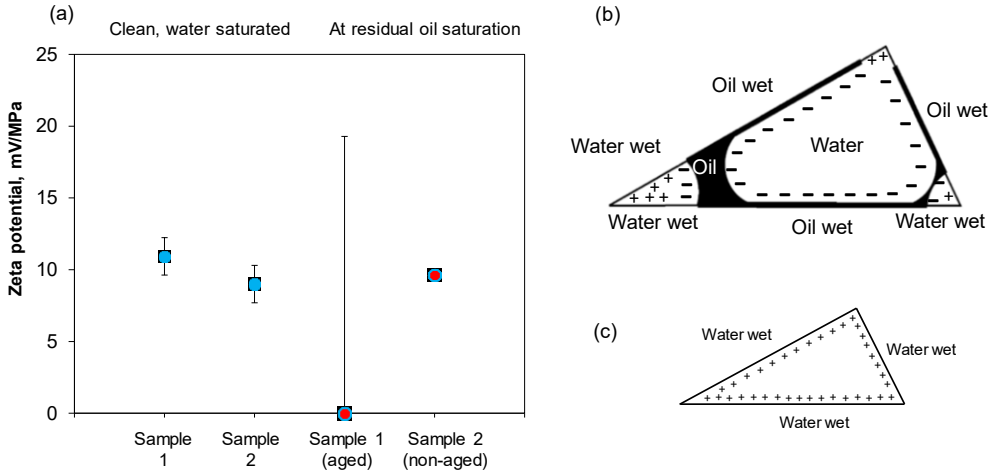



**Figure 2-10: Zeta potential measurements and wettability alteration at mineral surfaces after aging in formation brine (FMB) and oil proposed by *Jackson and Vinogradov,* (2012). (a) shows zeta potential for each sample, saturated with FMB brine (left), and saturated with FMB brine and residual oil (right). (b-c) show schematics of wettability alteration in carbonate sample saturated with FMB after aging and brine injection to the residual oil saturation. (b) Large pores are occupied by oil after primary drainage. (c) Small pores are not invaded by oil during primary drainage, and remain water-wet. After *Jackson and Vinogradov,* (2012).**

## 2.7. Summary

As a summary, the CSE was observed on initially mixed- or oil-wet chalk/carbonates when brines contain controlled salinity or compositions was used in SI or corefloods experiments. Experimental evidence showed that this can be successfully achieved by either lowering the ionic strength or increasing the concentration of PDIs in the imbibing/flooding brine. However, different conditions have been applied in each experiment, such as formation brine composition, crude oil properties, injection procedure and temperature. Thus results cannot be directly compared. Consequently, the underlying mechanisms responsible for improved oil recovery during CSW are still actively debated.

There are different methods to quantify wettability and wettability alteration during CSW in carbonates, including contact angle, Amott and USBM tests and zeta potential measurements. The last is highly affected by oil and brine compositions and can be obtained at conditions relevant to natural systems. Moreover, it could be used to quantify the wetting state of core samples (which are demonstrated in chapter 6), and determine optimum brine composition that lead to improved oil recovery from carbonate rocks during CSW (which are demonstrated in chapter 7).

Controls on surface charge and zeta potential of carbonates need to be fully addressed and examined at conditions relevant to natural systems in order to appropriately link between brine composition, wettability and oi recovery during CSW experiments. This is extensively discussed in the following chapter.

# Chapter 3.

# Zeta Potential of Artificial and Natural Calcite in Aqueous Solutions - Overview

## 3.1. Introduction

The properties of the calcite mineral surface and the interface between calcite and aqueous solution are of broad interest in many areas of science and engineering. Calcite is a common mineral, comprising approximately 4% of the Earth's crust, and surface reactions on calcite play an important role in many geochemical and environmental systems, as well as many areas of industry, including the manufacture of paper and cement (e.g. *Bapat*, 2012), the geologic storage of nuclear waste and $CO_2$ (e.g. *Hester and Harrison*, 2010), and the production of oil and gas (e.g. *Buckley et al.*, 1998; *Yousef et al.*, 2011; *Gomari et al.*, 2006; *Zhang and Austad*, 2006). However, despite the broad range of interest and applications, controls on calcite surface charge in aqueous solution, especially at conditions relevant to natural systems, have lagged behind because of the difficulties in probing such conditions in laboratories. Numerous papers have reported inconsistent or contradictory data and models, and there is still active debate over the relationship between calcite surface charge and electrolyte pH, the concentration of ions such as $Ca^{2+}$, $Mg^{2+}$, $CO_3^{2-}$ and $SO_4^{2-}$ in aqueous solution, the partial pressure of $CO_2$, the difference between natural and artificial calcite, and the role of dissolution and/or precipitation.

The focus of this chapter is the zeta potential of artificial and natural calcite in aqueous solution. The zeta potential is an important measure of the electrical potential at the mineral surface, and the magnitude and sign of the zeta potential

control the electrostatic interactions between the mineral surface and polar species in aqueous solution, between the mineral surface and other charged interfaces such as the water-air and water-oil interfaces (as shown in chapter 2), and between mineral particles in suspension including flocculation and dispersion. Measurements of zeta potential in low concentration solutions and at laboratory conditions are relatively straightforward, and most studies of the calcite mineral surface have reported measurements of zeta potential or the closely related property of electrophoretic mobility. Other approaches to determine surface charge, such as potentiometric titration, are challenging to apply in calcite because rapid dissolution kinetics and the buffering effect of carbonate ions in solution can affect the results. Thus the primary data source to understand calcite surface charge comprises measurements of zeta potential.

The aims of this chapter are twofold: (i) to collate and review previous measurements of zeta potential on natural and artificial calcite and carbonate as a resource for this thesis and future studies, (ii) to compare and contrast the results of these studies to determine key controls on zeta potential and where uncertainties remain.

## 3.2. Zeta Potential and the Electrical Double Layer

### 3.2.1. The Electrical Double Layer

The immersion of a calcite mineral in aqueous solution leads to a separation of electrical charge at the mineral-solution interface. An excess of charge at the mineral surface is balanced by a region of equal but opposite charge in the adjacent solution, in an arrangement often termed the electrical double layer (EDL; e.g. *Glover and Jackson*, 2010, *Glover*, 2015; see Figure 3-1). The charge at the mineral surface is balanced by a relative decrease in the concentration of co-ions (i.e. ions with the same charge as the surface) and increase in the concentration of counter-ions (i.e. ions with the opposite charge as the surface) in the adjacent solution. The region immediately adjacent to the mineral surface is typically termed

the Stern layer, and contains ions that are attached to the mineral surface; the Stern layer may be further divided into the inner and outer Helmoltz layers, defined by the inner and outer Helmoltz planes (the IHP and OHP shown in Figure 3-1a; note the inner and outer Helmholtz layers and associated planes are also sometimes termed the inner and outer Stern layers and planes). The IHP defines the location of ions that closely approach the mineral surface and are attached to surface sites (Figure 3-1a). The OHP defines the location of larger, typically hydrated ions that cannot enter the inner Helmholtz plane but which are nevertheless attached to the mineral surface (*Bard et al.*, 1980).

In most cases, the charge in the Stern layer does not exactly balance the surface charge, giving rise to a 'diffuse' or 'Gouy-Chapman' layer that contains the remaining excess charge in the solution required to ensure electrical neutrality of the EDL (e.g. *Kruyt and Overbeek*, 1960). The difference between the Stern and diffuse layers is that the co- and counter-ions in the diffuse layer are not attached to the mineral surface. At low ionic strength ($\lesssim 0.1\mathrm{M}$), the ion concentration in the diffuse layer decreases exponentially with distance from the OHP (Figure 3-1a). The electrical potential corresponding to the charge distribution within the EDL decreases linearly with distance from the mineral surface through the Stern layer, although there may be a difference in gradient between the inner and outer Helmholtz layers, and exponentially with distance from the OHP through the diffuse layer, falling to zero in the uncharged solution (Figure 3-1b).

### 3.2.2. Electrokinetic Phenomena

Electrokinetic phenomena arise when there is a relative motion between the excess charge in the diffuse layer of the EDL and the charged surface (*Hunter*, 1981). It is typically assumed that the excess charge in the diffuse layer is mobile only beyond a plane termed the 'shear' or 'slip' plane that lies a small distance away from the OHP (Figure 3-1).

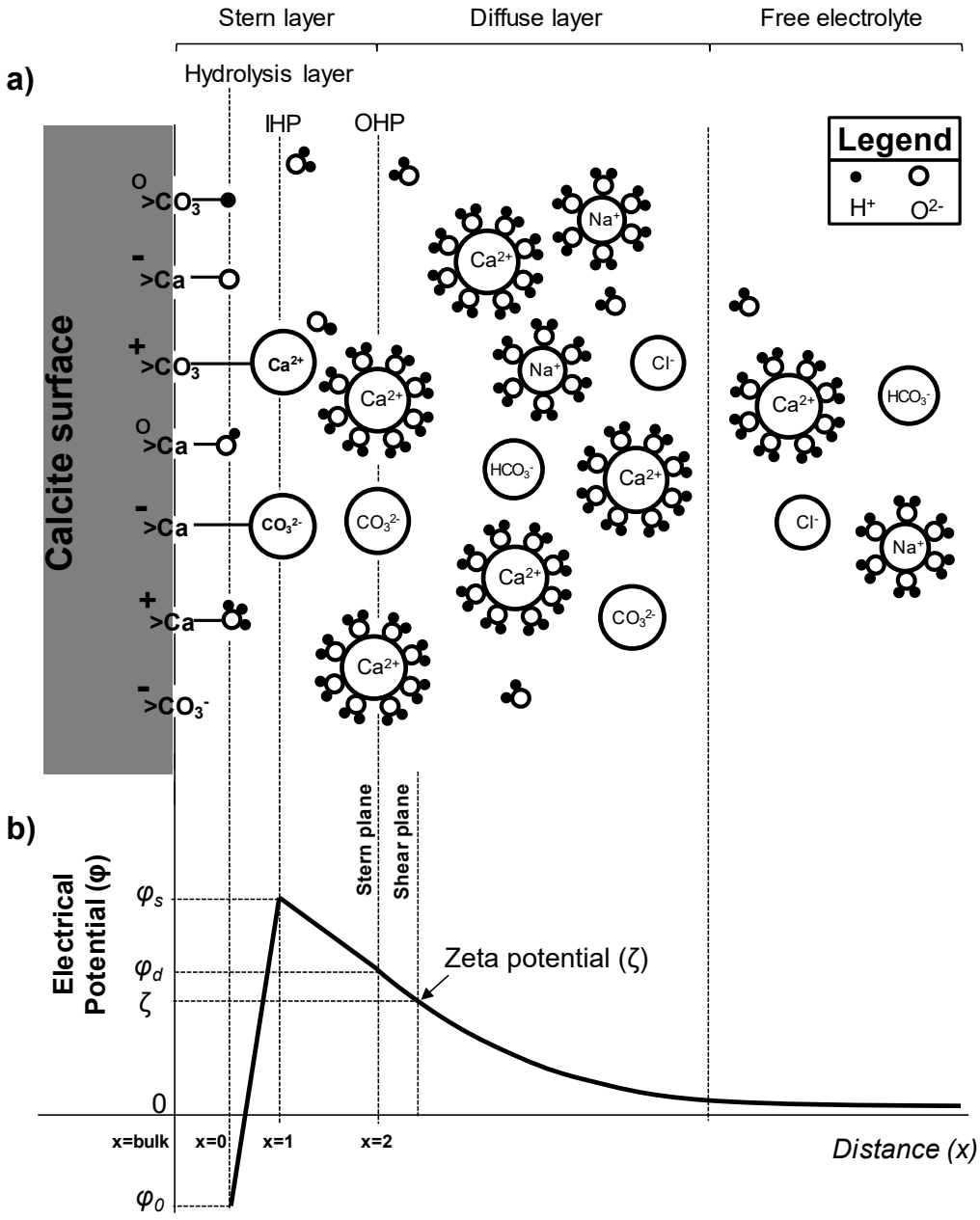



**Figure 3-1: Schematic representation of (a) the electrical double layer at the calcite-water interface and (b) the variation in the electrical potential with distance from the mineral surface. The surface speciation sites (>$CO_3H^0$, >$CaO^-$, >$CO_3Ca^+$, >$CaOH^0$, >$CaCO_3^-$, $CaOH_2^+$ and >$CO_3^-$) are from *Pokrovsky and Schott,* (2002). The Stern layer is described by three planes. The 0-plane (x=0) corresponds to the hydrolysis layer where H and OH are chemi-bonded to the bulk ions (*Stipp*, 1999). The 1-plane (x=1) denotes inner-sphere complexes and corresponds to the inner Helmholtz plane (IHP), while the 2-plane (x=2) denotes outer-sphere complexes and corresponds to the outer Helmholtz plane (OHP; *Wolthers et al.*, 2008). In (b) the mineral surface is negatively charged, consistent with the surface complexation model of *Heberling et al.,* (2011), but the zeta potential is positive because of adsorption of the lattice PDIs $Ca^{2+}$ and $CO_3^{2-}$.**

The zeta potential is the electrical potential at the shear plane. In some models of the EDL, it is assumed that the shear plane and the OHP are identical, in which case the zeta potential also represents the electrical potential at the OHP. Methods to determine the zeta potential make use of electrokinetic phenomena, most typically (1) electrophoresis, which is the mobilisation of charged particles, relative to a stationary solution, under the influence of an applied electrical field, and (2) streaming potential, which is the potential difference that arises when a solution is moved relative to a stationary solid under the influence of an applied pressure gradient (*Delgado et al.*, 2007).

#### 3.2.2.1 Electrophoretic Mobility Method

The electrophoretic method (termed here EPM) used to determine zeta potential is conducted on powdered samples suspended in the solution of interest. An electrical field $E$ is applied across the suspension and the resulting velocity $\boldsymbol{v}_e$ of the charged particles is measured with respect to the solution. The velocity is then normalized by the electrical field to yield the electrophoretic mobility $u_e$, which is typically treated as an isotropic quantity that can be related to the zeta potential by the Helmholtz-Smoluchowski equation for electrophoresis (*Delgado et al.*, 2007)

$$u_e = \frac{\varepsilon\zeta}{\mu}, \tag{3.1}$$

where $\varepsilon$ is the permittivity ($F \cdot m^{-1}$) and $\mu$ the viscosity ($Pa \cdot s$) of the solution. The zeta potential obtained using the EPM is an effective value across all the suspended particles; the zeta potential of individual particles (and, indeed, between the different faces of a given particle) may differ from the single value interpreted from EPM measurements.

Most previous studies (see below in section 3.4) used the EPM to interpret the zeta potential of calcite and natural carbonates using commercial zetameter instruments. These instruments require powdered samples to operate and have salinity and temperature limitations. It can be challenging to maintain stable

measurements using such instruments at the high ionic strength and at elevated temperatures typical of natural hydrocarbon systems (Strand et al., 2006, Zhang et al., 2007). Thus the EPM measurements may not reflect the natural conditions of interest for several reasons. First, crushed (powdered) samples may create 'fresh' mineral surface sites and hence increase the number of surface site available for adsorption/desorption; allowing more multivalent ions to be adsorbed and therefore increase the surface charge dramatically. Moreover, destroying the rock texture by crushing samples may affect the position of the shear plane; making it closer to the surface, which may result in higher zeta potential magnitudes (*Vernhet et al.*, 1994) compared to natural porous (uncrushed) medium. Second, the EPM requires a large volume of electrolyte versus solid phase compared to natural porous medium where the volumetric ratio of electrolyte to solid is much lower (e.g. when using intact core samples), which may be important in systems such as carbonates where dissolution and precipitation and/or adsorption and desorption may simultaneously modify the surface charge (Thompson and Pownall, 1989; Pierre et al., 1990). Third, the EPM is limited to the presence of only two phases (i.e. solid-liquid or liquid-liquid); hence it can not be used to represent the multiphase measurements when both non-aqueous phase liquids (NAPLs; e.g. oil) and electrolyte are present within the pore-space, as is often the case in subsurface hydrocarbon carbonate settings.

#### 3.2.2.2 Streaming Potential Method

The streaming potential method (termed here SPM) used to determine zeta potential is conducted using intact samples of porous materials, packed beds of particles, or surfaces through, or across, which the solution of interest is caused to flow. A pressure difference $\Delta P$ is applied across the sample and the resulting electrical potential difference $\Delta V$ is measured. For instance, in a water-wet surface, water reacts with the mineral surface, leaving an excess of negative charge on the mineral surface and an excess of positive charge in the adjacent water. This creates a separation in charge (in the diffuse layer of the EDL; Figure 3-2) at the

mineral-surface interface. If the fluid is subjected to a pressure gradient, causing it to move relative to the negatively charged mineral surface, some of the excess positive mobile charges in the diffuse layer of the EDL are transported with the flow (Figure 3-2). The net excess of these positive charges moving with the flow (denoted in Figure 3-2 by the length of the arrows) gives rise to an electrical convection, or so-called streaming, current. Under steady state conditions, this streaming current $I_s$ is globally balanced by an opposing conduction current $I_c$ to maintain electrical neutrality, so the total current in the sample is zero across any cross-section perpendicular to the induced pressure gradient. This conduction current is driven by an electrical potential, called the streaming potential (Figure 3-2).

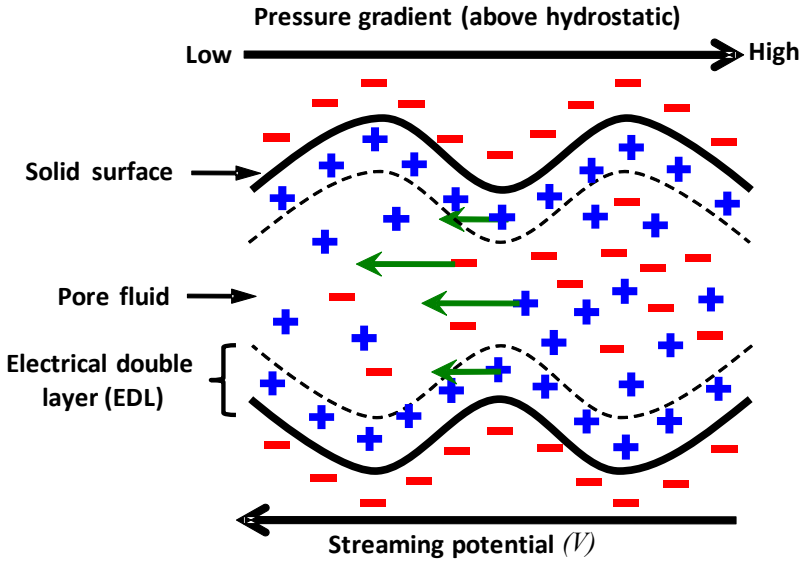



**Figure 3-2: The theory of streaming potential. A schematic showing a separation of charge in the electrical double layer (EDL) occurs due to a pressure gradient and at equilibrium streaming potential arises to maintain electrical neutrality. Adapted from *Jackson et al.,* (2012).**

The potential difference is then normalized by the pressure difference to yield the streaming potential coupling coefficient $C_{sp}$, which is typically treated as an isotropic quantity that relates the fluid pressure $\nabla P$ and streaming potential $\nabla V$ gradients when the total current density $j$ is zero,

$$\nabla V = C_{sp} \nabla P|_{j=0}. \tag{3.2}$$

The sign and magnitude of the streaming potential coupling coefficient $C_{sp}$ depends on several parameters: the electrical conductivity of the fluid $\sigma_f$, the surface conductivity $\sigma_s$, the fluid permittivity $\varepsilon$, the fluid dynamic viscosity $\mu$, and the zeta potential $\zeta$.

In order to develop an analytical relation between the various electrical properties in the case of a capillary; we start by considering the fluid velocity in a capillary, which is governed by Poiseuille's equation

$$v(z) = \frac{1}{4\mu}(r^2 - y^2)\frac{\Delta P}{L_c}, \tag{3.3}$$

where $v(z)$ is the velocity of the liquid (m s$^{-1}$), $\Delta P$ is the pressure drop (Pa) across the capillary measured over a tortuous path the fluid is taking through the medium $L_c$ (m) where $r$ is the capillary radius (m), and $y$ is the distance from the capillary wall at which the velocity is calculated (m), and using an incompressible fluid of viscosity $\mu$ (Pa s).

The streaming current is the flow rate multiplied by the charge density integrated over the capillary area, given by

$$I_s = \int_0^r 2\pi y \, v_z(y)\rho(y)dy. \tag{3.4}$$

This integration results in the total streaming current for all concentric shells of fluid within the capillary and is given by (*for detailed derivations see Appendix A*)

$$I_s = -\frac{\pi\varepsilon\zeta r^2}{\mu}\frac{\Delta P}{L_c}. \tag{3.5}$$

The opposing conduction current $I_c$ is derived from Ohm's law, and accounts for conductivities contribution from both the bulk conduction through the electrolyte occupying the capillary and surface conduction through the electrical double layer, gives

$$I_c = \sigma_f \frac{\pi r^2}{t}\frac{\Delta V}{L} + \sigma_s \frac{2\pi r}{t}\frac{\Delta V}{L};\ t = \frac{L_c}{L} \tag{3.6}$$

$$I_c = \pi r^2 \frac{\Delta V}{L_c}\left(\sigma_f + \frac{2\sigma_s}{r}\right), \tag{3.7}$$

where *t* is the tortuousity, which defines the straightness of the flow path and is the ratio of the actual tortuous path $L_c$ to the straight length of the capillary $L$, $\sigma_f$ is the electrical conductivity of the solution of interest ($S \cdot m^{-1}$) and $\sigma_s$ is the surface electrical conductivity ($S \cdot m^{-1}$).

At steady-state and electrical isolation conditions, the streaming current $I_s$ is balanced by the conduction current $I_c$. This assumes that both currents take the same 1-D path along the capillary; i.e. the flowing ions (or charges) and the opposing voltage take the same tortuous path. So, equation (3.2) can be used to determine the streaming potential coupling coefficient with $\nabla P$ and $\nabla V$ replaced by the stabilized $\Delta P$ and $\Delta V$. Equating both currents gives

$$I_c = -I_s = \pi r^2 \frac{\Delta V}{L_c}(\sigma_f + \frac{2\sigma_s}{r}) = \frac{\pi r^2}{\mu}\frac{\Delta P}{L_c}\varepsilon\zeta \tag{3.8}$$

$$\frac{\Delta V}{\Delta P} = C_{sp} = \frac{\varepsilon\zeta}{\mu(\sigma_f + \frac{2\sigma_s}{r})}. \tag{3.9}$$

The use of equation (3.9) to interpret the zeta potential in a porous medium has serval assumptions. First, this equation has been derived for a laminar flow through a single capillary tube where the excess charge and potential distribution (given be Poisson-Boltzman equation; see Appendix A) is considered at a planar interface in 1-D and is assumed to be reasonable at a curved interface when the local radius of curvature *r* is large compared to the double layer thickness $\kappa^{-1}$, i.e.

$$\kappa r \gg 1, \tag{3.10}$$

where $\kappa$ is the inverse Debye length which is a measure of the diffuse layer thickness ($nm^{-1}$). The Debye length is the distance from the surface at which the potential has decreased by a factor of the natural logarithm ‘‘e’’ (2.98).

Second, the assumption of using the SPM approach in a porous medium is that the pore sizes are much larger than the width of the diffuse layer, which may not always be the case in carbonates. The width of the diffuse layer is typically on the scale of a few nanometers (around 1-50 nm; *Hunter*, 1981); it is directly

proportional to the square root of the ionic strength and inversely proportional to the square root of temperature (see equation 2.12). For carbonates rocks with pore sizes in the range of 100 microns to a fraction of a micron (*Nurmi and Standen*, 1997), equation (3.9) can be assumed to be valid especially at high salinity when the EDL is thin (i.e. $\kappa^{-1} \ll r$). However, for carbonate rocks with pore sizes in the range of 10-100nm, it is highly questionable that equation (3.9) is valid.

Third, the streaming potential can indicate the average surface potential in a porous medium and is influenced by the pore size distribution. Therefore, the interpreted zeta potential is an average value and this can be significant when porous rocks of mixed mineralogy are used. The true zeta potential might be different from the interpreted value using the SPM but the two values should show similar trends when changes are made to the system (e.g. increasing temperature or introducing oil phase).

In brine-saturated rock samples, the streaming potential coupling coefficient is expressed in terms of the solution electrical conductivity $\sigma_f$, the apparent formation factor ($F_a$; i.e. at each salinity) and the intrinsic formation factor ($F_0$).

$$F_0 = \frac{\sigma_f}{\sigma_{rf}^{\sigma_s=0}} = \frac{\sigma_f}{\sigma_f \frac{\pi r^2}{At}}$$

$$F_a = \frac{\sigma_f}{\sigma_{rf}^{\sigma_s \neq 0}} = \frac{\sigma_f}{\sigma_f \frac{\pi r^2}{At} + \sigma_s \frac{2\pi r}{At}} \tag{3.11}$$

$$\sigma_f \frac{F_0}{F_a} = \sigma_f \frac{\sigma_f \frac{\pi r^2}{At} + \sigma_s \frac{2\pi r}{At}}{\sigma_f \frac{\pi r^2}{At}} = \sigma_f \left(1 + \frac{2\sigma_s}{r\sigma_f}\right) = (\sigma_f + \frac{2\sigma_s}{r})$$

$$C_{sp} = \frac{\varepsilon \zeta}{\mu \sigma_f \frac{F_0}{F_a}}, \tag{3.12}$$

where $\sigma_{rf}^{\sigma_s=0}$ is the saturated rock electrical conductivity with a concentrated solution with high electrical conductivity (i.e. the surface electrical conductivity is negligible; S m$^{-1}$), $\sigma_{rf}^{\sigma_s \neq 0}$ is the saturated rock electrical conductivity of the system saturated with the solution at salinity of interest (S m$^{-1}$), $F_a$ is the so-called apparent

formation factor (dimensionless) which is defined as the ratio of the fluid conductivity $\sigma_f$ to the system conductivity $\sigma_{rf}$ at salinity of interest and $F_0$ is the so-called intrinsic formation factor (dimensionless) which is defined as the ratio of the fluid conductivity $\sigma_f$ to the system conductivity $\sigma_{rf}$ when surface electrical conductivity is negligible. The intrinsic formation factor (an intrinsic property of the rock texture) is typically measured on the system saturated with a concentrated solution with high electrical conductivity (typically at $\sigma_f$ >0.4 S m$^{-1}$; e.g. *Jouniaux and Pozzi*, 1995; *Jaafar et al.*, 2009; *Vinogradov et al.*, 2010; see below chapter 4, section 4.2.4).

Also, equation (3.12) can be expressed in terms of the saturated rock conductivity $\sigma_{rf}$ and only the intrinsic formation factor $F_0$ (e.g. *Jaafar et al.*, 2009; *Vinogradov et al.*, 2010; *Alroudhan et al.*, 2016)

$$C_{sp} = \frac{\varepsilon\zeta}{\mu\sigma_{rf}F_0}. \tag{3.13}$$

When streaming potential measurements are obtained in porous media where surface conductivity is negligible, $F_a$ and $F_0$ are the same and the streaming potential coupling coefficient $C_{sp}$ can be related to the zeta potential by the Helmholtz-Smoluchowski equation for streaming potential (e.g. *Overbeek*, 1952; *Dukhin and Deriaguine*, 1974; *Hunter*, 1981)

$$C_{sp} = \frac{\varepsilon\zeta}{\sigma_f\mu}. \tag{3.14}$$

Equation (3.14) can be used in oil-brine-saturated rock samples when the surface conductivity is dramatically reduced. This is because oils conduct electricity minimally under normal conditions. Therefore, the contribution of the surface conductivity can be neglected compared to the bulk conductivity and the Helmholtz-Smoluchowski equation (eq. 3.14) can be valid in such conditions.

*(Detailed analysis of the interpretation of zeta potential from the SPM in the investigated carbonate samples in this thesis at different conditions can be found in the methodology sections of chapters 4, 5 and 6).*

## 3.3. Development of Surface Charge on Calcite in Aqueous Solution

### 3.3.1. Effect of pH

The development of surface charge on calcite in aqueous solution is complex because of the difficulties in separating dissolution from desorption and precipitation from adsorption on the mineral surface (*Stipp*, 1999; *Van Cappellen et al.*, 1993; *Wolthers et al.*, 2008). The surface charge of calcite appears to be affected by various variables (pH, $[Me^{2+}]$ and $pCO_2$; where $Me^{2+}$ denotes divalent metal ions such as $Ca^{2+}$ and $Mg^{2+}$), which they, in turn, control calcite dissolution (see below) (*Brady and House*, 1996). There are key differences between the charge development in metal oxides and calcite.

In most metal oxides, charge development occurs when mineral surfaces sites are hydrated to form amphoteric groups >MeOH (where Me denotes a metal ion and > denotes the crystal lattice) and these react either with $H^+$ or $OH^-$ ions according to (e.g. *Schindler and Stumm*, 1987; *Stumm et al.*, 1987)

$$>MeOH^0 + OH^- \Leftrightarrow >MeO^- + H_2O \quad (3.15)$$

$$>MeOH^0 + H^+ \Leftrightarrow >MeOH_2^+ \quad (3.16)$$

The relative abundance of negatively and positively charged surface sites depends on the relative concentration of $H^+$ and $OH^-$ in solution; these ions behave as 'potential determining ions' (PDIs) for the surface. Consequently, the net surface charge depends on the solution pH. It is therefore common to see surface charge and/or zeta potential plotted as a function of pH, with the surface charge and/or zeta potential becoming more negative as the pH increases and the deprotonation reaction (3.15) is favoured, and more positive as the pH decreases and the protonation reaction (3.16) is favoured (e.g. *Hohl et al.*, 1980; *Davis and Kent*, 1990). When the number of positively and negatively charged surface sites exactly balances, a surface charge of zero is observed and the corresponding pH is termed the 'point of zero charge' (PZC). A zeta potential of zero may also be observed and the corresponding pH is termed the 'iso-electric-point' (IEP) (e.g.

*Hunter*, 1981). The IEP and PZC may not coincide, for reasons discussed in more detail in the next section.

The surface of calcite differs from the metal oxides in several important respects. First, the mineral is soluble in aqueous solution and the lattice ions $Ca^{2+}$ and $CO_3^{2-}$ can be released into solution or deposited on the surface depending upon the solution pH (*Stumm*, 1992; *Somasundaran*, 2006). Second, atmospheric $CO_2$ in open system experiments can dissolve into solution, affecting the pH and the equilibrium concentrations of $Ca^{2+}$, $CO_3^{2-}$ and $HCO_3^-$ (e.g. *Eriksson et al.*, 2007). Third, the hydrated calcite surface contains protonated anion surface sites $>CO_3H^0$ as well as hydroxylated cation sites $>CaOH^0$ (e.g. *Pokrovsky and Schott*, 2002; *Van Cappellen et al.*, 1993). Evidence to support the presence of these sites has been provided by X-ray photoelectron spectroscopic (XPS) and infrared (IR) spectroscopic measurements (*Pokrovsky et al.*, 2000; *Stipp et al.*, 1994; *Stipp and Hochella*, 1991). The protonation and deprotonation reactions at these surface sites, and therefore the relative abundance of positively and negatively charged sites on the mineral surface, is pH dependent according to the following reactions (e.g. *Heberling et al.*, 2011; *Pokrovsky and Schott*, 2002; *Van Cappellen et al.*, 1993)

$$>CaOH^0 + OH^- \Leftrightarrow >CaO^- + H_2O \quad (3.17)$$

$$>CO_3H^0 + OH^- \Leftrightarrow >CO_3^- + H_2O \quad (3.18)$$

$$>CaOH^0 + H^+ \Leftrightarrow >CaOH_2^+ \quad (3.19)$$

Thus it would be expected that the surface charge, and hence the zeta potential, of calcite in aqueous solution are both determined by the pH, with $H^+$ and $OH^-$ behaving as the PDIs. Numerous studies have determined the variation in zeta potential with pH for a variety of calcite types and solution compositions (e.g. Figure 3-3 and Figure 3-4).

However, this analysis ignores the contribution of the lattice ions $Ca^{2+}$, $CO_3^{2-}$ in solution. Several experimental studies have shown that the zeta potential of calcite is independent of pH if the concentration of calcium (expressed in this paper as pCa, where p represents the negative logarithm; higher pCa corresponds to

lower $Ca^{2+}$ concentration and *vice versa*) is kept constant (e.g. *Foxall et al.*, 1979; *Cicerone et al.*, 1992; *Sondi et al.*, 2009; see Figure 3-5). Moreover, other studies have demonstrated a relationship between zeta potential and pCa (e.g. *Thompson and Pownall*, 1989; *Pierre et al.*, 1990; *Cicerone et al.*, 1992; *Alroudhan et al.*, 2016; see Figure 3-6 and Figure 3-7), and a strong dependence between the zeta potential of calcite and the excess of $Ca^{2+}$ ions at the mineral surface has been observed (*Huang et al.*, 1991). These data show that the development of charge on the calcite surface is more complex than the simple protonation and deprotonation reactions that occur at the surface sites of metal oxides (e.g. *Stipp*, 1999). Instead, the lattice ions $Ca^{2+}$ and $CO_3^{2-}$ adsorb onto the mineral surfaces through surface complexation reactions such as (e.g. *Van Cappellen et al.*, 1993; *Stipp*, 1999; *Wolthers et al.*, 2008; *Heberling et al.*, 2011)

$$>CO_3H^0 + Ca^{2+} \Leftrightarrow >CO_3Ca^+ + H^+ \quad (3.20)$$

and, in the presence of $CO_2$, reactions such as

$$>CaOH^0 + CO_2 \Leftrightarrow >CaCO_3^- + H^+ \quad (3.21)$$

$$>CaOH^0 + CO_2 \Leftrightarrow >CaHCO_3^0 \quad (3.22)$$

As discussed below, the concentration dependent adsorption of these lattice ions (and other potential determining ions) is the primary control on the zeta potential of calcite.

### 3.3.2. Potential Determining Ions

Surface diffraction studies have revealed well-ordered water layers a few Å (= $1 \times 10^{-10}$ m) above the calcium and carbonate ions on the mineral surface (*Fenter et al.*, 2000; *Fenter and Sturchio*, 2004; *Geissbühler et al.*, 2004; *Magdans et al.*, 2007; *Heberling et al.*, 2011). This is the hydrolysis plane of *Stipp,* (1999) and the 0-plane invoked in various surface complexation models (SCMs) of the calcite-water interface (*Wolthers et al.*, 2008; *Heberling et al.*, 2011; see also Figure 3-1a). Protonation and deprotonation reactions occur in this plane, but it does not contain the lattice ions $Ca^{2+}$ and $CO_3^{2-}$ or other adsorbed ion complexes.

These are confined to the 1- and 2-planes (or the a- and b-planes), which here we associate with the inner and outer Helmholtz planes respectively (Figure 3-1a). Most SCMs include ordered water layers at the 0-plane, and the pH-dependent protonation and deprotonation reactions (3.17) – (3.19) that occur at the sites defining the 0-plane (*Stipp*, 1999; *Wolthers et al.*, 2008; *Heberling et al.*, 2011). However, the SCM of *Heberling et al.* (2011) predicted that the charge at the 0-plane is only weakly pH dependent. The dominant surface species are $>CaOH^-$ and $>CaCO_3^-$, causing the 0-plane to be negatively charged across the pH range 5.5-11. Thus, unlike the >MeOH groups on oxide mineral surfaces, the calcite surface species $>CaOH^-$ and $>CaCO_3^-$ do not determine the pH dependence of the zeta potential. Rather, the potential at the OHP and, hence, the zeta potential, is instead controlled by adsorption of the potential-determining lattice ions $Ca^{2+}$ or $CO_3^{2-}$ at the 1- or 2-planes. The available evidence suggests that most of the adsorbed lattice PDIs are located at the 2-plane (*Wolthers et al.*, 2008; *Heberling et al.*, 2011).

Dissolution of calcite in aqueous solution is described by the following reaction:

$$CaCO_3\,(s) \Leftrightarrow Ca^{2+}\,(aq) + CO_3^{2-}(aq) \qquad (3.23)$$

The equilibrium conditions are defined by the pH, the concentration of the ionic species and, in open system conditions, the partial pressure of $CO_2$ ($pCO_2$) in solution (*Somasundaran et al.*, 1985; *Somasundaran*, 2006; *Somasundaran et al.*, 1985). Moreover, the concentration of lattice ion species available to adsorb onto the calcite surface is controlled by the reactions (*Eriksson et al.*, 2007):

$$CO_3^{2-}\,(aq) + H_2O\,(l) \Leftrightarrow HCO_3^-\,(aq) + OH^-\,(aq) \qquad (3.24)$$

$$HCO_3^-\,(aq) + H_2O\,(l) \Leftrightarrow H_2CO_3\,(aq) + OH^-\,(aq) \qquad (3.25)$$

$$H_2CO_3\,(aq) \Leftrightarrow H_2O\,(l) + CO_2\,(g) \qquad (3.26)$$

$$Ca^{2+}\,(aq) + H_2O\,(l) \Leftrightarrow Ca(OH)^+\,(aq) + H^+\,(aq) \qquad (3.27)$$

$$Ca^{2+}\,(aq) + HCO_3^-\,(aq) \Leftrightarrow CaHCO_3^+\,(aq) \qquad (3.28)$$

It can be seen from (3.23) - (3.28) that pH (and $pCO_2$) determines the $Ca^{2+}$ and $CO_3^{2-}$ concentrations in the solution at equilibrium. Apparent trends between zeta potential and pH therefore reflect the fact that pH and pCa are directly related at fixed $pCO_2$ (e.g. *Smallwood*, 1977). We confirm this experimentally in chapter 4. Thus, $H^+$ is not the key PDI for the calcite surface; rather, it is the lattice ion $Ca^{2+}$ (*Foxall et al.*, 1979; *Pierre et al.*, 1990; *Huang et al.*, 1991; *Cicerone et al.*, 1992; *Moulin and Roques*, 2003; *Alroudhan et al.*, 2016). Moreover, the PZC and IEP are not closely related. In principle, the PZC could be defined in terms of pH, as pH controls the protonation and deprotonation reactions at the 0-plane, However, in practice, the PZC is not observed over the pH range 5.5-11 (*Heberling et al.*, 2011). The IEP must be defined in terms of pCa, or in terms of the concentration of other PDIs for the calcite surface such as $Mg^{2+}$ as discussed below.

## 3.4. Experimental Measurements of Zeta Potential

Published measurements of zeta potential in calcite and natural carbonates in aqueous solution range from +29 mV to -39 mV (Figure 3-3 and Figure 3-4). As discussed below, the zeta potential depends upon the electrolyte concentration and composition, the nature of the calcite, sample preparation, experimental conditions and measurement method. However, limited reporting of the nature of the samples and experimental method, especially sample history, preparation and cleaning, and experimental conditions (especially pH, pCa and $pCO_2$), makes it challenging to systematically compare experimental data (see Table 3-1 for a summary). In this section, we review and discuss the data published to date, and summarize the key controls on zeta potential.

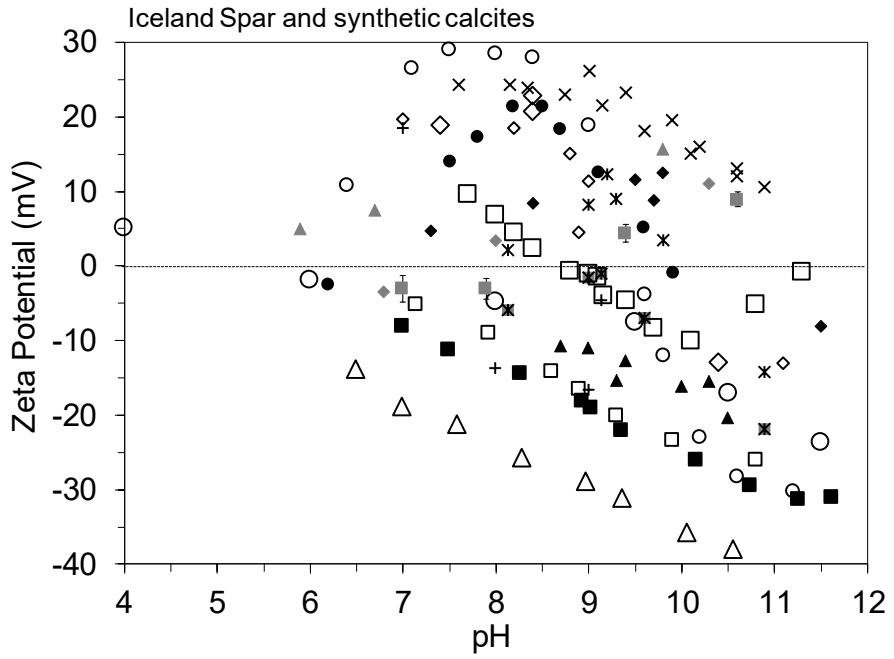



**Figure 3-3: Zeta potential of Iceland spar and synthetic calcite in indifferent electrolytes as a function of pH. Measurements were obtained using the electrophoretic mobility method (EPM), with the exception of *Somasundaran and Agar*, 1967) (diamonds) and *Thompson and Pownall*, 1989) (squares). Error bars are shown when reported by the source. Data from Somasundaran and Agar, (1967) in deionized water after different mixing times (♦: no mixing; ◊: after 1 week; ◇: after two months of mixing); Sampat Kumar et al., (1971) in deionised water (+); Siffert and Fimbel, (1984) in $10^{-2}$M NaCl electrolyte (∗: mass dispersed = 50 mg; grey ∗: 30 mg); Thompson and Pownall, (1989) in various electrolytes (■: NaCl ($5\times10^{-3}$M); □: NaCl ($5\times10^{-3}$M)/$NaHCO_3$ ($1\times10^{-3}$M); ☐: NaCl ($5\times10^{-3}$M)/$NaHCO_3$ ($1\times10^{-3}$M)/$H_2CO_3$/$Ca(OH)_2$); Cicerone et al., (1992) in $10^{-3}$M KCl electrolyte (▲); Vdović and Bišćan, (1998) in $10^{-3}$M NaCl electrolyte (○); Vdovic, (2001) in $10^{-3}$M NaCl electrolyte (●); Eriksson et al., (2007) in $5.56\times10^{-3}$M NaCl electrolyte (×); Sondi et al., (2009) in $10^{-3}$M NaCl electrolyte (△) and Kasha et al., (2015) in deionized water (○). Grey symbols show data from Mahani et al., (2016) in various electrolytes (▲: formation brine; ♦: seawater; ■: 25 times diluted seawater).**

## 3.4.1. Electrolyte Concentration and Composition

### 3.4.1.1 Effect of pH

Many studies have reported more negative values of zeta potential with increasing pH (e.g. *Thompson and Pownall*, 1989; *Pierre et al.*, 1990; *Cicerone et al.*, 1992; *Vdovic*, 2001; *Eriksson et al.*, 2007). For example, *Thompson and Pownall,* (1989) reported a close-to-linear relationship between zeta potential and pH (square data in Figure 3-3) using packed synthetic calcite and NaCl solution of ionic strength $5\times10^{-3}$ M (filled squares) and $NaCl/NaHCO_3$ of ionic strength $5\times10^{-4}$

M (open squares). Similarly, *Vdovic,* (2001) obtained a linear relationship between zeta potential and pH using natural carbonate powder samples suspended in $10^{-3}$ M NaCl electrolyte (filled and open circles in Figure 3-4).

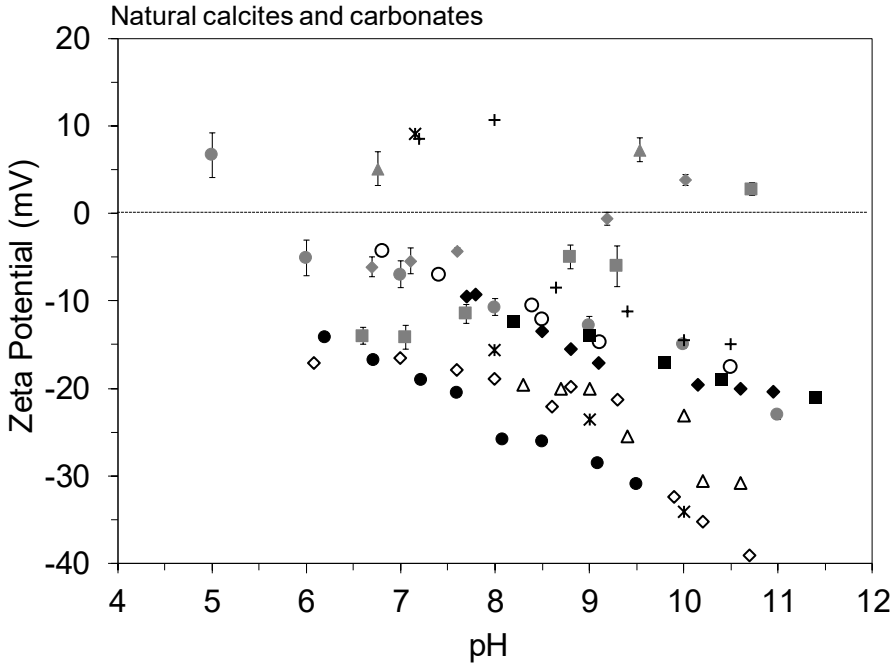



**Figure 3-4: Zeta potential of natural calcite and carbonate rocks in indifferent electrolytes as a function of pH. Error bars are shown when reported by the source. Data from Mishra, (1978) in $2x10^{-2}$M $NaClO_4$ electrolyte (+); Rao et al., (1989) in $2x10^{-3}$M $NaClO_4$ electrolyte (♦); Cicerone et al., (1992) in $10^{-3}$M KCl electrolyte (△); Vdović and Bišćan, (1998) in $10^{-3}$M NaCl electrolyte (◊); Patil et al., 1998 in $2x10^{-3}$M $NaNO_3$ electrolyte (✳); Vdovic, (2001) in $10^{-3}$M NaCl electrolyte (○: limestone; ●: lake sediment) and Somasundaran et al., (2005) in $10^{-3}$M $KNO_3$ electrolyte (■). Grey symbols show data on natural carbonate rocks in various electrolytes (●: deionized water containing 0.09 M $CaCl_2$ from Chen et al., 2014; ▲: formation brine; ♦: seawater; ■: 25 times diluted seawater, all from Mahani et al., 2016).**

However, there are numerous exceptions (e.g. *Somasundaran and Agar*, 1967; *Mishra*, 1978; *Siffert and Fimbel*, 1984; *Vdović and Bišćan*, 1998; *Chen et al.*, 2014; *Kasha et al.*, 2015; *Mahani et al.*, 2015; 2016). For example, *Siffert and Fimbel,* (1984) found that the zeta potential of synthetic calcite at equilibrium pH (9.1; Table 3-1a) could be either positive or negative, dependent on the dispersed mass. Away from the equilibrium pH, the zeta potential decreased with either increasing or decreasing pH (open and grey stars in Figure 3-3). *Vdović and Bišćan,* (1998) (open circles in Figure 3-3) and *Vdovic,* (2001) (filled circles in Figure 3-3) observed similar behaviour. The latter reported zeta potential values

that changed polarity with both increasing and decreasing pH, thus apparently defining two IEPs.

*Mahani et al.,* (2015) and *Mahani et al.,* (2016) reported an increasingly negative zeta potential with decreasing pH (grey triangles, diamonds and squares in Figure 3-3 and Figure 3-4), contrary to the trends reported above. However, as discussed in the previous section, SCMs for calcite suggest the electrical potential at the mineral surface is only weakly pH dependent, and experimental data have shown that the zeta potential is independent of pH if pCa is held constant (Figure 3-5). These data confirm that zeta potential is not directly controlled by pH, but rather by the concentration of lattice ions such as $Ca^{2+}$ and other PDIs discussed below.

**Table 3-1: Summary of published zeta potential of calcite and natural carbonates with varying pH and pCa. Table 3.1a reports studies focusing on the effect of varying pH. Table 3.1b reports studies focusing on the effect of varying pCa.**

**Table 3.1a.**

| Material | Method | Background electrolyte | Equilibrium condition | Equilibration time (hr) | Equilibrium pH ($pH_{EQ}$) | Open vs. closed system | Zeta potential at EQ. | $pH_{IEP}$ | IEP determination | Reference |
|---|---|---|---|---|---|---|---|---|---|---|
| Iceland spar | SPM | Deionized water ($HNO_3$/NaOH) | Calcite/water/air | 1440 | 8.2 | Open | Positive | 8.2 | Extrapolated | *Somasundaran and Agar,* (1967) |
| Iceland spar | SPM | $SiO_2$/$Na_2O$ | Calcite/water | N/A | 9.8 | Closed | Positive | 10.8 | Direct | *Fuerstenau et al.,* (1968) |
| Iceland spar | SPM | Deionized water | Calcite/water/$CO_2$ | N/A | 6.55 | $pCO_2$ = 0.23 | Negative | 6.55 | Direct | *Moulin and Roques,* (2003) |
| | | | | | 7.05 | $pCO_2$ = 0.023 | Negative | 7.05 | | |
| Iceland spar | SPM | Deionized water | Calcite/water/$CO_2$ | 24 - 720 | 5.8 | $pCO_2$ = 1 | Negative | 6.5 | Direct | *Heberling et al.,* (2011) |
| | | | | | 7.5 | $pCO_2 = 10^{-3.44}$ | Negative | 8.8 | | |
| | | | | | 8.3 | $pCO_2 = 10^{-5.2}$ | Negative | 9.4 | | |
| Iceland spar | EPM | Deionized water | Calcite/water | 24 | N/A | Closed | Negative | 5.4 | Extrapolated | *Kasha et al.,* (2015) |
| Iceland spar | EPM | Deionized water | Calcite/water/$CO_2$ | 1-2 | N/A | Open | Negative | 7.2-7.8 | Extrapolated | *Sampat Kumar et al.,* (1971) |
| Iceland spar | EPM | Formation water | Calcite/water | 24 | N/A | Closed | Positive | N/A | Direct | *Mahani et al.,* (2016) |
| | | Seawater (SW) | | | N/A | | Negative | 7.5 | | |
| | | 25 times diluted SW | | | 9.2 | | Negative | 8.5 | | |
| Synthetic calcite | EPM | $1x10^{-2}$, $5x10^{-2}$, $1.5x10^{-1}$M NaCl | Calcite/water/air | N/A | N/A | Open | Positive | N/A | N/A | *Foxall et al.,* (1979) |
| Synthetic calcite | EPM | $10^{-2}$M NaCl | Calcite/water | 10 | 9.1 | Closed | Pos – Neg | 10-11 | N/A | *Siffert and Fimbel,* (1984) |
| Synthetic calcite | SPM | $5 \times 10^{-3}$M NaCl | Calcite/water | 48 | 9.11-9.87 | Closed | Negative | N/A | N/A | *Thompson and Pownall,* (1989) |
| Synthetic calcite | SPM | $5 \times 10^{-3}$M NaCl/ $10^{-3}$M $NaHCO_3$ | Calcite/water | 48 | 9.11-9.87 | Closed | Negative | N/A | N/A | *Thompson and Pownall,* (1989) |
| Synthetic calcite | SPM | $5x10^{-4}$M $CaCl_2$ | Calcite/water | 48 | 9.11-9.87 | Closed | Positive | N/A | N/A | *Thompson and Pownall,* (1989) |

**Table 3.1a (continued)**

| Material | Method | Background electrolyte | Equilibrium condition | Equilibration time (hr) | Equilibrium pH ($pH_{EQ}$) | Open vs. closed system | Zeta potential at EQ. | $pH_{IEP}$ | IEP determination | Reference |
|---|---|---|---|---|---|---|---|---|---|---|
| Synthetic calcite | EPM | $10^{-2}$M NaCl | Calcite/water | 24 | 10 | Closed | Positive | 9.6 | Direct | *Pierre et al.,* (1990) |
| Synthetic calcite | EPM | $10^{-3}$M KCl | Calcite/water | 168 | 9.8-10 | Closed | Negative | N/A | N/A | *Cicerone et al.,* (1992) |
| Synthetic calcite | EPM | $10^{-3}$M KCl/$10^{-3}$M $CaCl_2$ | Calcite/water | 168 | 9.8-10 | Closed | Negative | N/A | N/A | *Cicerone et al.,* (1992) |
| Synthetic calcite | EPM | $10^{-3}$M KCl/$10^{-2}$M $CaCl_2$ | Calcite/water | 168 | 9.8-10 | Closed | Positive | N/A | N/A | *Cicerone et al.,* (1992) |
| Synthetic calcite | EPM | $10^{-3}$M NaCl | Calcite/water/air | Few | 8.6 | Closed | Positive | 9.8 | Direct | *Vdović and Bišćan,* (1998) |
| Synthetic calcite | EPM | $10^{-3}$M NaCl | Calcite/water/air | Few | 8.4 | Closed | Positive | 9.8 | Direct | *Vdovic,* (2001) |
| Synthetic calcite | EPM | 5.56x$10^{-3}$M NaCl | Calcite/water/$CO_2$ | 1 | 8-8.5 | Open | Positive | N/A | N/A | *Eriksson et al.,* (2007) |
| Synthetic calcite | EPM | $10^{-3}$M NaCl | Calcite/water/air | Few | 8.3 | Closed | Negative | N/A | N/A | *Sondi et al.,* (2009) |
| Natural calcite | EPM | 2x$10^{-3}$M $NaClO_4$ | Calcite/water | 0.5 | 9-10 | Closed | Negative | N/A | N/A | *Rao et al.,* (1989) |
| Natural calcite | EPM | 2x$10^{-2}$M $NaClO_4$ | Calcite/water/air | 0.5 | 8.2 | Open | Negative | 8.2 | Extrapolated | *Mishra,* (1978) |
| Natural calcite | EPM | $10^{-2}$M NaCl | Calcite/water | 24 | 10 | Closed | Negative | 9.4 | Direct | *Pierre et al.,* (1990) |
| Natural calcite | EPM | $10^{-3}$M KCl | Calcite/water | 168 | 9.8-10 | Closed | Negative | N/A | N/A | *Cicerone et al.,* (1992) |
| Natural calcite | EPM | $10^{-3}$M NaCl | Calcite/water/air | Few | 8.6 | Closed | Negative | N/A | N/A | *Vdović and Bišćan,* (1998) |
| Natural calcite | EPM | 2x$10^{-3}$M $NaNO_3$ | Calcite/water/air | 2.2 | 8.3 | Open | Negative | 7.8 | Extrapolated | *Patil et al.,* (1998) |
| Natural calcite | EPM | $10^{-3}$M NaCl | Calcite/water/air | Few | 8.4 | Closed | Negative | N/A | N/A | *Vdovic,* (2001) |
| Natural calcite | EPM | $10^{-3}$M $KNO_3$ | Calcite/water/air | 1 | N/A | Open | Negative | N/A | N/A | *Somasundaran et al.,* (2005) |
| Natural carbonate | EPM | Deionized water | Calcite/water | 1 | N/A | Closed | Negative | 5.2-5.8 | Extrapolated | *Chen et al.,* (2014) |
| Natural carbonate | EPM | Formation water | Calcite/water | 24 | N/A | Closed | Positive | N/A | Direct | *Mahani et al.,* (2016) |
| | | Seawater (SW) | | | N/A | | Negative | 9.25 | | |
| | | 25 times diluted SW | | | 9.2 | | Negative | 10.25 | | |

**Table 3.1b.**

| Material Type | Method | Background electrolyte | Equilibrium condition | Equilibration time (hr) | Equilibrium pH ($pH_{EQ}$) | Open vs. closed system | dζ/dpCa | $pCa_{IEP}$ | IEP determination | Reference |
|---|---|---|---|---|---|---|---|---|---|---|
| Iceland spar | Electro osmosis | NaCl/$Na_2CO_3$/$CaCl_2$ | Calcite/water | 2 | 9 | Closed | N/A | 3.33 | Extrapolated | *Douglas and Walker,* (1950) |
| Iceland spar | SPM on packed particles | Deionized water ($HNO_3$/NaOH) | Calcite/water/air | 1440 | 8.2 | Open | N/A | 4.25 | Extrapolated | *Somasundaran and Agar,* (1967) |
| Iceland spar | EPM | 0.571M NaCl | Calcite/water | 24 | N/A | Closed | N/A | 1.65-1.75 | Extrapolated | *Kasha et al.,* (2015) |
| Synthetic calcite | EPM | 1x$10^{-2}$, | Calcite/water/air | N/A | N/A | Open | -15.2 | 4.5 | Extrapolated | *Foxall et al.,* (1979) |
| | | 5x$10^{-2}$, | | | | | -12.8 | | | |
| | | 1.5x$10^{-1}$M NaCl | | | | | -9.3 | | | |
| Synthetic calcite | SPM | 2x$10^{-3}$M NaCl | Calcite/water | 48 | 9.11-9.87 | Closed | -12.7 | 2.02 | Extrapolated | *Thompson and Pownall,* (1989) |
| Synthetic calcite | SPM | 2x$10^{-3}$/$10^{-2}$M ($NaCl$/$NaHCO_3$) | Calcite/water | 48 | 9.11-9.87 | Closed | -10.2 | 1.92 | Extrapolated | *Thompson and Pownall,* (1989) |
| Synthetic calcite | SPM | 2x$10^{-3}$/$10^{-2}$M ($NaCl$/$CaCl_2$) | Calcite/water | 48 | 9.11-9.87 | Closed | -10.1 | 3.4 | Extrapolated | *Thompson and Pownall,* (1989) |

**Table 3.1b (continued)**

| Material Type | Method | Background electrolyte | Equilibrium condition | Equilibration time (hr) | Equilibrium pH ($pH_{EQ}$) | Open vs. closed system | dζ/dpCa | $pCa_{IEP}$ | IEP determination | Reference |
|---|---|---|---|---|---|---|---|---|---|---|
| Synthetic calcite | SPM | $2x10^{-3}/10^{-2}$M ($NaCl/H_2CO_3$) | Calcite/water | 48 | 9.11-9.87 | Closed | -10.8 | 4 | Extrapolated | *Thompson and Pownall*, (1989) |
| Synthetic calcite | SPM | $2x10^{-3}/10^{-2}/10^{-2}$M ($NaCl/NaHCO3/H_2CO_3$) | Calcite/water | 48 | 9.11-9.87 | Closed | -12.9 | 3.8 | Direct | *Thompson and Pownall*, (1989) |
| Synthetic calcite | SPM | $2x10^{-3}/10^{-2}/10^{-2}$M ($NaCl/NaHCO3/Ca(OH)_2$) | Calcite/water | 48 | 9.11-9.87 | Closed | -12.2 | 3.8 | Direct | *Thompson and Pownall*, (1989) |
| Synthetic calcite | EPM | $10^{-2}$M NaCl | Calcite/water | 24 | 10 | Closed | N/A | 3.3 | Direct | *Pierre et al.*, (1990) |
| Synthetic calcite | SPM | $10^{-5}$ – 0.01M $CaCl_2$ | Calcite/water | 120 | 9.3-9.9 | Closed | -8.34 | 4.38 | Extrapolated | *Huang et al.*, (1991) |
| Synthetic calcite | EPM | $10^{-3}$M KCl | Calcite/water | 168 | 9.8-10 | Closed | -14.5 (in the vicinity of IEP) | 2.7 | Direct | *Cicerone et al.*, (1992) |
| Natural calcite | EPM | $10^{-2}$M NaCl | Calcite/water | 24 | 10 | Closed | N/A | 4 | Direct | *Pierre et al.*, (1990) |
| Stevns Klint chalk | EPM | $CaCl_2$ and $NaSO_4$ in 0.571M NaCl | Chalk/water/air | 48 | Controlled at 8.4 | Closed | N/A | N/A | N/A | *Zhang and Austad*, 2006 |
| Natural carbonate | EPM | Deionized water (DI) | Calcite/water | 1 | Controlled at 8.4 | Closed | N/A | 0.2-0.75 | Extrapolated | *Chen et al.*, (2014) |
| Natural carbonate | SPM in intact samples | 0.05M NaCl | Calcite/water/ air | 168-720 | 8.2 | Closed | -5.29 | 0.61 | Direct | *Alroudhan et al.*, (2016) |
| | | 0.5M NaCl | | | | | -4.35 | 0.49 | | |
| | | 2M NaCl | | | | | -2.75 | 0.41 | | |

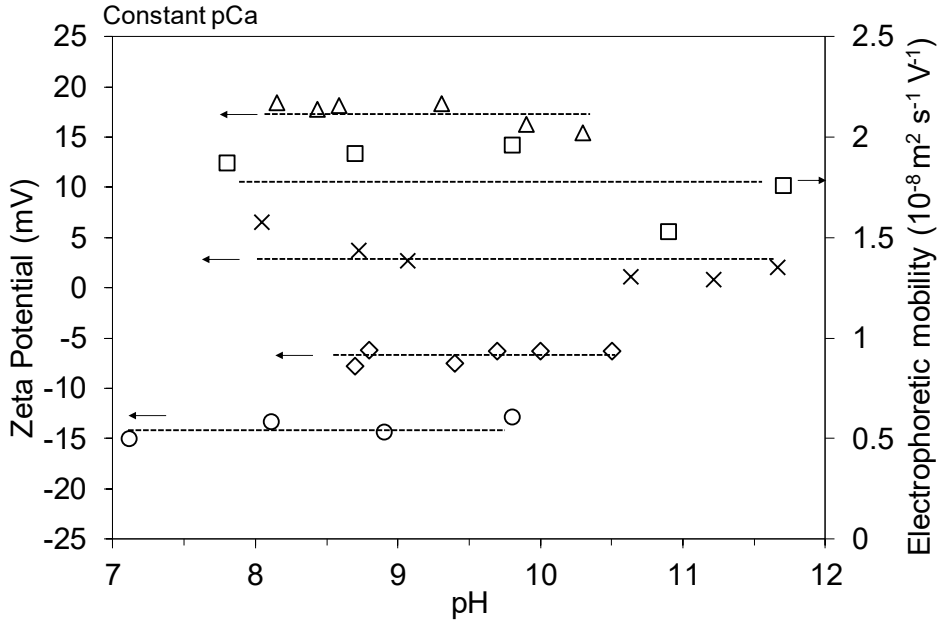



**Figure 3-5: Zeta potential and electrophoretic mobility of synthetic calcite and Iceland spar as a function of pH in experiments with constant pCa.Data are from synthetic calcite. Data from Foxall et al., (1979) in $10^{-3}$M NaCl electrolyte with pCa = 2.1 (□); Thompson and Pownall, (1989) in $5x10^{-4}$M $CaCl_2$ electrolyte with pCa = 3.3 (×); Cicerone et al., (1992) in $10^{-3}$M KCl electrolyte with pCa = 2 (△) and pCa = 3 (◇), and Sondi et al., (2009) in $10^{-3}$M NaCl electrolyte with pCa = 2 (○).**

#### 3.4.1.2 Effect of Ca and $CO_3$

Many authors have concluded that the principal PDIs for calcite are the lattice ions $Ca^{2+}$ and $CO_3^{2-}$ (e.g. *Berlin and Khabakov*, 1961; *Somasundaran and Agar*, 1967; *Mishra*, 1978; *Foxall et al.*, 1979; *Siffert and Fimbel*, 1984; *Thompson and Pownall*, 1989; *Pierre et al.*, 1990; *Huang et al.*, 1991; *Schramm et al.*, 1991; *Cicerone et al.*, 1992; *Vdović and Bišćan*, 1998; *Vdovic*, 2001). Consequently, the effect of $Ca^{2+}$ on the zeta potential has been the topic of several experimental studies (e.g. *Thompson and Pownall*, 1989; *Pierre et al.*, 1990; *Huang et al.*, 1991; *Cicerone et al.*, 1992; *Alroudhan et al.*, 2016; see Figure 3-6 and Figure 3-7). The consistent observation in these studies is that decreasing pCa yields more positive zeta potential, consistent with increased adsorption of $Ca^{2+}$ onto the calcite surface (Figure 3-1). However, significant differences in the magnitude and polarity of the zeta potential, in the gradient of zeta potential vs. pCa ($d\zeta$/dpCa), and in the IEP (expressed as pCa), have been reported (Figure 3-6 and Figure 3-7; Table 3-1b). The zeta potential varies between +20mV and -26mV, depending on calcite type and experimental conditions. Most studies report a linear or close-to-linear relationship between zeta potential and pCa, especially for pCa values close to the IEP, with the gradient $d\zeta$/dpCa in the range -8 to -15 mV/decade (Figure 3-6 and Figure 3-7).

A linear relationship is consistent with Nernstian behaviour of the calcite surface and suggests the electrical double layer is described by the Gouy–Chapman–Grahame model (e.g. Hunter, 1978). The relationship between zeta potential and pCa can then be expressed as (*Foxall et al.*, 1979):

$$\left.\frac{d\zeta}{dpCa}\right|_{\zeta\to 0} = \frac{-2.303\frac{kT}{ze}}{\left(1+\frac{C_d}{C_s}\right)\exp(\kappa\Delta)} \tag{3.29}$$

where $k$ is Boltzmann's constant, $T$ is the temperature, $z$ is the valence of the PDI, $e$ is the charge on an electron, $C_d$ and $C_s$ are the capacitance per unit area of the diffuse and Stern layers respectively, $\kappa$ is the Debye-Huckel reciprocal length, and $\Delta$ is the distance of the shear plane from the Stern plane (see Figure 3-1).

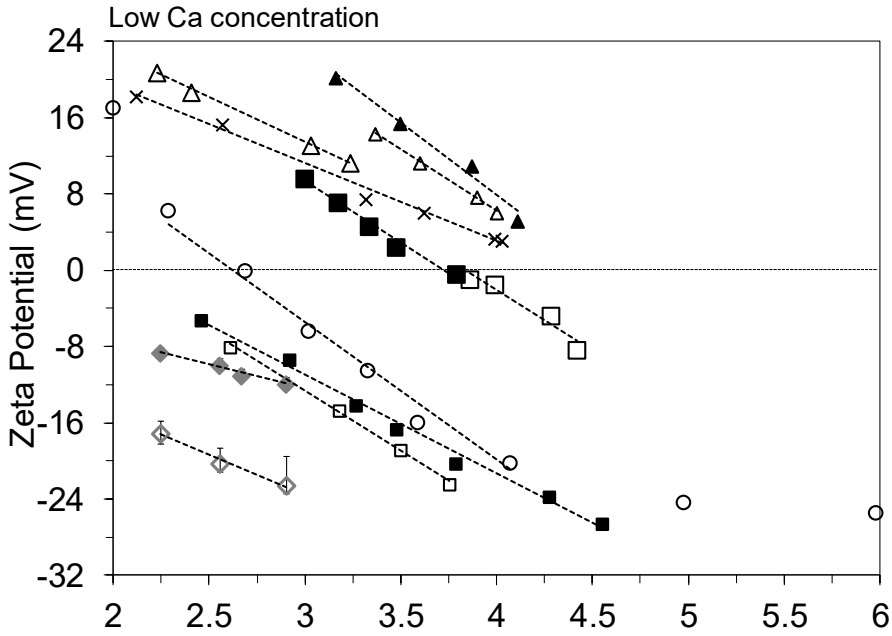



**Figure 3-6: Zeta potential of synthetic calcite and natural carbonate in indifferent electrolytes as a function of pCa at low Ca concentration only. Error bars are shown when reported by the source. All data are from powdered synthetic calcite with the exception of Alroudhan et al., (2016) (grey symbols). Data from Thompson and Pownall, (1989) in different aqueous compositions (■: NaCl ($2x10^{-3}$M)/$NaHCO_3$ ($10^{-2}$M); □: NaCl ($2x10^{-3}$); □: NaCl ($2x10^{-3}$M)/$NaHCO_3$ ($10^{-2}$M)/$Ca(OH)_2$ ($10^{-2}$M); ■: NaCl ($2x10^{-3}$M)/$NaHCO_3$ ($10^{-2}$M)/$H_2CO_3$ ($10^{-2}$M)); Foxall et al., (1979) in three different NaCl concentrations (▲: $1x10^{-2}$M; △: $5x10^{-2}$M; big △: $1.5x10^{-1}$M); Huang et al., (1991) in 0.01 $CaCl_2$ electrolyte (×) and Cicerone et al., (1992) in 10-3M KCl electrolyte (○). Grey diamonds show data from Alroudhan et al., (2016) on natural carbonate in 0.05M NaCl electrolyte at high pCa (♦: SPM data; ◊: EPM data); the full span of these data is shown in Figure 3-4.**

Zeta potential data obained at low ionic strength using the EPM method show a broadly consistent value of d$\zeta$/dpCa of approximately -13 mV/decade (Figure 3-6). Equation (3.29) can be used to match these data using one value of $C_s$ ~ 0.4 $Fm^{-2}$ and $\Delta =$ zero. For comparison, *Heberling et al.,* (2011) fitted their zeta potential data using a more sophisticated SCM with $C_s$ = 0.45 $Fm^{-2}$ and $\Delta = 0.33$ nm. Previous SCMs for calcite used unrealistically high $C_s$ values of 10 – 100 $Fm^{-2}$ (*Van Cappellen et al.*, 1993; *Pokrovsky and Schott*, 2002). However, a number of recent studies have reported non-linear relationships between zeta potential and pCa (e.g. *Zhang and Austad*, 2006; *Chen et al.*, 2014; *Kasha et al.*, 2015; see Figure 3-7). Moreover, a wide range of IEP (expressed as pCa) values have been reported (pCa of 1.92 – 4.5; Table 3-1b).

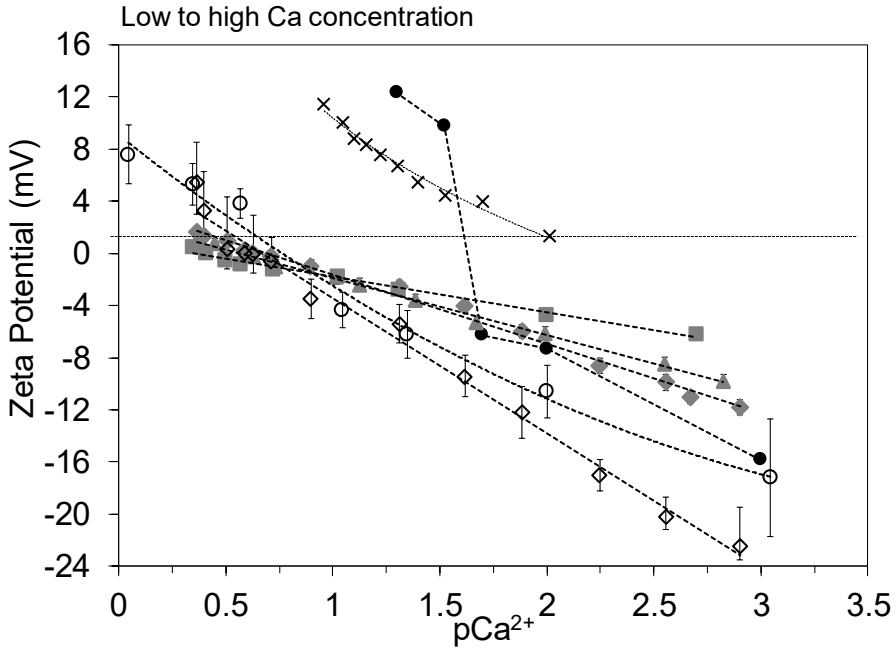



**Figure 3-7: Zeta potential of synthetic calcite and natural carbonate in indifferent electrolytes as a function of pCa at low and high Ca concentration. Error bars are shown when reported by the source. all data are from natural calcite and carbonate rocks, with the exception of Kasha et al., (2015) (filled symbols). Data from Zhang and Austad, (2006) on powdered Stevns Klint chalk in 0.571M NaCl electrolyte (×); Chen et al., (2014) in deionized water (○); Kasha et al., (2015) in synthesized brines equivalent to seawater composition (●) and Alroudhan et al., (2016) in 0.05M NaCl (◊). Grey symbols show data from Alroudhan et al., (2016) in intact natural carbonate rocks in various NaCl concentrations (♦: 0.05M; ▲: 0.5M; ■: 2M; all from; error bars are the same size or smaller than the symbols).**

As discussed in the following sections, the variability of these results might be attributed to differences in experimental conditions, including $pCO_2$, calcite type, measurement technique and the establishment of equilibrium. The effect of the carbonate ion on the zeta potential has received less attention than the calcium ion. The very limited data suggest that addition of $CO_3^{2-}$ makes the zeta potential more negative, consistent with increased adsorption of $CO_3^{2-}$ onto the calcite surface (e.g. *Douglas and Walker*, 1950; *Smallwood*, 1977).

### 3.4.1.3 Effect of pMg and $pSO_4$

The magnesium ion is also compatible with the calcite crystal lattice (*Bragg*, 1950). *De Groot and Duyvis,* (1966) suggested that $Ca^{2+}$ and $Mg^{2+}$ influence the zeta potential of calcite to a similar extent, but their dataset was very sparse,

comprising just five measurements (two for $Mg^{2+}$ and three for $Ca^{2+}$) at high pMg (i.e. at very low concentration; compare filled and open triangles in Figure 3-8). *Smallwood,* (1977) obtained a similar response (compare filled and open squares in Figure 3-8) over the same concentration range. More recent studies have found that the zeta potential becomes more positive with decreasing pMg (*Zhang et al.*, 2007; *Chen et al.*, 2014; *Alroudhan et al.*, 2016; see data represented by crosses, circles and diamonds in Figure 3-8). *Alroudhan et al.,* (2016) found that $Mg^{2+}$ behaved identically to $Ca^{2+}$ within experimental error over a wide range of pCa and pMg (0.4 – 3; compare filled and open diamonds). However, data showing the effect of pMg on zeta potential are still very scarce, especially at low pMg.

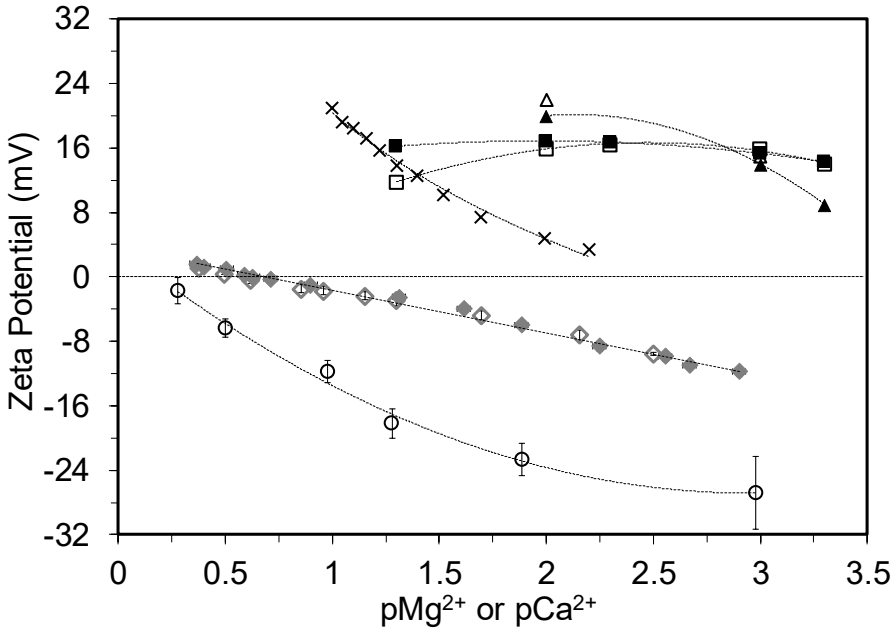



**Figure 3-8: Zeta potential of synthetic calcite and natural carbonate as a function of pMg. Error bars are shown when reported by the source. open symbols show zeta potential as a function of pMg. Data from De Groot and Duyvis, (1966) in deionized water (△); Smallwood, (1977) in deionized water (□); Zhang et al., (2007) in 0.571M NaCl electrolyte (×); Chen et al., (2014) in deionized water (○) and Alroudhan et al., (2016) in intact natural Portland carbonate in 0.05M NaCl electrolyte (◇; error bars for these data are the same size or smaller than the symbols). For comparison, filled symbols show measurements as a function of pCa when available from the same studies.**

A number of studies have also shown that the zeta potential is affected by the concentration of $SO_4^{2-}$, observing that the zeta potential becomes more negative with decreasing $pSO_4$ (*Smallwood*, 1977; *Zhang and Austad*, 2006; *Alroudhan et al.*, 2016; Figure 3-9). *Smallwood,* (1977) argued that $SO_4^{2-}$ is

adsorbed onto the calcite mineral surface, similar to the lattice ions $Ca^{2+}$, $Mg^{2+}$ and $CO_3^{2-}$, as indicated by its ability to reverse the polarity of the zeta potential (Figure 3-9). However, no other papers have reported an IEP in terms of $pSO_4$. *Zhang and Austad,* (2006) and *Alroudhan et al.,* (2016) both observed a linear relationship between zeta potential and $pSO_4$ for chalk and natural carbonate respectively, but the IEP was not encountered over the concentration range investigated (Figure 3-9). Data showing the effect of $pSO_4$ on zeta potential are still scarce and do not conclusively show that $SO_4^{2-}$ is a PDI for the calcite surface.

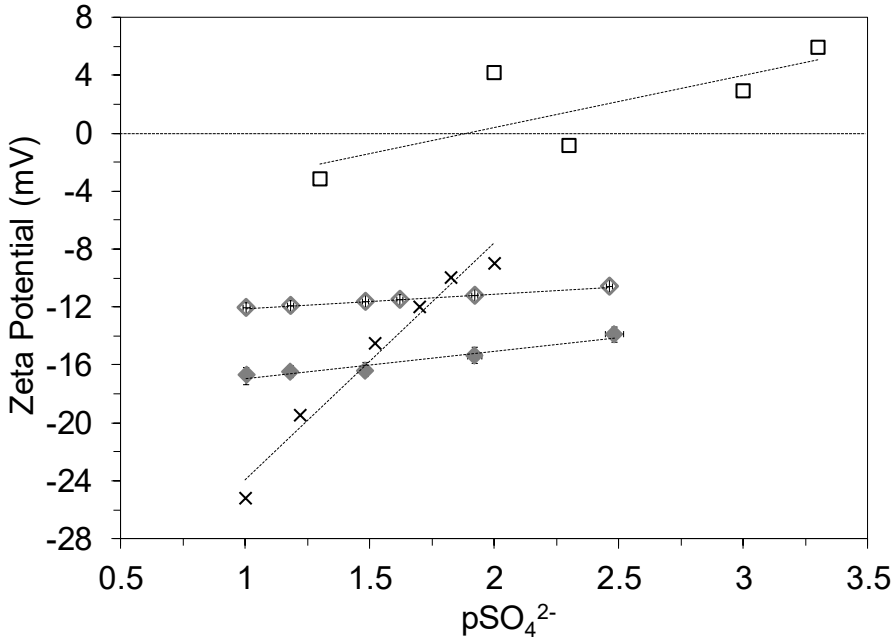



**Figure 3-9: Zeta potential of synthetic calcite and natural carbonate as a function of $pSO_4$. Error bars are shown when reported by the source. Data from Smallwood, (1977) on synthetic calcite in deionized water (□); Zhang and Austad, (2006) on Stevns Klint chalk in 0.571M NaCl electrolyte (×) and Alroudhan et al., (2016) in intact natural Portland carbonate in various NaCl electrolytes (◆: 0.05M; ◇: 0.5M; error bars are the same size or smaller than the symbols; data from).**

### 3.4.1.4 Indifferent Ions and Total Ionic Strength

Ions other than $Ca^{2+}$, $Mg^{2+}$, $CO_3^{2-}$ and $SO_4^{2-}$ are generally assumed to be indifferent to the calcite mineral surface; they have little or no tendency to adsorb onto the surface. It is well known that the zeta potential decreases in magnitude with increasing concentration of indifferent ions such as $Na^+$, $K^+$, $Cl^-$, reflecting contraction of the electrical double layer (EDL; e.g. *Vinogradov et al., 2010*). *Pierre*

*et al.,* (1990) obtained the same IEP (expressed as pH) on natural calcite irrespective of the concentration of NaCl (0, $10^{-3}$, $10^{-2}$ M), indicating that Na and Cl are indifferent ions. *Alroudhan et al.,* (2016) found that the sensitivity of zeta potential to pCa (i.e. $d\zeta/dpCa$) decreased as NaCl concentration increased, consistent with contraction of the EDL reducing the absolute magnitude of the zeta potential (Figure 3-7 and Table 3-1b). However, they also found that the IEP (as pCa) decreased with increasing NaCl concentration, which is not expected for indifferent ions. They suggested that at the high NaCl concentrations investigated (up to 2M), the ability of $Ca^{2+}$ ions to interact with calcite surface was reduced due to contraction of the EDL and increasing occupancy of hydrated $Na^{+}$ ions in the diffuse layer. However, data to support this hypothesis are scarce; few studies have obtained zeta potential measurements on calcite at high ionic strength (>0.1M).

### 3.4.2. Partial Pressure of $CO_2$

Variations in $pCO_2$ across different experiments may be one factor that explains the variation in reported values of IEP. In closed system experiments with controlled $pCO_2$, the very limited data available suggest that the IEP (expressed as pH) decreases with increasing $pCO_2$ (*Moulin and Roques*, 2003; *Heberling et al.*, 2011) (see Figure 3-10). Moreover, in open system experiments, *Somasundaran and Agar,* (1967) postulated that $pH_{IEP}$ was a function of mixing time of the sample powder in solution, due to an increase in $CO_2$ concentration in the suspension. They used this mechanism to explain the decrease in $pH_{IEP}$ they observed with increased mixing time. The reported $pH_{IEP}$ in closed system experiments is generally higher than the value in open system experiments, consistent with reduced access to $CO_2$ (Table 3-1a). The absence of, or limited access to, $CO_2$ in closed system experiments causes a decrease in carbonic acid formation (equation 3.27) and in turn increases $pH_{IEP}$ (*Somasundaran*, 2006).

The effect of $pCO_2$ on the IEP expressed as pCa or pMg is less studied. No studies have varied $pCO_2$ and pCa or pMg, or measured pCa or pMg whilst varying

$pCO_2$ and pH. Studies investigating the effect of pCa on zeta potential have typically been conducted in simple open or closed system conditions. In open system experiments, measured $pCa_{IEP}$ lies in the range of 4.25 – 4.5 (*Somasundran and Agar*, 1967; *Foxall et al.*, 1979; *Huang et al.*, 1991; Table 3-1b). In closed system experiments, reported $pCa_{IEP}$ values have a wider range of 0.4 - 4 and are always lower than the $pCa_{IEP}$ values reported in open system experiments (Table 3-1b). The broad range of $pCa_{IEP}$ observed in closed system experiments might be attributed to different amounts of $CO_2$ dissolved into solution during preparation (e.g. *Thompson and Pownall*, 1989) or the type of calcite used (synthetic vs. natural; *Pierre et al.*, 1990; see also the next section). Recent studies of zeta potential on natural carbonates in closed system experiments consistently show the lowest values of $pCa_{IEP}$ in the range 0.4-0.75 (*Chen et al.*, 2014; *Kasha et al.*, 2015; *Alroudhan et al.*, 2016). In closed system experiments, $pCO_2$ is fixed and, as we show in chapter 4, lower pCa corresponds to lower pH. Lower pH is equivalent to higher $pCO_2$ (e.g. *Heberling et al.*, 2011; see also reactions 3.24 – 3.28).

### 3.4.3. Natural versus Synthetic Calcite

The zeta potential has been measured on a wide variety of calcite samples with differing nature and origin which can be broadly subdivided into three types: (1) synthetic calcite (pure precipitated crystalline calcium carbonate), (2) Iceland spar (pure crystalline calcite of natural origin) and (3) natural carbonate (composed mostly of calcite with inorganic material or organic matter). Data for Iceland spar and synthetic calcite show both positive and negative values for a given value of pH (Figure 3-3 and Figure 3-4; Table 3-1a) and pCa (Figure 3-6, Table 3-1b). The broad range of zeta potential values observed for a given pH may reflect differences in the concentrations of PDIs such as $Ca^{2+}$ and $Mg^{2+}$ that were not measured in the experiments; they may also reflect differences in $pCO_2$ or, as discussed below, the equilibration method. The range of values observed for a given pCa is more difficult to explain, but most likely reflects differences in $pCO_2$

or the equilibration method; it may also reflect differences in the concentrations of other PDIs such as $Mg^{2+}$ and $SO_4^{2-}$.

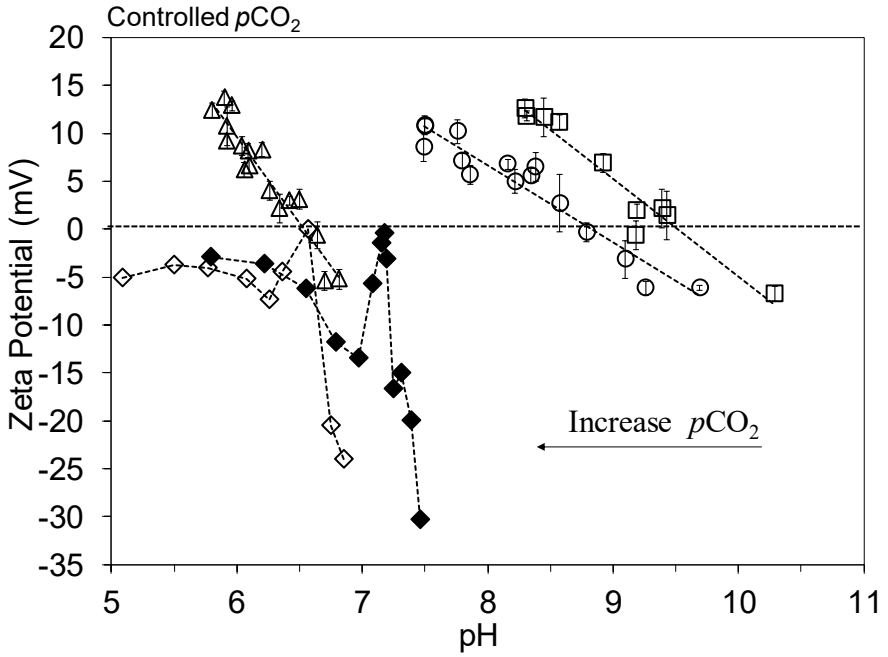



**Figure 3-10: Zeta potential of Iceland spar in deionized water with various $pCO_2$ as a function of pH. Error bars are shown when reported by the source. Data from Moulin and Roques, (2003) (◆: $pCO_2 = 0.023$; ◇: $pCO_2 = 0.234$) and Heberling et al., (2011) (△: $pCO_2 = 1$; ○: $pCO_2 = 10^{-3.44}$; □: $pCO_2 = 10^{-5.2}$).**

Data for natural calcite and carbonate rocks show less variability, with most studies returning negative values of zeta potential irrespective of pH; the few positive values in Figure 3-3 and Figure 3-4 were mostly obtained using natural brines rich in $Ca^{2+}$ where, as we show later, positive zeta potential is expected. *Berlin and Khabakov,* (1961) reported negative zeta potentials on 115 natural carbonate samples irrespective of pH. Likewise, with relatively few exceptions, the zeta potential on natural samples has been found to be negative at high pCa and positive at low pCa, although there is some variability in $pCa_{IEP}$ as discussed above (Figure 3-7). It has been suggested that the more negative zeta potentials typically observed in natural carbonates are due to the presence of organic matter incorporated in their structure during formation (*Vdović and Bišćan*, 1998; *Vdovic*, 2001). For example, *Vdovic,* (2001) obtained negative zeta potential on two natural carbonate samples over the whole pH range (filled and open circles in Figure 3-4);

however, they obtained a positive zeta potential on synthetic calcite (filled circles in Figure 3-3). Likewise, *Cicerone et al.,* (1992) found that natural (biogenetic) calcite (open triangles in Figure 3-4) bore a more negative zeta potential than pure calcite (filled triangles in Figure 3-3).

### 3.4.4. Measurement Technique

Measurements of zeta potential generally use either the electrophoretic mobility (EPM) method or the streaming potential method (SPM) introduced earlier. There appears to be no systematic difference in the reported IEP and both techniques have yielded a linear Nernstian relationship between zeta potential and pCa (Table 3-1; Figure 3-6 and Figure 3-7). However, only *Alroudhan et al.,* (2016) have compared the two techniques on the same (natural) calcite samples and electrolytes. Using the EPM method and natural (powdered) carbonate suspended in 0.05M NaCl electrolyte, they obtained a linear regression between zeta potential and pCa with a gradient of -10.45mV/decade, which they fitted using equation (3.29) and values of $C_s$ = 1.13 $Fm^{-2}$ and $\Delta = 0$. Note that this gradient is lower than obtained in previous studies on similar samples (as discussed above; see also Figure 3-6) and the value of $C_s$ used to obtain a match is higher. However, *Alroudhan et al.,* (2016) investigated electrolytes of higher total ionic strength than previous studies and their results suggest that $C_s$ increases with increasing total ionic strength.

Using the SPM method and the same natural (intact) carbonates and electrolytes, *Alroudhan et al.,* (2016) obtained the same IEP (expressed as pCa) within experimental error, but the gradient of a linear regression through the data was approximately two times smaller at -5.10 mV/decade. They argued that the shear plane is further away from the mineral surface in intact natural samples as opposed to powdered samples owing to the complex topology of the pore-space (see also *Vernhet et al.*, 1994 for similar comparisons on other materials), and fitted the SPM data using equation (3.29) with the same value of $C_s$ but a higher value of $\Delta = 0.245$nm. Thus differences in the observed sensitivity of zeta potential

to pCa (or the concentration of other PDIs) may reflect differences in the measurement technique and/or the nature of the sample (intact versus powdered).

### 3.4.5. Establishment of Equilibrium Between Sample and Electrolyte

Most studies equilibrate the calcite-electrolyte systems of interest for 48 hours or less prior to measuring the zeta potential (Table 3-1). Only a few studies have investigated longer equilibration times (e.g. *Somasundaran and Agar, 1967; Huang et al., 1991; Cicerone et al., 1992; Heberling et al., 2011; Alroudhan et al., 2016*). Some studies have reported equilibration times of an hour or less (e.g. *Sampat Kumar et al., 1971; Mishra, 1978; Rao et al., 1989; Eriksson et al., 2007; Chen et al., 2014*). *Heberling et al.,* (2011) investigated the difference between equilibrium and non-equilibrium measurements. In a study using natural intact limestone, *Alroudhan et al.,* (2016) found that the equilibrium pH in open system conditions was reached after 100 hours and sometimes more, and that it could take a factor of 2-3 times longer to reach the equilibrium pCa (e.g. Figure 3-11). Thus there is the risk that short equilibration times may not yield a stable equilibrium in pH and/or pCa, which will affect the measured zeta potential. Moreover, the equilibrium pH may be achieved before the equilibrium pCa, so assessing equilibration based on pH measurements alone may not be sufficient. As discussed above, values of the zeta potential on calcite are primarily controlled by pCa and the concentration of other PDIs such as $Mg^{2+}$, rather than pH. Therefore, it is important to ensure that equilibrium in the concentration of these PDIs has been reached prior to taking measurements. Inconsistent values of zeta potential obtained in some studies may reflect a lack of equilibration.

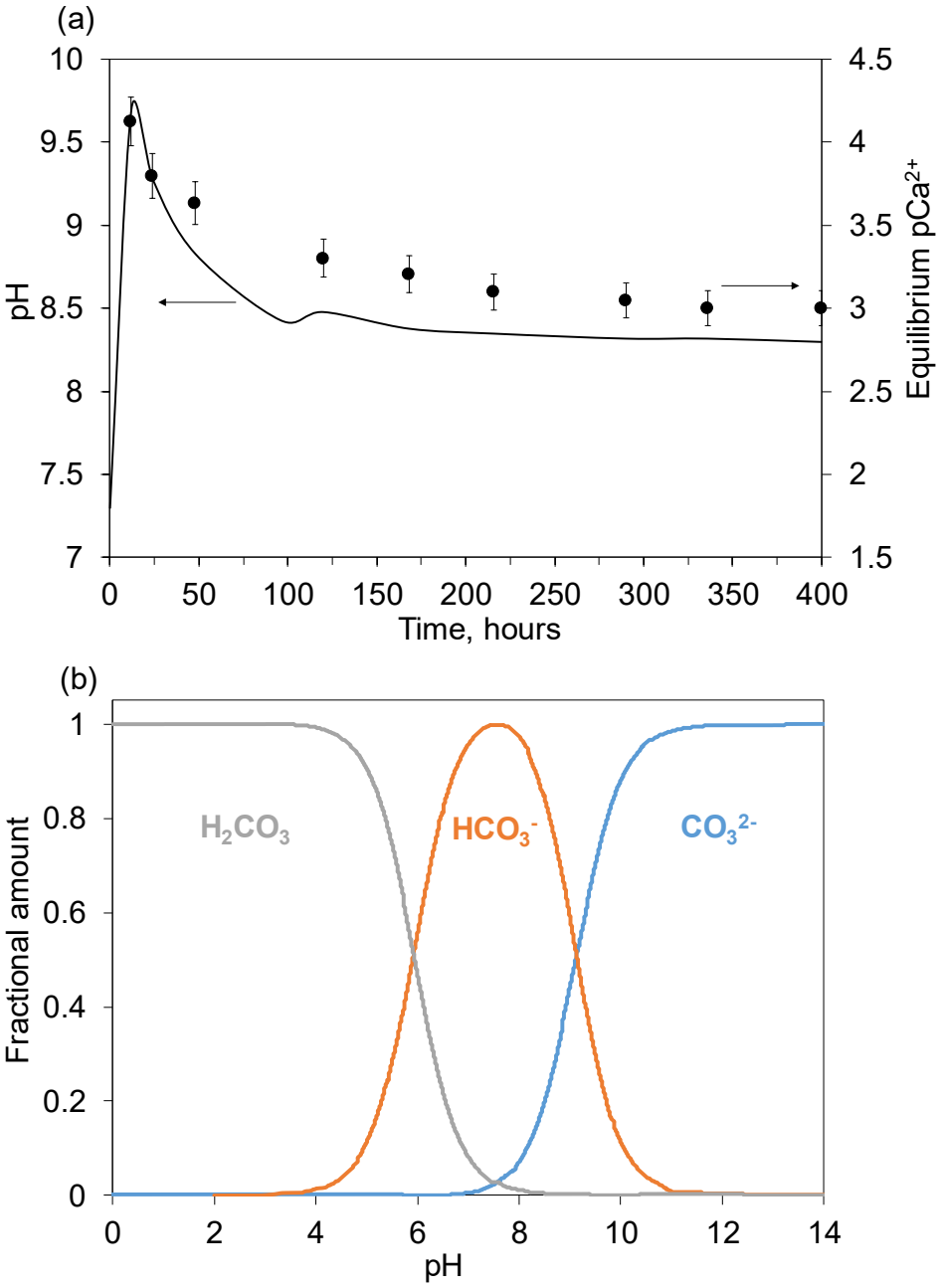



**Figure 3-11: Calcite-water-$CO_2$ equilibrium of natural Portland rock samples with deionised water.Plot (a) shows calcium concentration (expressed as pCa) and pH measured as a function of time during equilibration process. Plot (b) shows carbonate speciation into $H_2CO_3$, $HCO_3^-$, and $CO_3^{2-}$ as a function of pH. Modified from Alroudhan et al., (2016).**

## 3.5. Summary

Published measurements to date have typically observed linear, Nernstian relationships between zeta potential and pH, and between zeta potential and pCa, especially for values of pH and pCa close to the IEP. However, despite the clear relationship between zeta potential and pH obtained in such studies, the proton is not a PDI for calcite, as varying pH whilst holding pCa constant yields constant zeta potential within experimental error. Moreover, surface complexation models suggest that the calcite surface remains negatively charged over the pH range 5.5-11, and the surface charge is only weakly dependent on pH. The zeta potential is controlled instead by the concentration-dependent adsorption of lattice ions $Ca^{2+}$ and $CO_3^{2-}$ in the Stern layer, and also by the adsorption of $Mg^{2+}$ ions, although experimental data testing the effect of pMg are scarce. The few data available suggests that $Mg^{2+}$ behaves identically to $Ca^{2+}$ within experimental error. The $SO_4^{2-}$ ion has also been suggested as a PDI for the calcite surface, but the evidence is not conclusive. We provide further investigation of this parameter space using the SPM in natural carbonate in chapter 4.

A wide range of values of IEP (expressed as pCa) have been observed, depending upon whether the sample is natural or artificial, whether the experiments are open or closed to atmospheric $CO_2$, and the approach taken to equilibrate the sample and electrolyte prior to obtaining data. In open system experiments, measured $pCa_{IEP}$ lies in the range of 4.25 – 4.5, but in closed system experiments, $pCa_{IEP}$ has a wider range of 0.4 - 4 and is always lower than values reported in open system experiments. Natural samples generally show more negative values of zeta potential than artificial samples for a given value of pCa, and therefore yield lower values of $pCa_{IEP}$. Recent studies of zeta potential on natural carbonates in closed system experiments consistently show the lowest values of $pCa_{IEP}$ in the range 0.4 - 0.75. New data are provided next in chapter 4.

# Chapter 4.

# Measurements of Zeta Potential on Natural Limestone Rock Samples: Impact of Rock Type, PDI concentration and Ionic Strength

## 4.1. Introduction

As outlined in the chapter 3, few studies have reported measurements of zeta potential in carbonates at conditions relevant to natural subsurface systems. Most have explored synthetic calcite and dilute electrolytes with much lower total ionic strength and PDI concentration than subsurface brines. Moreover, most did not employ an experimental method that established equilibrium conditions of pH, $pCO_2$ and PDI concentration relevant to subsurface carbonates. PDIs (as discussed above) are those ions whose concentration in aqueous solution controls the polarity and magnitude of zeta potential, on the mineral surface (*Somasundaran and Agar*, 1967). The difference between sandstones and carbonates is that divalent ions (e.g. $Ca^{2+}$, $Mg^{2+}$ and $CO_3^{2-}$) are considered to be PDIs as they can alter the magnitude and polarity of the zeta potential; but not in sandstone where the zeta potential is only a function of the ionic strength and pH where $H^+$ and $OH^-$ are the PDIs.

The aim of this chapter is to report new measurements of zeta potential relevant to natural systems, with a particular emphasis on determining (i) the relationship between pH and pPDI ($Ca^{2+}$ and $Mg^{2+}$) in equilibrated calcite-electrolyte systems, given that no studies have measured pPDI whilst varying pH, or reported pH whilst varying pPDI, (ii) the effect of high concentrations of indifferent ions such as NaCl on the sensitivity of the zeta potential to pPDI, (iii)

whether $SO_4^{2-}$ is a PDI for the calcite mineral, and (iv) how the zeta potential is affected by pPDI over the concentration range found in natural brines. Only *Alroudhan et al.,* (2016) have probed this parameter space, and they used only a single rock type. Here we investigate two further natural carbonates to determine whether the results are rock-type specific.

We used the SPM described by Jackson and co-workers (*Jaafar et al.*, 2009; *Vinogradov et al.*, 2010; *Jackson et al.*, 2011; *Jackson and Vinogradov*, 2012; *Alroudhan et al.*, 2016) to measure the zeta potential. The SPM is applicable to intact natural samples, can be used to measure zeta potential at high ionic strength (> 2M), and can also be used during multiphase flow and at elevated temperature (*Jaafar et al.*, 2009; *Vinogradov et al.*, 2010; *Vinogradov and Jackson*, 2011; *Jackson and Vinogradov*, 2012; *Al Mahrouqi et al.*, 2015; *Alroudhan et al.*, 2016). The SPM measurements were complemented by chemical analysis of the effluent electrolyte, to monitor adsorption/desorption of ionic species during the experiments. The results have broad application to earth engineering processes such as hydrocarbon production and geological $CO_2$ storage, and we use them here to investigate the mechanisms that underpin the use of controlled injection brine compositions during waterflooding of hydrocarbon reservoirs (reported in chapter 2).

## 4.2. Methodology

### 4.2.1. Materials and Sample Preparation

We used two intact natural carbonate core samples that in x-ray diffraction (XRD; Appendix B) analysis appear to be mineralogically identical pure limestone that differ only in age and permeability (Table 4-1). Also shown in Table 4-1 are the properties of the Portland Limestone samples investigated by *Alroudhan et al.,* (2016), which we compare to the new results presented here when possible. The brines used were synthetic solutions of reagent-grade NaCl, $CaCl_2.2H_2O$, $Na_2SO_4$ and $MgCl_2.6H_2O$ salts (Sigma Aldrich, UK) in deionized water (DIW) from a filtered

system with electrical conductivity below 1 μS/cm. Table 4-2 lists the compositions of the electrolytes used, including synthetic formation brine (denoted FMB) typical of oil reservoirs and deep saline aquifers (e.g. *Romanuka et al.*, 2012), seawater (denoted SW) and different compositions derived from seawater; the seawater was twice (2dSW), ten times (10dSW), and twenty times (20dSW) diluted, and also had $SO_4$ added to yield twice (SW2S), three times (SW3S), and four times (SW4S) the concentration.

**Table 4-1: Properties and mineralogy of rock samples used in this study**

| Property/rock | Ketton | Estaillades | Portland |
|---|---|---|---|
| **Description** | Middle Jurassic Oolitic limestone from UK | Upper Cretaceous limestone from France | Upper Jurassic Ooparite limestone from UK |
| **Porosity** | 23% ±0.5 | 28% ±0.5 | 20% ±0.5 |
| **Permeability** | 1.4 darcy ±0.4 | 0.13 darcy ±0.02 | 0.005 darcy ±0.001 |
| **Intrinsic Formation Factor ($F_0$)** | 13.87 ±0.5 | 12.92 ±0.5 | 22.04 ±0.5 |
| **Compositions** | 97% calcite ($CaCO_3$)<br>3% magnesium* | 97% calcite ($CaCO_3$<br>3% magnesium* | 96.6% calcite ($CaCO_3$)<br>3.4% quartz |
| **Dimensions** | Length (L) =0.076 m<br>Diameter (D) =0.038 m | Length (L) =0.076 m<br>Diameter (D) =0.038 m | Length (L) =0.076 m<br>Diameter (D) =0.038 m |

***Magnesium ($Mg^{2+}$) is likely incorporated into the calcite structure as $MgCO_3$ or $CaMg(CO_3)_2$**

**Table 4-2: Properties and composition of brines used in chapter 4**

| Ions (M/L) | FMB | SW | SW2S | SW3S | SW4S | 2dSW | 10dSW | 20dSW |
|---|---|---|---|---|---|---|---|---|
| **Ions** | **Mol/l** | | | | | | | |
| $Na^+$ | 2 | 0.550 | 0.596 | 0.644 | 0.692 | 0.298 | 0.0596 | 0.0275 |
| $Cl^-$ | 3.020 | 0.620 | 0.618 | 0.618 | 0.618 | 0.309 | 0.0618 | 0.031 |
| $Ca^{2+}$ | 0.420 | 0.014 | 0.014 | 0.014 | 0.014 | 0.007 | 0.0014 | 0.0007 |
| $Mg^{2+}$ | 0.091 | 0.045 | 0.045 | 0.045 | 0.045 | 0.0225 | 0.0045 | 0.00225 |
| $SO_4^{2-}$ | 0.002 | 0.024 | 0.048 | 0.072 | 0.096 | 0.012 | 0.0024 | 0.0012 |
| $HCO_3^-$ | 0.005 | 0.001 | 0.001 | 0.001 | 0.001 | 0.005 | 0.0001 | 0.00005 |
| **Ionic strength (*IS*)** | 3.542 | 0.750 | 0.822 | 0.894 | 0.966 | 0.375 | 0.075 | 0.0375 |
| **pH** | 6.2 | 7.4 | 7.5 | 7.5 | 7.5 | 7.9 | 8.2 | 8.2 |

***** $Cl^-$ and $HCO_3^-$ concentrations are calculated using ion balance approach.**

The equilibrium condition of carbonate/electrolyte/$CO_2$ discussed previously in chapter 3 (see Figure 3-11) was replicated following the approach of

*Alroudhan et al.,* (2016). NaCl electrolytes of varying concentrations (0.05 – 5M) were equilibrated by leaving offcuts of the tested carbonate samples in a closed beaker containing an air gap to allow $CO_2$ to dissolve into solution, replicating the open-system conditions of carbonate deposition (*Stumm and Morgan*, 2012). The pH of the NaCl electrolyte (measured using a Five-Go Mettler-Toledo pH meter with their 3-in-1 pH electrode LE438, implementing where necessary the manufacturer's recommended calibration and correction procedures at high ionic strength) and $Ca^{2+}$ concentration (measured using Inductively Coupled Plasma Atomic Emission Spectroscopy, ICP-AES) were monitored until both reached constant value within experimental error. The equilibrium pH was found to be 8.3±0.1 for both Ketton and Estaillades, and the equilibrium pCa was found to be 2.8±0.1 and 3.1±0.1, respectively. The equilibrated NaCl solutions were termed NaCl-EQ and were then used directly in zeta potential measurements, or were modified by addition of $Ca^{2+}$, $Mg^{2+}$ and/or $SO_4^{2-}$.

Before SPM experiments begin, samples were cleaned using a standard cleaning procedure. Briefly, 50:50 toluene/methanol mixtures were used for virgin samples for 24 h prior flushing with methanol for another 24 h. Then, the cleaned samples were dried in vacuum chamber at 80$^{o}$C for 48 h prior saturating with the tested electrolyte concentration. To ensure the sample is cleaned properly and brought back to the original condition, a SPM experiment (using only NaCl-EQ brine) is always conducted before adding any PDI concentration. For samples that have been used in PDIs-SPM experiments, a special cleaning method was used as reported in *Alroudhan et al., (2016)*. This involves flushing the sample with 2 pore-volumes (PV) of deionized water (DIW) prior standard cleaning procedure. Then the cleaned saturated sample was flooded with another 4-5 PVs using 0.05M NaCl-EQ electrolyte. The conductivity of the effluent electrolyte was used as a measure for a successful cleaning, which should be within 5% tolerance compared to the original value obtained on the fresh sample using the same electrolyte. The experimental apparatus, used in this study, to measure streaming potential is the same as described in *Jaafar et al.,* (2009) (Figure 4-2).

Figure 4-1 shows the steps in single phase streaming potential experiments, leading to measurements of zeta potential, including rock-brine-$CO_2$ equilibration and sample cleaning procedures.

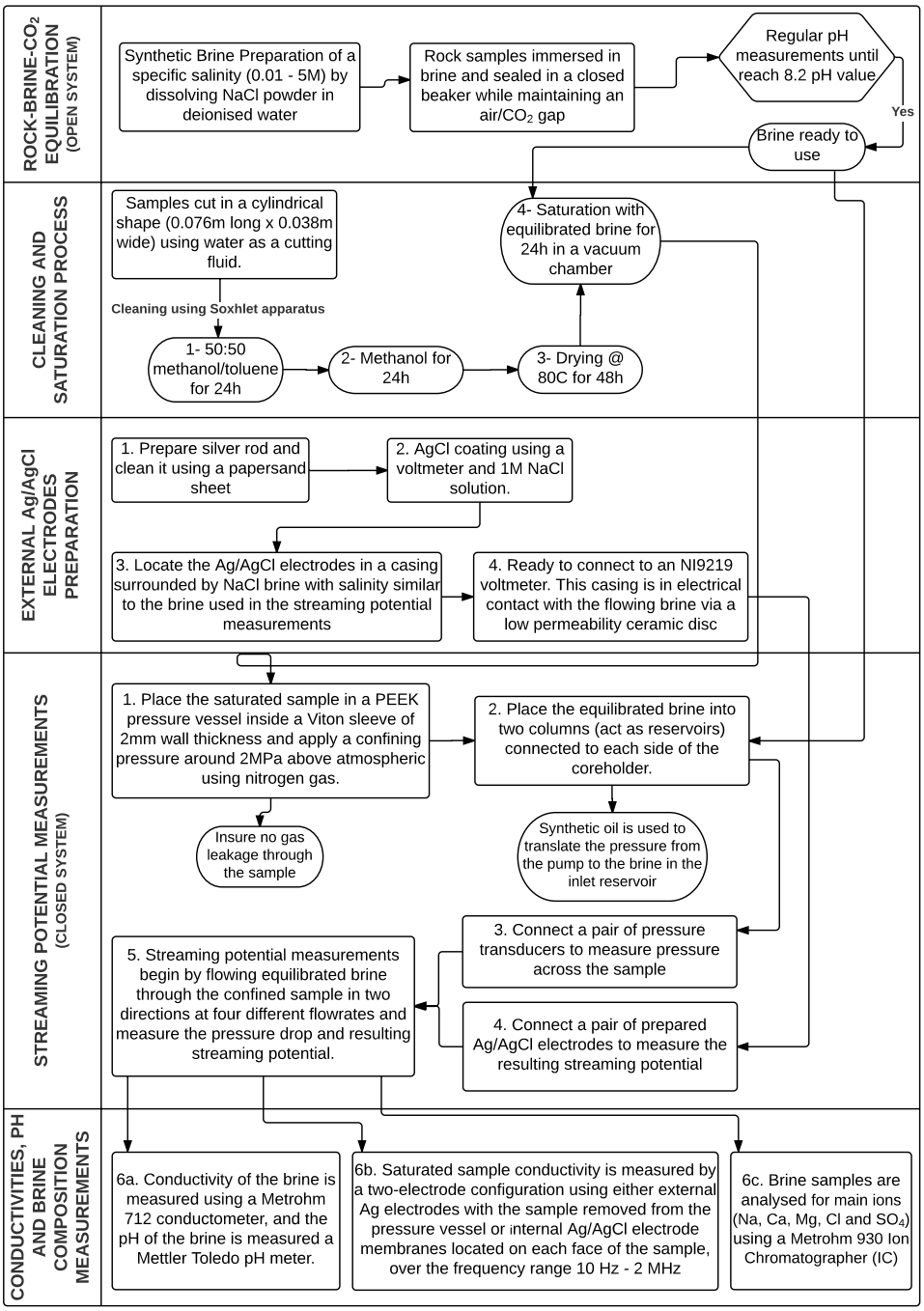



**Figure 4-1: A flowchart showing all steps conducted during streaming potential experiments on natural carbonates samples including brine and sample preparation, streaming potential measurements technique and brine composition measurements.**

### 4.2.2. Measurements of Streaming Potential Coupling Coefficient Using the Streaming Potential Method (SPM)

The apparatus used to measure streaming potential coupling coefficient and interpret zeta potential in our SPM is closed to the atmosphere, and the second stage of equilibration prior to measuring the zeta potential was to ensure equilibrium between the electrolyte of interest (NaCl-EQ with or without the addition of $Ca^{2+}$, $Mg^{2+}$ or $SO_4^{2-}$) and the rock sample at the closed-system conditions pertaining to a rock-brine system at depth. The carbonate core samples were confined within a Viton rubber sleeve of 2mm wall thickness embedded in a PEEK core holder with PEEK end caps. A Quizix QX-500 Stainless steel pump was used to induce a fluid pressure difference across the sample, causing brine to flow through the sample from reservoirs connected to each side of the core holder. Synthetic non-polar oil (MULTIPAR-H) was used to translate the induced pressure from the pump to the brine in the inlet reservoir, which maintains closed-system conditions. The use of synthetic oil allows air bubbles in the brine to be captured at the top of the oil layer in each reservoir, prevents exposure of brines to atmosphere and reduces corrosion of the pump. The pump maintains constant rate to high accuracy (with a maximum inlet pressure of 3.4 MPa, a minimum flowrate of 0.1 ml/min and a maximum of 500 ml/min) and flow can be directed in either direction through the sample by adjusting the flow valves (Figure 4-2). The repeated flow of the electrolyte through the sample at closed system conditions mimics migration of the electrolyte into the carbonate rock at depth. At regular intervals, the electrical conductivity and pH of the electrolyte in the reservoirs was measured, and equilibrium was assumed to have been reached when the conductivity and pH of the electrolyte in each reservoir differ by <5%. A minimum flowrate of 125ml/min was used for the high preamble core sample (Ketton) whereas a minimum of 10ml/min was applied for the lower permeability core sample (Estaillades). In general, 70kPa pressure gradient across the sample is sufficient to generate a recordable streaming potential.

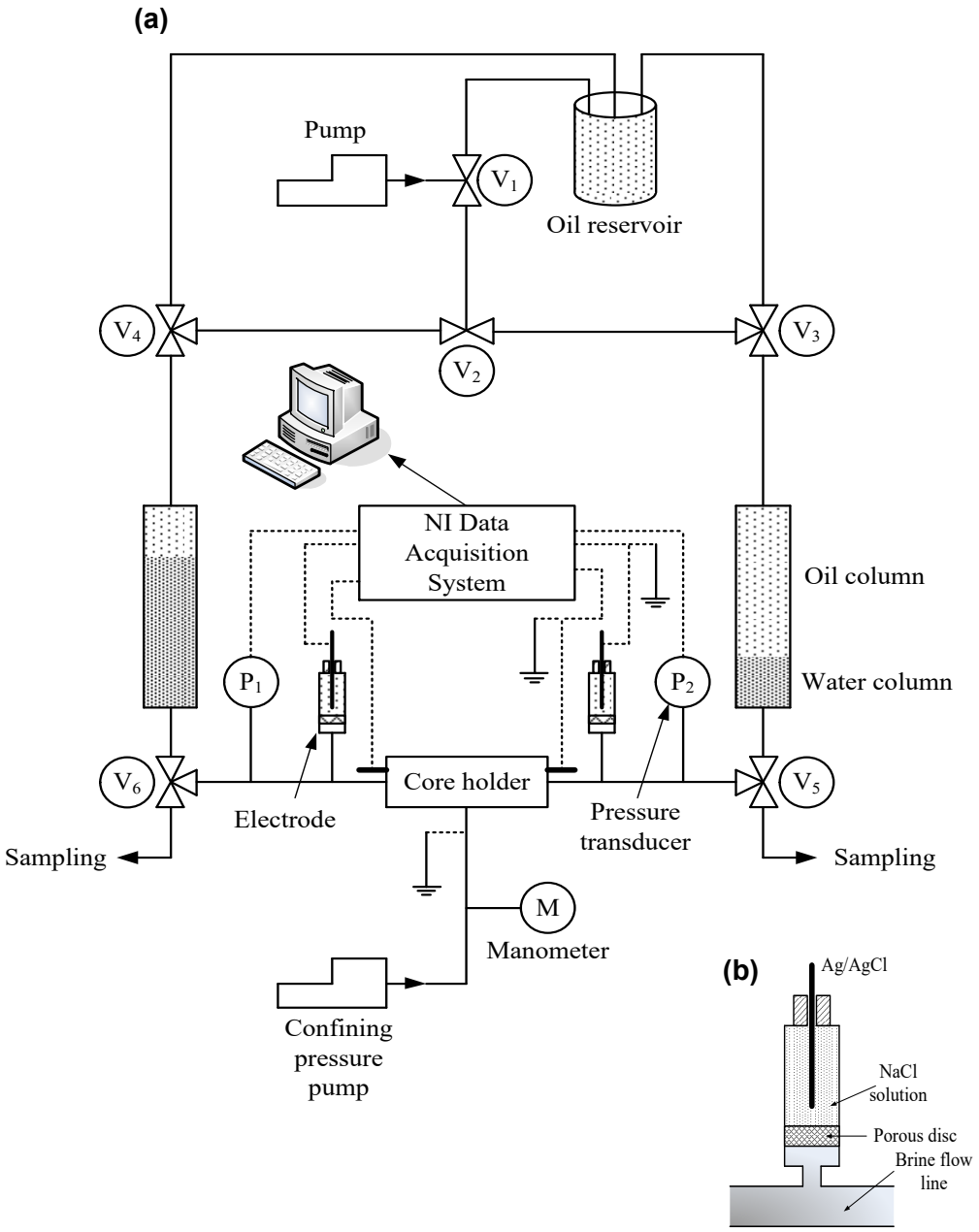



**Figure 4-2: Experimental apparatus for measuring streaming potential coupling coefficient. (a) shows pressure vessel (core holder), brine reservoirs where synthetic oil is used as a hydraulic fluid, flowlines (solid lines) connecting brine reservoirs with core holder, pressure transducers and externa electrodes and electrical connections (dashed lines). Pressure and voltage are recorded in LabVIEW using NI data acquisition system. In (b) a schematic showing the configuration of Ag/AgCl external electrode used to measure the streaming potential across the sample. Adapted from *Jaafar et al.*, 2009.**

The pressure difference across the sample was measured using a pair of Druck PDCR 810 pressure transducers (accuracy 0.1% of measured value, resolution 70 Pa) and the voltage across the sample was measured using non-

polarizing Ag/AgCl electrodes and a National Instruments an NI9219 voltmeter (internal impedance >1 GΩ, accuracy 0.18%, resolution 50 nV) (Figure 4-2).

The noise level of the measurements is dictated by the stability of the electrodes, rather than the performance of the voltmeter. To ensure that exclusion-diffusion potentials (e.g. *Revil*, 1999; *Leinov and Jackson*, 2014) were eliminated during measurements of the streaming potential, uniform and constant brine conductivity and pH in each reservoir, and uniform and constant temperature (23°C), were maintained within a 5% tolerance. Redox potentials were minimized by ensuring that the Ag/AgCl electrodes were the only metal in contact with the samples and brine.

SPM experiments began with equilibrium runs to equilibrate Ag/AgCl electrodes with the brine inside the electrode's case. The equilibrium runs stopped when the variation in static voltage (voltage at zero flow), $V_{static1}$ <5 μV. The first measurement of streaming coupling coefficient started by setting the Quizix pump to induce a pressure difference across the sample at constant flow rate. Both pressure and voltage were then recorded in LabVIEW using NI data acquisition system. The flow was stopped when stabilized values of pressure and voltage are reached with a variation of <10 μV and <5kP, respectively. The system was then allowed to relax back to a static mode and a second static voltage was measured, $V_{static2}$. Then, the flow was induced through the sample in opposite direction at the same rate until pressure and voltage stabilized with a variation of <10 μV and <5kPa, respectively. The system was allowed to relax and a third static voltage was recorded (e.g. Figure 4-7a,c).

This method is termed ''paired stabilization - PS''. The same workflow was repeated for different flow rates and stabilized voltages and pressure differences are recorded (Figure 4-7b,d). The voltage change is checked to have the same magnitude but opposite polarity in response to flow in each direction, confirming that electrode polarization effects are small (e.g., *Ball and Fuerstenau*, 1973) and that the measured electrical potential corresponds to the streaming potential.

Finally, a brine effluent sample was taken from a point straight after the core holder and the brine conductivity and pH and the conductivity of saturated samples were measured.

### 4.2.3. Measurements of Brine Conductivity, Brine Viscosity and Brine Permittivity

The conductivity of the brine was measured using a Metrohm 712 conductometer.

The brine viscosity was calculated by relating the brine conductivity to salinity and then relating salinity to viscosity using the approach of *Vinogradov et al.,* (2010) (Figure 4-3a, b). In this approach, we used the empirical correlation of *Worthington et al.,* (1990) for low brine conductivity (<1 S $m^{-1}$) because it shows a good agreement with published data in the CRC Handbook of Chemistry and Physics (*Weast et al.*, 1989) and *Sen and Goode,* (1992). For high brine conductivity (>1 S $m^{-1}$), the expression of *Worthington et al.,* (1990) fails and shows significant differences with published data (*Weast et al.*, 1989; *Sen and Goode*, 1992); therefore, we used a new polynomial function (4.14) of the same order as that suggested by *Worthington et al.,* (1990) fitted to published data in *Weast et al.,* (1989) and *Sen and Goode,* (1992)

$$C_f = 5.9738x10^{-7}\sigma_f^6 - 3.5136x10^{-5}\sigma_f^5 + 7.823x10^{-4}\sigma_f^4 - 8.0334x10^{-3}\sigma_f^3 + 4.0791x10^{-2}\sigma_f^2 + 3.4996x10^{-2}\sigma_f + 3.6104x10^{-2} \quad (4.1)$$

where $C_f$ is the brine salinity in M and the brine conductivity $\sigma_f$ is in S $m^{-1}$. Then, we calculated the brine viscosity at 23°C as a function of salinity by linearly interpolating the measured data at 20°C reported by *Weast et al.,* (1989) and that at 25°C reported by *Zhang and Han,* (1996) to yield values at 23°C (Figure 4-3c).

The electrical permittivity was calculated as a function of brine salinity using the correlation suggested by *Malmberg and Maryott,* (1956) and used by *Revil et al.,* (1999).

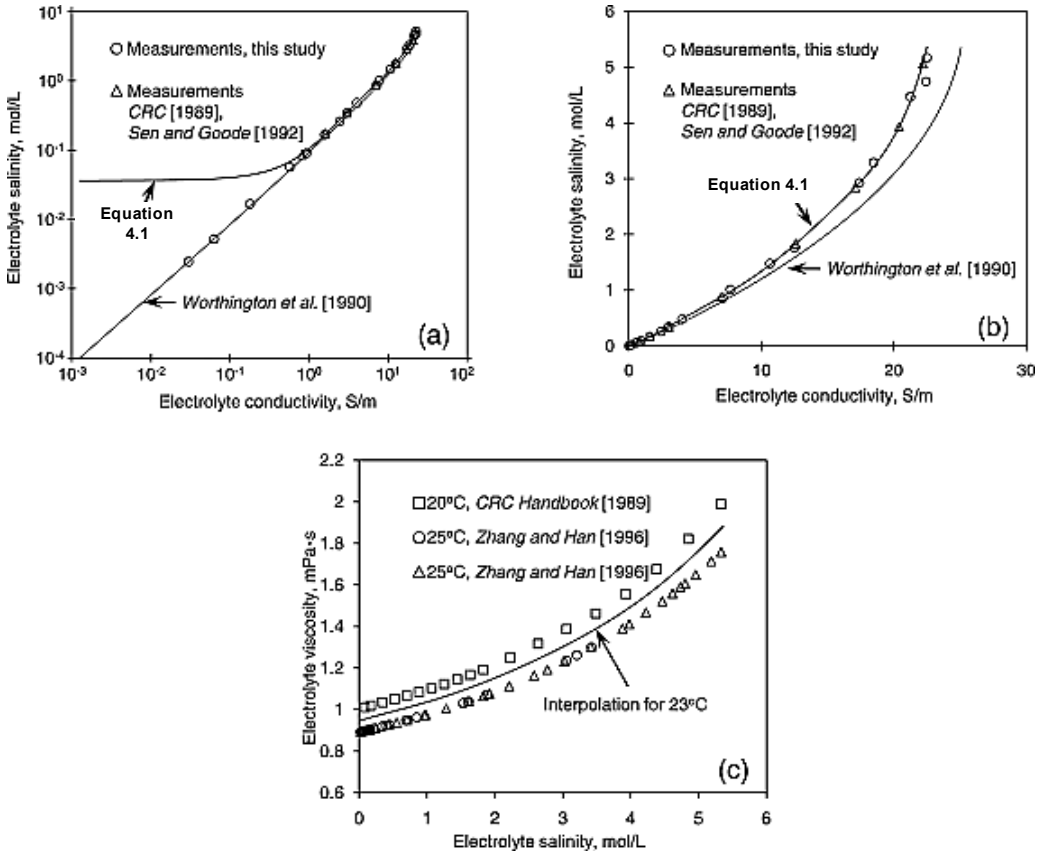



**Figure 4-3: The relationship between brine salinity and brine conductivity (a and b) and between brine viscosity and brine salinity (c). In (a) and (b), the expression using equation 4.1 is shown against that of *Worthington et al.,* (1990) and published data in the CRC Handbook of Chemistry and Physics (*Weast et al.*, 1989) and *Sen and Goode,* (1992). The data plotted in (a) log-log scale and (b) linear scale. In (c), the linear interpolation at 23°C between the two expressions is shown as solid line. After *Vinogradov et al.,* (2010).**

### 4.2.4. Measurements of Saturated Rock Conductivity

The saturated rock conductivity $\sigma_{rf}$ was measured at the end of each experiment in order to account for the effect of enhanced electrical conductivity through the EDL and calculate the formation factors (intrinsic $F_0$ and apparent $F_a$; see equation 3.12). We used a two external Ag/AgCl electrode configuration (with the sample removed from the pressure vessel) over the frequency range 10 Hz to 2 MHz on a QuadTech7600 Precision LCR meter instrument. The instrument computed the measured frequency *f* (in Hz) the corresponding total impedance *Z* (in ohm), and the resistance $R_s$ (in ohm) at each frequency value (e.g. Figure 4-4).

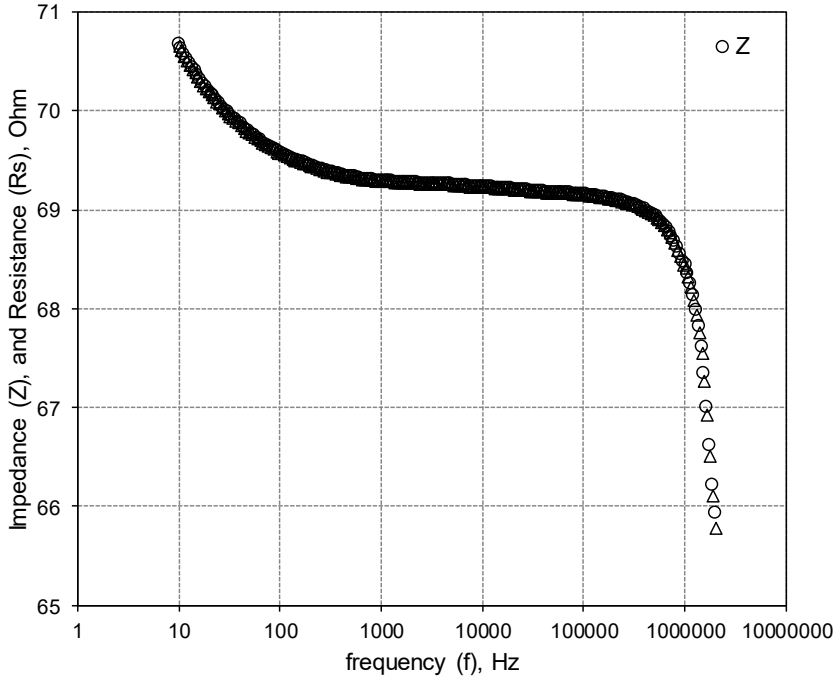



**Figure 4-4: The measured impedance and electrical resistance of 2M NaCl saturated sample of the Estaillades limestone as a function of the frequency range 10 Hz-2 MHz.**

These parameters allowed the resulting reactance *X* (in ohm) to be calculated as a function of the resistance $R_s$ (e.g. Figure 4-6),

$$X = \sqrt{(Z^2 - {R_s}^2)} \tag{4.2}$$

The value of measured resistance *R* that corresponds to the minimum reactance is taken to be the resistance of the sample to direct current (e.g. Figure 4-5). The saturated rock conductivity $\sigma_{rf}$ was then calculated using

$$\sigma_{rf} = \frac{L}{R\pi r^2} \tag{4.3}$$

where *L* is the length of core sample (m) and *r* is the sample's radius (m).

This method was used in the single phase (only brine; this chapter) and the multiphase (brine and oil) experiments (chapters 6 and 7). For the elevated temperature experiments (chapter 5), an internal Ag/Ag/Cl electrodes attached to the end of sample faces were used (see Figure 5-1b), and the saturated rock conductivity was measured inside the oven without removing the sample from the pressure vessel. This was done using the same QuadTech7600 Precision LCR

meter (remains outside oven) and the internal electrodes (inside the oven) were connected to the LCR meter using copper coaxial cables.

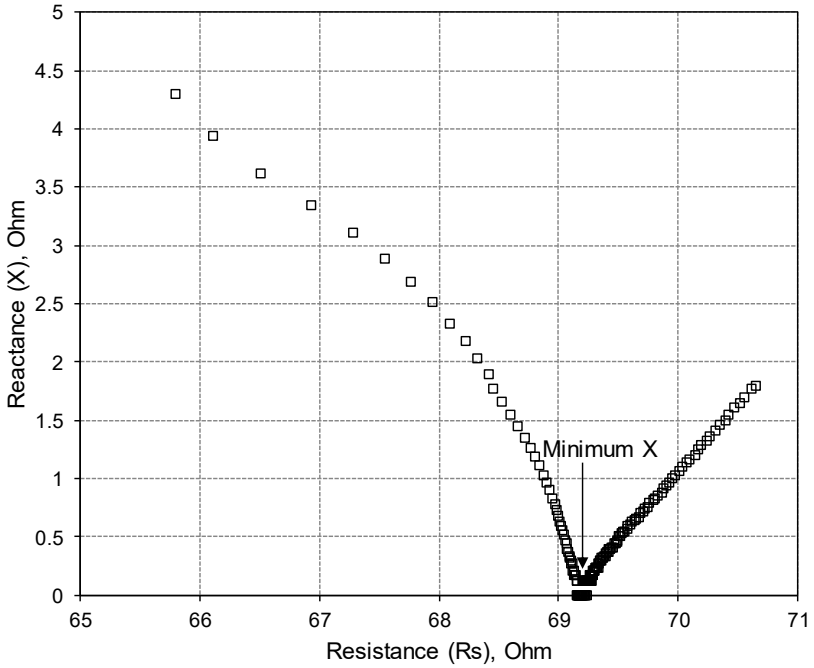



**Figure 4-5: The calculated reactance (*X*) as a function of the meausred electrical resistance of 2M NaCl saturated sample of the Estaillades limestone. The minimum reactance corresponds to resistance (R) of 69.15 ohm.**

### 4.2.5. Measurements of the Intrinsic Formation Factor

The intrinsic formation factor (as discussed in section 3.2.2.2) is essential to account for the effect of enhanced electrical conductivity through the EDL, especially at low ionic strengths (<0.1M), when calculating the zeta potential as shown in equations (3.12) and (3.13). It is also an important property to correct for zeta potential measurements at elevated temperature as will be shown in chapter 5. The intrinsic formation factor $F_0$ is unique for each rock type and obtained from the linear regression between electrical conductivities of fluid $\sigma_f$ and fluid-saturated rock ($\sigma_{rf}$); typically, at high ionic strengths (e.g. Figure 4-6).

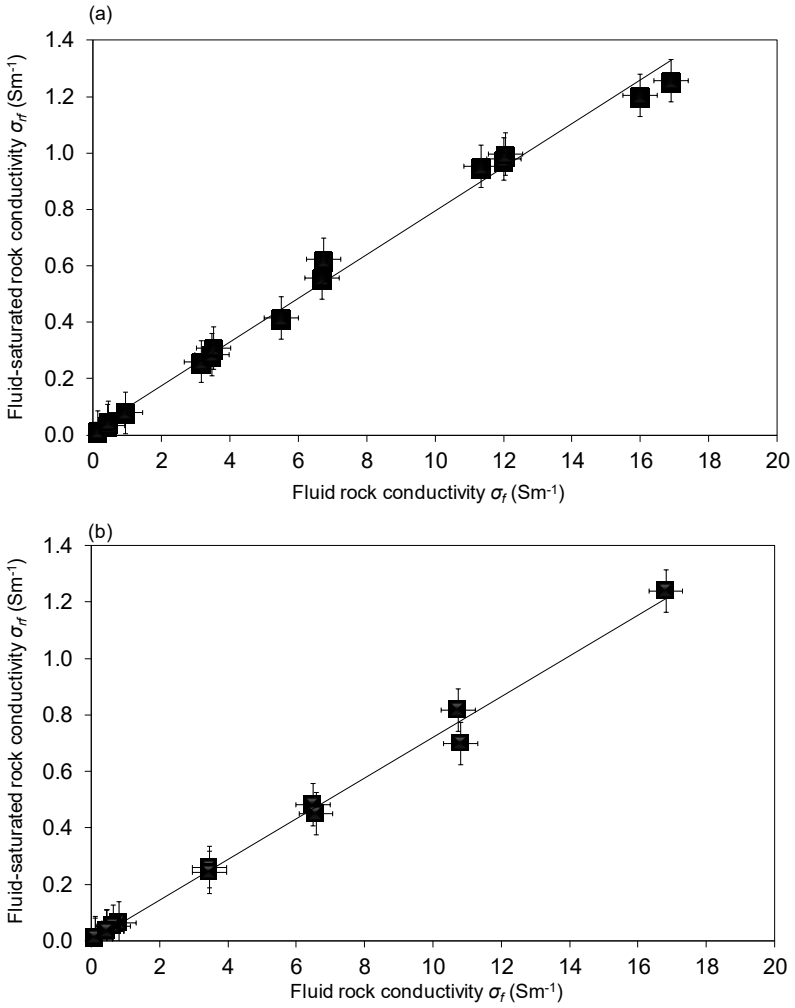



**Figure 4-6: Saturated sample conductivity of (a) Ketton and (b) Estaillades samples versus NaCl-EQ brine conductivity. One linear regression can be fitted through all points and the reciprocal of the slope yields the intrinsic formation factor, which is used in equation (3.13).**

Figure 4-6 shows that the data follows linear trend even at brine conductivities <1 S m$^{-1}$, which indicates that the bulk conductivity always dominates in the range of salinities used in this thesis (≥ 0.01M). *Vinogradov et al.,* (2010) showed that the trend between electrical conductivities of fluid and fluid-saturated rock levels off at brine conductivities <0.4 S m$^{-1}$ (equivalent to 0.036 M). In carbonates, we did not observe this levelling off (Figure 4-6a,b). Including all data, we calculated the intrinsic formation factor $F_0$ as the reciprocal of the slope of the linear regression through the data. Values of $F_0$ for the three carbonate rock types investigated here are reported in Table 4-1.

### 4.2.6. Interpretation of the Zeta Potential

The zeta potential was calculated from the measured streaming potential coupling coefficient, electrical conductivities, brine permittivity and dynamic viscosity using either equation (3.12) or (3.13). Both equations yield the same zeta potential value. It is noted that the interpreted value using these equations is the corrected zeta potential, which varies slightly (< 2 mV) from the interpreted value using well known Helmholtz Smoluchowski equation (3.14) (see Table E-1 in Appendix E).

Recall that the SPM approach is only valid when pore sizes are much larger than the width of the diffuse layer (given by the inverse of the Debye length; $\kappa^{-1}$). The pore size distribution for the three investigated carbonate samples here (Ketton, Estaillades and Portland) was studied previously by Blunt and co-workers in Imperial College (refer to *Nayef*, 2015). Three different methods were used to derive the pore size distribution against normalized frequency: (1) nuclear magnetic resonance (NMR), (2) mercury injection capillary pressure (MICP) and (3) pore scale modelling (PSM) (see Figure 2.12 in *Nayef*, 2015). Their results showed that the pore throat sizes range 0.01 to 50 μm in the Estaillades limestone; 0.01 to 100 μm in the Ketton limestone and 0.01 to 10 μm in the Portland limestone.

At ambient temperature ($T = 295.15\ K$), the Debye length $\kappa$ (using equation 2.1; $\kappa = 56.2\sqrt{IS/T}$) varies between 0.328 $nm^{-1}$ in the lowest investigated ionic strength (0.01M) and 7.315 $nm^{-1}$ in the highest investigated ionic strength (5M); and $\kappa r$ ranges from 3.271 in the smallest pore in 0.01M to 731,476 in the largest pore in 5M ionic strength. Therefore, we conclude that the relationship $\kappa r \gg 1$ is valid in all pores and thus equations (3.12) and (3.13) may be used.

### 4.2.7. Measurements of Electrolyte Composition

Electrolyte samples were analysed before and after the SPM experiments for key ions ($Na^+$, $Ca^{2+}$, $Mg^{2+}$ and $SO_4^{2-}$). We used ICP-AES for cations and Ion Chromatography (IC) for anions with appropriate dilution where necessary. The

ICP-AES analysis was carried out in the Analytical Chemistry Laboratory at the Natural History Museum London; the IC analysis was carried out in the TOTAL Laboratory for Reservoir Physics at Imperial College London. Instrument error was determined by using certified solutions containing $Na^+$, $Ca^{2+}$, $Mg^{2+}$ and $SO_4^{2-}$ and the error calculated from the standard deviation of five repeat measurements of each solution. The errors revealed to be quite small; 3.5% for $Ca^{2+}$ and $Mg^{2+}$, 3% for $Na^+$ and 0.5% for $SO_4^{2-}$. These errors are not changed with background salinity as all samples were diluted to a measurable range prior to analyses. Therefore, applying these error percentages to real salinity values will show small concentration error bars at high salinity and large error bars at low salinity.

### 4.2.8. Design of Experiments

We conducted three sets of experiments. In the first, the sensitivity of zeta potential to variations in NaCl concentration was tested using the equilibrated NaCl-EQ solutions described above. In these experiments, the concentration of $Ca^{2+}$, $Mg^{2+}$ and $SO_4^{2-}$ was dictated by the equilibration process; no additional salts containing these ionic species were added to the NaCl-EQ solutions. In the second, the sensitivity of the zeta potential to variations in $Ca^{2+}$, $Mg^{2+}$ and $SO_4^{2-}$ concentration was tested by adding salts containing these ionic species over the range found in natural brines (0.007 – 0.42M for $Ca^{2+}$ and $Mg^{2+}$; 0.002 – 0.096M for $SO_4^{2-}$) to NaCl-EQ solutions of two different ionic strengths (0.5M and 2M). The 0.5M NaCl concentration represents seawater and is similar to the 'ZP brine' of *Zhang and Austad,* (2006) and *Zhang et al.,* (2007), allowing direct comparison of results. The 2M NaCl concentration represents the saline brines found in many saline aquifers and hydrocarbon reservoirs (e.g. *Romanuka et al.*, 2012). In the second set of experiments, we investigated for the first time the relationship between pCa (or pMg) and pH. Note that in the experiments reported here, precipitation of salts such as $CaSO_4$ and $MgCO_3$ in the pore-space was prevented because each ion of interest ($Ca^{2+}$, $Mg^{2+}$ or $SO_4^{2-}$) was added to NaCl-EQ electrolyte containing only trace or zero concentration of cations or anions other

than Na and Cl. In the third, the sensitivity of zeta potential to varying multiple PDIs was tested using SW as a reference point. In one type of experiments, SW was twice (2dSW), ten times (10dSW), and twenty times (20dSW) diluted. In another type, $SO_4$ was added to SW to yield twice (2SW), three times (3SW), and four times (4SW) the concentration.

## 4.3. Results

Streaming potentials were measured using the paired-stabilization method of *Vinogradov et al.,* (2010) and typical raw results are shown in Figure 4-7a,c.

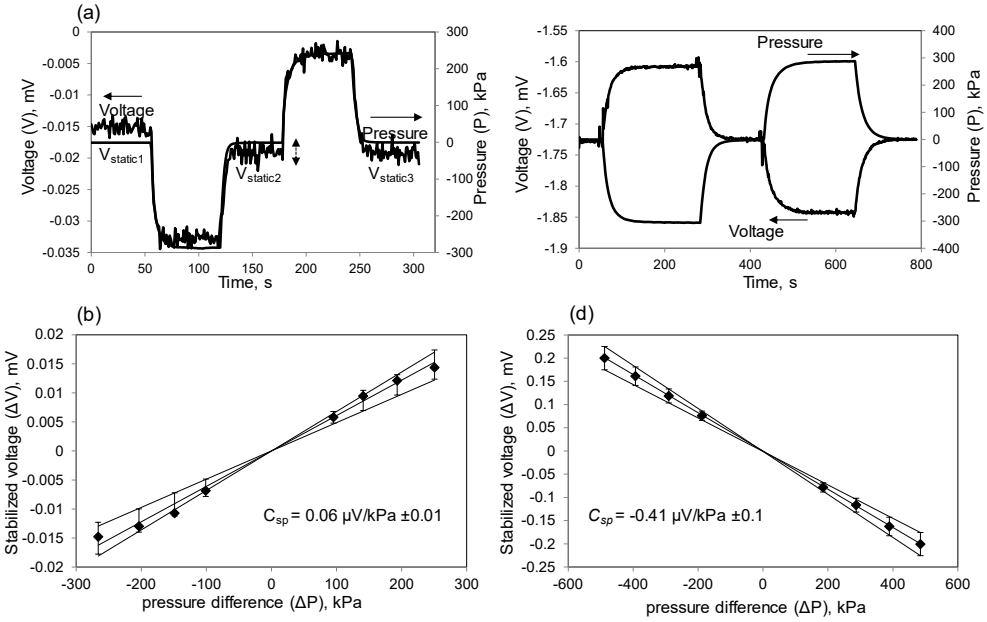



**Figure 4-7: Typical results from streaming potential measurements (SPM) experiments on natural carbonate samples. (a, c) show results for Ketton and (b, d) show results for Estaillades. In (a), injected brine is 0.5M NaCl-EQ with 0.28M Ca. In (c), injected brine is SW contains twice $SO_4$ concentration (SW2S) (b and d) show stabilized voltage against stabilized pressure difference for Ketton and Estaillades at four different flowrates. The error bars represent the voltage fluctuations around the stabilized value and the uncertainty in the reported $C_{sp}$ reflects the variability in the linear regression that can be forced through the data within experimental error.**

The stabilized voltage was plotted against the stabilized pressure difference across the sample for four different flow rates and a linear regression through the data yielded the streaming potential coupling coefficient (Figure 4-7b,d). The uncertainty in the streaming potential coupling coefficient arising from the range of

linear regressions that can be forced through the stabilized voltage and pressure data was used to determine the associated experimental error in zeta potential reported in the following sections.

### 4.3.1. Impact of $Na^+$ Concentration on Zeta Potential

We begin by reporting the effect of NaCl concentration on zeta potential. When possible, we compare results from the Ketton and Estaillades samples investigated here against the Portland sample studied by *Alroudhan et al.,* (2016). Figure 4-8a shows the zeta potential as a function of NaCl concentration (in M) for all three natural carbonate samples.

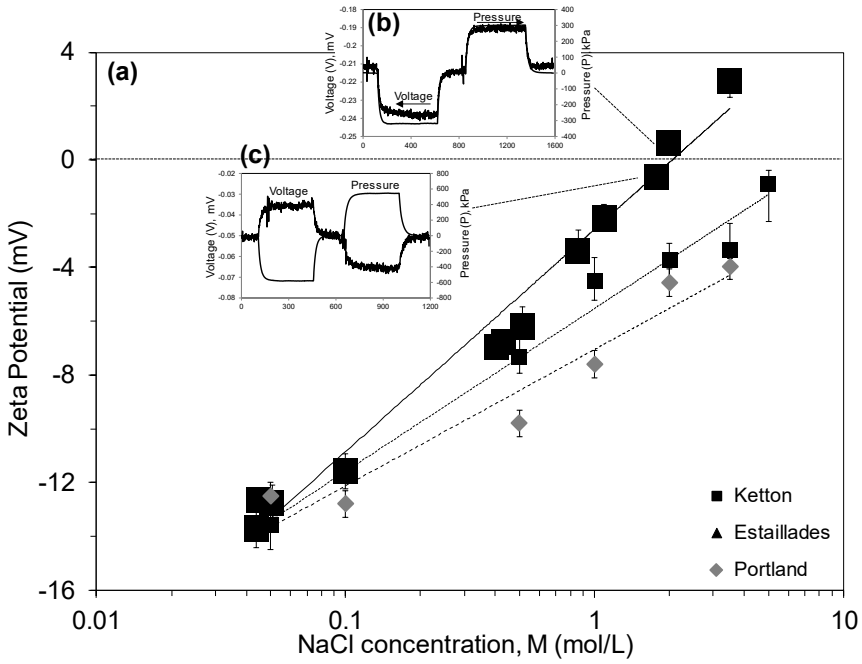



**Figure 4-8: Effect of NaCl concentration on zeta potential on the Ketton (squares) and Estaillades (triangles) samples.Data obtained on the Portland carbonate sample by Alroudhan et al. (2016) are shown for comparison (grey diamonds). The inset plots (b) and (c) show typical example measurements of voltage and pressure against time from the SPM used to determine the zeta potential. When pressure and voltage respond in the same sense the zeta potential is positive and vice-versa. The polarity of the zeta potential is accurately determined even when its value is close to zero.**

A linear regression can be fitted to the data from each rock type (with $R^2 > 0.97$) but the gradient of the regression differs between samples. The Estaillades sample (filled triangles) shows the highest gradient (-8.08 ± 0.52 mV/M) and the

Portland sample (filled grey diamonds) the lowest gradient (-5.08 ± 0.47 mV/M) with the Ketton sample (filled squares) in between (-6.11 ± 0.49 mV/M).

At low NaCl concentration (<0.1M) the zeta potential is negative and identical (within experimental error) for all three samples. However, as NaCl concentration increases, the zeta potentials diverge with $\zeta_{Portland} > \zeta_{Ketton} > \zeta_{Estaillades}$. Moreover, the zeta potential of the Estaillades samples becomes positive at NaCl concentration >1.9M, whereas the other two samples yield negative zeta potential over the entire concentration range investigated. The inset plots Figure 4-8b and Figure 4-8c show there is no ambiguity in the polarity of the zeta potential: for a NaCl concentration of 1.8M the streaming potential, and hence zeta potential, of the Estaillades sample is clearly negative (-0.56mV ± 0.33) and becomes positive (0.72mV ± 0.33) for a NaCl concentration of 2M. As discussed above, $Na^+$ and $Cl^-$ are believed to be indifferent ions to the calcite mineral surface and their presence is expected to affect the magnitude, but not the polarity, of the zeta potential.

### 4.3.2. Impact of $Ca^{2+}$, $Mg^{2+}$ and $SO_4^{2-}$ Concentration on Zeta Potential

We next investigate the impact of the concentration of the confirmed and suggested PDIs $Ca^{2+}$, $Mg^{2+}$ and $SO_4^{2-}$ on the zeta potential. We plot concentration as pPDI and, in all cases, the highest pPDI values reported correspond to the equilibrium concentrations in the NaCl-EQ electrolytes. Plotting PDIs concentration in this way is analogous to plotting the proton concentration as pH, although we do not account for the non-ideal nature of the electrolyte (i.e. we plot the negative logarithm of PDIs concentration rather than activity). Figure 4-9a shows the impact of pCa and pMg on the zeta potential of Estaillades, and the impact of pCa on the zeta potential of Ketton, for two different NaCl concentrations (0.5M and 2M) typical of subsurface brines; also shown for comparison are the data from Portland obtained by *Alroudhan et al.,* (2016).

We find that the zeta potential consistently becomes more positive with decreasing pCa or pMg. Moreover, the response to pCa and pMg is identical within

experimental error for the Estaillades carbonate, irrespective of NaCl concentration. *Alroudhan et al.,* (2016) also found that pCa and pMg behaved identically for the Portland carbonate, although they investigated a lower NaCl concentration of 0.05M and their data are not shown here.

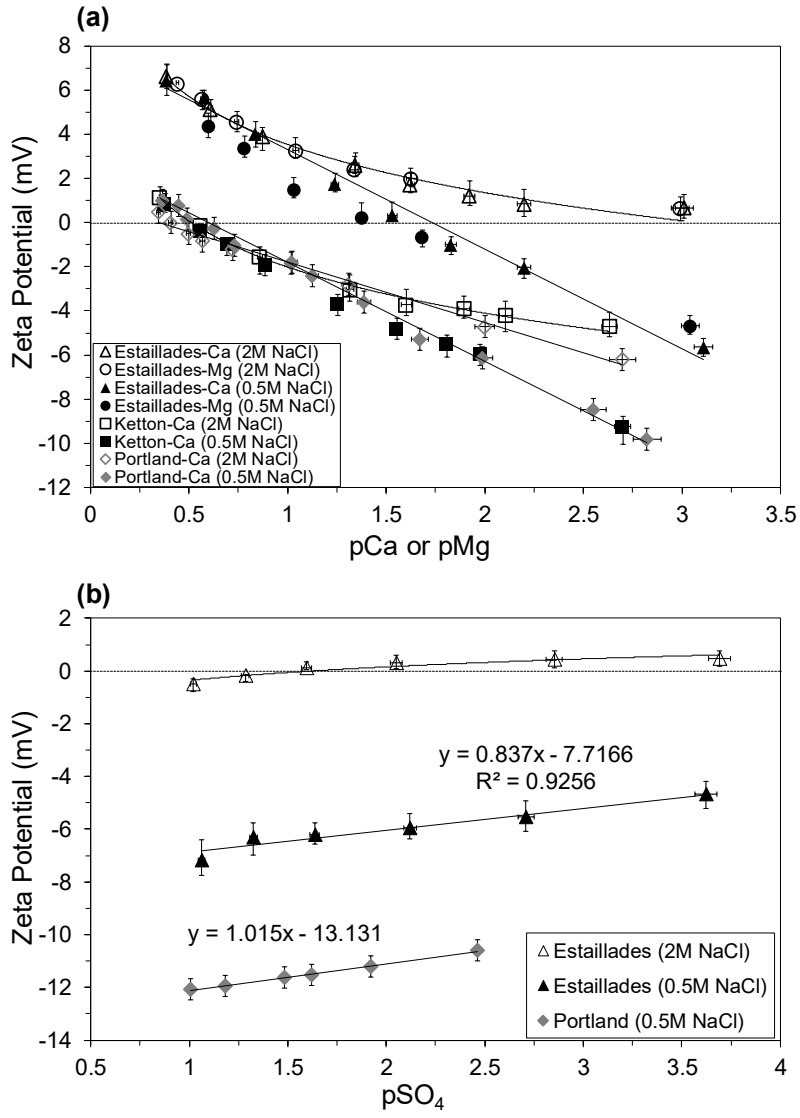



**Figure 4-9: Zeta potential versus (a) pCa and pMg, and (b) $pSO_4$ for the Ketton and Estaillades samples at different NaCl concentrations. Data obtained on the Portland carbonate sample by Alroudhan et al. (2016) are shown for comparison (diamonds).**

The response of the zeta potential to pCa or pMg is generally sample specific and depends on the NaCl concentration. At the lower (0.5M) NaCl concentration investigated here, Ketton and Portland exhibit identical behaviour over the entire pCa range investigated: a linear regression provides an excellent

fit to the data ($R^2 > 0.98$) with a gradient of -4.5±0.25 mV/decade and an $pCa_{IEP}$ of 0.5±0.03. A linear regression with the same gradient also provides an excellent fit to the Estaillades data at the lower NaCl concentration investigated; however, $pCa_{IEP}$ is much higher at 1.7±0.03. Nernstian (linear) behaviour is therefore always observed at the lower NaCl concentration over the entire pCa and pMg range investigated, but the IEP is different for the Estaillades sample. Fitting the Gouy-Chapman-Grahame model (equation 3.29) to these data yields $C_s$ = 1 $Fm^{-2}$ and $\Delta$ = 0.245 nm, similar to the values obtained for Portland carbonate by *Alroudhan et al.,* (2016) and within the range used by *Heberling et al.,* (2011).

At the higher (2M) NaCl concentration investigated here, the Ketton carbonate continues to show linear, Nernstian behaviour close to the IEP with a gradient and IEP identical to that obtained using 0.5M NaCl within experimental error, but the behaviour becomes non-linear (non-Nernstian) away from the IEP at high pCa. The Portland sample shows linear, Nernstian behaviour over the entire pCa range investigated with an identical IEP within experimental error but a lower gradient of -2.86±0.25 mV/decade. The Estaillades carbonate exhibits notably different behaviour, with the zeta potential remaining positive over the entire pCa/pMg range investigated, and non-Nernstian behaviour at high pCa. *Cicerone et al.,* (1992) also observed non-Nernstian behavior far from IEP and related that to variations in the Stern layer capacitance or to breakdown of the Gouy-Chapman-Grahame model.

Increasing $pSO_4$ consistently yields more positive zeta potential, although the sensitivity is much less than that observed when varying pCa or pMg (Figure 4-9b). A linear regression yields a good fit to the data at the lower NaCl concentration investigated here ($R^2 > 0.92$) with a consistent gradient of 0.84 ±0.2 mV/decade for both the Estaillades and Portland carbonates. A key feature is that an apparent IEP of $pSO_4$ = 1.59 is observed for the Estaillades sample in 2M NaCl electrolyte. It is also notable that the difference in absolute zeta potential between the different carbonate samples observed in Figure 4-8 persists in Figure 4-9, with $\zeta_{Portland} > \zeta_{Ketton} > \zeta_{Estaillades}$.

### 4.3.3. Relationship Between pH and pCa or pMg

Figure 4-10a shows the relationship between the equilibrium pH and pCa or pMg obtained across all of the experiments reported here.

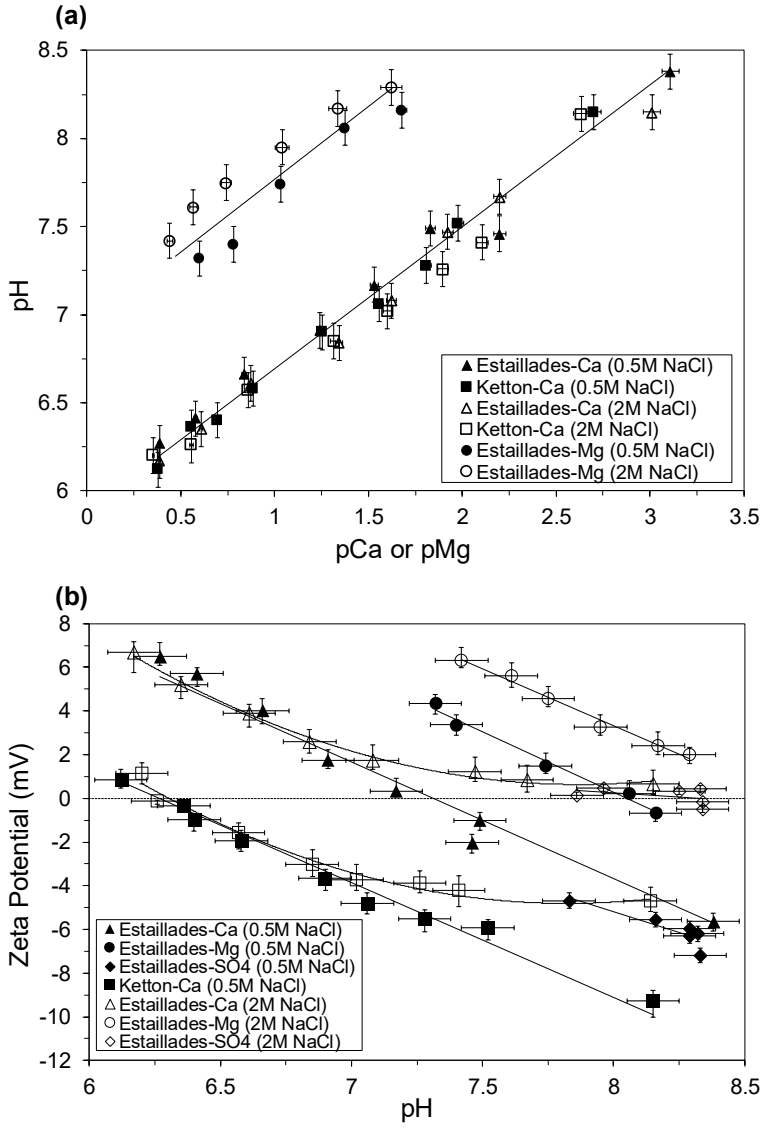



**Figure 4-10: Relationship between pH, pCa (or pMg) and zeta potential from the SPM experiments reported in this study. (a) Relationship between pH and pCa or pMg obtained from all the experiments shown in Figure 8, along with linear regressions to the data. (b) Data shown in Figure 4-9 replotted against pH using the linear regression shown in (a).**

A linear regression provides an excellent fit to the data ($R^2 > 0.98$) with a gradient of 0.81, irrespective of NaCl concentration, rock sample or PDI varied, although the value of pH is consistently higher in the experiments varying pMg as compared

to those varying pCa. These data confirm that equilibrium pH and pPDI are related at fixed $pCO_2$ via equations (3.24) – (3.28). It is possible to plot the data obtained here against pH and obtain an apparently strong correlation (Figure 4-10b) even though pCa and pMg were the controlled parameters.

### 4.3.4. Impact of Varying Multiple PDIs

Here, we report measurements of zeta potential on Estaillades and Ketton in electrolytes containing multiple PDIs ($Ca^{2+}$, $Mg^{2+}$ and $SO_4^{2-}$) at concentrations found in typical formation saline brines (FMB; Table 4-2) and sweater (SW; Table 4-2). FMB yields a positive zeta potential while SW yields a negative zeta potential (Figure 4-11a), and FMB is rich in Ca concentration whilst SW is rich in $SO_4$. Estaillades has larger magnitude of positive zeta potential in FMB (+7.13mV) and smaller negative value in SW (-1.48mV) compared to Ketton (+1.15mV in FMB and –5.83mV in SW).

We also investigate the effect of the two CSW approaches reported in chapter 2 (i.e. Bulk dilution of SW or addition of $SO_4^{2-}$ to SW) on zeta potential of Ketton and Estaillades rock samples. Figure 4-11b shows that modification of the SW composition by either lowering the ionic strength (bulk dilution) or increasing ionic strength (adding $SO_4^{2-}$) further increases the magnitude of the negative zeta potential in both carbonate samples. However, the rate of change of zeta potential with increasing ionic strength (through addition of $SO_4^{2-}$) is less than that observed with decreasing ionic strength (by dilution). It is noticed that the impact of $SO_4^{2-}$ on zeta potential is quite similar with or without the presence of other PDIs (compare Figure 4-9b and Figure 4-11b).

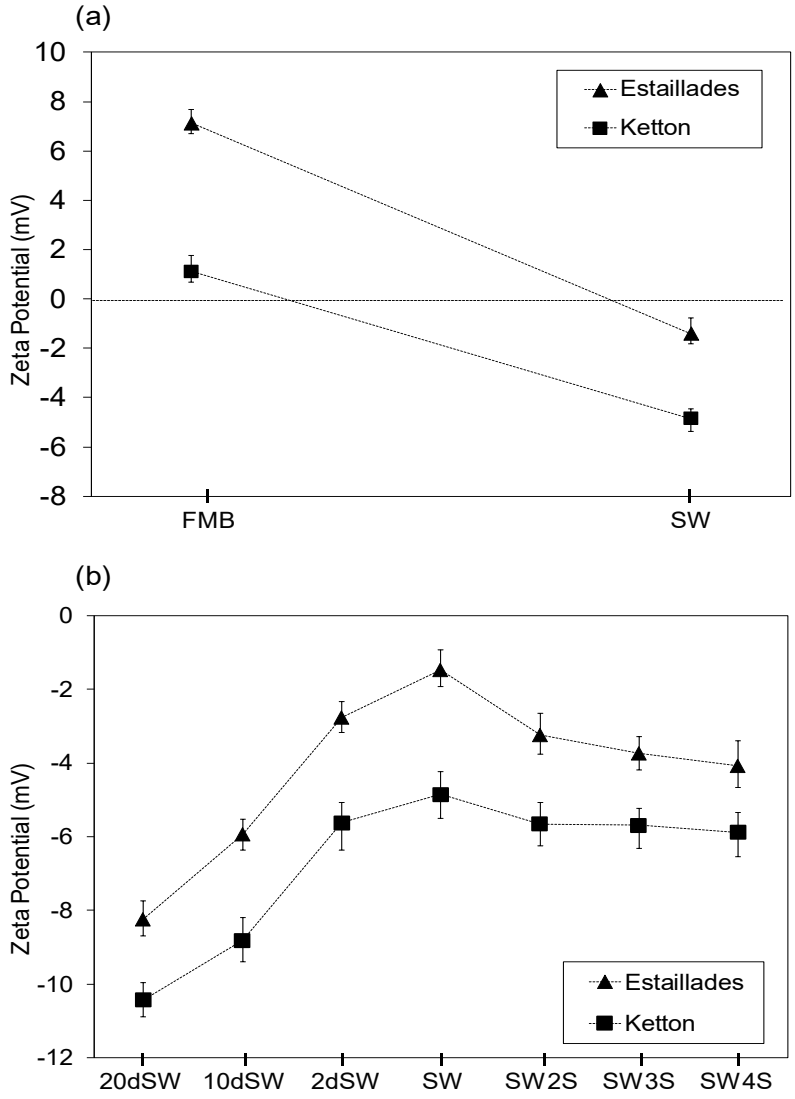



**Figure 4-11: Impact of formation brine (FMB), seawater (SW) and derived compositions from SW on zeta potential of Ketton and Estaillades (a) in FMB and SW and (b) by either varying $SO_4^{2-}$ concentration in SW up to four times, or bulk dilution of SW up to 20 times dilution.**

## 4.4. Discussion

### 4.4.1. Impact of Indifferent Ions

The results presented here show a clear relationship between the concentration of indifferent ions $Na^+$ and $Cl^-$ and the zeta potential on natural carbonate (Figure 4-8). Such a relationship is expected owing to collapse of the double layer with increasing ionic strength, but if double layer collapse is the only

control on zeta potential, then the zeta potential should be proportional to the logarithm of NaCl concentration (as a proxy for ionic strength; e.g. *Glover et al.*, 2012). Consequently, the dependence of zeta potential on NaCl concentration observed in Figure 4-8 cannot result only from double layer collapse. Figure 4-12 shows the equilibrium pCa and $pSO_4$ as a function of NaCl concentration, corresponding to the zeta potential data shown in Figure 4-8. Note that pMg remained large and approximately constant at 4.19±0.03 for all samples irrespective of NaCl concentration (i.e. the $Mg^{2+}$ concentration is small). pCa generally decreases with increasing NaCl concentration (Figure 4-12a); hence, given that zeta potential becomes more positive with decreasing pCa, these data are consistent with the more positive zeta potential observed with increasing NaCl concentration in Figure 4-8.

### 4.4.2. Impact of Carbonate Type

The results obtained here also show that natural carbonate samples that appear identical in XRD display different zeta potential behaviour. The Estaillades carbonate, in particular, behaves differently to the Ketton and Portland carbonates, showing inversion of the zeta potential with increasing NaCl concentration (Figure 4-8), higher values of $pCa_{IEP}$/$pMg_{IEP}$ compared to Ketton and Portland (Figure 4-9a), and also an apparent IEP expressed as $pSO_4$ (Figure 4-9b). The Estaillades carbonate released the least $SO_4^{2-}$ during equilibration with the NaCl solutions, while the Portland sample released the most $SO_4^{2-}$ (Figure 4-12b), consistent with the observed differences in zeta potential ($\zeta_{Portland} > \zeta_{Ketton} > \zeta_{Estaillades}$) in Figure 4-8 and Figure 4-9.

We hypothesize that Ketton and Portland contain undetected sources of $SO_4^{2-}$ which affects the pristine zeta potential, yielding more negative values and lower $pCa_{IEP}$ than Estaillades. Natural carbonates can incorporate a number of different minerals, including clays, organic matter, apatite, anhydrite or quartz, that yield a more negative zeta potential than pure calcite (*Smani et al.*, 1975; *Cicerone et al.*, 1992; *Somasundaran*, 2006).

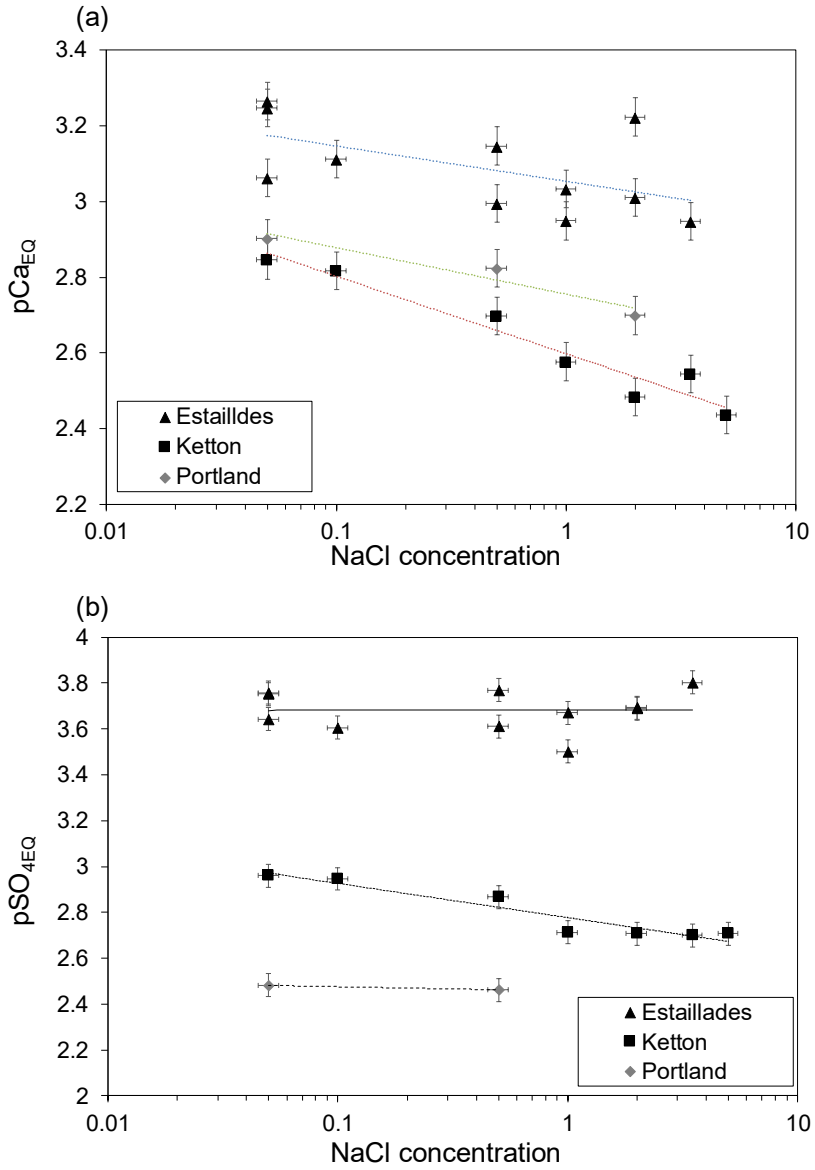



**Figure 4-12: Equilibrium pCa (a) and $pSO_4$ (b) versus NaCl concentration for the Ketton (squares) and Estaillades (triangles) samples. Data obtained on the Portland carbonate sample by Alroudhan et al. (2016) are shown for comparison (diamonds).**

The contrasting behaviour of Estaillades carbonate may also reflect differences in the affinity of $Ca^{2+}$ and $CO_3^{2-}$ for the mineral surface. *Pierre et al.,* (1990) suggested that the IEP is governed by the relative magnitude of the equilibrium constants $K_{Ca}$ and $K_{CO3}$ governing the adsorption of $Ca^{2+}$ and $CO_3^{2-}$ ions on the calcite mineral surface. The IEP shifts to lower pCa if $K_{CO3} > K_{Ca}$; that is, if the calcite surfaces show greater affinity for $CO_3^{2-}$ than $Ca^{2+}$. *Pierre et al.*

(1990) found the IEP differed for synthetic and natural calcite and argued that this reflected the differing affinity for $Ca^{2+}$ and $CO_3^{2-}$. The Pierre et al. model suggests that the Estaillades carbonate investigated here has a much lower affinity to $CO_3^{2-}$ (and greater affinity to $Ca^{2+}$) than the Ketton and Portland carbonates at equilibrium conditions.

A third plausible explanation for the differences in zeta potential behaviors between the three carbonates rocks investigated here could simply be the number of surface sites where surface complexes of calcium and carbonate are present. The number of surface sites per unit area (surface site density) is usually taken as 5 sites/$(nm)^2$ (*Davis and Kent*, 1990). However, *Hiorth et al.,* (2010) found that 2 sites/$(nm)^2$ gives much better fit to the experimental data (discussed in chapter 2) in their chemical model. The difference in the surface site density may reflect differences in the adsorption of $Ca^{2+}$ and $CO_3^{2-}$ or any divalent ions (e.g. $Mg^{2+}$ and $SO_4^{2-}$) on the mineral surface, which in turn affects the magnitude and polarity of zeta potential.

### 4.4.3. $SO_4$ as a PDI for Calcite

Several studies have suggested that the $SO_4^{2-}$ ion is a PDI for calcite (e.g. *Smallwood*, 1977; *Zhang and Austad*, 2006). However, these studies did not measure changes in pCa or pMg in response to changing $pSO_4$. Here we find that pCa systematically decreases in response to decreasing $pSO_4$ (Figure 4-13a), suggesting that calcium desorbs from the mineral surface as the concentration of $SO_4^{2-}$ in solution increases. Moreover, the zeta potential change in response to addition of $SO_4^{2-}$ correlates with the change in pCa (Figure 4-13b). Hence we suggest that $SO_4^{2-}$ is not a PDI for calcite; rather, it controls zeta potential only by triggering desorption of $Ca^{2+}$ from the mineral surface. We observe a linear relationship between zeta potential and ΔpCa with similar gradient (4.5 mV/decade; $R^2$>0.95) to that obtained in the experiments where pCa was varied.

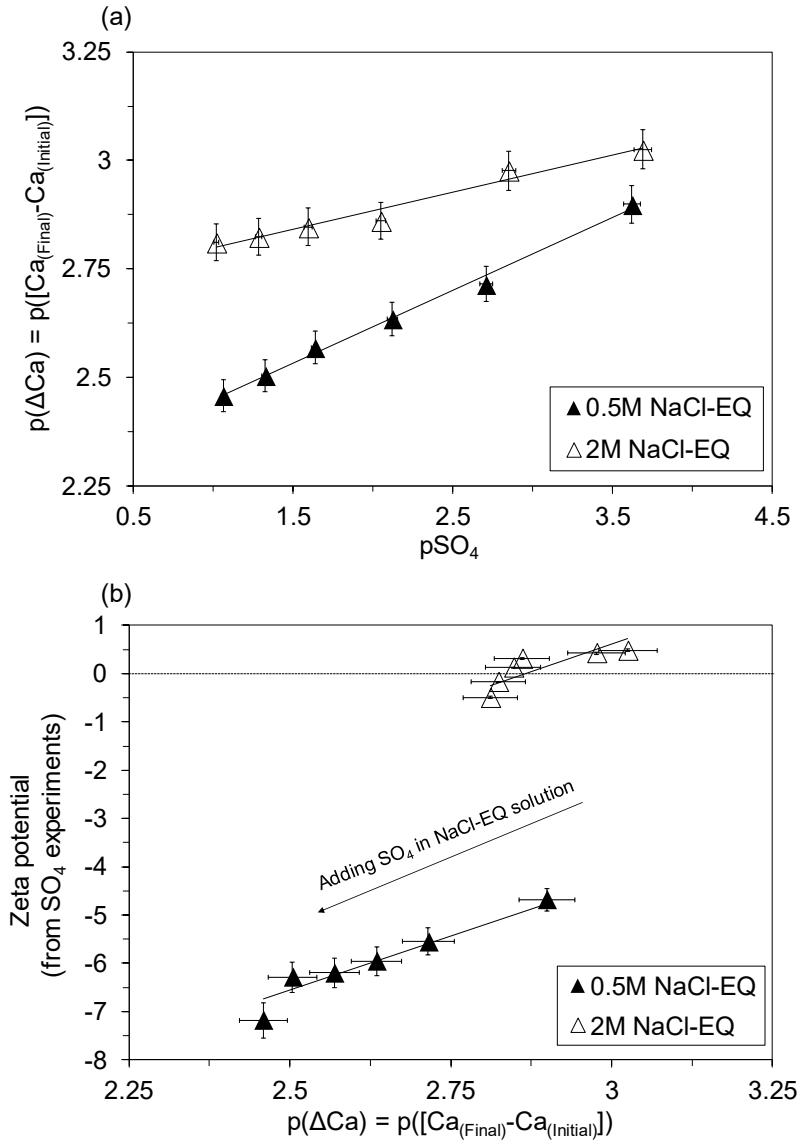



**Figure 4-13: Impact of $pSO_4$ on $Ca^{2+}$ concentration and zeta potential measured on the Estaillades sample. (a) Cumulative change in pCa measured during the experiments shown in Figure 4-9b in which $SO_4$ was added to pre-equilibrated NaCl brine. (b) Zeta potential from the experiments shown in Figure 4-9b plotted against the change in pCa recorded in (a).**

### 4.4.4. Implications for Wettability Alteration and Hydrocarbon Recovery in Carbonate Reservoirs

In carbonate rock formations with positively charged mineral surfaces, an attractive electrostatic force will act between the mineral surfaces and the negatively charged oil-brine interface, promoting wettability alteration to oil-wet conditions (e.g. *Buckley et al.*, 1989; *Hiorth et al.*, 2010). Several studies have

suggested that carbonate rocks saturated with natural brines rich in $Ca^{2+}$ and $Mg^{2+}$ ions have positively charged mineral surfaces so are likely to be oil-wet (e.g. *Jackson and Vinogradov*, 2012; *Chen et al.*, 2014; *Mahani et al.*, 2015; 2016; *Alroudhan et al.*, 2016). The wettability of a reservoir plays a key role in the efficiency with which the oil can be produced. However, we find here considerable variability in the IEP expressed as pCa, suggesting that some carbonates will be positively charged in contact with natural brines, and others will not. The SPM used here is a suitable technique to determine the zeta potential of intact reservoir rock samples saturated with natural brine (e.g. *Jackson and Vinogradov*, 2012).

In many reservoirs, water is injected to maintain the pressure and displace oil towards production wells. If the concentration of $Ca^{2+}$ or $Mg^{2+}$ in the injected water can be modified to fall below the IEP, either selectively or by bulk dilution in CSW process, the zeta potential will change polarity from positive to negative as shown in Figure 4-11. The polarity change leads to electrostatic repulsion between the mineral surfaces and the negatively charged oil-brine interface. This may promote wettability alteration to water-wet conditions, releasing previously adsorbed oil from the calcite mineral surfaces and therefore improving oil recovery (e.g. *Mahani et al.*, 2016). The subtle change of zeta potential with increasing $SO_4^{2-}$ observed in Figure 4-11 can be used as an explanation for no improved oil recovery exhibited in SI experiments conducted on various carbonate rock types by *Romanuka et al.,* (2012). Stevns Klint chalk surface was a clear exception and showed an increased oil recovery with increasing $SO_4^{2-}$ concentration.

Furthermore, most previous reported values of the IEP expressed as pCa suggest that considerable reduction in Ca concentration is required to change the polarity of calcite (Table 3-1). However, our results suggest that far less dilution may be required in some natural carbonates (e.g. Ketton and Portland); in others, the IEP may never be encountered and the mineral surfaces may remain positively charged (e.g. Estaillades). The carbonate-rock-specific relationship between zeta potential and PDI concentration observed here may explain why CSW in some cases yields increased recovery and in other cases does not (e.g. *Alotaibi et al.*,

2010; *Romanuka et al.*, 2012). Work relevant to CSW in chapters 6 and 7 emphases on testing the link between brine composition, zeta potential and increased oil recovery using integrated experiments with consistent materials and experimental conditions.

## 4.5. Conclusions

Experimental studies of the zeta potential of calcite and carbonate have reported a broad range of values with numerous inconsistent results. Yet the primary data source to understand calcite surface charge comprises measurements of zeta potential, so it is important to understand the key controls on zeta potential and why studies have reported apparently contradictory values. A comprehensive review of the literature in chapter 3, supplemented by experimental data new to this study, suggests that:

- The potential determining ions (PDIs) for the carbonate mineral surface are the lattice ions $Ca^{2+}$, $Mg^{2+}$ and $CO_3^{2-}$. The zeta potential is controlled by the concentration-dependent adsorption of these ions within the Stern layer, primarily at the Outer Helmholtz Plane (OHP). Given this, the Iso-Electric Point (IEP) at which the zeta potential is zero should be expressed as pCa (or pMg). It should not be reported as pH, similar to most metal oxides.
- The pH does not directly control the zeta potential. Varying the pH whilst holding pCa constant yields constant zeta potential. The pH affects the zeta potential only by moderating the equilibrium pCa for a given $CO_2$ partial pressure ($pCO_2$).
- Experimental studies that appear to yield a systematic relationship between pH and zeta potential are most likely observing the relationship between pCa and zeta potential, with pCa responding to the change in pH. New data presented here show a consistent linear relationship between equilibrium pH and equilibrium pCa irrespective of sample or solution ionic strength.

- The surface charge is weakly dependent on pH through protonation and deprotonation reactions that occur within a hydrolysis layer immediately adjacent to the mineral surface. The Point of Zero Charge (PZC) at which the surface charge is zero could be expressed as pH, but surface complexation models suggest the surface is negatively charged over the pH range 5.5-11.
- Several studies have suggested that $SO_4^{2-}$ is also a PDI for the calcite surface, but new data presented here indicate that the value of $pSO_4$ affects zeta potential only by moderating the equilibrium pCa.
- Natural carbonate typically yields a more negative zeta potential than synthetic calcite, most likely due to the presence of impurities including clays, organic matter, apatite, anhydrite or quartz, that yield a more negative zeta potential than pure calcite. New data presented here show that apparently identical natural carbonates display differing zeta potential behavior, most likely due to the presence of small volumes of these impurities.
- It is important to ensure that equilibrium, defined in terms of the concentration of PDIs, has been reached prior to taking measurements. Inconsistent values of zeta potential obtained in some studies may reflect a lack of equilibration.
- The results have broad application to key engineering processes such as the use of modified injection brine composition to increase oil recovery in a process termed controlled salinity waterflooding (CSW). The carbonate-rock-specific relationship between zeta potential and PDI concentration obtained here may explain why CSW in some cases yields increased recovery and in other cases does not.

# Chapter 5.

# Temperature-Dependence of the Zeta Potential in Intact Natural Carbonates

## 5.1. Introduction

As discussed in chapter 3, most of studies on measurements of zeta potential in calcite and carbonate were conducted at low ionic strength and laboratory temperatures; however, natural brines have much higher salinity. Moreover, in many subsurface settings, including hydrocarbon reservoirs (e.g. Gulamali et al., 2011; Saunders et al., 2012), deep saline aquifers (e.g. Moore et al., 2004) and hydrothermal systems (e.g. Revil and Pezard, 1998; Suski et al., 2008), there are carbonate rocks at elevated temperature, yet the temperature dependence of the zeta potential in carbonates has not well studied. No measurements above laboratory temperature are available in the literature. The aim of this chapter is to determine the temperature-dependence of the zeta potential in natural carbonates over the range 22–120°C.

## 5.2. Methodology

### 5.2.1. Materials and Sample Preparation

The natural carbonate core samples used in this chapter were Ketton, Estaillades and Portland, identical to those used in chapter 4. The properties of the tested samples were previously summarized in Table 4-1. We investigated three types of electrolytes. One electrolyte contained 0.01M NaCl (ionic strength

comparable to potable water); the second contained 0.5M NaCl (ionic strength comparable to seawater). Both electrolytes also contained small but unbuffered amounts of Ca and other ions, having been equilibrated with the limestone sample of interest prior to measuring the zeta potential. The third comprised of compositions typical to natural SW and different compositions derived from SW reported previously in Table 4-2. Appropriate initial conditions of carbonate/water/$CO_2$ equilibrium were replicated here following the approach described in section 4.4.1. The equilibrated NaCl electrolytes (denoted NaCl-EQ) were used directly in our streaming potential experiments, or were modified by addition of $Ca^{2+}$, $Mg^{2+}$ and/or $SO_4^{2-}$.

The samples were cleaned following the enhanced cleaning procedure outlined in section 4.2.1. These samples were used in previous streaming potential experiments reported in chapter 4. The first experiment at laboratory temperature is compared against previous results obtained on the same samples at different brine compositions. The interpreted zeta potential should match within ±0.5mV to previous measurements.

### 5.2.2. Measurements of Zeta Potential using the SPM at Elevated Temperature

We measured the zeta potential of the intact limestone samples using the streaming potential method (SPM) at elevated temperature recently developed by *Vinogradov and Jackson,* (2015) and applied by them to intact sandstone samples. Their experimental set-up was modified from that described by *Jaafar et al.,* (2009) and *Vinogradov et al.,* (2010) to allow measurements at elevated temperature (see Figure 5-1). The main difference was that the electrolytes used to saturate the core samples and in the reservoirs (columns) were already pre-equilibrated with the carbonate materials, ensuring constant pH and conductivity of the electrolyte across the whole system (in loaded samples and reservoir columns). As the SPM has been described previously, we provide only a short overview here. The sample was confined in a PEEK core holder and placed in an oven along with the

reservoirs (columns) that supply electrolyte to the sample, and the electrodes used to measure the electrical potential across the sample. The oven had temperature controlled to ±0.5°C. The pump used to flow the electrolyte through the sample remained outside of the oven and Multipar oil was used as a hydraulic fluid to force electrolyte from one reservoir, through the sample, and into the other reservoir, via flowlines that pass through the wall of the oven from the reservoirs to the pump. The conductivity and pH of the electrolytes were measured over the tested temperature range 22-80°C. The saturated-sample conductivity was measured over the entire temperature range investigated using pair of internal Ag/AgCl membranes at the two sample-end faces (; inside the oven; Figure 5-1b) following the approach described in *Vinogradov and Jackson,* (2011). The electrolyte-saturated samples were placed in a Viton rubber sleeve embedded in a PEEK core holder and the confining pressure of about 1.5MPa was used with a backpressure applied at 80 and 120°C to avoid reaching a water-boiling point.

The streaming potential was measured using the 'paired-stabilization' (PS) method of *Vinogradov and Jackson,* (2011). In this method, the pump is used to flow the electrolyte through the sample at constant rate until stable pressure and voltage are recorded across the sample (e.g. Figure 5-2a). The flow direction is then reversed at the same rate. A symmetric response confirms that electrode polarization effects are small and that the measured electrical potential corresponds to the streaming potential. These PS experiments are repeated at 3 or 4 different flow rates and the stabilized voltage for each experiment plotted as a function of the stabilized pressure difference (e.g. Figure 5-2b). The gradient of a linear regression through these data yields the streaming potential coupling coefficient ($C_{sp}$), which is related to the zeta potential ($\zeta$) via equation (3.13) which accounts for the effect of surface electrical conductivity.

The intrinsic formation factors (at 22°C) were available from previous chapter (Table 4-1) and we obtained $\sigma_f$, $\mu$ and $\varepsilon$ as a function of temperature and ionic strength using the approach of *Saunders et al.,* (2012) (see below; also, see Appendix A in *Saunders et al.*, 2012).

#### 5.2.2.1 Brine Conductivity as a Function of Temperate and Salinity

The brine conductivity $\sigma_f$ (in S m$^{-1}$) was calculated from temperature $T$ (in $^{o}$C) and salinity $C_f$ (in M) using the equation provided by *Sen and Goode,* (1992)

$$\sigma_f = (5.6 + 0.27T - 0.00015T^2)C_f - \frac{2.36+0.099T}{1.0+0.214C_f^{1/2}}C_f^{3/2}. \quad (5.1)$$

It is noted that the conductivity of brine increases as both temperature and salinity increase.

#### 5.2.2.2 Brine Viscosity as a Function of Temperate

The brine viscosity $\mu$ (in Pa s) was calculated as a function of temperature $T$ (in $^{o}$C) and salinity $C_f$ (in M) using the correlation described by *Kestin and Shankland,* (1984)

$$\mu(T, C_f) = \mu(T, 0) \text{ x } \mu_r(T, C_f) \quad (5.2)$$

where

$$log_{10}\left(\frac{\mu(T,0)}{\mu(20,0)}\right) = \frac{1}{(96+T)}[(20-T)(1.2378 - 1.303 \text{ x } 10^{-3} \text{ x } (20-T) + 3.06 \text{ x } 10^{-6}(20-T)^2 + 2.55 \text{ x } 10^{-8}(20-T)^3] \quad (5.3)$$

and

$$\mu(20,0) = 0.001002. \quad (5.4)$$

The relative viscosity $\mu_r$ as a function of temperature at a given salinity $C_f$ is given by

$$log_{10}\left(\mu_r(T, C_f)\right) = A(C_f) + B(C_f) log_{10}\left(\frac{\mu(T,0)}{\mu(20,0)}\right) \quad (5.5)$$

where

$$A(C_f) = 3.3324 \text{ x } 10^{-2}C_f + 3.624 \text{ x } 10^{-3}C_f^2 - 1.879 \text{ x } 10^{-4}C_f^3 \quad (5.6)$$

and

$$B(C_f) = -3.96 \text{ x } 10^{-2}C_f + 1.02 \text{ x } 10^{-2}C_f^2 - 7.02 \text{ x } 10^{-4}C_f^3. \quad (5.7)$$

The brine viscosity therefore decreases as the temperature increases for a given salinity above 1 M. However, the effect of temperature on viscosity for salinities up to 1 M is almost negligible.

#### 5.2.2.3 Brine Permittivity as a Function of Temperate

The brine permittivity $\varepsilon$ (in F m$^{-1}$) was calculated from the relative permittivity $\varepsilon_r$ (in F m$^{-1}$), which is a function of temperature and salinity, and the vacuum permittivity $\varepsilon_0$ ($= 8.854187\text{x}10^{-12}$ F m$^{-1}$)

$$\varepsilon = \varepsilon_r \varepsilon_0. \tag{5.8}$$

The relative permittivity $\varepsilon_r$ of brine at a given temperature *T* and normality *N* was calculated using the equations given in *Stogryn,* (1971)

$$\varepsilon_r(T, N) = \varepsilon_r(T, 0) \text{ x } a(N) \tag{5.9}$$

where

$$\varepsilon_r(T, 0) = 87.74 - 0.40008T + 9.398 \text{ x } 10^{-4}T^2 + 1.41 \text{ x } 10^{-6}T^3 \tag{5.10}$$

$$a(N) = 1.0 - 0.2551N + 5.151 \text{ x } 10^{-2}N^2 - 6.889 \text{ x } 10^{-3}N^3 \tag{5.11}$$

and

$$N = \hat{C}_f(1.707 \text{ x } 10^{-2} + 1.205 \text{ x } 10^{-5}\hat{C}_f + 4.058 \text{ x } 10^{-9}\hat{C}_f^2 \tag{5.12}$$

where, $\hat{C}_f$ is the salinity of brine (in parts per thousands) (*Malmberg and Maryott*, 1956).

Thus, the brine permittivity decreases with both temperature and salinity.

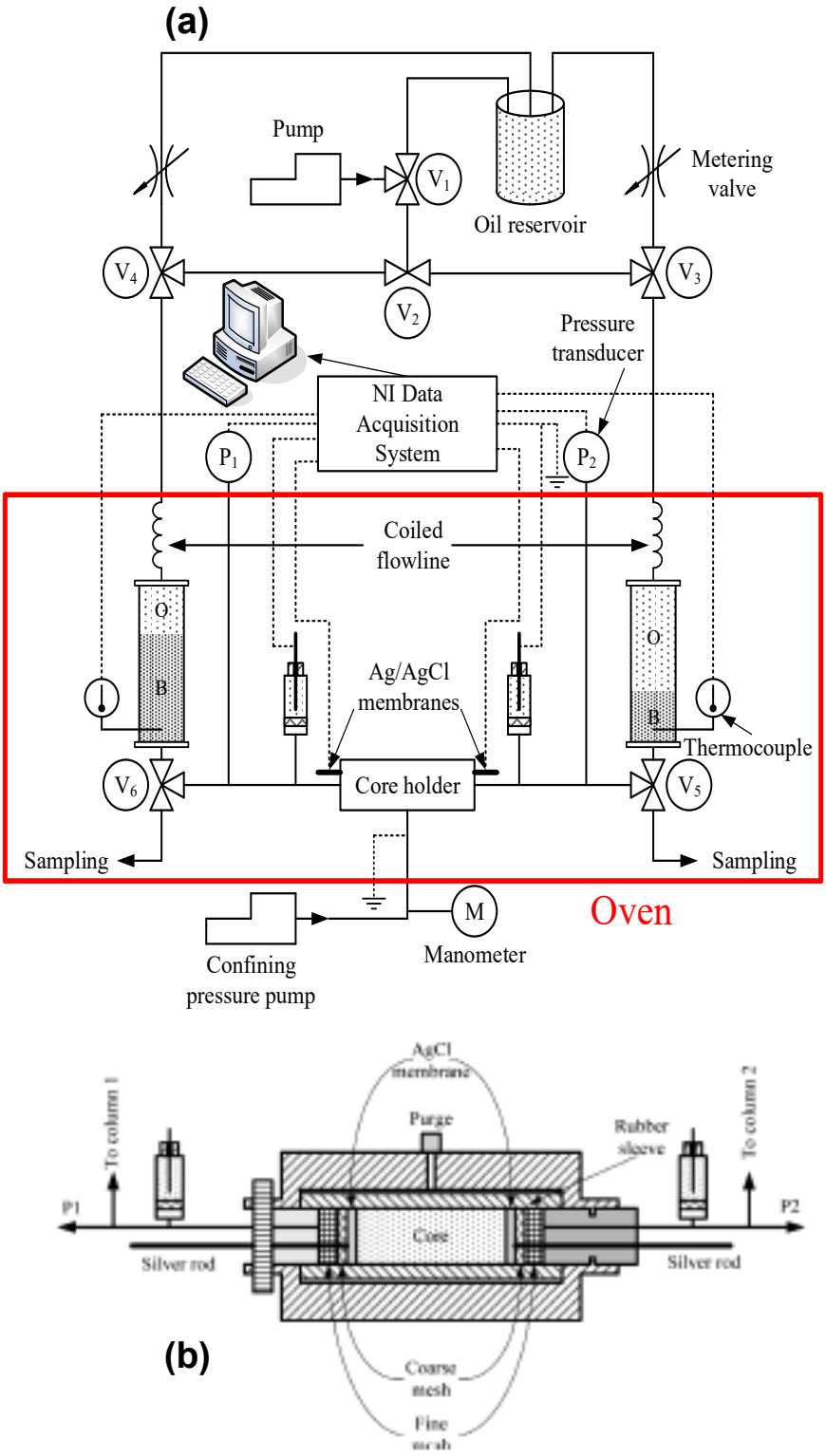



**Figure 5-1: Experimental apparatus in measuring streaming potential coupling coefficient at elevated temperature. (a) Coreflooding and the SPM apparatus. (b) Internal AgCl electrodes (membranes) are located on each face of the sample and used to measure sample conductivity.**

## 5.3. Results

### 5.3.1. Impact of NaCl Ionic Strength

Typical raw results of the PS experiments are shown in Figure 5-2a,b. Figure 5-2c and Figure 5-2d show the measured sample electrical conductivity and electrolyte pH of all experiments over the range of temperatures investigated. The sample conductivity increases with temperature almost linearly (Figure 5-2c), and the conductivity also increases with the electrolyte ionic strength; the higher the electrolyte concentration the higher the conductivity. Electrolyte pH is constant within experimental error in all investigated samples and electrolytes (Figure 5-2d). Figure 5-2e and Figure 5-2f show the temperature dependent change in streaming potential coupling coefficient for the 0.01M and 0.5M electrolytes respectively. The streaming potential coupling coefficient is negative for all samples, and decreases in magnitude with increasing temperature at low ionic strength (Figure 5-2e) but is constant within experimental error in high ionic strength (Figure 5-2f).

Figure 5-3 shows the temperature dependence of the zeta potential and calcium concentration (expressed as pCa) for the 0.01M (Figure 5-3a,b) and 0.5M (Figure 5-3c,d) electrolytes. At low ionic strength, zeta potential and equilibrium pCa (negative logarithm of calcium concentration) both decrease in magnitude with increasing temperature (Figure 5-3a,b). A linear regression provides a good fit to the temperature dependence of the zeta potential for the Estaillades and Portland samples with a common gradient of 0.04 mV/ºC (adjusted $R^2$ = 0.897 for Estaillades; adjusted $R^2$ = 0.974 for Portland) but a power law regression of the form $a = bT^c$ is required to obtain a similar quality of fit to the data from the Ketton sample (adjusted $R^2$ = 0.958) with $b$ = -41.46 mV and $c$ = -0.409. A linear regression also provides a good fit to the temperature dependence of pCa for the Estaillades and Portland samples with a common gradient of -0.0024 decade/ºC (adjusted $R^2$ = 0.977 for Estaillades; adjusted $R^2$ = 0.896 for Portland), but again a power law regression is required to obtain a similar quality of fit to the data from the Ketton sample (adjusted $R^2$ = 0.844) with $b$ = 3.23 and $c$ = -0.067.

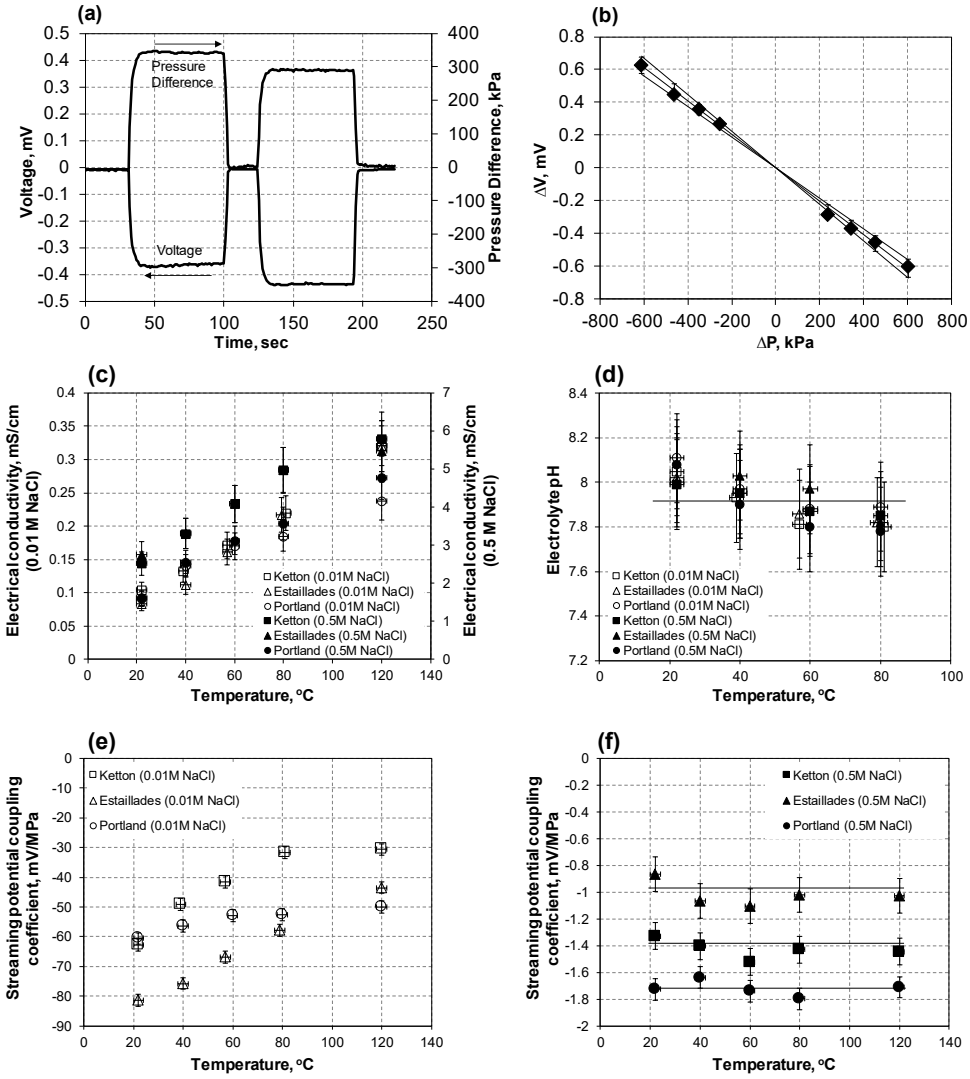



**Figure 5-2: Experimental results of NaCl electrolytes at elevated temperatures. (a) shows typical paired stabilization results obtained at a flowrate of 80 ml min$^{-1}$ on Estaillades sample saturated with 0.5M NaCl electrolyte at 80°C. Note that the directions of voltage and pressure are opposite to each other, thus the streaming potential coupling coefficient is negative. (b) shows a typical plot of stabilized voltage against stabilized pressure difference at four different flowrates; here, the linear regression has $R^2$=0.998. The slope of the linear regression yields a value for the streaming potential coupling coefficient for this rock sample, temperature and ionic strength of $C_{sp}$= -1.02±0.1 mV MPa$^{-1}$. The error bars reflect the voltage fluctuations around the stabilized value and the uncertainty in $C_{sp}$ reflects the variability in the linear regression that can be forced through the data within experimental error. (c) shows the electrical conductivity of the saturated samples as a function of temperature: filled symbols denote 0.5M NaCl electrolyte and are plotted against the right-hand axis; empty symbols denote 0.01M NaCl electrolyte and are plotted against the left-hand axis. (d) shows the electrolyte pH as a function of temperature: filled symbols 0.5M NaCl electrolyte; empty symbols denote 0.01M NaCl electrolyte. (e & f) show streaming potential coupling coefficient as a function of temperature for 0.01M NaCl electrolyte in (e) and. 0.5M NaCl electrolyte in (f).**

The absolute magnitude of the zeta potential and calcium concentration (expressed as pCa) for each sample consistently follows the order Portland > Estaillades > Ketton.

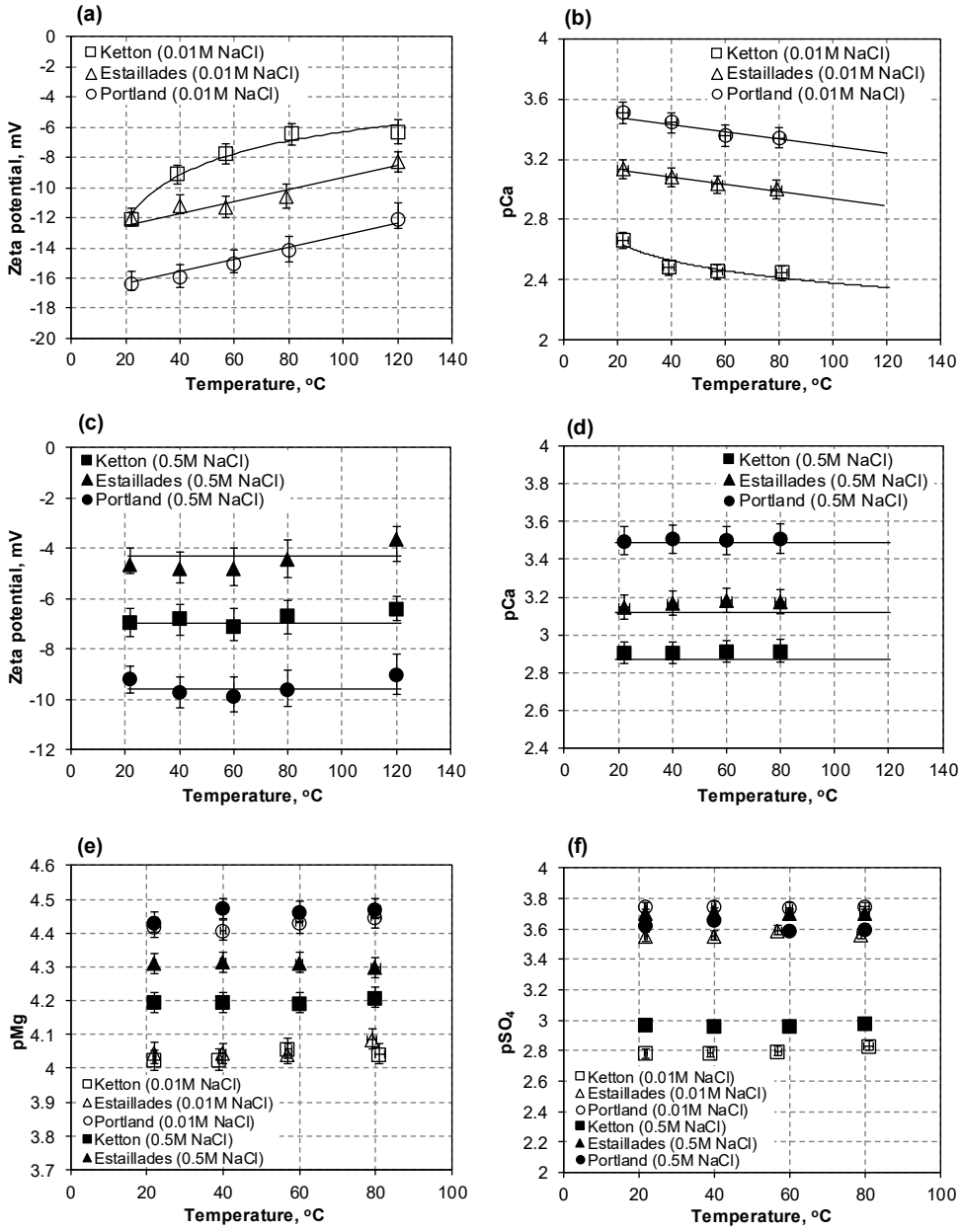



**Figure 5-3: Zeta potential and equilibrium pCa, pMg and $pSO_4$ as a function of temperature. Plots (a) and (b) show zeta potential and pCa as a function of temperature at low ionic strength (0.01M NaCl electrolyte). Plots (c) and (d) show zeta potential and pCa as a function of temperature at high ionic strength (0.5M NaCl electrolyte). The equilibrium pCa was measured for temperatures in the range 22-80°C and extrapolated to higher temperature using the regressions obtained. Plots (e) and (f) show pMg and $pSO_4$ as a function of temperature for all samples and electrolytes.**

At high ionic strength, both zeta potential and calcium concentration are independent of temperature within experimental error (Figure 5-3c,d). The absolute magnitude of the zeta potential for each sample consistently follows the order Portland > Ketton > Estaillades (Figure 5-3c). However, the calcium concentration (expressed as pCa) follows the order Portland > Estaillades > Ketton (Figure 5-3d). Dissolution of the sample during equilibrium of the rock/electrolyte system therefore yielded a non-zero concentration of $Ca^{2+}$ in the electrolyte that was temperature dependent at low ionic strength, but constant for a given sample at high ionic strength.

The equilibration process also yielded non-zero concentrations of $Mg^{2+}$ and $SO_4^{2-}$ which were independent of temperature irrespective of ionic strength, but varied between samples (Figure 5-3e, f). The difference in equilibrium pMg between the three samples is small and follows the trend in pCa, so pMg is lower in the Ketton sample and higher in the Portland sample; see Figure 5-3e). The equilibrium $pSO_4$ is always lower in the Ketton sample (Figure 5-3f), consistent with previous results obtained at room temperature (see chapter 4). We discuss the significance of these ions in solution in terms of their impact on zeta potential in the Discussion section.

### 5.3.2. Effect of SW Dilution and Addition of $SO_4$ to SW on Zeta Potential at 80°C

We finish by reporting zeta potential measurements on synthetic electrolytes equivalent to typical natural SW and SW modified compositions at 80°C in Estaillades and Ketton. SW was diluted twice (2dSW), ten times (10dSW) and twenty times (20dSW), and $SO_4$ was added to yield four times (4SW) the natural seawater concentration. The results are compared against data obtained at room temperature (shown in Figure 4-11). In both rocks, the zeta potential at 80°C follows the same trend observed at room temperature (22°C); i.e. the zeta potential is negative in SW and becomes increasingly negative as the SW is diluted or $SO_4^{2-}$ is added (Figure 5-4). Moreover, for SW, 2dSW and SW4S, there is no

change in the magnitude of zeta potential within experimental error between 22°C and 80°C (compare empty and filled symbols in Figure 5-4a). However, as SW diluted to 10 and 20 times, zeta potential at 80°C is less negative compared to 22°C (Figure 5-4a). Figure 5-4b shows the response of zeta potential of the two samples at both temperatures against ionic strength. The zeta potential is independent of temperature at ionic strength ≥ 0.375M and decreases in magnitude with increasing temperature at ionic strength ≤ 0.075M.

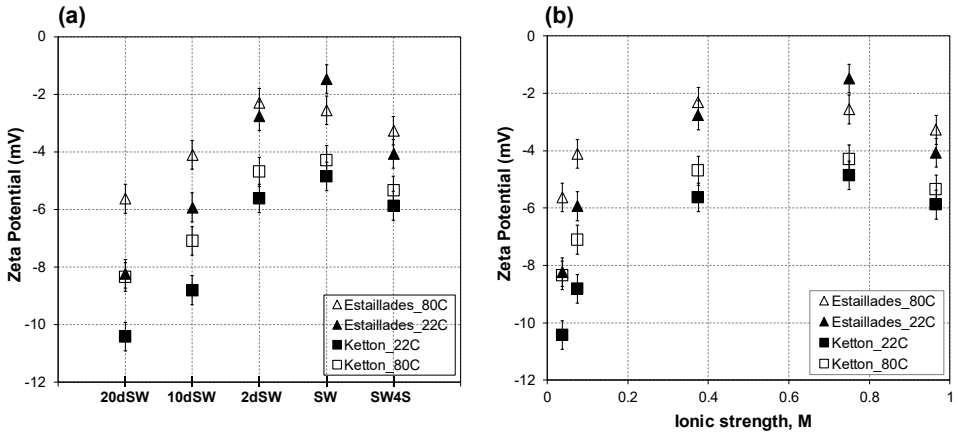



**Figure 5-4: Effect of seawater dilution and addition of $SO_4$ to seawater on zeta potential of natural carbonates at 80°C. Results are compared against measurements in room temperature reported in Figure 4-11b. In (b), zeta potential of the same compositions plotted as a function of ionic strength.**

## 5.4. Discussion

### 5.4.1. Effect of Varying NaCl Concentration on Temperature Dependence of Zeta Potential

We observe a clear and consistent temperature dependence of the zeta potential in natural carbonates which is the same across the three different limestone samples investigated here but depends on the ionic strength of the electrolyte. At the lower ionic strength tested (0.01M NaCl), the zeta potential decreases in magnitude with increasing temperature, while at the higher ionic strength tested (0.5M NaCl), we find that the zeta potential remains constant within experimental error. This behaviour is similar to that observed in natural sandstones

by *Vinogradov and Jackson,* (2015): they also found that the zeta potential decreased in magnitude with increasing temperature at lower ionic strength (0.01M NaCl, consistent with that investigated here) but remained constant at higher ionic strength (0.5M NaCl, as in this study). However, they found that the zeta potential at a given temperature was the same within experimental error across the three sandstone samples investigated. Moreover, they also found that the electrolyte pH decreased in magnitude with increasing temperature at low ionic strength but remained constant at high ionic strength. Here we find the value of zeta potential is different for each limestone sample. Moreover, the pH remained constant within experimental error, irrespective of temperature or ionic strength.

The negative values of zeta potential obtained here for all three carbonate samples investigated are consistent with previously reported values on natural carbonates and calcites at the equilibrium pH = 8.2 (e.g. *Berlin and Khabakov*, 1961). However, there are no published data on the temperature dependence of the zeta potential on calcite or natural carbonates against which the results obtained here can be compared. All previously published data were obtained at laboratory temperature (see chapter 4; e.g. *Foxall et al.*, 1979; *Thompson and Pownall*, 1989; *Pierre et al.*, 1990; *Huang et al.*, 1991; *Cicerone et al.*, 1992; *Chen et al.*, 2014; *Alroudhan et al.*, 2016).

These studies have shown that, unlike metal oxides such as silica, the proton is not the key potential determining ion (PDI) for the calcite surface. While pH does control the protonation and deprotonation reactions that occur at the calcite mineral surface, the variation in surface charge over the pH range 5.5-11 is small (e.g. *Heberling et al.*, 2011). The zeta potential is instead controlled by the concentration-dependent adsorption of the lattice ions $Ca^{2+}$ and $Mg^{2+}$ on the mineral surface (refer to chapter 3). The $SO_4^{2-}$ ion has also been suggested as a PDI for calcite (e.g. *Pierre et al.*, 1990; *Alroudhan et al.*, 2016). The zeta potential of the natural limestone samples investigated here is therefore controlled by pCa, pMg and $pSO_4$.

The equilibrium pMg and $pSO_4$ observed in our experiments was constant for a given sample and electrolyte irrespective of temperature (Figure 5-3a, b). At the higher ionic strength tested, the equilibrium pCa was also constant for a given sample and electrolyte irrespective of temperature. However, at the lower ionic strength tested, the equilibrium pCa decreased with increasing temperature (i.e. the concentration of $Ca^{2+}$ increased; Figure 5-3b). Moreover, at the lower ionic strength, a clear correlation between zeta potential and pCa was obtained for a given sample, yielding a linear (Nernstian) regression with a gradient of -15 mV/decade for the Portland and Estaillades samples (adjusted $R^2$>0.91) and -20 mV/decade for the Ketton sample (adjusted $R^2$=0.90) (Figure 5-5a). Previous studies on these and similar natural samples have also observed a Nernstian relationship between zeta potential and pCa with similar gradients but in room temperature experiments (refer to Figure 3-6). At the higher ionic strength, the data clustered at one value of pCa and zeta potential for each sample (Figure 5-5a).

The temperature dependence of the zeta potential in sandstones observed by *Vinogradov and Jackson,* (2015) was explained by them in terms of the temperature dependence of the electrolyte pH (i.e. the concentration of the proton, the PDI for the silica surface). Here, we find that the temperature dependence of the zeta potential for a given carbonate sample can be explained by the temperature dependence of the electrolyte pCa (i.e. the concentration of the calcium ion, the PDI for the calcite surface). At the lower ionic strength investigated, both the zeta potential and pCa decrease with increasing temperature (Figure 5-3a,b) and the change in zeta potential reflects a Nernstian response to the change in pCa (Figure 5-5a). At the higher ionic strength investigated, both the zeta potential and pCa remain constant irrespective of temperature (Figure 5-3c,d) but the constant zeta potential nonetheless reflects a Nernstian response to the change in pCa (Figure 5-5b).

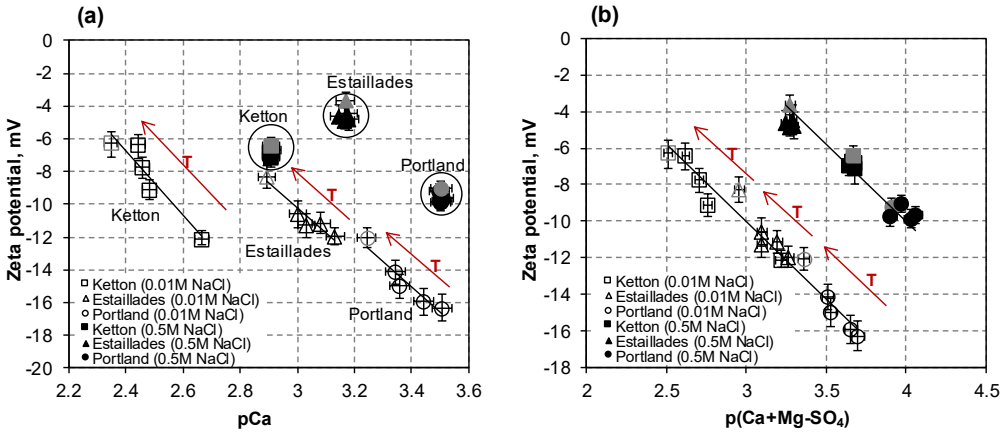



**Figure 5-5: Relationship between zeta potential and PDI concentration. (a) Zeta potential plotted against pCa. (b) Zeta potential plotted against p(Ca+Mg–$SO_4$). Red arrows represent increasing temperature from 22°C to 120°C. Grey symbols are extrapolated values at 120°C.**

The relationship between zeta potential and equilibrium pCa explains the temperature dependence of the zeta potential for a given limestone sample, but does not explain the difference in zeta potential observed at a given pCa/temperature between the three investigated limestone samples. For example, the Ketton sample recorded a larger negative zeta potential than the Estaillades sample at high ionic strength, even though the calcium concentration was higher (i.e. pCa was lower; see Figure 5-5a). The difference in zeta potentials can be accounted for by also including the variations in equilibrium pMg and p$SO_4$ observed across the different samples (Figure 5-3e, f). The difference in the zeta potential response of the three samples tested can be accounted for by plotting the zeta potential against the total concentration of PDIs (expressed as p(Ca+Mg-$SO_4$)). We choose to plot concentration in this way as the lattice ions $Ca^{2+}$ and $Mg^{2+}$ have an identical impact on zeta potential within experimental error, while the $SO_4^{2-}$ ion acts to reduce the effect of pCa; see chapter 4. The empirical expression p(Ca+Mg-$SO_4$) explains the different trends observed between the three limestone samples where at low ionic strength we see $|\zeta|_{Portland} > |\zeta|_{Estaillades} > |\zeta|_{Ketton}$ but at high ionic strength we find $|\zeta|_{Portland} > |\zeta|_{Ketton} > |\zeta|_{Estaillades}$. Plotted in this way, the zeta potential varies linearly with PDI concentration irrespective of sample type, temperature and ionic strength, with an identical gradient of -8 mV/decade (adjusted $R^2$>0.93) (Figure 5-5b).

The simplest plausible mechanism to account for the observed response of zeta potential with temperature can be explained by carbonate dissolution. At low ionic strength, we expect the pH to decrease as observed by *Vinogradov and Jackson,* (2015) in natural sandstones; however, the pH in our experiments is buffered at the equilibrium value (Figure 5-2d) by small concentrations of $Ca^{2+}$, $Mg^{2+}$ and $HCO_3^-$ present in the equilibrated electrolytes. In our closed system, the expected decrease in the pH with increasing temperature is buffered by an increase in the concentrations of $Ca^{2+}$ (as shown in Figure 5-3b). The source of $Ca^{2+}$ ions must be carbonate dissolution. With an increase in temperature, the solubility of $Ca^{2+}$ ions increase, allowing them to preferentially leave the carbonate surface and resulting to an increase of hydrated $Ca^{2+}$ concentration near the carbonate surface (in the diffuse layer of the EDL); hence a decrease in the zeta potential (becoming less negative). At high ionic strength, *Vinogradov and Jackson,* (2015) observed no change in pH with temperature. Hence, we expect no mineral dissolution and so no change in pCa (Figure 5-3d).

More complicated processes might involve a preferential hydrolysis of surface calcium and carbonate after dissolution as postulated by *Somasundaran and Agar,* (1967) according to the following mechanisms

$$CaCO_3 \longrightarrow Ca^{2+} + CO_3^{2-} \quad (5.13)$$

$$H_2O \longrightarrow H^+ + OH^- \quad (5.14)$$

$$Ca^{2+} + OH^- \longrightarrow CaOH^+ \quad (5.15)$$

$$CO_3^{2-} + H^+ \longrightarrow HCO_3^- \quad (5.16)$$

As per reaction (5.13), dissolution of carbonate at elevated temperature (because of a decrease in pH) will produce more calcium and carbonate. Excess of $H^+$ and $OH^-$, due to dissociation of water molecules, as temperature increases (reaction 5.14) are consumed by excess of $Ca^{2+}$ and $CO_3^{2-}$ at the same rate, which shifts reactions (5.15) and (5.16) to the right with increasing temperature. This might explain the observed constant pH with temperature. Moreover, reaction (5.13) suggests that the relative concentration of positive and negative sites on the surface would remain unchanged, in agreement with *Stumm,* (1992). Stumm

assumes that at this pH range of 8.2 (equilibrium pH in calcite-water system in equilibrium with $CO_2$), surface species do not contribute to the overall electroneutrality of the aqueous suspension. We argue that the increased concentration of positive PDI ($Ca^{2+}$) at low ionic strength will lead to more positive zeta potential, although the surface charge might remain the same.

At high ionic strength, *Vinogradov and Jackson,* (2015) observed no change in pH with temperature. Hence, we expect no mineral dissolution and so no change in pCa (Figure 5-3d).

### 5.4.2. Implications for Controlled Salinity Waterflooding (CSW)

We have shown that zeta potential of natural carbonate is independent of temperature at high ionic strength (≥ 0.375M) and decreases with temperature at low ionic strength (≤ 00375M) irrespective of electrolyte composition (Figure 5-4). Typical formation brines (e.g. *Austad et al.*, 2011; *Romanuka et al.*, 2012), seawater (e.g. *Strand et al.*, 2006; *Karoussi and Hamouda*, 2007; *Zhang et al.*, 2007; *Yousef et al.*, 2011) and when $SO_4$ is added to SW are of ionic strength higher than threshold value of 0.375M. These results suggest that zeta potential measurements of natural carbonate in natural brines (e.g. formation brines and seawater; ionic strength ≥0.5M) at room temperature may be applied *in situ*. Thus the measurements at laboratory conditions may be used to correlate zeta potential to wettability and oil recovery at reservoir conditions of salinity and temperature. At low ionic strength, the zeta potential may be noticeably lower than that measured in experiments at laboratory conditions.

As discussed in section 4.4.4, the repulsive electrostatic forces between the negatively charged mineral surfaces and the negatively charged oil-brine interface increase with increasing the negative zeta potential at mineral-brine interface, promoting wettability alteration to water-wet conditions. This can be largely achieved through bulk dilution rather than addition of $SO_4$ even at reservoir temperature, which might further explain why no additional oil recovery was

observed in reported SI and coreflood experiments when $SO_4$ was added to SW (e.g. *Fernø et al.*, 2011; *Romanuka et al.*, 2012).

## 5.5. Conclusion

We find that the temperature dependence of the zeta potential in natural carbonates saturated with NaCl electrolytes depends on ionic strength. The zeta potential is negative and decreases in magnitude with increasing temperature at low ionic strength but is independent of temperature at high ionic strength; consistent with published zeta potential data in intact natural sandstones. The equilibrium calcium concentration also decreases with increasing temperature at low ionic strength but independent of temperature at high ionic strength. The temperature dependence of zeta potential can be correlated with the temperature dependence of pCa and shows a Nernstian linear relationship. The difference in response of the three carbonate samples tested can be accounted for by also including the variations in pMg and $pSO_4$ to the temperature dependent variation in pCa. pH remains unchanged with temperature at low and high ionic strengths. The zeta potential measurements in natural brines (e.g. saline aquifers, formation brines or seawater; ionic strength ≥0.5M) at laboratory conditions may be applied *in situ*. The results have broad application relevant to engineering processes and hydrothermal fields and might explain previous CSW experiments in carbonate at elevated temperatures when incremental oil recovery was mostly achieved during bulk dilution rather than addition of $SO_4$.

# Chapter 6.

# Quantification of Carbonate Rock Wettability Using Streaming Potential Measurements

## 6.1. Introduction

Multiphase flow in subsurface reservoir rock is controlled by the pore-scale distribution of the fluid phases, which in turn depends on the wettability of the rock mineral surfaces (e.g. *Kennedy et al.*, 1955; *Abdallah et al.*, 1986; *Hirasaki*, 1991). There is a wide span of wettability which results in a wide range of reservoir performance. The difference in wettability arises from the differences in the fraction of total surface areas wetted preferentially by water (preferentially water-wet) or by oil (preferentially oil-wet). Several quantitative and qualitative; direct and indirect methods have been discussed in chapter 2 (section 2.6) with their advantages and disadvantages in quantifying the wettability of rock samples.

The aim of this chapter is to determine whether wettability can be characterised from measurements of the zeta potential on intact carbonate rock samples, obtained using the streaming potential method (SPM). It has previously been shown that streaming potential in carbonates saturated with brine and crude oil is sensitive to the wetting state (*Jackson and Vinogradov*, 2012) and it is well known that surface charge/zeta potential plays a key role in determining rock wetting state (*Buckley et al.*, 1989; *Hirasaki*, 1991; *Buckley and Liu*, 1998; *Buckley et al.*, 1998). However, there has been no attempt to systematically relate variations in wettability to variations in the zeta potential.

We show that the SPM can be used to characterise wettability in laboratory experiments much quicker than traditional Amott or USBM tests; is sensitive to the

entire range of wettability and data can be obtained during the conventional coreflooding experiments used to measure (for example) permeability and relative permeability. We have seen that the SPM can be used to measure zeta potential at reservoir conditions of high salinity brine (chapter 4), multiphase flow (*Vinogradov and Jackson,* 2011) and elevated temperature (chapter 5). Moreover, the SPM could be used to determine zeta potential *in-situ* using, for example, a modified version of the modular dynamic tester (MDT) tool or similar, by inducing flow in the reservoir and measuring the pressure and voltage response. Such a tool would be of great utility in reservoir characterisation. There is, therefore, the potential to develop a new method to characterise wettability both in the laboratory, and *in-situ* in the reservoir, if a quantifiable and predictable relationship can be demonstrated between the rock wettability and the zeta potential obtained using SPM.

## 6.2. Methodology

### 6.2.1. Materials and Sample Preparation

The rock samples used in the experiments were Estaillades and Portland natural limestones (Table 4-1). We used five brines in our coreflooding experiments (Table 6-1): (1) a simple NaCl brine (denoted NaB) with total ionic strength of 2M; (2) artificial formation brine FMB1 which is identical to the one used by *Alroudhan et al.,* (2016); (3) artificial formation brine FMB2 which is identical to that used in chapter 4; (4) seawater (denoted SW; similar to *Strand et al.*, 2006); and (5) seawater diluted 20 times (denoted 20dSW). The brines used represent salinity and compositions typical of hydrocarbon reservoirs (e.g. *Romanuka et al.*, 2012). Five different types of natural crude oil were used to alter the wettability of carbonate samples (Table 6-2). Brine and rock preparation procedures and brine-composition measurements were the same as reported in section 4.2.1 and 4.2.3.

**Table 6-1: Properties and composition of brines used in chapter 6**

| | NaB | FMB1 | FMB2 | SW | 20dSW |
|---|---|---|---|---|---|
| **Ions** | mol/l | | | | |
| **$Na^+$** | 2 | 2 | 2 | 0.55 | 0.0275 |
| **$Cl^-$** | 2 | 2.98 | 3.02 | 0.62 | 0.031 |
| **$Ca^{2+}$** | 0.0003 | 0.42 | 0.42 | 0.014 | 0.0007 |
| **$Mg^{2+}$** | 0.00004 | 0.07 | 0.091 | 0.045 | 0.00225 |
| **$SO_4^{2-}$** | 0.0002 | 0.0033 | 0.002 | 0.024 | 0.0012 |
| **Ionic Strength** | 2.000 | 3.477 | 3.537 | 0.749 | 0.0375 |
| **pH** | 8.2 | 6.3 | 6.3 | 7.4 | 8.2 |

**Table 6-2: Properties of the oils used in chapters 6 and 7**

| Oil Type | Acid Number (AN) | Base Number (BN) | Asphaltene, % |
|---|---|---|---|
| **Oil A** | 0.37 | 2.02 | 3.49 |
| **Oil B** | 0.15 | 0.8 | 0.05 |
| **Oil C** | 0.2 | 1.77 | 2.9 |
| **Oil D** | 0.05 | 0.4 | 0.1 |
| **Oil E** | 0.2 | 1.2 | 2.3 |

### 6.2.2. Aging to Alter Wettability

Initially, brine-saturated samples were confined in the core flooding apparatus and then flooded with >5 pore volumes (PV) of crude oil at constant rate of approximately 0.1 ml $min^{-1}$ (equivalent to a linear flow rate of 0.8 ft $day^{-1}$) until no more water was produced. Then, the injection rate was increased gradually to 10 ml $min^{-1}$ (equivalent to a linear flow rate of 42 ft $day^{-1}$) to reduce the capillary end effect during this drainage process. The variation in $S_{wi}$ was achieved using a porous plate (e.g. *Jadhunandan and Morrow*, 1995). The lowest $S_{wi}$ measured with this method was 0.35 with use of a B05M1 five-bar ceramic porous plate (purchased from Soilmoisture Equipment Corp) of approximately 31% porosity and similar diameter to the core sample. The core samples at $S_{wi}$ were then aged for four weeks in oil-filled containers at 80°C. The aging period is comparable to aging times used in *Jadhunandan and Morrow,* (1995).

### 6.2.3. Spontaneous Imbibition (SI) and Coreflood Tests

After aging, the residual oil saturation ($S_{or}$) was established by first allowing spontaneous water imbibition, leaving the samples in cells filled with brine identical to the initial-formation brine. SI is a long process and its time varies depending on sample type, brine and oil compositions and experimental conditions. Various SI times have been reported in literature. *Jadhunandan and Morrow,* (1995) used three weeks in sandstone cores. *Strand et al.,* (2006) used a range of SI times from 10 to 20 days, while *Zhang and Austad,* (2006) used 20 to 35 days in chalk cores. In this study, four weeks was used, similar to the time used by *Romanuka et al.,* (2012) in carbonate core samples with similar properties. The produced oil volume was measured at regular intervals using the scale at the top of the Amott cell.

After SI, the samples were mounted in the same coreflooding apparatus used to measure the streaming potential and flooded with >10 PV of the same brine. The coreflooding experiments were performed at a constant field rate of approximately 1 ft day$^{-1}$ (0.1 ml min$^{-1}$) until no more oil was produced. This flowrate was assumed to be representative of the real hydrocarbon reservoirs. It is usually difficult to attain residual oil saturations during the (laboratory) coreflooding experiments on small core plug samples, due to capillary end effects arising by the discontinuity of capillarity in the wetting phase at the end-phase of the core sample. In most of the laboratory experiments performed at field rates (i.e. low rates), only remaining rather than residual oil saturation is reached. In our coreflood tests performed here, the injection rate was increased gradually, after 10 PVs, to a maximum rate that gives a pressure difference of approximately 700 kPa across the core sample to ensure all mobile phase was produced and the capillary end effects were reduced. The maximum rate varied between 6 and 12 ml min$^{-1}$, depending on the permeability of the core sample. We assumed that residual rather than remaining oil saturation has been measured; however, it may not be the case in each experiment and the increase in flow rate may not fully eliminate these problems associated with capillary end effects.

In one suite of experiments, oil was injected into dry samples and the oil-saturated samples were aged to induce wettability alteration. The dry samples were saturated with the oil phase in a vacuum oven for 48 hours. Then, the oil-saturated samples were flooded with >5 PV of the same oil. This was done to ensure that no air bubbles were trapped in the sample. The rest of the aging procedure, and the establishment of $S_{or}$, was the same as described above.

This approach allowed the wettability to be determined using Amott water index ($I_w$). It must be noted that the SI and coreflood tests were conducted at room temperature.

### 6.2.4. Measurement of Amott Water Index ($I_w$)

The wettability of the samples was determined by measuring the wettability index of water using the well-known Amott method (*Amott*, 1959)

$$I_w = \frac{V_{wsp}}{V_{wt}} = \frac{S_{spw} - S_{cw}}{1 - S_{cw} - S_{or}}, \quad (6.1)$$

where $V_{wsp}$ is the volume of water spontaneously imbibed and $V_{wt}$ is the total volume of water imbibed by both SI and coreflooding as described in the previous sections. $S_{spw}$ is the water saturation after the imbibition process, $S_{cw}$ is the connate water saturation and $S_{or}$ is the residual oil saturation after coreflooding.

### 6.2.5. Measurement of Zeta Potential at $S_w$ =1 and $S_w$=1-$S_{or}$

The zeta potential of brine saturated samples, and of samples saturated with brine and oil at the residual saturation ($S_{or}$), was measured using the SPM as described in section 4.2.2.

The intrinsic formation factor (at $S_w$ = 1) and electrical conductivity were available in Table 4-1. For the multi-phase experiments, the formation factor was evaluated at residual oil saturation and for each of the used brines by relating the electrical conductivity of the brine to that of the rock sample. Note that the formation factors at residual oil saturation increased by a factor of 5 to 12 compared to the

formation factors at $S_w$ = 1 (compare Table E-1 and E-7 in Appendix E). This reflects the decreasing contribution of surface conductivity (as oil is minimally conductive) and the domination of the bulk conductivity. Thus it was reasonable to neglect surface conductivity in these experiments and used the Helmholtz Smoluchowski equation (3.14) to calculate the zeta potentials at $S_w$=1-$S_{or}$. We assumed that at every salinity used, a new intrinsic formation factor was established due to the variation of fluid distribution inside the pore spaces, especially in the core samples where the incremental oil recovery was observed. In this case, the apparent formation factor at each salinity and saturation was equal to the intrinsic formation factor. (i.e. $F_a = F$).

The measurements of saturated rock conductivity, brine conductivity brine viscosity and brine permittivity were the same as described in chapter 4 section 4.2.

Note that the zeta potential obtained at $S_w$=1-$S_{or}$ is an effective value because it reflects the contribution of different values of the zeta potential at rock-brine and oil-brine interfaces. Uncertainty in the reported value of zeta potential reflects the range of possible regressions that can be fitted to the measured streaming potential data within experimental error (e.g. see Figure 4-7).

### 6.2.6. Design of Experiments

In this chapter, the coreflooding and SPM experiments were designed to investigate how the interpreted zeta potential from these measurements are affected by: (i) the aging process (i.e. whether the samples were aged or not), (ii) the wetting state established using the same aging procedure at different initial water saturation ($S_{wi}$), (iii) the crude oil type and (iv) the ionic strength of injection brines (high vs. low). Two types of initial brine were used to saturate the samples before primary drainage; NaB in Portland and FMB2 in Estaillades samples. Note that experiments in Portland samples were previously reported by *Alroudhan,* (2015). For all coreflood experiments carried out in this chapter and chapter 7, the

primary waterflooding was conducted using brine identical to that with which the rock sample was saturated.

We follow the approach of *Jadhunandan and Morrow,* (1995) to establish different degree of wettability. This was achieved by aging the samples with different initial brine saturations after primary drainage, for each oil type and brine composition investigated. These samples are termed 'aged' henceforth. The mixed-wet condition is likely to be a result of some fractional wettability, in which the largest pores are occupied by oil and have the potential to become oil-wet, whilst small pores are not invaded by oil, due to the high capillary entry pressure, and remain wetted by water (*Brown and Fatt*, 1956; *Kovscek et al.*, 1993). In a different suite of experiments used for comparison, samples were also drained to establish the same $S_{wi}$ but were not aged. These samples are termed 'non-aged'. The completely water-wet samples were not exposed to oil (i.e. $S_{wi}$=1) and the results obtained for these samples correspond to those reported for fully brine-saturated samples in chapter 4. These samples are termed 'brine-only'. The most oil-wet samples were saturated only with oil prior to aging ($S_{wi}$=0), and these samples are termed 'oil-only'. It should be noted that the zeta potential in all samples containing oil was measured at the residual oil saturation ($S_w$=1-$S_{or}$), i.e. after the SI and coreflooding stages when only the brine of interest was flowing in the pore-space and oil was not mobile.

Table 6-3 summarizes the experiments conducted on Portland and Estaillades carbonate samples at different conditions. For example, to guide the reader through Table 4: 'Aged/P3' test ID means the SPM experiment was conducted on 'aged' Portland sample # 3, which was initially saturated with NaB and brought down to initial water saturation '$S_{wi}$' of 0.39 using oil A. After SI test using NaB (identical to that with which the sample was saturated and aged), coreflooding experiments started first with NaB and the streaming potential was conducted on the sample saturated with NaB and oil A at $S_{or}$ (note the flowing fluid was only NaB). Then the flowing brine was switched to FMB1 and the streaming potential was carried out again. In all experiments, no change in $S_{or}$ was observed

after flooding with second or third brine composition (i.e. no low salinity effect was observed).

**Table 6-3: Summary of the experiments conducted in chapter 6**

| Test ID | Initial Brine | Oil Type | $S_{wi}$ | $1-S_{or}$ | $I_w$ | Brines Used in Waterflooding |
|---|---|---|---|---|---|---|
| **Brine-Only/P1** | NaB | Oil A | 1 | 1 | 1 | NaB – FMB1 |
| **Non-Aged/P2** | NaB | Oil A | 0.57 | 0.79 | 0.9 | NaB – FMB1 |
| **Aged/P3** | NaB | Oil A | 0.39 | 0.75 | 0.17 | NaB – FMB1 |
| **Aged/P4** | NaB | Oil A | 0.71 | 0.88 | 0.13 | NaB – FMB1 |
| **Aged/P5** | NaB | Oil A | 0.17 | 0.53 | 0.09 | NaB – FMB1 |
| **Oil-Only/P6** | NaB | Oil A | 0 | 0.30 | 0.04 | NaB – FMB1 |
| **Brine-Only/E1** | FMB2 | Oil B | 1 | 1 | 1 | FMB2 – SW – 20dSW |
| **Non-Aged/E2** | FMB2 | Oil B | 0.57 | 0.8 | 0.64 | FMB2 – SW – 20dSW |
| **Aged/E3** | FMB2 | Oil B | 0.67 | 0.86 | 0.19 | FMB2 – SW – 20dSW |
| **Aged/E4** | FMB2 | Oil B | 0.71 | 0.92 | 0.14 | FMB2 – SW – 20dSW |
| **Aged/E5** | FMB2 | Oil B | 0.35 | 0.86 | 0.09 | FMB2 – SW – 20dSW |
| **Oil-Only/E6** | FMB2 | Oil B | 0 | 0.50 | 0.03 | FMB2 – SW – 20dSW |
| **Aged/E7** | FMB2 | Oil D | 0.46 | 0.84 | 0.09 | FMB2 |
| **Aged/E8** | FMB2 | Oil E | 0.42 | 0.87 | 0.06 | FMB2 |
| **Oil-Only/E9** | FMB2 | Oil C | 0 | 0.47 | 0.03 | FMB2 |
| **Oil-Only/E10** | FMB2 | Oil D | 0 | 0.49 | 0.05 | FMB2 |
| **Oil-Only/E11** | FMB2 | Oil E | 0 | 0.52 | 0.04 | FMB2 |

## 6.3. Results

### 6.3.1. Impact of Water Saturation ($S_w = 1-S_{or}$) and Rock Conductivity on Zeta Potential

We start by investigating the relationship between the interpreted zeta potential and water saturation ($1-S_{or}$). Zeta potential measurements were obtained on Portland samples and residual oil A in NaB and FMB1 (Figure 6-1; see

*Alroudhan*, 2015); and on Estaillades samples and residual oil B in FMB2, SW and 20dSW (Figure 6-2).

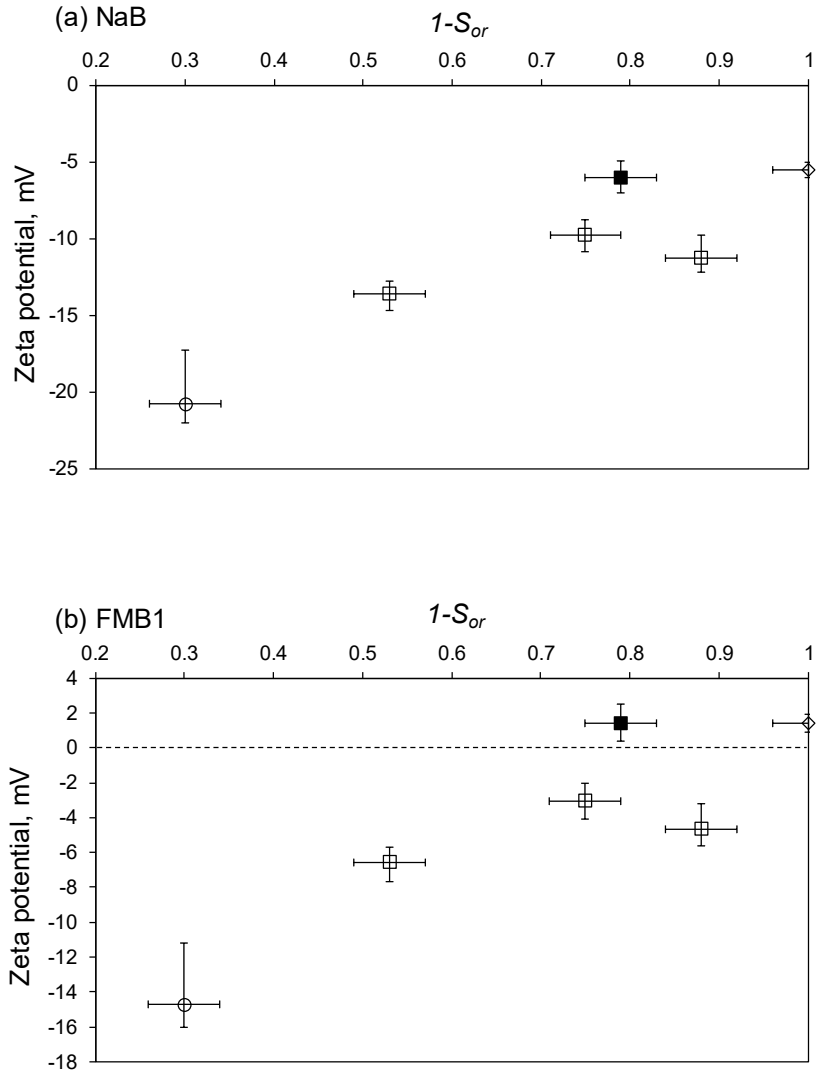



**Figure 6-1: Zeta potential as a function of water saturation ($S_w=1-S_{or}$) for the Portland samples aged with oil A in (a) 2M NaCl and (b) formation brine (FMB1). Empty circle represents aging in the absence of water ('oil-only'), empty squares represent aged samples in presence of water, filled square represents the water-wet case (no aging) and the diamond represents the single phase ('water-only'; $S_w=1$).**

The values of the zeta potential for the 'water-only' and 'non-aged' samples are identical within experimental error for each brine in both samples (compare empty diamonds and filled squares in both figures), suggesting that the lack of aging caused the oil to fail to adhere to the mineral surfaces, leaving them water-wet. For Portland, the 'aged' samples yield more negative zeta potential compared

to ‘water-only’ samples (compare the diamonds and open squares in Figure 6-1a, b) and the ‘oil-only’ samples show the most negative zeta potential (empty circles in Figure 6-1a, b). It is noted that the (negative) value is larger in magnitude for the NaB (-20.7 mV) than for the FMB1 (-14.7 mV; compare circles in Figure 6-1a, b), owing to higher divalent cation concentrations (Ca+Mg) in FMB compared to NaB (Table 6-1). In contrast, the aged Estaillades samples with oil B, (open squares in Figure 6-2a, b, c) yield more positive/less negative zeta potential compared to the ‘water-only’ samples (open diamonds in Figure 6-2a, b, c), whilst the ’oil-only’ samples (open circles in Figure 6-2a, b, c) show the most positive/least negative zeta potential (+10.73, +3.53 and -1.87 mV for FMB2, SW and 20dSW, respectively). Switching from FMB2 to SW and 20dSW results in the zeta potential becoming more negative for all the experiments (Figure 6-2).

The results shown in Figure 6-1 and Figure 6-2 demonstrate that there is no unambiguous correlation between the zeta potential and water saturation (1-$S_{or}$), i.e. the same value of the zeta potential (within experimental uncertainty given by the error bars) can be related to different values of 1-$S_{or}$ and *vice versa*. For example, the zeta potential of Estaillades in FMB2 is +7.13mV ±0.3 mV at both 1-$S_{or}$ = 1 (water-only sample) and 1-$S_{or}$ = 0.8 (non-aged sample; Figure 6-2a). Moreover, the aged samples show different values of zeta potential at the same value of 1-$S_{or}$, within experimental error, for all investigated brines (Figure 6-2a, b, c). For Portland, the ‘aged’ samples show a wider spread in 1-$S_{or}$ values compared to ‘aged’ Estaillades samples but the unclear trend still maintains particularly at 1-$S_{or}$ range 0.7 – 0.8 (Figure 6-1).

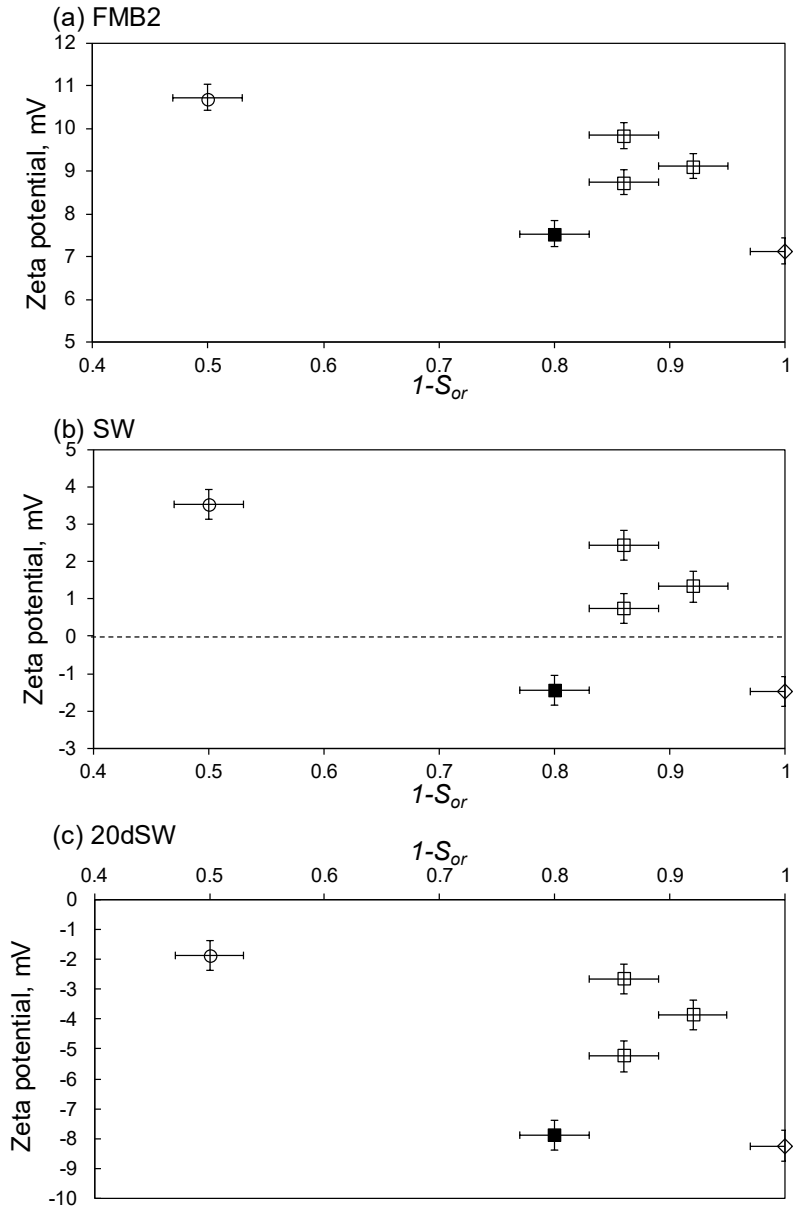



**Figure 6-2: Zeta potential as a function of water saturation ($S_w$=*1-$S_{or}$*) for the Estaillades samples aged with oil B in (a) formation brine (FMB2), (b) seawater (SW) and (c) diluted SW (20dSW).Empty circle represents aging in the absence of water ('oil-only'), empty squares represent aged samples in presence of water, filled square represents the water-wet case (no aging) and the diamond represents the single phase ('water-only'; $S_w$=1).**

Furthermore, we observed no correlation between saturated rock conductivity and zeta potential, similar to 1-$S_{or}$. The same rock conductivity can be measured in aged samples having different effective zeta potential values and *vice versa* (e.g. Figure 6-3a). Likewise, no unambiguous correlation was observed between rock conductivity, and wettability expressed as log($I_w$) as shown in Figure

6-3b. Thus water saturation or electrical conductivity measurement cannot be used to quantitatively characterise wettability.

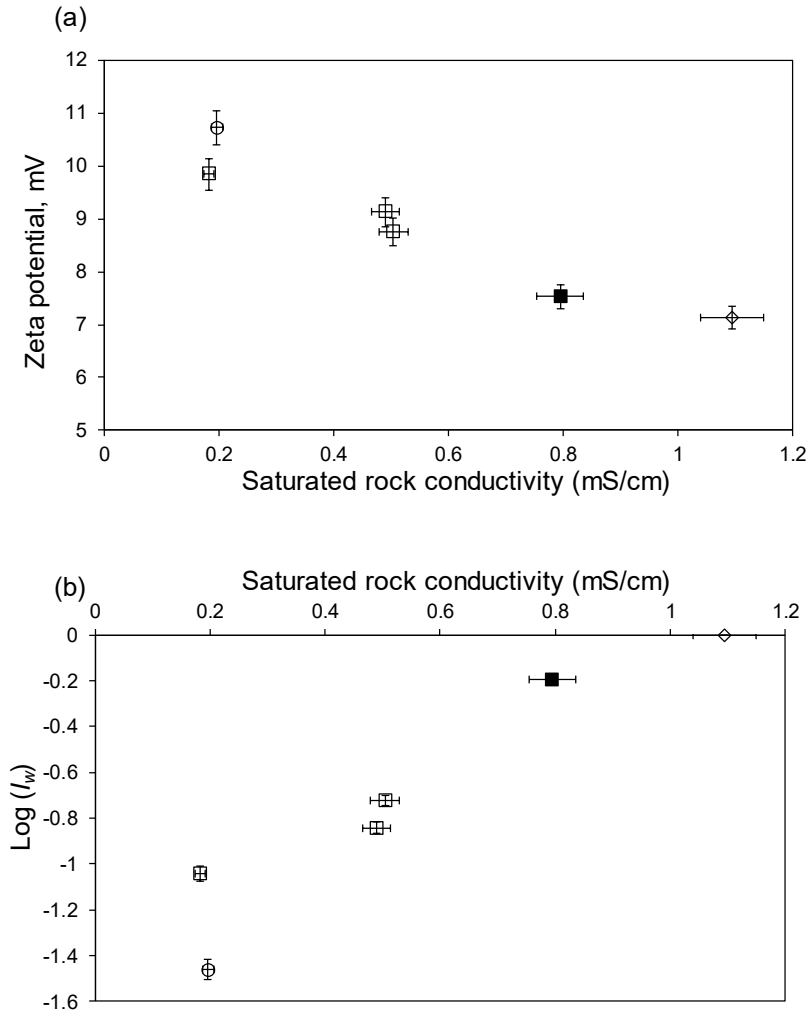



**Figure 6-3: Impact of rock conductivity on zeta potential and wettability for the Estaillades samples aged with oil B in formation brine (FMB2).(a) shows zeta potential as a function of saturated rock conductivity at different wetting state and (b) shows wettability (expressed as log $I_w$) as a function of saturated rock conductivity.**

### 6.3.2. Impact of Wettability on Zeta Potential

Here, we investigate the impact of wettability on zeta potential. Figure 6-4 and Figure 6-5 show the relationship between the Amott Index to water, expressed as log($I_w$), and the zeta potential. Figure 6-4 present the data obtained for oil A using the Portland samples; and Figure 6-5 shows the results from oil B using the

Estaillades samples containing different brines. A linear regression can be ascribed to each of the rock/brine/oil combinations and expressed as

$$\zeta\ (I_w)\ = C \cdot log(I_w) + \zeta_{Sw=1} \tag{6.2}$$

$$C = \frac{d\zeta}{d(\log(I_w))}, \tag{6.3}$$

where *C* denotes the dependence of the zeta potential on log($I_w$), and $\zeta_{Sw=1}$ is the zeta potential measured on the rock fully saturated with brine; i.e. in strongly water-wet conditions (brine-only experiments) when log($I_w$) = 0. It must be noted that this correlation (using equation 6.2) only works in mixed wet rocks ($I_w$ <0) and fails in strongly oil-wet rocks ($I_w$ = 0; as log($I_w$) yields ∞).

In Portland experiments with oil A, equation (6.2) yields a good fit to the measured data ($R^2$ > 0.83) with *C* = +9.1 mV for both high salinity brines. $\zeta_{Sw=1}$ = -5 mV for the NaB, and $\zeta_{Sw=1}$ = +1.5 mV for the FMB1. Decreasing $I_w$ (i.e. decreasing water-wetness) consistently yields more negative zeta potential for both brines. For oil B in Estaillades, equation (6.2) yields a better fit to the measured data ($R^2$ > 0.99). However, the gradient (*C*) in FMB2 is inversed and much smaller in magnitude (*C* = -2.5 mV) compared to that obtained for oil A in Portland samples; moreover, (*C*) increases in magnitude from -2.5 to -3.4 and to -4.8 mV as the brine composition changes from FMB2 to SW and 20dSW (Figure 6-5). In Estaillades, $\zeta_{Sw=1}$ is found to +7.1 mV for the FMB2, -1.48 mV for the SW and -8.4 mV for the 20dSW brine, which is identical within experimental error to those reported for fully brine-saturated samples in Figure 4-11. For oil B, decreasing $I_w$ (i.e. decreasing water-wetness) consistently yields more positive zeta potential.

Unlike water saturation and rock conductivity, there is a clear and consistent relationship between wettability, expressed as log($I_w$), and zeta potential irrespective of brine and oil compositions. The gradient (*C*) appears to be independent of brine composition at high ionic strength, i.e. for a given type of rock and crude oil, (*C*) is identical within the experimental uncertainty for both high ionic strength brines: NaB and FMB1 (Figure 6-4). However, (*C*) becomes dependent on brine composition at lower ionic strength (SW and 20dSW; Figure 6-5).

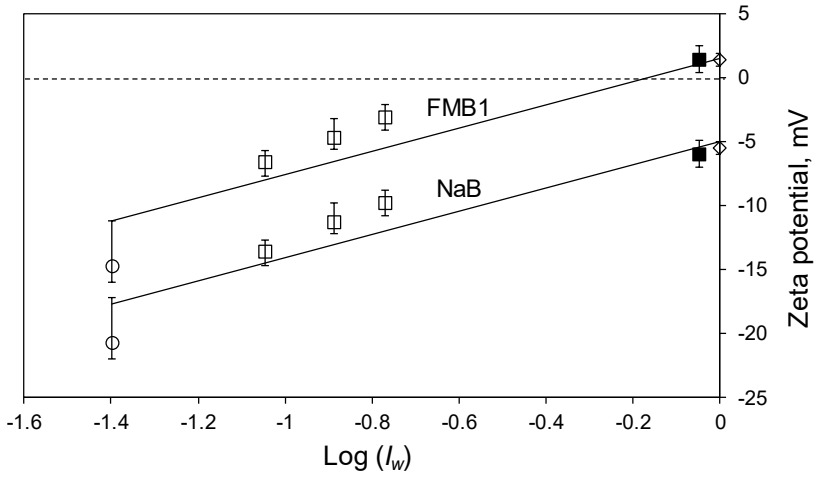



**Figure 6-4: Zeta potential as a function of water wetting index for oil A using the Portland samples saturated with 2M NaCl (NaB) or formation brine (FMB1) and residual oil saturation. Wettability increases towards oil-wet as log($I_w$) increases towards -∞.**

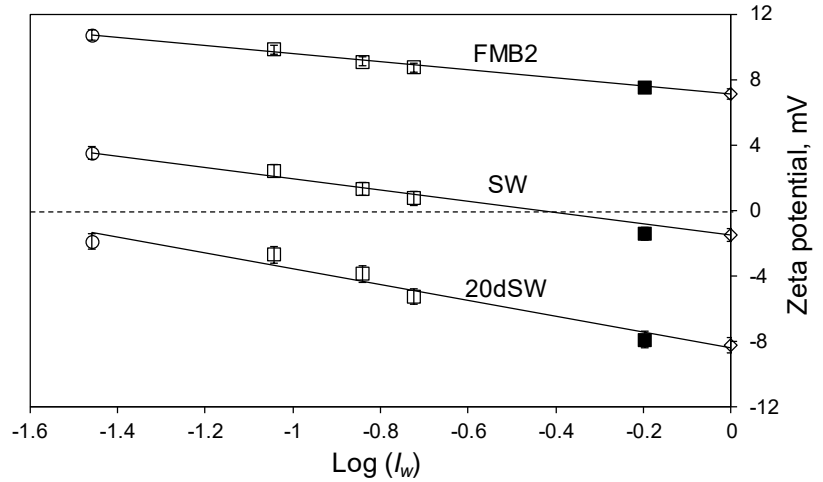



**Figure 6-5: Zeta potential as a function of water wetting index for oil B using the Estaillades samples saturated with formation brine (FMB2), seawater (SW) and 20dSW and residual oil saturation. Wettability increases towards oil-wet as log($I_w$) increases towards -∞.**

### 6.3.3. Impact of Varying Oil Composition on Zeta Potential

For other three oils (C-E; Table 6-2) reported in Table 3, we use the same rock type (Estaillades) to eliminate any possibility that the rock type might have an effect in the measured effective zeta potential. Figure 6-6 shows zeta potential as a function of water wetting index for oils (C-E) using the Estaillades samples saturated with FMB2 and residual oil saturation; also shown for comparison are the data from oil B in FMB2. Two clear and distinct trends in zeta potential with

log($I_w$) are obtained. In one, observed for oils C, D and E, the zeta potential becomes increasingly negative with decreasing $I_w$ (similar to oil A; Figure 6-4). In the other, observed for oil B, the zeta potential becomes increasingly positive with decreasing $I_w$. Note that similar trend in zeta potential with wettability observed for crude oils C, D, and E ($C$ = +3.7 mV; $R^2$ > 0.94), which suggests that these oils wet the surfaces of Estaillades samples to a similar extent.

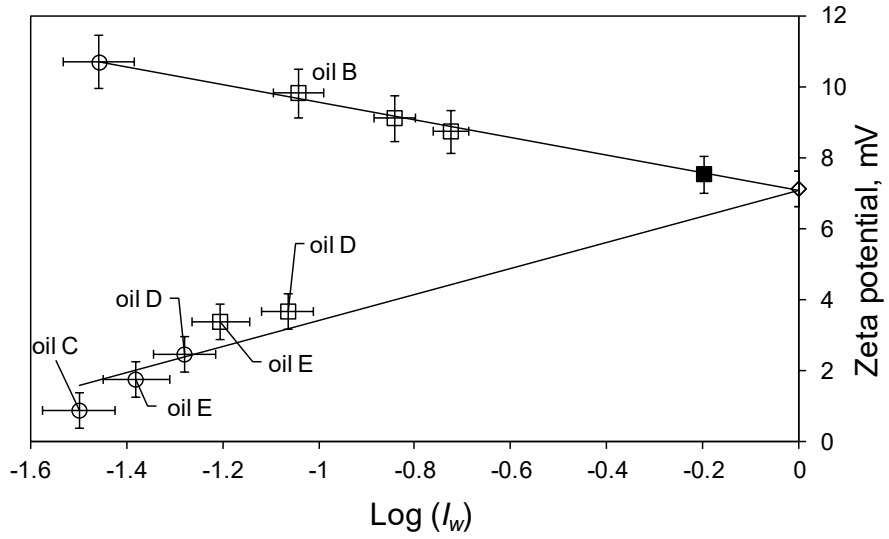



**Figure 6-6: Zeta potential as a function of water wetting index for each of the four oils tested (B-E) using the Estaillades samples saturated with formation brine (FMB2) and residual oil saturation. Empty circles represent aging in the absence of water ('oil-only'), empty squares represent aged samples in presence of water, filled square represents non-aged sample and the diamond symbol represents water-only sample.**

## 6.4. Discussion

### 6.4.1. The Relationship Between Wettability and Zeta Potential

We observe a clear and consistent linear relationship between the zeta potential and Amott wettability index of water, expressed as log($I_w$), for all investigated natural carbonate samples, brines and crude oils. In equation (6.2), the slope of the regression ($C$) indicates the dependence of zeta potential on wettability. It also indicates the polarity of crude oil-brine zeta potential and therefore we term it Crude Oil Zeta Potential Indicator (COZPI; if COZPI is negative, oil-brine interface is positively charged and *vice versa* as discussed

later). We will use the term COZPI, instead of the gradient, throughout the discussion section. For each Crude Oil Brine Rock (COBR) mixed wet system, a unique COZPI can be identified.

The relationship between the wettability index and the zeta potential observed here can be explained by the varying proportions of water-wet and oil-wet surfaces encountered by the flowing brine during the streaming potential measurement (Figure 6-7). In water-wet conditions, the brine flows within continuous layers adjacent to the mineral surfaces wetted by water, and the resulting zeta potential reflects the pristine mineral-brine interface, which here we found is positively charged in formation brines (Figure 6-7a). The 'non-aged' samples reflect water-wet conditions and yield zeta potential values similar to 'brine-only' samples (as shown in Figure 6-4 and Figure 6-5; black squares and diamonds). *Jackson and Vinogradov,* (2012) showed that introducing residual, immobile oil into the pore-space without aging does not affect the effective zeta potential because the residual oil does not replace the brine at the mineral surface. Thus, zeta potential is not affected by the presence of immobile, discontinuous bubbles of oil that reside in the middle of larger pores (Figure 6-7b). As the wetting state becomes mixed-wet, the flowing brine encounters some oil-wet mineral surfaces, yielding the effective zeta potential different from that measured during the single-phase ('brine-only') experiments. The effective zeta potential in this case comprises superposed contributions of mineral-brine and oil-brine interfaces and the resulting zeta potential lies between the 'brine-only' and the 'oil-only' values (*Jackson and Vinogradov*, 2012).

The 'oil-only' samples were aged with no brine present prior to the measurement of the zeta potential, and we hypothesise that the oil in these samples, after aging and subsequent waterflooding down to $S_{or}$, wets most but not all of the mineral surfaces. Large pores are occupied by oil and become oil-wet after aging. However, small pores are not invaded by oil during primary drainage, due to the high capillary entry pressure, and become water-wet after waterflooding. Thus the interpreted effective zeta potential is more influenced by the oil-brine

interface and therefore shifts towards the magnitude and polarity of the oil-brine interface zeta potential. When the oil-brine zeta potential is negative (as observed for A, C, D and E; with a positive COZPI), the effective zeta potential of the sample becomes more negative (Figure 6-7c). When the effective zeta potential becomes increasingly positive (like the case for oil B), the oil must have a positive charge at the oil-brine interface (Figure 6-7d). Additional experiments in SW and 20dSW confirm this trend and obtained linear regression (with a negative COZPI) provides an excellent fit to the data (Figure 6-5a, b, c). Note that the pH remained above 6 in all experiments (e.g. Table 6-1 and Table 4-2). This is the first time that positive zeta potential at the oil-brine interface has been reported in salinity and pH typical of natural brines.

Zeta potential measurements obtained using the streaming potential measurements are therefore sensitive to the wetting state, regardless of oil, if two conditions are met. First, the zeta potential at the mineral-brine and oil-brine interfaces must differ in magnitude and/or polarity. Second, variations in wettability must reflect differing proportions of water-wet and oil-wet mineral surfaces in the pore-space. These conditions are typically met in carbonate reservoirs, where the mineral-brine interface is often positively charged (e.g. *Jackson and Vinogradov*, 2012; *Mahani et al.*, 2015; *Mahani et al.*, 2016), and those parts of the pore-space contacted by oil become oil-wet (*Kovscek et al.*, 1993). Thus streaming potential measurements, yielding zeta potential data sensitive to the pore-level proportion of oil- and water-wet mineral surfaces, offer a new route to determine wettability in carbonate reservoirs. In the following sections we investigate the parameters that control the zeta potential at the mineral-brine and oil-brine interfaces, and also provide some discussion on forces responsible for the stability of wetting films along with the implication of our method for *in-situ* wettability characterisation.

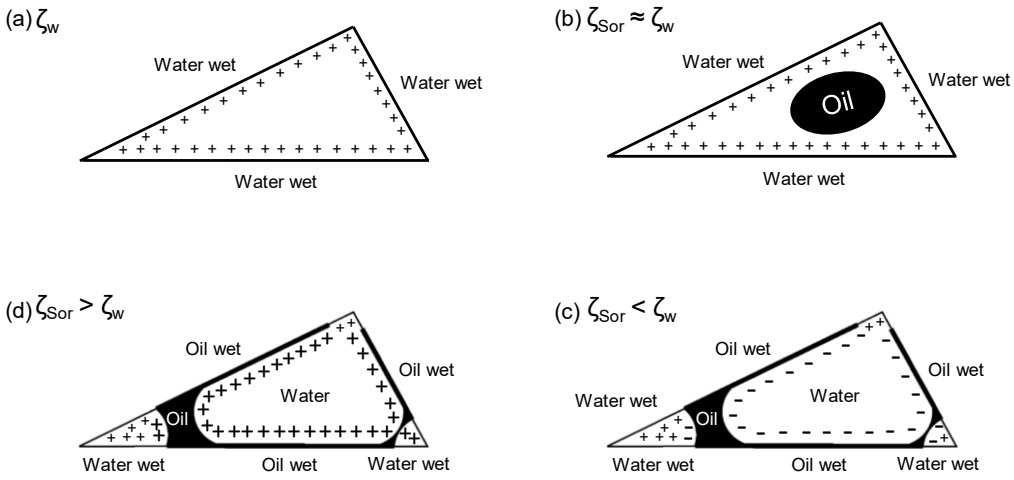



**Figure 6-7: Schematics showing postulated wettability of mineral- and oil-brine interfaces in carbonate samples using oils (A-E) in formation brines. (a) Saturated with water, (b) with water and residual oil without aging and (c, d) with water and residual oil after aging. In (c), oil having a negatively charged oil-brine interface and in (d), oil having a positively charged oil-brine interface. Large pores are showing here; smaller pores are expected to be water-wet in non-aged and aged samples; and oil-wet in oil-only samples. Figure is adapted from *Jackson and Vinogradov,* (2012).**

### 6.4.2. Controls on Zeta Potential of Mineral-Brine and Oil-Brine Interfaces

The zeta potential at carbonate-brine interface is strongly affected by brine ionic strength and composition, primarily $Ca^{2+}$ and $Mg^{2+}$ concentration (as shown in chapter 4). Much less attention has been given to the oil-brine interfacial charge. The available data suggest that the interface is negatively charged at pH > 4.5 but can become positive at lower pH. However, the data are limited and were acquired using emulsions of oil in simple NaCl or $CaCl_2$ electrolytes at low ionic strength in the commercial zetameters discussed above (*Chow and Takamura*, 1988; *Buckley et al.*, 1989; *Beattie and Djerdjev*, 2004; *Hirasaki and Zhang*, 2004; *Alotaibi and Nasr-El-Din*, 2011; *Alotaibi and Yousef*, 2016). It can be challenging to maintain a stable suspension in such experiments, especially at the high ionic strength typical of natural brines (*Beattie and Djerdjev*, 2004; *Alotaibi and Yousef*, 2016).

In our multiphase experiments, we need to consider the controls on the zeta potential at the two interfaces. The zeta potential at mineral-brine interface depends on Ca and Mg concentrations in brine but not on pH, similar to 'brine-

only' experiments (as demonstrated experimentally in chapter 4). Therefore, when we switch from NaB to FMB1 in Figure 6-4, the concentrations of Ca and Mg increase and make the zeta potential of the mineral-brine interface more positive (Figure 6-4). When we switch from FMB2 to SW and 20dSW, concentrations of Ca and Mg decease and make the mineral-brine interface zeta potential more negative (as shown in Figure 6-5).

On the other hand, the zeta potential at the oil-brine interface depends strongly on pH at low ionic strength (*Buckley et al.*, 1989; *Nasralla et al.*, 2013). The zeta potential increases almost linearly towards more positive values as pH decreases. However, at high ionic strength, the pH dependence of the zeta potential is significantly less pronounced (*Nasralla et al.*, 2013). The pH dependence of the zeta potential at the oil-brine interface is similar to the observations published on silica-brine (*Kosmulski et al.*, 2002) and anatase-brine systems (*Kosmulski and Rosenholm*, 1996). The results obtained for oil A and high salinity electrolytes NaB and FMB1 showed that the zeta potential measured in oil-wet samples decreased by the same amount relative to the 'brine-only' values (compare circles and diamond for both electrolytes in Figure 6-4). Thus we conclude that the zeta potential at the oil-brine interface is identical for both brines, within the experimental error, although pH varies between 8.2 (in NaB) and 6.2 (in FMB1). When a similar fraction of pore walls is wetted by oil A, a similar wetting behaviour is established (see the identical $1\text{-}S_{or}$=0.3 in Figure 6-1a, b and identical $\log(I_w)$=-1.4 in Figure 6-4 for NaB and FMB1). Therefore, COZPI for both COBR systems is identical within the experimental uncertainty (in Figure 6-4).

As we switch from FMB2 (pH 6.2) to SW (pH 7.4) and later to 20dSW (pH 8.2), the pH dependence of the oil-brine zeta potential becomes stronger due to the lower ionic strength. In this case, the increase in pH from 6.2 (FMB2) to 8.2 (20dSW) causes the zeta potential at the oil-brine interface to increase in magnitude (Figure 6-5). Note that for crude B the oil-brine interface is positively charged; therefore, the zeta potential at the oil-brine interface becomes progressively more positive with increasing pH and the effective zeta potential also

shifts towards more positive values relative to the 'brine-only' values, as shown in Figure 6-5 (compare the differential potential between diamonds and circles for all three electrolytes). During the transition from SW to 20dSW, the zeta potential at both interfaces also increases in magnitude due to the EDL expansion. As a result of all the effects, COZPI increases in magnitude from -2.5mV (in FMB2) to -3.4mV (in SW) and -4.8mV (in 20dSW) (Figure 6-5). We conclude that a unique value of COZPI will characterise each COBR system at lower ionic strength (<1M).

### 6.4.3. Crude Oil Composition and Polarity of Oil-Brine Interface

We investigated five types of natural crude oils in this study and observed a linear regression between the zeta potential and the water wetting index for all oils (Figure 6-4, Figure 6-5 and Figure 6-6). All oils investigated (A-E) are characterised by higher base number (BN) relative to acid number (AN) and with asphaltene content (AS) that ranges from a relatively high in oil A to a relatively low in oil B (Table 6-2). *Buckley and Liu,* (1998) stated that any of oil properties alone cannot be considered the key property in wettability alteration. Rather, it is a combination of asphaltene, acid and base numbers that provide a qualitative indication of the extent to which a specific type of crude oil in a particular COBR system can alter the rock wettability. For carbonates in brine rich with multivalent cations system, oils with high BN or relatively high asphaltene content can enhance the wettability alteration towards more oil-wet (*Buckley and Liu*, 1998).

We have also shown that all but oil B give a negative zeta potential at the oil-brine interface. The low asphaltene content in oil B might contribute to the observed positive zeta potential at the oil-brine interface. However, we find no direct correlation between oil composition and magnitude or polarity of oil-brine interface; the similar zeta potentials measured with oils C, D and E (Figure 6-6) corresponds to different values of BN, AN, and asphaltene (Table 6-2).

### 6.4.4. Successful Wettability Alteration with Charged Interfaces of the Same Polarity at High Ionic Strength

In this section, we provide a possible explanation to the results obtained in Portland-Oil A-NaB and Estaillades-Oil B-FMB2 systems. Despite the fact that both the oil-brine and mineral-brine interfaces had the electrical potential of the same polarity in these experiments, the rock wettability was successfully altered as suggested by the non-zero log($I_w$).

It has been shown in section 2.5 that the stability of the wetting film on the mineral surface depends on the disjoining pressure, which is partly controlled by the electrostatic force between mineral-brine and oil-brine interfaces (*Hirasaki*, 1991; *Hiorth et al.*, 2010; *Israelachvili*, 1985; more detailed analysis is discussed in next chapter when we present our CSW results). When the two interfaces have the same polarity, the electrostatic force is repulsive and the wetting film is stable. It becomes attractive between two opposing charged interfaces and hence the wetting film can collapse, promoting oil-wetness to the mineral surfaces.

Here, we observed a wettability alteration in Portland aged with oil A and NaB (Figure 6-4) and Estaillades aged with oil B and FMB (Figure 6-5). In both cases, it was possible to alter the rock wettability to oil-wet although the two interfaces had the same polarity (negative for oil A and NaB and positive for oil B and FMB2). We hypothesise that at high ionic strengths the wetting films at concave areas of the mineral surfaces were stable, while the stability of the wetting films adjacent to the convex areas was significantly reduced and these surfaces became oil-wet; consistent with the disjoining pressure model presented by *Hirasaki,* (1991). During coreflooding, such as that investigated in Portland and oil A in which NaB was replaced by FMB1 or in Estaillades and oil B in which FMB2 was replaced by SW and then 20dSW, the electrostatic force became attractive and increased in magnitude, leading to a lower disjoining pressure and increasingly unstable water films. Thus the wettability was altered to more oil-wet conditions and no incremental recovery was observed.

### 6.4.5. Practical Application of Wettability Characterisation using the SPM Method

The practical implementation of this experimental method will involve measurements of the wettability index ($I_w$) and the zeta potential in a preserved or aged rock samples using formation brine of interest. To fully characterise rock wetting behaviour two more measurements are required to provide the two end-points of the linear regression: the measurements carried out at 'brine-only' and 'oil-only' conditions. The obtained regression (COZPI) from the zeta potential vs. log($I_w$) plot gives indication about the surface charge of oil-brine interface (if COZPI is negative the oil-brine interface is positively charged and *vice versa*) and the wettability index of the system. This will offer a new, quick and accurate route to determine and quantify the wettability in carbonate reservoirs, which might also be used to screen carbonate oil reservoirs for successful controlled salinity waterflooding which is usually accompanied by wettability alteration. Due to its simplicity, SPM could be used downhole using a modified tool similar to Modular Dynamic Tester (MDT). The possibility of *in-situ* characterisation of formation wettability is of a high importance for many industrial applications, including hydrocarbon reservoirs and $CO_2$ sequestration and trapping sites.

## 6.5. Conclusions

We report here measurements of the zeta potential on two intact natural limestones containing natural crude oils aged at various values of initial brine saturation and different brine compositions. Three key conclusions may be drawn from the results reported here. (1) There is a clear relationship between zeta potential interpreted from streaming potential measurements and wettability expressed in terms of the Amott water index ($I_w$). Thus, the SPM method is efficient in characterising wettability of COBR system in natural conditions of pH and ionic strength with undistorted pore structure and with both brine and oil present in the pore-space at the same time. (2) The oil-brine interface can be positively charged

at the high pH and ionic strength relevant to the formation brines found in many carbonate reservoirs. This might explain why brine dilution used as EOR has not always resulted in improved oil recovery, which simply could be that oil was positively charged and dilution only increased oil wetness. (3) COZPI provides the essential means to quantitatively characterise wettability. The finding implies that wettability can accurately be predicted (quantitatively), it can be modified to a specific value by adjusting brine concentration, composition and pH. The results have significance in allowing petrophysics laborites to conduct streaming potential measurements as a complementary measurement to the Special Core Analysis (SCAL), and oil service companies to (perhaps) consider deploying the SPM downhole for *in-situ* wettability characterisation.

# Chapter 7.

# Designing the Brine Composition: Improved Oil Recovery from Carbonate During Controlled Salinity Waterflooding

## 7.1. Introduction

We have seen in chapter 2 that the most typical CSW approaches are either lowering the ionic strength of imbibing/flooding brine by switching from formation brine to seawater (e.g. Figure 2-3d) and/or to dilute formation brine or seawater (e.g. Figure 2-3b-c). Other shows CSE by attuned the concentration of one or more of the divalent ions $Ca^{2+}$, $Mg^{2+}$ or $SO_4^{2-}$ (e.g. Figure 2-2a, b, c). The problem is that CSE is not observed in all cases and CSW in carbonates remains unclear with many contradictory results. Consequently, there is no method to predict the optimum CSW composition to maximize oil recovery for a given COBR system.

Recall that several studies have suggested a link between wettability and zeta potential in carbonates (e.g. *Strand et al.*, 2006; *Zhang et al.*, 2007; *Jackson and Vinogradov*, 2012; *Yousef et al.*, 2012a; *Mahani et al.*, 2015; *Alroudhan et al.*, 2016), although none have yet shown a direct correlation between changes in zeta potential, wettability and improved recovery during CSW.

The aim of this chapter is to establish a relationship between brine composition, wettability and oil recovery during CSW experiment using the SPM method. We demonstrated in chapter 6 that the oil-water interface can be positively or negatively charged at the high pH and ionic strength relevant to the formation brines found in many carbonate reservoirs. We show that the zeta potential at both the mineral-water and oil-water interfaces must be determined when assessing the

optimum brine composition for CSW in carbonates. Improved recovery during CSW in carbonates is observed only if the change in brine composition yields a zeta potential at each interface that has the same polarity, such that a repulsive electrostatic force acts between the interfaces and stabilizes a water film on the mineral surface. Studies that have failed to observe improved recovery using the conventional (dilution) approach to CSW, or by designing some other change in water composition that yields more negative mineral surfaces, were most likely dealing with a positively charged oil-water interface that had not been diagnosed.

We provide a new method to allow the optimum brine composition for CSW in carbonates to be determined based on measurements of the zeta potential at both the oil-brine and mineral-brine interfaces, along with new insight into the mineral-surface-scale mechanisms underpinning CSW. The results have broad application and significance in allowing oil companies to design water injection strategies that yield improved oil recovery from carbonate reservoirs.

## 7.2. Methodology

Estaillades core samples (Table 4-1) and four crude oils (B, C, D and E; Table 6-2) were used in the experiments reported here. Three different brine compositions were also tested (Table 7-1). The first set comprised FMB, SW and 20dSW; identical to those used in chapters 4 and 6. The other tested brines comprised two sets each containing three synthetic brines; each set had the same ionic strength but varying $Ca^{2+}$ concentrations. The aging and establishment of $S_{or}$ procedures were the same as reported in sections 6.2.2 and 6.2.3. We followed the same SPM methodology described in section 6.2.5 to measure the zeta potential at $S_w = 1$ and $S_w = 1\text{-}S_{or}$.

A tertiary CSW approach was adopted in which the core sample was first flooded with the same brine used during aging until no more oil was produced (i.e. the residual oil saturation $S_{or}$ had been reached, usually after >10 pore-volumes-injected (PVI) of the brine of interest). Thereafter, the injected brine was changed

to one with modified composition for a minimum of 10 PVI or until no further oil was produced. Four different waterflooding sequences were used. The first followed a typical low salinity waterflood (LSW): the sample was first aged and then flooded with the formation brine, before switching to seawater and then dilute seawater (FMB -> SW -> 20dSW). The second inverted the typical LSW: the sample was aged and then flooded with dilute seawater, before switching to seawater and then formation brine (20dSW -> SW -> FMB).

The third and fourth flooding sequences were designed to test the relative importance of changing the total ionic strength of the injected brine versus changing the concentration of $Ca^{2+}$ which is known to play a key role in controlling the zeta potential of calcite. In the third flooding sequence, the sample was aged and then flooded with the formation brine. Then $Ca^{2+}$ was progressively stripped out of subsequent waterfloods (see compositions FdCa1, FdCa2 and FdCa3 in Table 7-1) but the ionic strength was kept constant by adjusting the concentration of NaCl. In the fourth flooding sequence, the sample was aged and then flooded with pre-equilibrated NaCl. Then $Ca^{2+}$ was progressively added to subsequent waterfloods (see compositions NaCa1, NaCa2 and NaCa3 in Table 7-1) whilst keeping the ionic strength constant by adjusting the concentration of NaCl.

**Table 7-1: Properties and composition of brines used in chapter 7**

| | FMB | SW | 20dSW | FdCa1 | FdCa2 | FdCa3 | NaCa1 | NaCa2 | NaCa3 |
|---|---|---|---|---|---|---|---|---|---|
| **Ions** | | | | | | | | | |
| $Na^+$ | 2 | 0.550 | 0.0275 | 2.840 | 3.218 | 3.259 | 1.959 | 1.581 | 0.741 |
| $Cl^-$ | 3.020 | 0.620 | 0.031 | 3.312 | 3.428 | 3.442 | 1.987 | 1.861 | 1.581 |
| $Ca^{2+}$ | 0.420 | 0.014 | 0.0007 | 0.140 | 0.014 | 0.0003 | 0.014 | 0.140 | 0.420 |
| $Mg^{2+}$ | 0.091 | 0.045 | 0.00225 | 0.091 | 0.091 | 0.091 | 0.00004 | 0.00004 | 0.00004 |
| $SO_4^{2-}$ | 0.002 | 0.024 | 0.0012 | 0.002 | 0.002 | 0.002 | 0.0002 | 0.0002 | 0.0002 |
| Ionic strength | 3.537 | 0.749 | 0.0375 | 3.537 | 3.537 | 3.537 | 2.001 | 2.001 | 2.001 |
| pH | 6.3 | 7.4 | 8.2 | 6.58 | 6.76 | 7.24 | 7.23 | 6.65 | 6.29 |

## 7.3. Results

### 7.3.1. Brine Composition and the Zeta Potential of Water-Wet Carbonate Samples

We begin by reporting the effect of the tested brine compositions on the zeta potential of strongly water-wet samples saturated only with the brine of interest (Figure 7-1). The zeta potential of the sample in FMB was positive, consistent with previous studies of natural carbonates, but became negative in contact with SW and increasingly negative as the seawater was diluted (Figure 7-1a), consistent with previous results obtained in Figure 4-11. Thus a typical LSW (FMB -> SW -> 20dSW) yields increasingly negative zeta potential at the mineral-brine interfaces and *vice versa* during the inverted LSW (20dSW -> SW -> FMB; Figure 7-1a). Removing the calcium ions from formation brine also yielded increasingly negative zeta potential, while adding $Ca^{2+}$ ions to NaCl brine yielded increasingly positive zeta potential (Figure 7-1b). However, the change was smaller in magnitude than that observed when switching from formation brine to seawater and then dilute seawater. Moreover, removing $Ca^{2+}$ from the formation brine failed to invert the polarity of the zeta potential.

The next section shows that the polarity of the zeta potential at the oil-brine interface plays a key role in controlling whether improved recovery is observed during CSW. As shown previously in chapter 6, oils C, D and E have a negative zeta potential at oil-brine interface (Figure 6-6). However, oil B have a positive zeta potential at the oil-brine interface, which is larger in magnitude than the positive zeta potential at the mineral-brine interface (Figure 6-6). The experiments reported here test the hypothesis that IOR during CSW occurs only when the electrostatic repulsion between the oil-brine and mineral-brine interfaces increases in response to the change in brine composition during waterflooding.

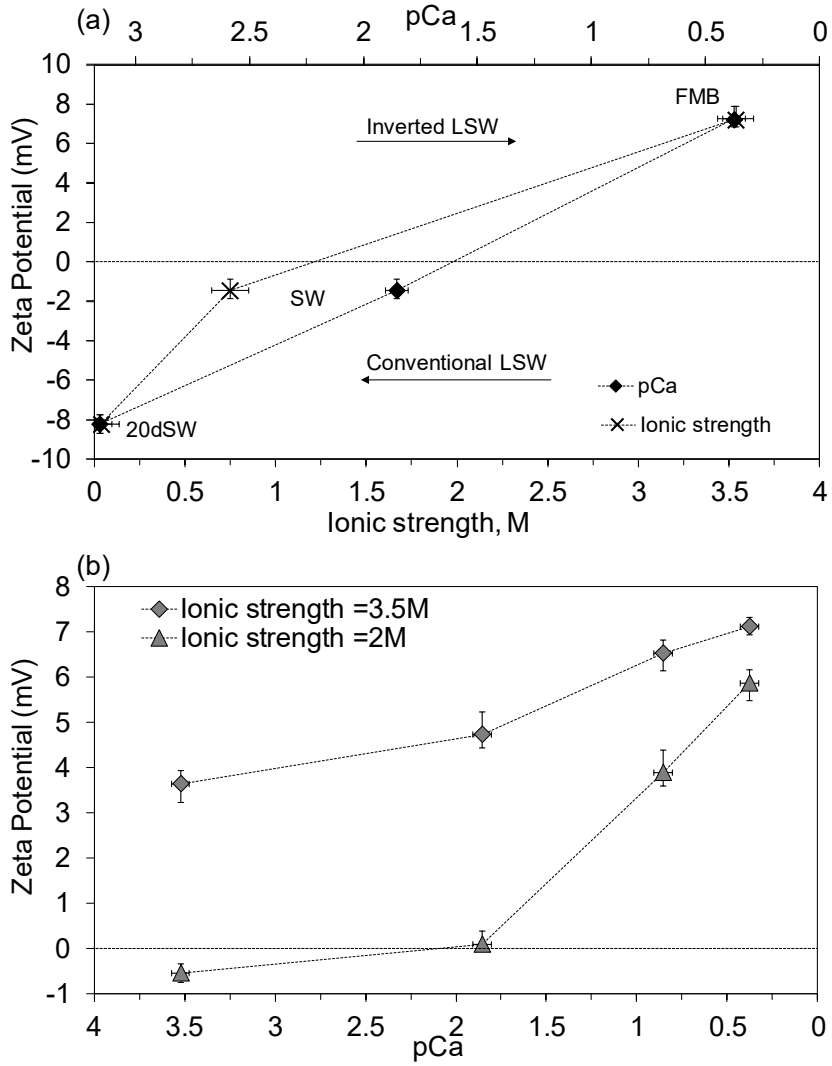



**Figure 7-1: Impact of brine composition on the zeta potential of water-wet carbonate samples in formation brine (FMB), seawater (SW), diluted seawater (20dSW) and varying Ca in FMB and 2M NaCl. (a) Effect of varying composition from formation brine (FMB) to seawater (SW) to dilute seawater (20dSW). Data are plotted against ionic strength on the lower horizontal axis and pCa on the upper horizontal axis, where p represents the negative logarithm. (b) Effect of varying calcium concentration at two different values of (constant) total ionic strength (2M and 3.5M which is comparable to FMB). Data are plotted against pCa.**

### 7.3.2. Controlled Salinity Waterflooding with Varying Ionic Strength

We now report coreflooding experiments and zeta potential measurements during conventional tertiary LSW (FMB -> SW - > 20dSW; Figure 7-2a, b) and inverted LSW (20dSW -> SW -> FMB; Figure 7-2d, e). As discussed previously,

conventional LSW yields more negative zeta potential at the mineral-brine interface; inverted LSW yields more positive zeta potential (Figure 7-1a).

All three crude oils C, D and E with a negative zeta potential at the oil-brine interface showed modest but measureable incremental recovery during conventional LSW; the results of one example LSW using crude oil E are shown in Figure 7-2a. Moreover, there is a clear correlation for each sample between the incremental oil recovered and the incremental change in the zeta potential of the sample as the injected brine composition was changed: oil recovery increased as the zeta potential became more negative (Figure 7-2c). In contrast, oil B showed no incremental recovery during conventional LSW (Figure 7-2b) and there is therefore no correlation between change in zeta potential and incremental recovery (Figure 7-2c).

During inverted LSW, crude oils C, D and E showed no incremental recovery; the results of one example LSW using crude oil E are shown in Figure 7-2d. However, oil B showed the largest incremental recovery of all the crude oils tested (Figure 7-2e). Moreover, incremental recovery for oil B increased as the sample zeta potential became more positive (Figure 7-2f). We conclude that CSW is successful only if the zeta potential at the mineral-brine changes to become more negative when the oil-brine interface is negatively charged in the formation brine, and *vice-versa*.

It is noted that (in general) the recoveries are high (>70%; Figure 7-2), and hence the residual oil saturation is low, after first waterflooding. This is not the case in real carbonate reservoirs where the recovery factor using conventional waterflooding is low (refer to chapter 2). In our experiments, the high recoveries and low $S_{or}$ were only achieved after injecting many pore volumes (≥10 PVs) than would be applied in the field (usually 1 to 3 PVs).

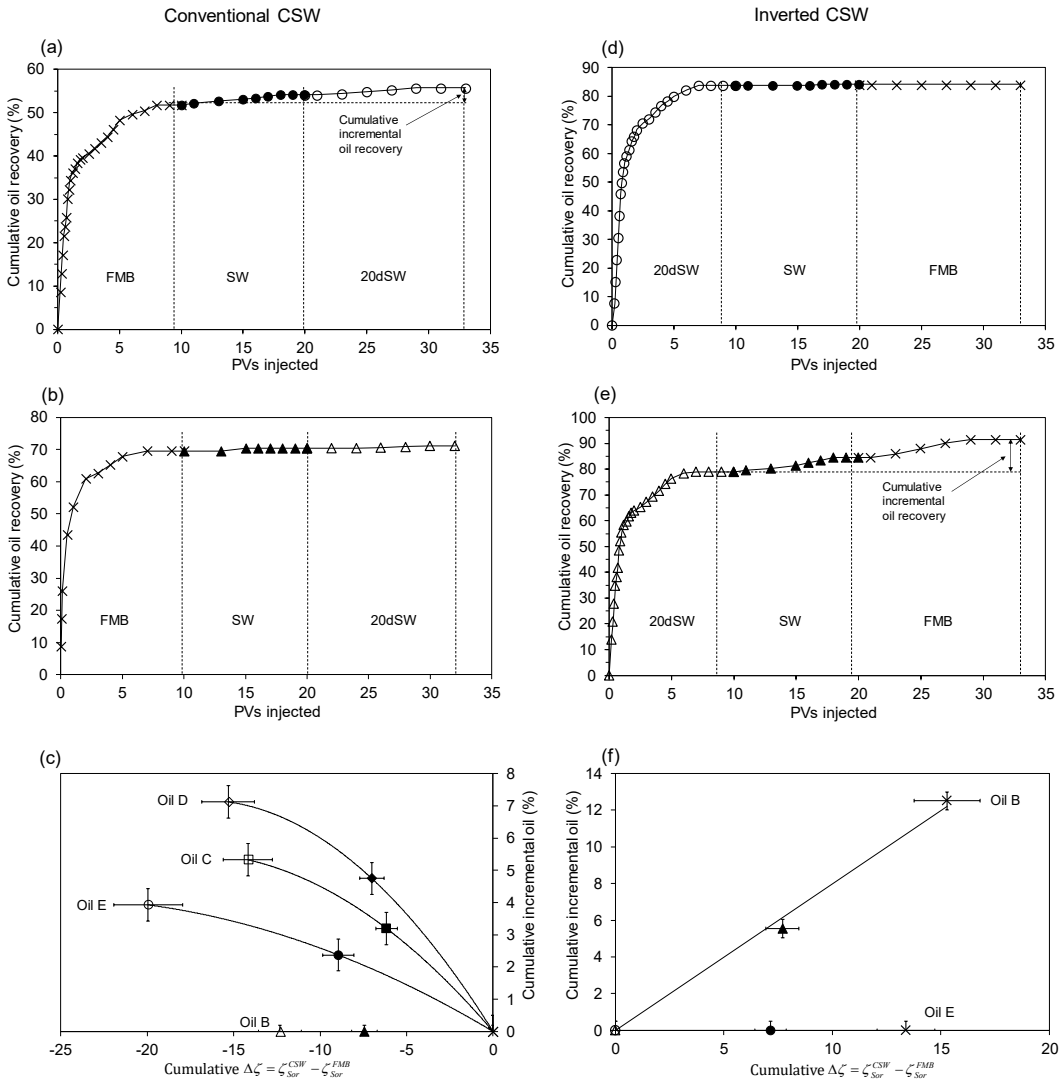



**Figure 7-2: Effect of conventional low salinity waterflooding LSW (FMB -> SW - > 20dSW) and inverted LSW (20dSW -> SW - > FMB) on oil recovery and zeta potential change. (a, b, c) show conventional LSW results and (d, e, f) show inverted LSW results. Examples of (a) successful results of LSW and (d) unsuccessful results of inverted LSW using crude oil E. Examples of (b) unsuccessful results of LSW and (e) successful results of inverted LSW using crude oil B. Vertical dashed lines in (a, b, d, e) indicate when the streaming potential measurements are conducted. (c, f) Relationship between the incremental oil recovered and the incremental change in the zeta potential of the sample as the injected brine composition was changed during LSW and inverted LSW. Subscript FMB indicates formation brine in (c) and 20dSW in (f).**

### 7.3.3. Controlled Salinity Waterflooding with Varying Ca Concentration

In the conventional and inverted LSW experiments described previously, both the total ionic strength, and the $Ca^{2+}$ concentration, changed between the

FMB, SW and 20dSW brines used. We finish by testing the effect of eliminating the change in ionic strength, comparing waterflood experiments in which the $Ca^{2+}$ concentration was progressively decreased at constant ionic strength (FdCa1-3 in Table 7-1), and in which the $Ca^{2+}$ concentration was progressively increased at constant ionic strength (NaCa1-3 in Table 7-1). As discussed previously, removal of $Ca^{2+}$ yields more negative zeta potential at the mineral-brine interface; addition of $Ca^{2+}$ yields more positive zeta potential (Figure 7-1b).

All three crude oils C, D and E with a negative zeta potential at the oil-brine interface showed modest but measureable incremental recovery when Ca was removed; the results of one example using crude oil C are shown in Figure 7-3a. There is again a clear correlation for each sample between the incremental oil recovered and the incremental change in the zeta potential of the sample: oil recovery increased as the zeta potential became more negative (Figure 7-3b). In contrast, oil B showed incremental recovery when Ca was added (Figure 7-3c). Incremental recovery for oil A increased as the sample zeta potential became more positive (Figure 7-3d).

We conclude that the composition of the brine is not important so long as CSW causes the appropriate changes in zeta potential at the mineral-brine interface. To observe IOR, the mineral surface must change to have a more negative zeta potential when the oil-brine interface is negatively charged in the formation brine, and *vice-versa*.

Overall our results show favourable waterflood recoveries – almost certainly more favourable than a strongly water-wet case. So, while incremental recovery may be associated with a move to more water-wet conditions, the waterflood response is still evidently mixed-wet, and this may indeed be the ideal wettability state for recovery.

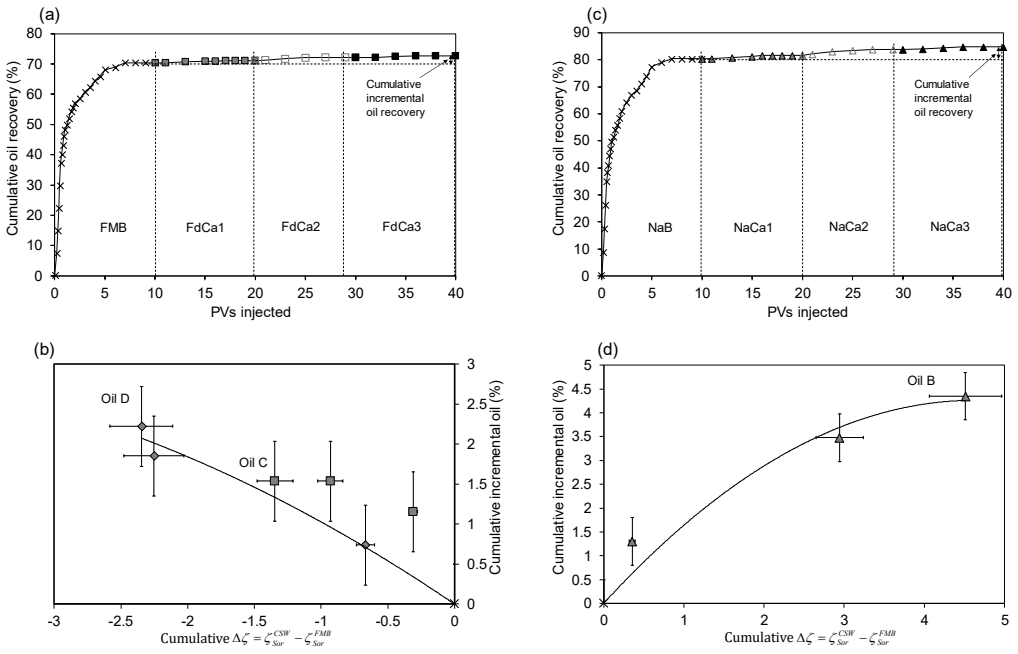



**Figure 7-3: Effect of decreasing/increasing Ca concentration on oil recovery and zeta potential change. Successful examples (a) when Ca is removed using crude oil C and (c) when Ca is added using crude oil B. Vertical dashed lines in (a, c) indicate when the streaming potential measurements are conducted. (b, d) Relationship between the incremental oil recovered and the incremental change in the zeta potential of the sample as Ca concentration in the injected brine composition was changed. Subscript FMB indicates formation brine in (b) and 2M NaCl in (d).**

### 7.3.4. Correlation Between Zeta Potential and Improved Oil Recovery

To determine whether there is a general expression that relates IOR to zeta potential irrespective of the zeta potential of the oil-brine interface, we plot incremental recovery against a normalized zeta potential ($\zeta_n$) defined as (Figure 7-4)

$$\zeta_n = \left| \frac{\zeta_{Sor}^{CSW} - \zeta_{Sor}^{FMB}}{\zeta_{Sor}^{CSW} - \zeta_{Sw=1}^{CSW}} \right| \tag{7.1}$$

where $\zeta_{Sor}^{CSW}$ denotes the zeta potential of the aged sample after waterflooding with the chosen brine of controlled composition, $\zeta_{Sor}^{FMB}$ denotes the zeta potential of the sample saturated crude oil at the residual saturation ($S_w = 1 - S_{or}$) after waterflooding with the brine in which with the core sample was aged and $\zeta_{Sw=1}^{CSW}$ denotes the zeta potential of the sample saturated with the chosen controlled

salinity brine when $S_w = 1$. The numerator in (7.1) gives the change in zeta potential during controlled salinity waterflooding; the denominator gives the difference in zeta potential in aged sample after waterflooding with chosen brine of controlled salinity and in water-wet sample, indicating the degree of wettability. It is noted that as the sample becomes more water-wet, the term $\zeta_{Sor}^{CSW} - \zeta_{Sw=1}^{CSW}$ gets smaller and $\zeta_n$ increases in magnitude (Figure 7-4). Plotted in this way it is clear that incremental recovery correlates with the change in zeta potential induced by CSW when normalized against the difference in zeta potential before and after wettability alteration irrespective of oil composition or flooding sequences.

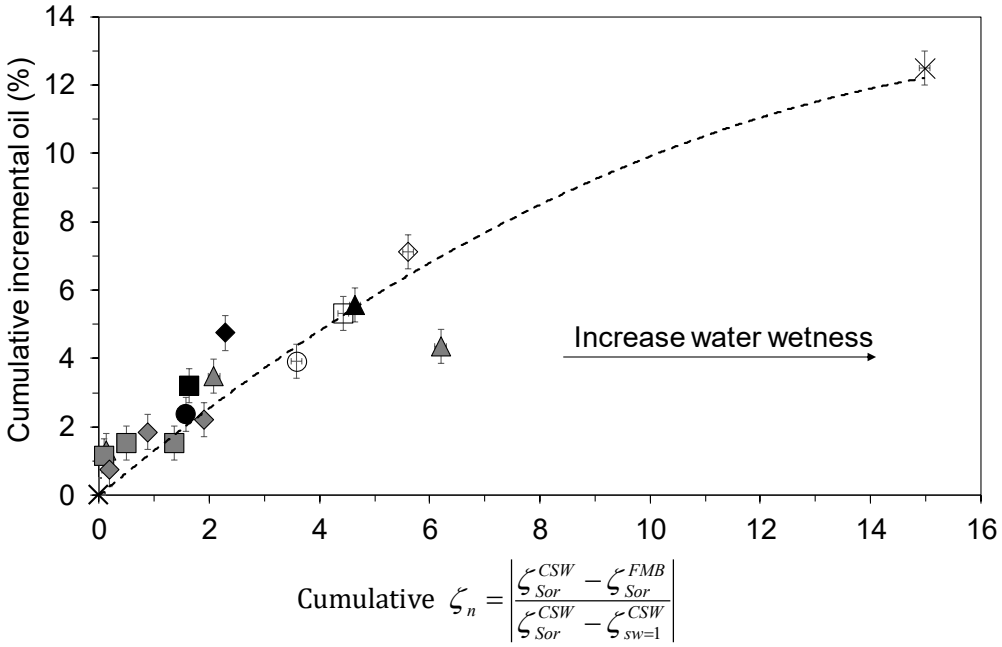



**Figure 7-4: Summary of results showing cumulative incremental oil recovery against cumulative normalised zeta potential irrespective of the zeta potential of the oil-brine interface. $\zeta_{Sor}^{CSW} - \zeta_{Sor}^{FMB}$ gives the change in zeta potential during controlled salinity waterflooding and $\zeta_{Sor}^{CSW} - \zeta_{Sw=1}^{CSW}$ gives the difference in zeta potential in aged sample after waterflooding with the chosen brine of controlled salinity and in a water-wet sample, indicating the degree of wettability; increased water wetness when $\zeta_{Sor}^{CSW} - \zeta_{Sw=1}^{CSW}$ goes smaller in magnitude. Cross shows data in FMB, filled symbols show data in SW and empty symbols show data in 20dSW. Grey symbols show results of decreasing Ca (squares for oil C and diamonds for oil D) and increasing Ca (triangles for oil B).**

## 7.4. Discussion

The results presented here demonstrate that the zeta potential at both the mineral-water and oil-water interfaces must be determined when designing the optimum water composition for CSW in carbonates. Improved recovery is observed only if the change in water composition yields a zeta potential at each interface that has the same polarity. If the oil-water interface is negatively charged, modifying the injected water composition to produce a more negative zeta potential on the mineral surfaces yields improved recovery. The conventional approach of diluting formation brine and/or seawater is successful in this case. However, if the oil-water interface is positively charged, the injection water composition must be modified to yield a more positive zeta potential on the mineral surfaces.

The results can be explained at the mineral-surface-scale by considering the stability of a thin water film on the mineral surface that wets and separates the mineral surface from the oil phase. As discussed in chapter 6, the stability of a wetting film depends on the disjoining pressure, which is the sum of the contributions from van der Waals forces, structural forces and electrostatic forces (e.g. *Israelachvili*, 1985; Figure 7-5a). The Van der Waals force is always attractive, which means that its contribution to the disjoining pressure is negative (dashed line in Figure 7-5a). The structural force is always repulsive, so its contribution to the disjoining pressure is positive (dotted line in Figure 7-5a).

The contribution of the electrostatic force to the disjoining pressure can be positive or negative depending upon the zeta potential at the mineral-brine and oil-brine interfaces (solid lines in Figure 7-5a). If the zeta potentials have the same polarity, then the electrostatic force is repulsive so the contribution of the electrostatic force to the disjoining pressure is positive and *vice-versa* (compare pale grey lines against dark grey lines in Figure 7-5a). The magnitude of the contribution of the electrostatic force decreases with increasing ionic strength (*Buckley et al.*, 1989; *Hirasaki*, 1991; *Buckley et al.*, 1998; compare high and low IS lines in Figure 7-5a).

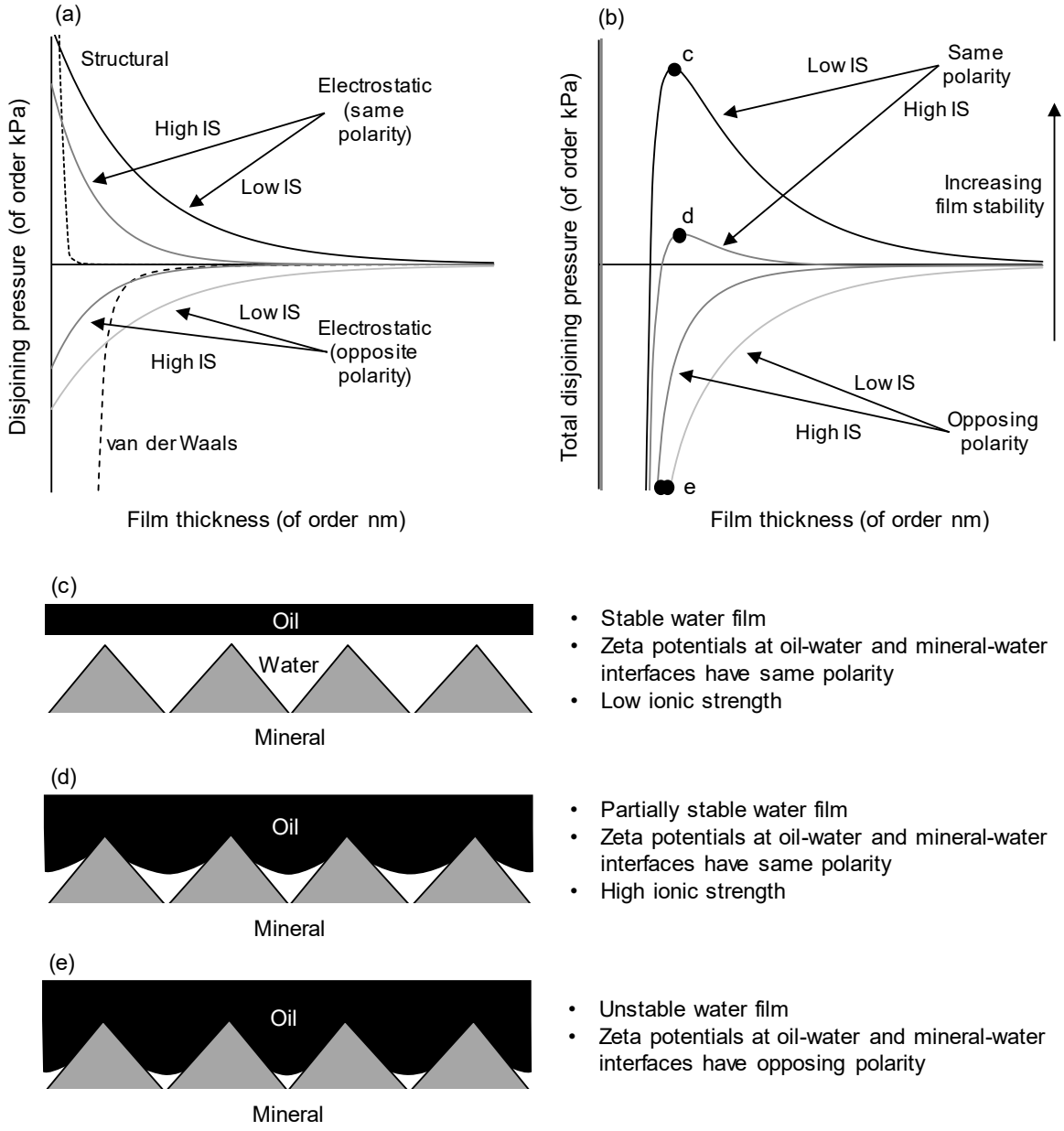



**Figure 7-5: Impact of disjoining pressure on water film thickness and wettability.(a) Schematic of the various contributions of van der Waals (dashed line), structural (dotted line) and electrostatic (solid lines) on the disjoining pressure. When the oil-water and mineral-water interfaces have the same polarity, the contribution of electrostatic forces is positive (black and dark grey lines); when they have opposing polarity, the contribution is negative (light grey lines). The contribution of electrostatic forces is larger at low ionic strength (IS) than at high IS. (b) Total disjoining pressure corresponding to (a). The labels c-e correspond to figures (c) – (e) which show schematically the water film on a rough mineral surface. The mineral surfaces are water-wet where the film is stable, but can become oil-wet where the film has collapsed.**

The condition for a stable water film is that the disjoining pressure (Π) has a maximum which satisfies (*Hirasaki*, 1991)

$$\Pi_{\max} \geq P_o - P_w - \frac{2\sigma}{r} = P_c - \frac{2\sigma}{r} > 0 \qquad (7.2)$$

where $P_o$ (Pa) is the oil pressure, $P_w$ (Pa) is the water pressure, $P_c$ is the oil-water capillary pressure (Pa), $\sigma$ is the oil-water interfacial tension (N $m^{-1}$), and $r$ is the local radius of curvature of the mineral surface (m); Figure 7-5b). The value of $r$ is positive for a concave surface and negative for a convex surface. Thus the water film on a rough pore surface first becomes unstable at an asperity (*Hirasaki*, 1991). When the oil-brine and mineral-brine zeta potentials have the same polarity, the water film can be stable (dark grey lines in Figure 7-5b). However, at high ionic strength, only the concave parts of the pore-surfaces host stable water films, whereas at low ionic strength, the water film is stable irrespective of the surface topology. Evidence to support this model comes from nano-scale imaging using cryogenic broad ion-beam polishing in combination with scanning electron microscopy, which has imaged direct contacts between oil and quartz mineral surfaces at asperities in water-wet sandstone samples (*Israelachvili*, 1985). When the oil-brine and mineral-brine zeta potentials have opposing polarity, the water film is unstable (pale grey lines in Figure 7-5b).

The data obtained here are consistent with the observation that the mineral surfaces in carbonate reservoirs containing typical formation brines rich in $Ca^{2+}$ and $Mg^{2+}$ often have a positive zeta potential. If the oil-brine interface has a negative zeta potential (as in oils C-E investigated here), then the water film is unstable because the zeta potentials at the mineral-brine and oil-brine interfaces have opposing polarity and the electrostatic force is attractive. Consequently, polar components in the oil adsorb onto the mineral surfaces causing the surfaces to become oil-wet (Figure 7-5e; location ‘e’ on Figure 7-5b). During a conventional LSW, such as that investigated here in which formation brine was replaced by seawater and then dilute seawater, the zeta potential at the mineral brine interface becomes more negative. Consequently, the electrostatic force becomes repulsive

and increases in magnitude, leading to a higher disjoining pressure and increasingly stable water films. Thus the wettability alters towards more water-wet conditions (Figure 7-5c; location ‘c’ on Figure 7-5b). Oil previously adsorbed on the mineral surfaces is released and incremental oil recovery is observed.

However, if the oil-brine interface has a positive zeta potential (as in Oil B investigated here), the water film is partially stable because the zeta potentials at the mineral-brine and oil-brine interfaces have the same polarity and the electrostatic force is weakly repulsive. Consequently, the polar components in the oil adsorb onto a smaller area of the pore-space (Figure 7-5d; location ‘d’ on Figure 7-5b). During a conventional LSW, the zeta potential at the mineral brine interface becomes more negative. Consequently, the electrostatic force becomes attractive and increases in magnitude, leading to a lower disjoining pressure and increasingly unstable water films (Figure 7-5e; location ‘e’ on Figure 7-5b). Thus there is no tendency to re-establish the water wetting layers and no incremental recovery is observed.

In the reverse LSW investigated here, wettability alteration occurred during aging with crude oil B and dilute seawater because the attractive electrostatic force between the positively charged oil-brine interface and the negatively charged mineral-brine interface yielded an unstable water film (Figure 7-5e; location ‘e’ on Figure 7-5b). During CSW, changing the injected brine composition to seawater and then formation brine caused the zeta potential at the mineral-brine interface to become less negative and then positive, leading to increasingly stable water films (Figure 7-5d; location ‘d’ on Figure 7-5b). Thus the wettability was altered towards more water-wet conditions, oil was released from the mineral surfaces and incremental oil recovery was observed.

Decreasing the $Ca^{2+}$ concentration has a similar effect to simple dilution (and *vice versa*) because varying $Ca^{2+}$ changes the zeta potential of the mineral-brine interface, thus affecting the electrostatic contribution to the disjoining pressure. However, changes in zeta potential in response to changes in $Ca^{2+}$ concentration were less pronounced for the carbonate sample investigated here

than the changes in zeta potential observed during conventional and inverted LSW. Thus the IOR was less pronounced.

The experimental method demonstrated here provides a practical approach to determine the optimum brine composition for CSW in carbonates. The first step is to determine the wettability and zeta potential of preserved or aged samples saturated with the crude oil and formation brine of interest (as shown in chapter 6), and compare the zeta potential with strongly-water samples. Our results, along with previous studies, suggest that IOR during CSW will be observed only if the initial wetting state is mixed- to oil-wet (*Austad et al.*, 2007; *Puntervold et al.*, 2007; *Shariatpanahi et al.*, 2010; *Austad et al.*, 2011; *Rashid et al.*, 2015).

If the zeta potential of the aged samples is more negative than that of the water-wet samples, then the oil-brine interface is negatively charged and the injection brine should be modified to yield a more negative zeta potential at the mineral-brine interface. Previous studies have shown that this can be achieved by simple dilution or by reducing the concentration of $Ca^{2+}$ and/or $Mg^{2+}$. Addition of $SO_4^{2-}$ can also yield more negative zeta potential.

If the zeta potential of the aged samples is more positive than that of the water-wet samples, then the oil-brine interface is positively charged and the injection brine should be modified to yield a more positive zeta potential at the mineral-brine interface. Previous studies have shown that this can be achieved by increasing the concentration of $Ca^{2+}$ and/or $Mg^{2+}$.

If the zeta potential of the water-wet and aged samples is the same but wettability alteration has clearly occurred, then the zeta potential of the mineral-brine and oil-brine interfaces is the same within experimental error. If the zeta potential is negative, then the injection brine should be modified to yield a more negative zeta potential at the mineral-brine interface and *vice-versa*.

## 7.5. Conclusions

The zeta potential at both the mineral-water and oil-water interfaces must be determined when designing the optimum brine composition for CSW in carbonates. The experimental method presented here allows this to be done using intact core samples saturated with the crude oil and brine of interest. Results reported here demonstrated that improved recovery during CSW in carbonates is observed if the change in brine composition yields a zeta potential at each interface that has the same polarity, such that a repulsive electrostatic force acts between the interfaces and stabilizes a water film on the mineral surface.

If the oil-water interface is negatively charged, modifying the injected water composition to produce a more negative zeta potential on the mineral surfaces yields improved recovery. The conventional approach of diluting formation brine and/or seawater is successful in this case. However, if the oil-water interface is positively charged, the injection water composition must be modified to yield a more positive zeta potential on the mineral surfaces. This can be achieved by increasing the concentration of Ca or Mg ions. Studies that have failed to observe improved recovery using the conventional (dilution) approach to CSW, or some other change in water composition designed to yield more negative mineral surfaces, were most likely dealing with a positively charged oil-water interface that had not been diagnosed. These results have broad application and significance in allowing oil companies to design water injection strategies that yield improved oil recovery from carbonate reservoirs.

# Chapter 8.

# Summary, Conclusions and Future Work

## 8.1. Summary and Conclusion

Understanding the controls on improved oil recovery during controlled salinity waterflooding (CSW) in carbonate rocks is essential as the majority of the world's oil reserves are hosted in carbonate reservoirs and yet, the proportion of oil recovered from carbonate rocks is low. In this work, we investigated the pore- to mineral-surface-scale mechanism(s) responsible for improved oil recovery during CSW using zeta potential interpreted from streaming potential measurements (SPM) on intact natural carbonate samples in natural brines and crude oils. The study involved four main components; (1) determination of key controls on zeta potential at mineral-brine and oil-brine interfaces, (2) effect of temperature on zeta potential, (3) impact of wettability on zeta potential and (4) designing the optimum CSW composition to maximize oil recovery for a given crude oil-brine-rock (COBR) system. To date, the mechanisms responsible for enhanced oil recovery during CSW are still actively debated; and no reliable method has been published that relates brine composition with zeta potential change, wettability and oil recovery.

The zeta potential of carbonate is controlled by the concentration-dependent adsorption of the lattice ions Ca, Mg and $CO_3$ within the Stern layer. A Nernstian relationship between zeta potential and pCa or pMg was observed over the range of typical natural brines; whilst, addition of $SO_4$ was found to affect zeta potential by moderating Ca in solution. In typical formation brines found in many carbonate reservoirs, concentrations of Ca and Mg are high which make the zeta

potential of the carbonate surface positive. Reduction of Ca and/or Mg concentration, either selectively or by bulk dilution, or injection of seawater (rich in $SO_4$) can invert the polarity yielding negative zeta potential. This may promote wettability alteration to water-wet conditions, releasing previously adsorbed oil from the calcite mineral surfaces and therefore improving oil recovery, providing that oil-brine interface is negatively charged. The carbonate-rock-specific relationship between zeta potential and PDI concentration observed here suggests that far less dilution may be required in some natural carbonates (e.g. Ketton and Portland); in others, inversion of polarity may never be encountered and the mineral surfaces may remain positively charged (e.g. Estaillades). The results may explain why CSW in some cases yields increased recovery and in other cases does not.

The thesis reports the first zeta potential measurements on carbonates at elevated temperatures typical to petroleum systems. The temperature dependence of the zeta potential was found to be strongly correlated with the temperature dependence of pCa. The zeta potential decreases with temperature at low ionic strength and independent of temperature at high ionic strength irrespective of brine composition. Given this, zeta potential measurements of natural carbonate in natural brines (e.g. FMB and SW; ionic strength ≥0.5M) at laboratory conditions may be applied *in situ*.

The thesis also develops an integrated approach that uses streaming potential measurements in intact samples to link zeta potential to brine composition, wettability and oil recovery during CSW with consistent materials and experimental conditions. The zeta potential was found to be strongly correlated with rock wettability, which offers a quick and cheap method to characterize wettability than existing laboratory methods. Likewise, improved oil recovery (IOR) during CSW was found to be strongly correlated with changes in zeta potential which must be determined at both the mineral-water and oil-water interfaces when designing the injection brine composition for CSW. Results reported here demonstrate that the oil-water interface can be positively charged at the high pH

and ionic strength relevant to many carbonate reservoirs. IOR during CSW was observed when the change in brine composition induces a repulsive electrostatic force between the oil-brine and mineral-brine interfaces that stabilizes a wetting water film. Studies that have failed to observe IOR using the conventional (dilution) approach to CSW, or some other change in water composition designed to yield more negative mineral surfaces, were most likely dealing with a positively charged oil-water interface.

## 8.2. Implications

The experimental method demonstrated in this thesis have useful applications to petrophysics laboratories and oil companies as follows:

- The streaming potential measurements can be conducted in laboratory coreflooding experiments as part of SCAL measurements to offer a quick and robust method in characterising wettability and screening reservoir rocks for successful CSW.
- The SPM can be integrated with MDT tool to be used as *in-situ*-measurements of wettability to identify parts of the filed or reservoir suitable for deployment of CSW.
- The SPM method can offer oil companies a rapid route in determining rock wettability and designing optimum brine composition and water injection strategies that yield improved oil recovery from carbonate reservoirs. The practical approach must involve measurement of zeta potential in aged/preserved and clean reservoir core plugs saturated with formation brine of interest to determine zeta potential of the mineral-brine and oil-brine interfaces. This gives an indication of the surface charge of the oil-brine interface and the wettability index of the system. If the zeta potential of aged/preserved reservoir core plug is more negative than that of clean sample, then oil-brine interface is negatively charged and water injection strategies can include a simple bulk dilution, lowering Ca or Mg concentration or addition of

$SO_4$. If the zeta potential of aged/preserved reservoir core plug showed more positive value compared to that of clean sample, then oil must have a positive oil-brine interface. In this case, increasing concentration of Ca and/or Mg should yield improved oil recovery.

## 8.3. Future Work

Despite the progress that has been made in understanding the electrokinetic behaviour of natural carbonate in the presence of natural brine and crude oils, and demonstrating the relationship between zeta potential, brine compositions, wettability and oil recovery to understand the adsorption/desorption processes at the carbonate surface during CSW, key questions remain and further work is required to address them.

- Different electrokinetic behaviour between apparently identical limestone samples is not fully understood. We have demonstrated that in chapter 4, the three investigated carbonate rocks; Ketton, Estaillades and Portland, have different magnitude of zeta potential and different iso-electric points. We attributed these differences to the possibility of some inorganic materials (e.g. anhydrite) incorporated into their structures based on the chemical analysis of effluent electrolytes. Moreover, we have shown that $SO_4^{2-}$ is not a PDI for carbonates and it only facilitate the $Ca^{2+}$ concentration in solution through adsorption/desorption processes. Further work using chemical modelling that couples reactions in the bulk aqueous and at the carbonate surface and assesses dissolution/precipitation processes might be needed to support our observations.
- In chapter 5, we have demonstrated the effect of elevated temperature on NaCl-EQ electrolytes, SW and various modifications of SW. Although the impact of PDIs on zeta potential at higher temperatures are embedded in SW compositions, the separate effect of $Ca^{2+}$, $Mg^{2+}$, and $SO_4^{2-}$, on zeta potential at elevated temperatures has not been addressed in this study. Moreover, the

impact of dilution of SW and addition of $SO_4^{2-}$ to SW has been shown at only one temperature value (80$^o$C). Studying the effect of different water injection strategies, reported in chapter 7, at different reservoir temperatures would be of immense usefulness to further understand the efficiency of CSW in carbonates at reservoir conditions.

- Despite the significance of our finding that the oil-brine interface can be positively charged at natural conditions of pH and salinity, it was only observed in one crude oil using one carbonate rock type. More work would be required to support our hypothesis on different natural carbonate rocks or sandstone core samples using the same oil to imitate the wettability and CSW experiments conducted here using natural Estaillades samples.
- We have seen that in chapter 7, Estaillades samples give very modest oil recovery during the modification of $Ca^{2+}$ concentration in the injection brine, which might be attributed to a higher positive zeta potential at the mineral-brine interface compared to Ketton and Portland (as demonstrated in chapter 4). A better result might have been obtained if Ketton or Portland rocks were used, as these samples showed a lower positive/higher negative zeta potential at natural brines (FMB and SW). Thus the repulsive electrostatic forces between the mineral-brine and oil-brine interfaces would expected to be higher during different CSW strategies compared to the results obtained from Estaillades samples; therefore, higher IOR.
- Also, in chapter 7, our waterflood experiments have shown favourable recoveries and low residual oil saturations. This was achieved after injecting more than 10 PVs. However, this may not be representative of the real waterflood response in the hydrocarbon reservoirs where pore-volume injected is far less than 10 PVs (typically 1 to 3 PVs). Having zeta potential measurements as a function of PV injected make the system more realistic and representative of waterflood performance in real reservoirs. We suggest looking into how zeta potential and wettability is related to oil recovery for different numbers of pore volume injected, and this could be used to design the

optimal brine composition. For most of the waterflooding experiments on mixed-wet plugs, significant recovery is always observed from the first pore volume with slower recovery later (post-breakthrough). More experiments could be done where zeta potential can be measured at different numbers of PV injected (possibly with the use of porous plate), and link it to remaining oil saturation and oil recovery. This can further be correlated to the relationship between wettability index and total oil recovery for different brine compositions (e.g. Figure 2.18) in order to design an optimal salinity, at which the electrostatic forces between the mineral-brine and oil-brine interfaces are maximized, at realistic conditions similar to the real waterflooding performance.

- Validating our streaming potential measurements during CSW using pore network modelling that addresses zeta potential change at the mineral-brine and oil-brine interfaces and oil recovery, or a simple capillary tube model, would be highly beneficial.
- Finally, in all multiphase experiments, the mobile phase was brine, which is not the case in hydrocarbon reservoirs where oil and brine flow. Thus, a better understanding of streaming potential coupling coefficient during multiphase flow is advantageous to characterise wettability and CSW as in real reservoir.

# References….


Abdallah, W., Buckley, J. S., Carnegie, A., Edwards, J., Herold, B., Fordham, E., Graue, A., Habashy, T., Seleznev, N. & Signer, C. (1986). Fundamentals of wettability. *Technology, 38***,** 1125-1144.

Adamson, A. W. (1976). *Physical chemistry of surfaces*, John Wiley & Sons, New York.

Al-Attar, H. H., Mahmoud, M. Y., Zekri, A. Y., Almehaideb, R. & Ghannam, M. (2013). Low-salinity flooding in a selected carbonate reservoir: Experimental approach. *Journal of Petroleum Exploration and Production Technology, 3***,** 139-149. doi: 10.1007/s13202-013-0052-3.

Al-Maamari, R. S. & Buckley, J. S. (2003). Asphaltene precipitation and alteration of wetting: The potential for wettability changes during oil production. *SPE Reservoir Evaluation & Engineering, 6***,** 210-214. doi: 10.2118/84938-PA.

Al Mahrouqi, D., Vinogradov, J. & Jackson, M. (2015). Understanding controlled salinity waterflooding in carbonates using streaming potential measurements. *Proceedings of the SPE Latin American and Caribbean Petroleum Engineering Conference, 18-20 November, Quito, Ecuador. SPE-177242-MS*. doi: 10.2118/177242-MS.

Alotaibi, M. B., Azmy, R. & Nasr-El-Din, H. A. (2010). Wettability challenges in carbonate reservoirs. *Proceedings of the SPE Improved Oil Recovery Symposium, 24-28 April, Tulsa, Oklahoma, USA. SPE-129972-MS*. doi: 10.2118/129972-MS.

Alotaibi, M. B. & Nasr-El-Din, H. A. (2011). Electrokinetics of limestone particles and crude-oil droplets in saline solutions. *SPE Reservoir Evaluation & Engineering, 14***,** 604-611. doi: 10.2118/151577-PA.

Alotaibi, M. B., Nasr-El-Din, H. A. & Fletcher, J. J. (2011a). Electrokinetics of limestone and dolomite rock particles. *SPE Reservoir Evaluation & Engineering, 14***,** 594-603. doi: 10.2118/148701-PA.

Alotaibi, M. B., Nasralla, R. A. & Nasr-El-Din, H. A. (2011b). Wettability studies using low-salinity water in sandstone reservoirs. *SPE Reservoir Evaluation & Engineering, 14***,** 713-725. doi: 10.2118/149942-PA.

Alotaibi, M. B. & Yousef, A. (2016). The role of individual and combined ions in waterflooding carbonate reservoirs: Electrokinetic study. *SPE Reservoir Evaluation & Engineering*. doi: 10.2118/177983-PA.

Alroudhan, A. (2015). Wettability characterization using streaming potential measurements*. PhD thesis*, Imperial College London.

Alroudhan, A., Vinogradov, J. & Jackson, M. (2016). Zeta potential of intact natural limestone: Impact of potential-determining ions Ca, Mg and $SO_4$. *Colloids and*

*Surfaces A: Physicochemical and Engineering Aspects*. doi: 10.1016/j.colsurfa.2015.11.068.

AlShaikh, M. & Mahadevan, J. (2016). Impact of brine composition on calcite wettability: A sensitivity study. *SPE Journal, 21*. doi: 10.2118/172187-PA.

Amott, E. (1959). Observations relating to the wettability of porous rock. *Transactions of the AIME, 216***,** 156-162.

Andersen, M., Thomas, D. & Teeters, D. (1988). A new formation wettability test: The dynamic wilhelmy plate wettability technique. *Proceedings of the SPE Enhanced Oil Recovery Symposium, 16-21 April, Tulsa, Oklahoma* SPE-17368-MS. doi: 10.2118/17368-MS.

Anderson, W. (1986a). Wettability literature survey Part 1: Rock/oil/brine interactions and the effects of core handling on wettability. *Journal of Petroleum Technology, 38***,** 1,125-1,144. doi: 10.2118/13932-PA.

Anderson, W. (1986b). Wettability literature survey Part 2: Wettability measurement. *Journal of Petroleum Technology, 38***,** 1,246-1,262. doi: 10.2118/13933-PA.

Austad, T., RezaeiDoust, A. & Puntervold, T. (2010). Chemical mechanism of low salinity water flooding in sandstone reservoirs. *Proceedings of the SPE Improved Oil Recovery Symposium, 24-28 April, Tulsa, Oklahoma, USA*. SPE-129767-MS. doi: 10.2118/129767-MS.

Austad, T., Shariatpanahi, S., Strand, S., Black, C. & Webb, K. (2011). Conditions for a low-salinity enhanced oil recovery (EOR) effect in carbonate oil reservoirs. *Energy & fuels, 26***,** 569-575. doi: 10.1021/ef201435g.

Austad, T. & Standnes, D. C. (2003). Spontaneous imbibition of water into oil-wet carbonates. *Journal of Petroleum Science and Engineering, 39***,** 363-376. doi: 10.1016/S0920-4105(03)00075-5.

Austad, T., Strand, S., Madland, M. V., Puntervold, T. & Korsnes, R. I. (2007). Seawater in chalk: An EOR and compaction fluid. *Proceedings of the International Petroleum Technology Conference, 4-6 December, Dubai, U.A.E.* . IPTC-11370-MS. doi: 10.2523/IPTC-11370-MS.

Ball, B. & Fuerstenau, D. (1973). A review of the measurement of streaming potentials. *Minerals Science and Engineering 5***,** 267-277.

Bapat, J. D. (2012). *Mineral admixtures in cement and concrete*, CRC Press, Taylor & Francis, New York

Bard, A. J., Faulkner, L. R., Leddy, J. & Zoski, C. G. (1980). *Electrochemical methods: Fundamentals and applications*, Wiley, New York.

Beattie, J. K. & Djerdjev, A. M. (2004). The pristine oil/water interface: Surfactant-free hydroxide-charged emulsions. *Angewandte Chemie International Edition, 43***,** 3568-3571. doi: 10.1002/anie.200453916.

Berg, S., Cense, A., Jansen, E. & Bakker, K. (2010). Direct experimental evidence of wettability modification by low salinity. *Petrophysics, 51*.

Bergeron, V. & Radke, C. (1995). Disjoining pressure and stratification in asymmetric thin-liquid films. *Colloid and Polymer Science, 273***,** 165-174. doi: 10.1007/BF00654014.

Berlin, T. S. & Khabakov, A. V. (1961). Difference in the electrokinetic potentials of carbonate sedimentary rocks of different origin and composition. *Geochemistry*, 217-230.

Bernard, G. G. (1967). Effect of floodwater salinity on recovery of oil from cores containing clays. *Proceedings of the SPE California Regional Meeting, 26-27 October, Los Angeles, California* SPE-1725-MS. doi: 10.2118/1725-MS.

Blunt, M. J. (2001). Flow in porous media: Pore-network models and multiphase flow. *Current Opinion in Colloid & Interface Science, 6*, 197-207. doi: 10.1016/S1359-0294(01)00084-X.

Bradley, H. B. (1987). *Petroleum engineering handbook*, Society of Petroleum Engineers, Richardson, Texas.

Brady, P. V. & House, W. (1996). Surface-controlled dissolution and growth of minerals. In*:* BRADY, P. V. (ed.), *Physics and Chemistry of Mineral Surfaces.* VRV Press, New York.

Bragg, W. L. (1950). *Atomic structure of minerals*, Cornell University Press, New York.

Brown, R. J. & Fatt, I. (1956). Measurements of fractional wettability of oil fields' rocks by the nuclear magnetic relaxation method. *Proceedings of the SPE Fall Meeting of the Petroleum Branch of AIME, 14-17 October, Los Angeles, California* SPE-743-G. doi: 10.2118/743-G.

Buckley, J. & Liu, Y. (1998). Some mechanisms of crude oil/brine/solid interactions. *Journal of Petroleum Science and Engineering, 20*, 155-160. doi: 10.1016/S0920-4105(98)00015-1.

Buckley, J., Liu, Y. & Monsterleet, S. (1998). Mechanisms of wetting alteration by crude oils. *SPE Journal, 3*, 54-61. doi: 10.2118/37230-PA.

Buckley, J. & Morrow, N. (1990). Characterization of crude oil wetting behavior by adhesion tests. *Proceedings of the SPE/DOE Enhanced Oil Recovery Symposium, 22-25 April, Tulsa, Oklahoma* SPE-20263-MS. doi: 10.2118/20263-MS.

Buckley, J., Takamura, K. & Morrow, N. (1989). Influence of electrical surface charges on the wetting properties of crude oils. *SPE Reservoir Engineering, 4*, 332-340. doi: 10.2118/16964-PA.

Buckley, J. S., Bousseau, C. & Liu, Y. (1996). Wetting alteration by brine and crude oil: from contact angles to cores. *SPE Journal, 1*, 341-350. doi: 10.2118/30765-PA.

Chen, L., Zhang, G., Wang, L., Wu, W. & Ge, J. (2014). Zeta potential of limestone in a large range of salinity. *Colloids and Surfaces A: Physicochemical and Engineering Aspects, 450*, 1-8. doi: 10.1016/j.colsurfa.2014.03.006.

Chow, R. S. & Takamura, K. (1988). Electrophoretic mobilities of bitumen and conventional crude-in-water emulsions using the laser Doppler apparatus in the presence of multivalent cations. *Journal of Colloid and Interface Science, 125*, 212-225. doi: 10.1016/0021-9797(88)90070-7

Christenson, H. K. & Israelachvili, J. N. (1987). Direct measurements of interactions and viscosity of crude oils in thin films between model clay surfaces. *Journal of Colloid and Interface Science, 119*, 194-202. doi: 10.1016/0021-9797(87)90259-1

Cicerone, D. S., Regazzoni, A. E. & Blesa, M. A. (1992). Electrokinetic properties of the calcite water interface in the presence of magnesium and organic-matter. *Journal of Colloid and Interface Science, 154*, 423-433. doi: 10.1016/0021-9797(92)90158-i.

Davis, J. A. & Kent, D. (1990). Surface complexation modeling in aqueous geochemistry. *Reviews in Mineralogy and Geochemistry, 23*, 177-260.

De Groot, K. & Duyvis, E. (1966). Crystal form of precipitated calcium carbonate as influenced by adsorbed magnesium ions. *Nature, 212*, 183-184. doi: 10.1038/212183a0.

Delgado, A. V., Gonzalez-Caballero, F., Hunter, R. J., Koopal, L. K. & Lyklema, J. (2007). Measurement and interpretation of electrokinetic phenomena. *Journal of Colloid and Interface Science, 309*, 194-224. doi: 10.1016/j.jcis.2006.12.075.

Donaldson, E. C., Thomas, R. D. & Lorenz, P. B. (1969). Wettability determination and its effect on recovery efficiency. *SPE Journal, 9*, 13-20. doi: 10.2118/2338-PA.

Douglas, H. & Walker, R. (1950). The electrokinetic behaviour of Iceland Spar against aqueous electrolyte solutions. *Transactions of the Faraday Society, 46*, 559-568. doi: 10.1039/TF9504600559.

Downs, H. & Hoover, P. (1989). *Oil field chemistry: Enhanced recovery and production stimulation*, American Chemical Society, Washington, DC.

Dukhin, S. S. & Deriaguine, B. V. (1974). *Surface and colloid science: Electrokinetic phenomena*, John Wiley & Sons, New York.

Eriksson, R., Merta, J. & Rosenholm, J. B. (2007). The calcite/water interface: Surface charge in indifferent electrolyte media and the influence of low-molecular-weight polyelectrolyte. *Journal of Colloid and Interface Science, 313*, 184-193. doi: 10.1016/j.jcis.2007.04.034.

Evans, D. F. & Wennerström, H. (1999). *The colloidal domain: Where physics, Chemistry, Biology, and Technology Meet*, Wiley-VCH, New York.

Fathi, S. J., Austad, T. & Strand, S. (2010). "Smart Water" as a wettability modifier in chalk: The effect of salinity and ionic composition. *Energy & Fuels, 24*, 2514-2519. doi: 10.1021/ef901304m.

Fenter, P., Geissbühler, P., DiMasi, E., Srajer, G., Sorensen, L. B. & Sturchio, N. C. (2000). Surface speciation of calcite observed in situ by high-resolution X-ray reflectivity. *Geochimica et Cosmochimica Acta, 64*, 1221-1228. doi: 10.1016/S0016-7037(99)00403-2.

Fenter, P. & Sturchio, N. C. (2004). Mineral–water interfacial structures revealed by synchrotron X-ray scattering. *Progress in Surface Science, 77*, 171-258. doi: 10.1016/j.progsurf.2004.12.001.

Fernø, M. A., Grønsdal, R., Åsheim, J., Nyheim, A., Berge, M. & Graue, A. (2011). Use of sulfate for water based enhanced oil recovery during spontaneous imbibition in chalk. *Energy & Fuels, 25*, 1697-1706. doi: 10.1021/ef200136w.

Foxall, T., Peterson, G. C., Rendall, H. M. & Smith, A. L. (1979). Charge determination at calcium salt/aqueous solution interface. *Journal of the Chemical Society, Faraday*

*Transactions 1: Physical Chemistry in Condensed Phases, 75*, 1034-1039. doi: 10.1039/F19797501034.

Fuerstenau, M. C., Gutierrez, G. & Elgillani, D. A. (1968). The influence of sodium silicate in non metallic flotation systems. *Transactions of the AIME, 241*, 319.

Gandomkar, A. & Rahimpour, M. R. (2015). Investigation of low-salinity waterflooding in secondary and tertiary enhanced oil recovery in limestone reservoirs. *Energy & Fuels, 29*, 7781-7792. doi: 10.1021/acs.energyfuels.5b01236.

Geissbühler, P., Fenter, P., DiMasi, E., Srajer, G., Sorensen, L. & Sturchio, N. (2004). Three-dimensional structure of the calcite–water interface by surface X-ray scattering. *Surface Science, 573*, 191-203. doi: 10.1016/j.susc.2004.09.036.

Glover, P. W. & Jackson, M. D. (2010). Borehole electrokinetics. *The Leading Edge, 29*, 724-728. doi: 10.1190/1.3447786

Glover, P. W. J., Walker, E. & Jackson, M. D. (2012). Streaming-potential coefficient of reservoir rock: A theoretical model. *Geophysics, 77*, D17-D43. doi: 10.1190/geo2011-0364.1.

Gomari, K. R., Hamouda, A. & Denoyel, R. (2006). Influence of sulfate ions on the interaction between fatty acids and calcite surface. *Colloids and Surfaces A: Physicochemical and Engineering Aspects, 287*, 29-35. doi: 10.1016/j.colsurfa.2006.03.018.

Gulamali, M. Y., Leinov, E. & Jackson, M. D. (2011). Self-potential anomalies induced by water injection into hydrocarbon reservoirs. *Geophysics, 76*, F283-F292. doi: 10.1190/1.3596010.

Gupta, R., Smith, P. G., Hu, L., Willingham, T. W., Cascio, M. L., Shyeh, J. J. & Harris, C. R. (2011). Enhanced waterflood for Middle East carbonate cores - Impact of injection water composition. *Proceedings of the SPE Middle East Oil and Gas Show and Conference, 25-28 September, Manama, Bahrain* SPE-142668-MS. doi: 10.2118/142668-MS.

Hassenkam, T., Pedersen, C. S., Dalby, K., Austad, T. & Stipp, S. L. S. (2011). Pore scale observation of low salinity effects on outcrop and oil reservoir sandstone. *Colloids and Surfaces A: Physicochemical and Engineering Aspects, 390*, 179-188. doi: 10.1016/j.colsurfa.2011.09.025.

Heberling, F., Trainor, T. P., Lützenkirchen, J., Eng, P., Denecke, M. A. & Bosbach, D. (2011). Structure and reactivity of the calcite–water interface. *Journal of Colloid and Interface Science, 354*, 843-857. doi: 10.1016/j.jcis.2010.10.047.

Hester, R. E. & Harrison, R. M. (2010). *Carbon capture: Sequestration and storage*, Royal Society of Chemistry, London.

Hiorth, A., Cathles, L. M. & Madland, M. V. (2010). The impact of pore water chemistry on carbonate surface charge and oil wettability. *Transport in Porous Media, 85*, 1-21. doi: 10.1007/s11242-010-9543-6.

Hirasaki, G. (1991). Wettability: Fundamentals and surface forces. *SPE Formation Evaluation, 6*, 217-226. doi: 10.2118/17367-PA.

Hirasaki, G. & Zhang, D. L. (2004). Surface chemistry of oil recovery from fractured, oil-wet, carbonate formations. *SPE Journal, 9*, 151-162. doi: 10.2118/88365-PA.

Hohl, H., Sigg, L. & Stumm, W. (1980). Characterization of surface chemical properties of oxides in natural waters: The role of specific adsorption in determining the surface charge. In*:* K., M. C. & L., J. O. (ed.), *Particulates in Water.* Advances in Chemistry; American Chemical Society: Washington, DC.

Huang, Y. C., Fowkes, F. M., Lloyd, T. B. & Sanders, N. D. (1991). Adsorption of calcium ions from calcium chloride solutions onto calcium carbonate particles. *Langmuir, 7***,** 1742-1748. doi: 10.1021/la00056a028.

Hunter, R. J. (1981). *Zeta potential in colloid science : Principles and applications*, Academic Press, New Yotk.

Israelachvili, J. (1985). *Intermolecular and surface forces*, Academic press, New York.

Jaafar, M. Z., Vinogradov, J. & Jackson, M. D. (2009). Measurement of streaming potential coupling coefficient in sandstones saturated with high salinity NaCl brine. *Geophysical Research Letters, 36*. doi: 10.1029/2009gl040549.

Jackson, M. D., Gulamali, M. Y., Leinov, E., Saunders, J. H. & Vinogradov, J. (2012). Spontaneous potentials in hydrocarbon reservoirs during waterflooding: Application to water-front monitoring. *SPE Journal, 17***,** 53-69. doi: 10.2118/135146-PA.

Jackson, M. D. & Vinogradov, J. (2012). Impact of wettability on laboratory measurements of streaming potential in carbonates. *Colloids and Surfaces A-Physicochemical and Engineering Aspects, 393***,** 86-95. doi: 10.1016/j.colsurfa.2011.11.005.

Jackson, M. D., Vinogradov, J., Saunders, J. H. & Jaafar, M. Z. (2011). Laboratory measurements and numerical modeling of streaming potential for downhole monitoring in intelligent wells. *SPE Journal, 16***,** 625-636. doi: 10.2118/120460-PA.

Jadhunandan, P. P. & Morrow, N. R. (1995). Effect of wettability on waterflood recovery for crude-oil/brine/rock systems. *SPE Reservoir Engineering, 10***,** 40-46. doi: 10.2118/22597-PA.

Johnson, R. E. & Dettre, R. H. (1969). Wettability and contact angles. In*:* MATIJEVIC, E. (ed.), *Surface and Colloid Science.* Wiley Interscience, New York.

Jouniaux, L. & Pozzi, J. P. (1995). Streaming potential and permeability of saturated sandstones under triaxial stress: Consequences for electrotelluric anomalies prior to earthquakes. *Journal of Geophysical Research: Solid Earth, 100***,** 10197-10209. doi: 10.1029/95JB00069.

Karoussi, O. & Hamouda, A. A. (2007). Imbibition of sulfate and magnesium ions into carbonate rocks at elevated temperatures and their influence on wettability alteration and recovery. *Energy & Fuels, 21***,** 2138-2146. doi: 10.1021/ef0605246.

Karoussi, O. & Hamouda, A. A. (2008). Macroscopic and nanoscale study of wettability alteration of oil-wet calcite surface in presence of magnesium and sulfate ions. *Journal of Colloid and Interface Science, 317***,** 26-34. doi: 10.1016/j.jcis.2007.09.045.

Kasha, A., Al-Hashim, H., Abdallah, W., Taherian, R. & Sauerer, B. (2015). Effect of $Ca^{2+}$, $Mg^{2+}$ and $SO_4^{2-}$ ions on the zeta potential of calcite and dolomite particles aged with stearic acid. *Colloids and Surfaces A: Physicochemical and Engineering Aspects, 482***,** 290-299. doi: 10.1016/j.colsurfa.2015.05.043.

Kennedy, H. T., Burja, E. O. & Boykin, R. S. (1955). An investigation of the effects of wettability on oil recovery by water flooding. *The Journal of Physical Chemistry, 59*, 867-869.

Kestin, J. & Shankland, I. R. (1984). Viscosity of aqueous NaCl solutions in the temperature range 25–200 C and in the pressure range 0.1–30 MPa. *International Journal of Thermophysics, 5*, 241-263. doi: 10.1007/BF00507835.

Klemme, H. & Ulmishek, G. F. (1991). Effective petroleum source rocks of the world: Stratigraphic distribution and controlling depositional factors. *AAPG Bulletin, 75*, 1809-1851.

Kosmulski, M., Hartikainen, J., Mączka, E., Janusz, W. & Rosenholm, J. B. (2002). Multiinstrument study of the electrophoretic mobility of fumed silica. *Analytical Chemistry, 74*, 253-256. doi: 10.1021/ac015584h.

Kosmulski, M. & Rosenholm, J. B. (1996). Electroacoustic study of adsorption of ions on anatase and zirconia from very concentrated electrolytes. *The Journal of Physical Chemistry, 100*, 11681-11687. doi: 10.1021/jp960315u.

Kovscek, A., Wong, H. & Radke, C. (1993). A pore-level scenario for the development of mixed wettability in oil reservoirs. *AIChE Journal, 39*, 1072-1085. doi: 10.1002/aic.690390616.

Kruyt, H. & Overbeek, J. (1960). *An introduction to physical chemistry for biologists and medical students*, Holt, Rinehart and Winston, New York.

Lager, A., Webb, K. J., Black, C. J. J., Singleton, M. & Sorbie, K. S. (2008). Low salinity oil recovery - An experimental investigation. *Petrophysics, 49*, 28-35.

Leinov, E. & Jackson, M. (2014). Experimental measurements of the SP response to concentration and temperature gradients in sandstones with application to subsurface geophysical monitoring. *Journal of Geophysical Research: Solid Earth, 119*, 6855-6876. doi: 10.1002/2014JB011249.

Ligthelm, D. J., Gronsveld, J., Hofman, J., Brussee, N., Marcelis, F. & van der Linde, H. (2009). Novel waterflooding strategy by manipulation of injection brine composition. *Proceedings of the SPE EUROPEC/EAGE Conference and Exhibition, 8-11 June, Amsterdam, The Netherlands* SPE-119835-MS. doi: 10.2118/119835-MS.

Ma, S., Zhang, X., Morrow, N. & Zhou, X. (1999). Characterization of wettability from spontaneous imbibition measurements. *Journal of Canadian Petroleum Technology, 38*. doi: 10.2118/99-13-49.

Madland, M. V., Hiorth, A., Omdal, E., Megawati, M., Hildebrand-Habel, T., Korsnes, R. I., Evje, S. & Cathles, L. M. (2011). Chemical alterations induced by rock–fluid interactions when injecting brines in high porosity chalks. *Transport in Porous Media, 87*, 679-702. doi: 10.1007/s11242-010-9708-3.

Magdans, U., Torrelles, X., Angermund, K., Gies, H. & Rius, J. (2007). Crystalline order of a water/glycine film coadsorbed on the (104) calcite surface. *Langmuir, 23*, 4999-5004. doi: 10.1021/la0636659.

Mahani, H., Keya, A. L., Berg, S., Bartels, W.-B., Nasralla, R. & Rossen, W. R. (2015). Insights into the mechanism of wettability alteration by low-salinity flooding (LSF) in carbonates. *Energy & Fuels, 29*, 1352-1367. doi: 10.1021/ef5023847.

Mahani, H., Keya, A. L., Berg, S. & Nasralla, R. (2016). Electrokinetics of carbonate/brine interface in low-salinity waterflooding: Effect of brine salinity, composition, rock type, and pH on ζ-potential and a surface-complexation model. *SPE Journal*. doi: 10.2118/181745-PA.

Malmberg, C. & Maryott, A. (1956). Dielectric constant of water from

0° to 100°C. *Journal of Research of the National Bureau of Standards, 56***,** 1-8.

McGuire, P. L., Chatham, J. R., Paskvan, F. K., Sommer, D. M. & Carini, F. H. (2005). Low salinity oil recovery: An exciting new EOR opportunity for Alaska's North Slope. *Proceedings of the SPE Western Regional Meeting, 30 March-1 April, Irvine, California* SPE-93903-MS. doi: 10.2118/93903-MS.

Mishra, S. (1978). The electrokinetics of apatite and calcite in inorganic electrolyte environment. *International Journal of Mineral Processing, 05***,** 69-83. doi: 10.1016/0301-7516(78)90006-6

Mohammed, M. & Babadagli, T. (2015). Wettability alteration: A comprehensive review of materials/methods and testing the selected ones on heavy-oil containing oil-wet systems. *Advances in Colloid and Interface Science, 220***,** 54-77. doi: 10.1016/j.cis.2015.02.006.

Moore, J. R., Glaser, S. D., Morrison, H. F. & Hoversten, G. M. (2004). The streaming potential of liquid carbon dioxide in Berea sandstone. *Geophysical Research Letters, 31***,** L17610. doi: 10.1029/2004GL020774.

Morrow, N. & Buckley, J. (2011). Improved oil recovery by low-salinity waterflooding. *Journal of Petroleum Technology, 63***,** 106-112. doi: 10.2118/129421-JPT.

Morrow, N., Ma, S., Zhou, X. & Zhang, X. (1994). Characterization of wettability from spontaneous imbibition measurements. *Proceedings of the Petroleum Society of Canada Annual Technical Meeting, June 12 - 15, Calgary, Alberta* PETSOC-94-47. doi: 10.2118/94-47.

Morrow, N. & McCaffery, F. (1978). Displacement studies in uniformly wetted porous media. In*:* PADDAY, J. F. (ed.), *Wetting, Spreading and Adhesion.* Academic Press, New York.

Morrow, N. R. (1975). The effects of surface roughness on contact: angle with special reference to petroleum recovery. *Journal of Canadian Petroleum Technology, 14***,** 42-53. doi: 10.2118/75-04-04.

Morrow, N. R. (1990). Wettability and its effect on oil recovery. *Journal of Petroleum Technology, 42***,** 1,476-1,484. doi: 10.2118/21621-PA.

Morrow, N. R., Cram, P. J. & McCaffery, F. (1973). Displacement studies in dolomite with wettability control by octanoic acid. *SPE Journal, 13***,** 221-232. doi: 10.2118/3993-PA.

Moulin, P. & Roques, H. (2003). Zeta potential measurement of calcium carbonate. *Journal of Colloid and Interface Science, 261***,** 115-126. doi: 10.1016/S0021-9797(03)00057-2.

Nasralla, R. A., Bataweel, M. A. & Nasr-El-Din, H. A. (2013). Investigation of wettability alteration and oil-recovery improvement by low-salinity water in sandstone rock.

*Journal of Canadian Petroleum Technology, 52*, 144-154. doi: 10.2118/146322-PA.

Nasralla, R. A. & Nasr-El-Din, H. A. (2012). Double-layer expansion: Is it a primary mechanism of improved oil recovery by low-salinity waterflooding? *SPE Reservoir Evaluation & Engineering, 17*, 49-59. doi: 10.2118/154334-PA.

Nasralla, R. A. & Nasr-El-Din, H. A. (2014). Impact of cation type and concentration in injected brine on oil recovery in sandstone reservoirs. *Journal of Petroleum Science and Engineering, 122*, 384-395. doi: 10.1016/j.petrol.2014.07.038.

Nayef, A. (2015). Capillary trapping and oil recovery in altered-wettability carbonate rock. *PhD thesis*, Imperial College London.

Nurmi, R. & Standen, E. (1997). Carbonates: The inside story. *Middle East Well Evaluation Review, 18*, 28-41.

Overbeek, J. T. G. (1952). Electrochemistry of the double layer. In*:* KRUYT, H. R. (ed.), *Colloid Science.* Elsevier, Amsterdam-Huston-New York-London.

Patil, M., Shivakumar, K., Prakash, S. & Rao, R. B. (1998). Effect of organic reagents on the zeta potentials of graphite, quartz and calcite minerals. *Journal of Surface Science and Technology, 14*, 280-285. doi: 10.18311/jsst/1998/2122

Pierre, A., Lamarche, J., Mercier, R., Foissy, A. & Persello, J. (1990). Calcium as potential determining ion in aqueous calcite suspensions. *Journal of Dispersion Science and Technology, 11*, 611-635. doi: 10.1080/01932699008943286.

Pokrovsky, O., Mielczarski, J., Barres, O. & Schott, J. (2000). Surface speciation models of calcite and dolomite/aqueous solution interfaces and their spectroscopic evaluation. *Langmuir, 16*, 2677-2688. doi: 10.1021/la980905e.

Pokrovsky, O. & Schott, J. (2002). Surface chemistry and dissolution kinetics of divalent metal carbonates. *Environmental Science & Technology, 36*, 426-432. doi: 10.1021/es010925u.

Puntervold, T., Strand, S. & Austad, T. (2007). Water flooding of carbonate reservoirs: Effects of a model base and natural crude oil bases on chalk wettability. *Energy & Fuels, 21*, 1606-1616. doi: 10.1021/ef060624b.

Rao, K. H., Antti, B.-M. & Forssberg, E. (1989). Mechanism of oleate interaction on salt-type minerals part I. Adsorption and electrokinetic studies of calcite in the presence of sodium oleate and sodium metasilicate. *Colloids and Surfaces, 34*, 227-239. doi: 10.1016/0166-6622(88)80101-X

Rashid, S., Mousapour, M. S., Ayatollahi, S., Vossoughi, M. & Beigy, A. H. (2015). Wettability alteration in carbonates during “Smart Waterflood”: Underlying mechanisms and the effect of individual ions. *Colloids and Surfaces A: Physicochemical and Engineering Aspects, 487*, 142-153. doi: 10.1016/j.colsurfa.2015.09.067.

Revil, A. (1999). Ionic diffusivity, electrical conductivity, membrane and thermoelectric potentials in colloids and granular porous media: A unified model. *Journal of Colloid and Interface Science, 212*, 503-522. doi: 10.1006/jcis.1998.6077

Revil, A. & Pezard, P. (1998). Streaming electrical potential anomaly along faults in geothermal areas. *Geophysical Research Letters, 25*, 3197-3200. doi: 10.1029/98GL02384.

Revil, A., Schwaeger, H., Cathles, L. & Manhardt, P. (1999). Streaming potential in porous media: 2. Theory and application to geothermal systems. *Journal of Geophysical Research: Solid Earth, 104*, 20033-20048. doi: 10.1029/1999JB900090.

Rezaeidoust, A., Puntervold, T., Strand, S. & Austad, T. (2009). Smart water as wettability modifier in carbonate and sandstone: A discussion of similarities/differences in the chemical mechanisms. *Energy & Fuels, 23*, 4479-4485. doi: 10.1021/ef900185e.

Romanuka, J., Hofman, J., Ligthelm, D. J., Suijkerbuijk, B. M. J. M., Marcelis, A. H. M., Oedai, S., Brussee, N. J., van der Linde, H. A., Aksulu, H. & Austad, T. (2012). Low salinity EOR in carbonate *Proceedings of the SPE Improved Oil Recovery Symposium, 14-18 April, Tulsa, Oklahoma, USA. SPE-153869-MS*. doi: 10.2118/153869-MS.

Sakuma, H., Andersson, M. P., Bechgaard, K. & Stipp, S. L. S. (2014). Surface tension alteration on calcite, induced by ion substitution. *The Journal of Physical Chemistry C, 118*, 3078-3087. doi: 10.1021/jp411151u.

Sampat Kumar, V. Y., Mohan, N. & Biswas, A. K. (1971). Fundamental studies on the role of carbon dioxide in a calcite flotation system. *Transactions of the AIME, 250*, 182-186.

Saunders, J. H., Jackson, M. D., Gulamali, M. Y., Vinogradov, J. & Pain, C. C. (2012). Streaming potentials at hydrocarbon reservoir conditions. *Geophysics, 77*, E77-E90. doi: 10.1190/geo2011-0068.1.

Schindler, P. W. & Stumm, W. (1987). The surface chemistry of oxides, hydroxides, and oxide minerals. In*:* STUMM, W. (ed.), *Aquatic Surface Chemistry: Chemical Processes at the Particle-Water Interface.* John Wiley & Sons, New York.

Schramm, L. L., Mannhardt, K. & Novosad, J. J. (1991). Electrokinetic properties of reservoir rock particles. *Colloids and Surfaces, 55*, 309-331. doi: 10.1016/0166-6622(91)80102-t.

Sen, P. N. & Goode, P. A. (1992). Influence of temperature on electrical-conductivity on shaly sands. *Geophysics, 57*, 89-96. doi: 10.1190/1.1443191.

Shariatpanahi, S. F., Strand, S. & Austad, T. (2010). Evaluation of water-based enhanced oil recovery (EOR) by wettability alteration in a Low-permeable fractured limestone oil reservoir. *Energy & Fuels, 24*, 5997-6008. doi: 10.1021/ef100837v.

Shehata, A. M., Alotaibi, M. B. & Nasr-El-Din, H. A. (2014). Waterflooding in carbonate reservoirs: Does the salinity matter? *SPE Reservoir Evaluation & Engineering, 17*, 304-313. doi: 10.2118/170254-PA.

Siffert, D. & Fimbel, P. (1984). Parameters affecting the sign and magnitude of the eletrokinetic potential of calcite. *Colloids and Surfaces, 11*, 377-389. doi: 10.1016/0166-6622(84)80291-7.

Smallwood, P. (1977). Some aspects of the surface chemistry of calcite and aragonite Part I: An electrokinetic study. *Colloid and Polymer Science, 255*, 881-886. doi: 10.1007/BF01617095.

Smani, M., Blazy, P. & Cases, J. (1975). Beneficiation of sedimentary Moroccan phosphate ores. *Transactions of the AIME, 258*, 168-182.

Somasundaran, P. (2006). *Encyclopedia of surface and colloid science*, CRC press Taylor & Francis, New York.

Somasundaran, P. & Agar, G. (1967). The zero point of charge of calcite. *Journal of Colloid and Interface Science, 24*, 433-440. doi: 10.1016/0021-9797(67)90241-X

Somasundaran, P., Amankonah, J. O. & Ananthapadmabhan, K. (1985). Mineral-solution equilibria in sparingly soluble mineral systems. *Colloids and Surfaces, 15*, 309-333. doi: 10.1016/0166-6622(85)80081-0

Somasundaran, P., Deo, Namita, D. & Puspendu Natarajan, K. A. (2005). Role of biopolymers on bacterial adhesion and mineral beneficiation. *Minerals and Metallurgical Processing, 22*, 1-11.

Sondi, I., Bišćan, J., Vdović, N. & Škapin, S. D. (2009). The electrokinetic properties of carbonates in aqueous media revisited. *Colloids and Surfaces A: Physicochemical and Engineering Aspects, 342*, 84-91. doi: 10.1016/j.colsurfa.2009.04.012.

Soraya, B., Malick, C., Philippe, C., Bertin, H. J. & Hamon, G. (2009). Oil recovery by low-salinity brine injection: Laboratory results on outcrop and reservoir cores. *Proceedings of the SPE Annual Technical Conference and Exhibition, 4-7 October, New Orleans, Louisiana* SPE-124277-MS. doi: 10.2118/124277-MS.

Standnes, D. C. & Austad, T. (2000). Wettability alteration in chalk: 1. Preparation of core material and oil properties. *Journal of Petroleum Science and Engineering, 28*, 111-121. doi: 10.1016/S0920-4105(00)00083-8.

Stipp, S. (1999). Toward a conceptual model of the calcite surface: Hydration, hydrolysis, and surface potential. *Geochimica et Cosmochimica Acta, 63*, 3121-3131. doi: 10.1016/S0016-7037(99)00239-2.

Stipp, S., Eggleston, C. & Nielsen, B. (1994). Calcite surface structure observed at microtopographic and molecular scales with atomic force microscopy (AFM). *Geochimica et Cosmochimica Acta, 58*, 3023-3033. doi: 10.1016/0016-7037(94)90176-7

Stipp, S. L. & Hochella, M. F. (1991). Structure and bonding environments at the calcite surface as observed with X-ray photoelectron spectroscopy (XPS) and low energy electron diffraction (LEED). *Geochimica et Cosmochimica Acta, 55*, 1723-1736. doi: 10.1016/0016-7037(91)90142-R

Stogryn, A. (1971). Equations for calculating the dielectric constant of saline water (correspondence). *IEEE Transactions on Microwave Theory and Techniques, 19*, 733-736. doi: 10.1109/TMTT.1971.1127617.

Strand, S., Austad, T., Puntervold, T., Hognesen, E. J., Olsen, M. & Barstad, S. M. F. (2008). "Smart Water" for oil recovery from fractured limestone: A preliminary study. *Energy & Fuels, 22*, 3126-3133. doi: 10.1021/ef800062n.

Strand, S., Hognesen, E. J. & Austad, T. (2006). Wettability alteration of carbonates - Effects of potential determining ions ($Ca^{2+}$ and $SO_4^{2-}$) and temperature. *Colloids and Surfaces A: Physicochemical and Engineering Aspects, 275*, 1-10. doi: 10.1016/j.colsurfa.2005.10.061.

Stumm, W. (1992). *Chemistry of the solid-water interface: Processes at the mineral-water and particle-water interface in natural systems*, John Wiley & Sons, New Yotk.

Stumm, W. & Morgan, J. J. (2012). *Aquatic chemistry: chemical equilibria and rates in natural waters*, John Wiley & Sons, New York.

Stumm, W., Wehrli, B. & Wieland, E. (1987). Surface complexation and its impact on geochemical kinetics. *Croat. Chem. Acta, 60*, 429.

Suski, B., Ladner, F., Baron, L., Vuataz, F.-D., Philippossian, F. & Holliger, K. (2008). Detection and characterization of hydraulically active fractures in a carbonate aquifer: Results from self-potential, temperature and fluid electrical conductivity logging in the Combioula hydrothermal system in the southwestern Swiss Alps. *Hydrogeology Journal, 16*, 1319-1328. doi: 10.1007/s10040-008-0302-5.

Tang, G. Q. & Morrow, N. R. (1997). Salinity, temperature, oil composition, and oil recovery by waterflooding. *SPE Reservoir Engineering, 12*, 269-276. doi: 10.2118/36680-PA.

Tang, G. Q. & Morrow, N. R. (1999). Influence of brine composition and fines migration on crude oil/brine/rock interactions and oil recovery. *Journal of Petroleum Science and Engineering, 24*, 99-111. doi: 10.1016/s0920-4105(99)00034-0.

Tanino, Y. & Blunt, M. J. (2013). Laboratory investigation of capillary trapping under mixed-wet conditions. *Water Resources Research, 49*, 4311-4319. doi: 10.1002/wrcr.20344.

Thompson, D. W. & Pownall, P. G. (1989). Surface electrical-properties of calcite. *Journal of Colloid and Interface Science, 131*, 74-82. doi: 10.1016/0021-9797(89)90147-1.

Treiber, L. & Owens, W. (1972). A laboratory evaluation of the wettability of fifty oil-producing reservoirs. *SPE Journal, 12*, 531-540. doi: 10.2118/3526-PA.

Tucker, M. E. & Wright, V. P. (1990). Carbonate mineralogy and chemistry. *Carbonate Sedimentology.* Blackwell Publishing Ltd., Oxford, UK.

Van Cappellen, P., Charlet, L., Stumm, W. & Wersin, P. (1993). A surface complexation model of the carbonate mineral-aqueous solution interface. *Geochimica et Cosmochimica Acta, 57*, 3505-3518. doi: 10.1016/0016-7037(93)90135-J.

Vdovic, N. (2001). Electrokinetic behaviour of calcite - The relationship with other calcite properties. *Chemical Geology, 177*, 241-248. doi: 10.1016/s0009-2541(00)00397-1.

Vdović, N. & Bišćan, J. (1998). Electrokinetics of natural and synthetic calcite suspensions. *Colloids and Surfaces A: Physicochemical and Engineering Aspects, 137*, 7-14. doi: 10.1016/S0927-7757(97)00179-9

Vernhet, A., Bellon-Fontaine, M. & Doren, A. (1994). Comparison of three electrokinetic methods to determine the zeta potential of solid surfaces. *Journal de Chimie Physique, 91*, 1728-1747.

Vinogradov, J., Jaafar, M. Z. & Jackson, M. D. (2010). Measurement of streaming potential coupling coefficient in sandstones saturated with natural and artificial brines at high salinity. *Journal of Geophysical Research-Solid Earth, 115*, B12204. doi: 10.1029/2010jb007593.

Vinogradov, J. & Jackson, M. D. (2011). Multiphase streaming potential in sandstones saturated with gas/brine and oil/brine during drainage and imbibition. *Geophysical Research Letters, 38***,** L01301. doi: 10.1029/2010gl045726.

Vinogradov, J. & Jackson, M. D. (2015). Zeta potential in intact natural sandstones at elevated temperatures. *Geophysical Research Letters, 42***,** 6287-6294. doi: 10.1002/2015GL064795.

Vledder, P., Gonzalez, I. E., Carrera Fonseca, J. C., Wells, T. & Ligthelm, D. J. (2010). Low salinity water flooding: Proof of wettability alteration on a field wide scale. *Proceedings of the SPE Improved Oil Recovery Symposium, 24-28 April, Tulsa, Oklahoma, USA* SPE-129564-MS. doi: 10.2118/129564-MS.

Wagner, O. & Leach, R. (1959). Improving oil displacement efficiency by wettability adjustment. *Transactions of the AIME, 216***,** 65-72. doi: 10.2118/1101-G.

Weast, R. C., Astle, M. J. & Beyer, W. H. (1989). *CRC handbook of chemistry and physics*, CRC press Boca Raton, Florida.

Webb, K. J., Black, C. J. J. & Al-Ajeel, H. (2003). Low salinity oil recovery - log-inject-log. *Proceedings of the SPE Middle East Oil Show, 9-12 June, Bahrain* SPE-81460-MS. doi: 10.2118/81460-MS.

Webb, K. J., Black, C. J. J. & Edmonds, I. J. (2005). Low salinity oil recovery-The role of reservoir condition corefloods. *Proceedings of the 13th EAGE Symposium on Improved Oil Recovery, Budapest, Hungary*. EAGE-C18.

Willhite, G. (1986). *Waterflooding*, Society of Petroleum Engineers, Richardson, Texas.

Wolthers, M., Charlet, L. & Van Cappellen, P. (2008). The surface chemistry of divalent metal carbonate minerals; a critical assessment of surface charge and potential data using the charge distribution multi-site ion complexation model. *American Journal of Science, 308***,** 905-941. doi: 10.2475/08.2008.02.

Worthington, A., Hedges, J. & Pallatt, N. (1990). SCA guidelines for sample preparation and porosity measurements of electrical resistivity samples. *The Log Analyst, 31***,** 20-28.

Yi, Z. & Sarma, H. K. (2012). Improving waterflood recovery efficiency in carbonate reservoirs through salinity variations and ionic exchanges: A promising low-cost "Smart-Waterflood" approach. *Proceedings of the SPE Abu Dhabi International Petroleum Conference and Exhibition, 11-14 November , Abu Dhabi, UAE* SPE-161631-MS. doi: 10.2118/161631-MS.

Yousef, A. A., Al-Saleh, S. & Al-Jawfi, M. S. (2012a). Improved/enhanced oil recovery from carbonate reservoirs by tuning injection water salinity and ionic content. *Proceedings of the SPE Improved Oil Recovery Symposium, 14-18 April, Tulsa, Oklahoma, USA* SPE-154076-MS. doi: 10.2118/154076-MS.

Yousef, A. A., Al-Saleh, S. H., Al-Kaabi, A. & Al-Jawfi, M. S. (2011). Laboratory investigation of the impact of injection-water salinity and ionic content on oil recovery from carbonate reservoirs. *SPE Reservoir Evaluation & Engineering, 14***,** 578-593. doi: 10.2118/137634-PA.

Yousef, A. A., Liu, J., Blanchard, G., Al-Saleh, S., Al-Zahrani, T., Al-Zahrani, R., Al-Tammar, H. & Al-Mulhim, N. (2012b). Smartwater flooding: industry's first field test in carbonate reservoirs. *Proceedings of the SPE Annual Technical Conference and*

*Exhibition, 8-10 October, San Antonio, Texas, USA* SPE-159526-MS. doi: 10.2118/159526-MS.

Zahid, A., Shapiro, A., Stenby, E. H. & Yan, W. (2012). Managing injected water composition to improve oil recovery: A case study of North Sea chalk reservoirs. *Energy & Fuels, 26***,** 3407-3415. doi: 10.1021/ef2008979.

Zahid, A., Stenby, E. H. & Shapiro, A. A. (2010). Improved oil recovery in chalk: Wettability alteration or something else? *Proceedings of the SPE EUROPEC/EAGE Annual Conference and Exhibition, 14-17 June, Barcelona, Spain* SPE-131300-MS. doi: 10.2118/131300-MS.

Zhang, H.-L. & Han, S.-J. (1996). Viscosity and density of water + sodium chloride + potassium chloride solutions at 298.15 K. *Journal of Chemical & Engineering Data, 41***,** 516-520. doi: 10.1021/je9501402.

Zhang, P., Tweheyo, M. T. & Austad, T. (2007). Wettability alteration and improved oil recovery by spontaneous imbibition of seawater into chalk: Impact of the potential determining ions $Ca^{2+}$, $Mg^{2+}$, and $SO_4^{2-}$. *Colloids and Surfaces A: Physicochemical and Engineering Aspects, 301***,** 199-208. doi: 10.1016/j.colsurfa.2006.12.058.

Zhang, P. M. & Austad, T. (2006). Wettability and oil recovery from carbonates: Effects of temperature and potential determining ions. *Colloids and Surfaces A: Physicochemical and Engineering Aspects, 279***,** 179-187. doi: 10.1016/j.colsurfa.2006.01.009.

# Appendices

## Appendix A: Streaming Potential Measurements: Application to Porous Media

In many (but not all) electrokinetic phenomena, a fluid moves with respect to a solid surface. This leads to an arrangement of charge on the solid surface and in the adjacent fluid, which is referred to as the electrical double layer at the interface. There is an excess of counter-charge (and a deficit of co-charge) in the fluid adjacent to the solid surface. The charges in the fluid respond to three forces: (1) the electrical potential, (2) the diffusion force and (3) the bulk movement of charge carried by the flow of liquid (advection). The charge and potential distribution and at the planar interface follows Poisson's equation, which relates the electrostatic potential (or the electric field) to the electrical charge density (charge per unit volume)

$$\nabla.(-\varepsilon\nabla V) = \rho, \qquad \text{A.1}$$

and if the permittivity ε is constant

$$\nabla^2 V = -\frac{\rho}{\varepsilon}, \qquad \text{A.2}$$

where $\rho$ is the electrical charge density (C $m^{-3}$), ε is the electrical permittivity ($Fm^{-1}$) and $V$ is the electrical potential (volt).

The ion distribution in the fluid is assumed to be determined by the Boltzmann equation. This assumes

- The ions are point charges
- The solvent is continuous and characterized by a constant permittivity
- The only work done in bringing an ion from the bulk (where the electrical field is, by definition, zero) to a certain point in the electrical field close to the solid

surface is $z_i eV$. This neglects (a) the work done in displacing the solvent, (b) the change in potential energy due to local reorientation of the solvent around the ion and (c) the effect of the other ions on the electrostatic potential experienced by a given ion.

We need to consider one dimension only for charge distribution adjacent to a flat solid surface with uniform surface charge density. Then the Boltzmann equation is determined by assuming that, at equilibrium, the chemical (diffusion force) and electrical forces exactly balance and integrating from the bulk solution (where $V = 0$ and $n_i = n_i^0$) to yield

$$n_i = n_i^0 \exp(-z_i eV/kT), \qquad \text{A.3}$$

where $n_i^0$ is the number density of *i*-th ions in the bulk solution, $z_i$ is the ion valence, $e$ is the elementary charge, $k$ is Boltzmann constant, and $T$ is the temperature. Note that $n_i^0 = 1000 C N_A$, where $C_e$ is electrolyte concentration in Mol/L and $N_A$ is Avogadro's number ($6.022 \times 10^{23}$).

The volume charge density of all present species is therefore

$$\rho = \sum_i n_i ze. \qquad \text{A.4}$$

Combining (A.2), (A.3) and (A.4) yields the Poisson-Boltzmann equation

$$\nabla^2 V = \frac{d^2V}{dx^2} = -\frac{1}{\varepsilon}\sum_i n_i ze \exp(-z_i eV/kT). \qquad \text{A.5}$$

Equation (A.5) relates the associated charge density of the ions present to the electrical potential. A symmetrical electrolyte is a solution whose cations and anions have the same valence e.g., 1:1 as in NaCl or KCl (The Great Soviet Encyclopaedia, 1970). Symmetrical electrolyte solutions have equal positive and negative ions in their bulk ($n_+^0 = n_-^0 = 2n^0$) for which case the Debye length is $\kappa^{-1}$ (nm), which is given by

$$\kappa = \sqrt{\frac{2n^0 z^2 e^2}{\varepsilon kT}}. \qquad \text{A.6}$$

The Debye-Huckel approximation approach assumes $V$ is small everywhere in double layer so $z_i eV << kT$ and we can re-write Poisson-Boltzmann equation as

$$\nabla^2 V = \frac{d^2V}{dx^2} = \kappa^2 V, \quad \text{A.7}$$

which has the solution

$$V(x) = V_0 \exp(-\kappa x), \quad \text{A.8}$$

where $x$ is the distance from the surface to the shear plane. Equation (A.8) is valid for $V_0$ < 25.7 mV at 25°C. At the share plane, the electrical potential is the zeta potential ($i.e.\ V(x) = \zeta$). Thus equation (A.8) can be expressed as

$$\zeta = V_0 \exp(-\kappa x)\,, \kappa = \sqrt{\frac{2ISe^2}{\varepsilon kT}}, V_0 \ll 25mV, \quad \text{A.9}$$

where $IS$ is the ionic strength of the solution and $\kappa$ is the Debye-Huckel reciprocal length ($nm^{-1}$).

Now, in order to develop an analytical relation between the various electrical properties in the case of a capillary, we consider the excess charge transported with the flow through a single capillary

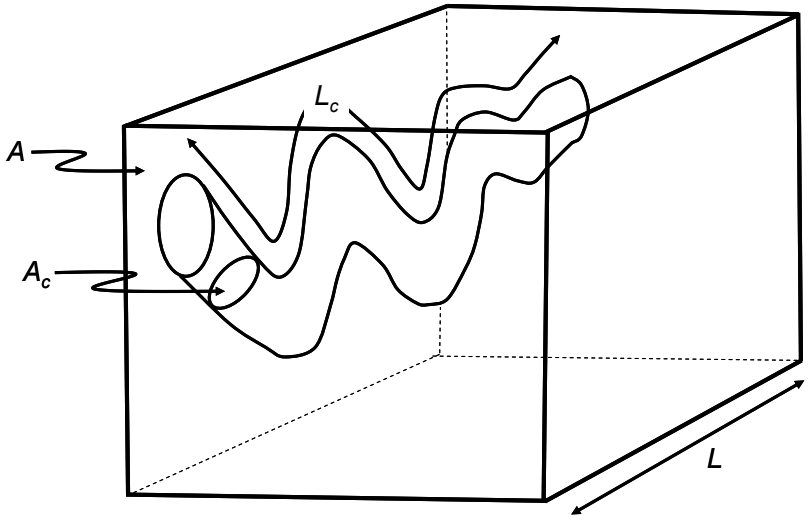



**Figure A- 1: The bundle of capillary tube models (Jackson, 2010).**

We assume the currents follow approximately the same 1-D path along the capillary. Also, the Poisson-Boltzman equation is assumed to be reasonable at a

curved interface when the local radius of curvature *r* is large compared to the double layer thickness so

$$\kappa r \gg 1. \qquad \text{A.10}$$

We start by considering the fluid velocity in a capillary, which is governed by Poiseuille's equation:

$$v(z) = \frac{1}{4\mu}(r^2 - y^2)\frac{\Delta P}{L_c}, \qquad \text{A.11}$$

where $v(z)$ is the velocity of the liquid, $\Delta P$ is the pressure drop across the rock sample measured over a tortuous path the fluid is taking through the medium $L_c$ where *r* is the capillary radius, and *y* is the distance from the capillary wall at which the velocity is calculated, and using an incompressible fluid of viscosity $\mu$.

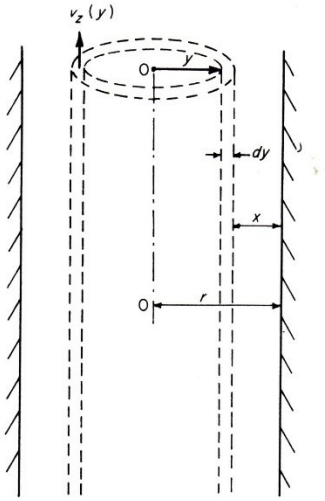



**Figure A- 2: A schematic showing the double layer in a capillary**

The streaming current is the flow rate multiplied by the charge density integrated over the capillary area, given by

$$I_s = \int_0^r 2\pi y\, v_z(y)\rho(y)dy. \qquad \text{A.12}$$

Double layer is confined to a thin region near the wall of the capillary, so we are only interested in charge transport in this region where *r* - *y* is small and use this to linearize Poiseulle's equation (close to the capillary wall)

$$r^2 - y^2 \approx 2r(r - y). \qquad \text{A.13}$$

Then substitute $x = (r - y)$, so

$$I_s = \int_0^r 2\pi(r-x)\frac{rx}{2\mu}\frac{\Delta P}{L_c}\rho(x)dx\,. \qquad \text{A.14}$$

When $x$ is small (close to the capillary wall), equation (A.14) can be linearized, so

$$r^2(x - \frac{x^2}{r}) \approx r^2 x \qquad \text{A.15}$$

and

$$I_s = \frac{\pi r^2}{\mu}\frac{\Delta P}{L_c}\int_0^r x\rho(x)dx. \qquad \text{A.16}$$

Now substitute for $\rho(x)$ using Poisson's equation (A.2) and integrate by parts

$$I_s = -\frac{\pi r^2 \varepsilon}{\mu}\frac{\Delta P}{L_c}\int_0^r x\frac{d^2V}{dx^2}dx \qquad \text{A.17}$$

$$I_s = -\frac{\pi r^2 \varepsilon}{\mu}\frac{\Delta P}{L_c}\left[\left(x\frac{dV}{dx}\right)_{x=0}^{x=r} - \int_0^r \frac{dV}{dx}dx\right] \qquad \text{A.18}$$

$$I_s = -\frac{\pi r^2 \varepsilon}{\mu}\frac{\Delta P}{L_c}\int_\zeta^0 dV\,. \qquad \text{A.19}$$

This integration results in the total streaming current for all concentric shells of fluid within the capillary and is given by

$$I_s = -\frac{\pi\varepsilon\zeta r^2}{\mu}\frac{\Delta P}{L_c}. \qquad \text{A.20}$$

When there is a fluid movement, charges within the diffuse layer move down a pressure gradient relative to the Stern layer. Thus, the streaming current $I_s$ and the associated steaming potential are generated. In order to maintain electrical neutrality, the conduction current $I_c$ is established. The conduction current $I_c$ is derived from Ohm's law, and accounts for conductivity contributions from both the bulk fluid $\sigma_f$ and the surface (fluid within the EDL) $\sigma_s$ gives

$$I_c = \left(\sigma_f + \frac{2\sigma_s}{r}\right)\pi r^2 \frac{\Delta V}{L_c}. \quad \text{A.21}$$

At steady-state and electrical isolation conditions, the streaming current $I_s$ is balanced by the conduction current $I_c$. This assumes that the path both currents take is practically the same i.e., the ions flow and the opposing voltage flow take the same tortuous path within the rock sample. Equating both gives

$$I_c = -I_s = \frac{\pi r^2}{t}\frac{\Delta V}{L}(\sigma_f + \frac{2\sigma_s}{r}) = \frac{\pi r^2}{\mu}\frac{\Delta P}{L_c}\varepsilon\zeta, \quad \text{A.22}$$

where $t$ is the tortuousity, which defines the straightness of the flow path and is the ratio of the actual tortuous path $L_c$ to the straight length of the capillary $L$.

The change in the potential is measured as function of pressure drop across the rock sample, which gives the coupling coefficient as (*Jackson and Vinogradov*, 2011)

$$\frac{\Delta V}{\Delta P} = C_{sp} = \frac{\varepsilon\zeta}{\mu\left(\sigma_f + \frac{2\sigma_s}{r}\right)} = \frac{\varepsilon_w\zeta}{\mu_w\sigma_{rw}F_0}, \quad \text{A.23}$$

where $F_0$ is the intrinsic formation factor, which is the ratio of the conductivity value of the brine to the conductivity of the fully saturated rock when the surface conductivity is negligible, $\Delta V$ is the stabilized voltage, and $\Delta P$ is the stabilized pressure measured across the plug.

This simplifies to the Helmholtz-Smoluchowski equation when the surface conductivity is negligible

$$\frac{\Delta V}{\Delta P} = C_{sp} = \frac{\varepsilon\zeta}{\mu\sigma_f}. \quad \text{A.24}$$

# Appendix B: XRD Data for Ketton, Estaillades and Portland

XRD analysis was carried out in the X-ray Laboratory at the Natural History Museum London. The measurements were obtained on powdered samples and Block-like samples (of the same size as core plugs used in this project). Off-cuts of fresh samples were cleaned for 48 hours in methanol and then crushed using a jaw crusher. A Tema Mill with an agate vessel was then used to obtain a fine powder of the sample. The results show that all investigated carbonate samples consist mainly of calcite with traces of magnesium as shown in Table 4-1 (Figures B-1:4).

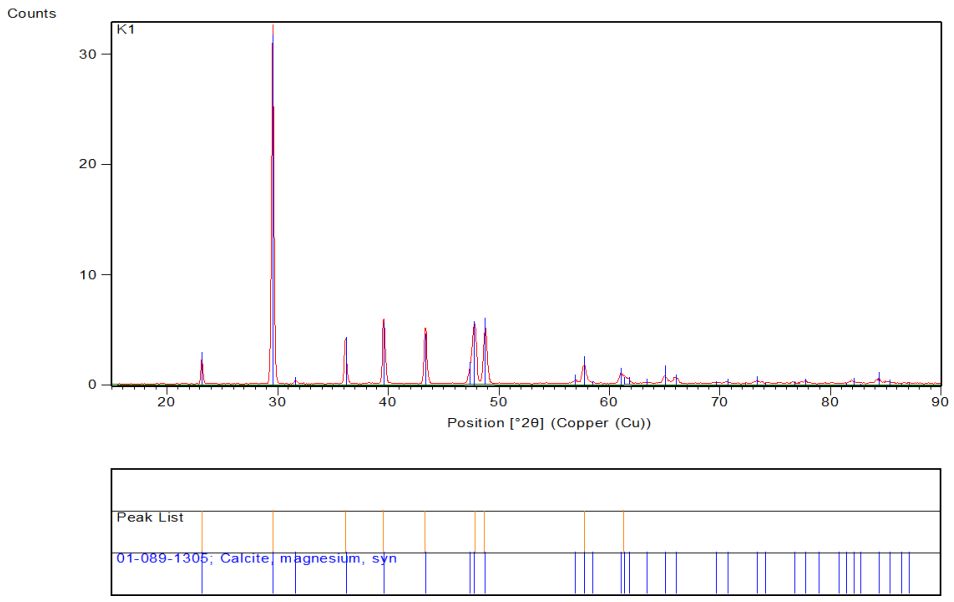



**Figure B- 3: XRD pattern on Ketton K1 block sample**

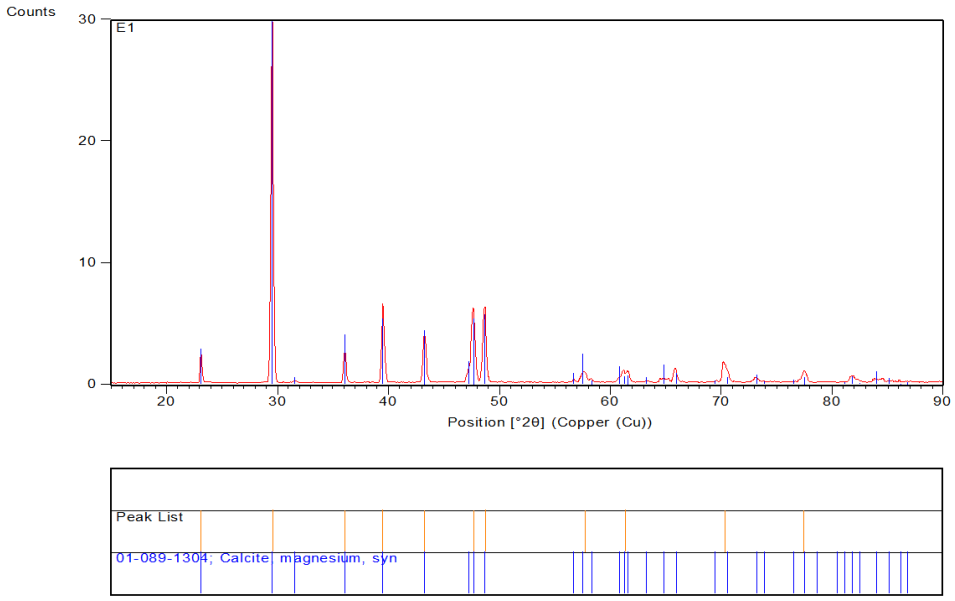



**Figure B- 4: XRD pattern on Estaillades E1 block sample**

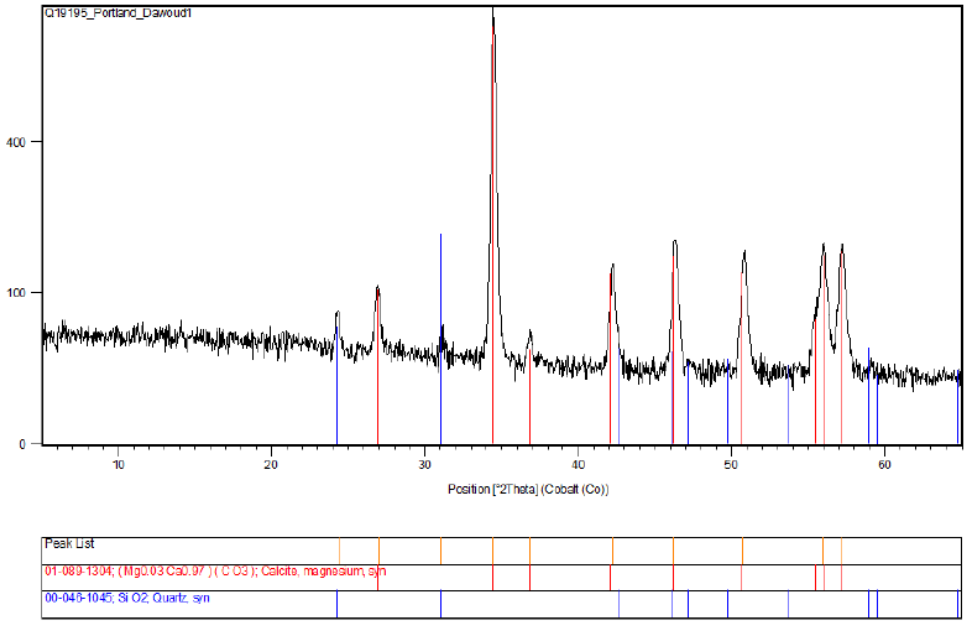



**Figure B- 5: XRD pattern on Portland powdered sample**

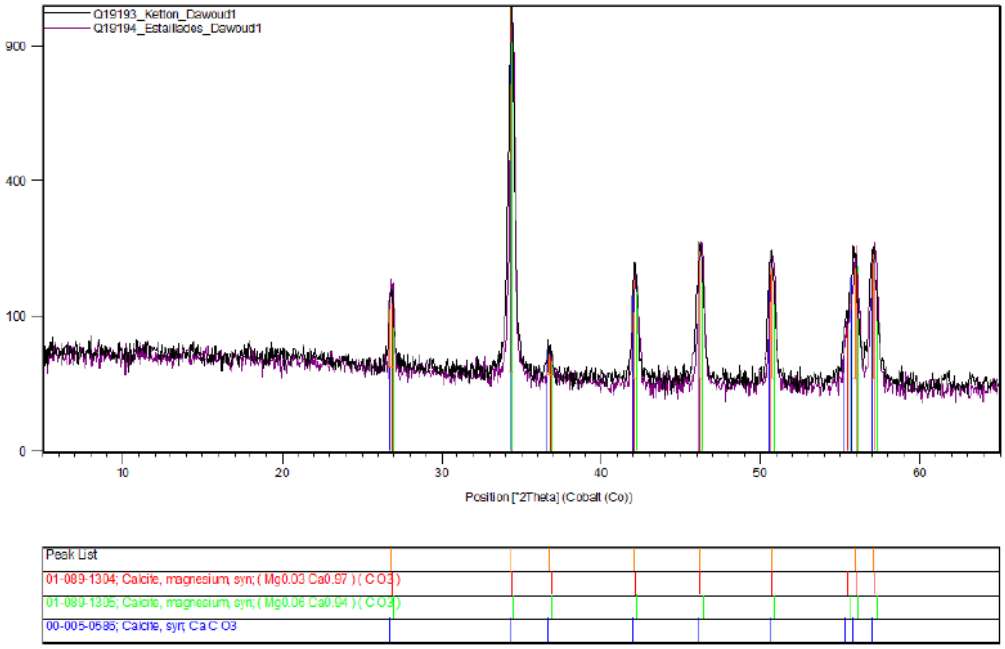



**Figure B- 6: XRD pattern on Ketton and Estaillades powdered samples**

# Appendix C: Determination of Rock Permeability and Porosity and Fluid Saturation

## C.1 Rock Permeability

The rock permeability of the tested samples was measured using the same experimental apparatus used for the SPM and coreflooding experiments shown in Figure 4-2. Darcy equation was used to determine the core samples permeability

$$k = \frac{Q\mu L}{A\Delta P}, \tag{C.1}$$

where $k$ is the rock permeability ($m^2$), $Q$ is the volumetric flow rate ($m^3$), $\mu$ is the brine viscosity (P.s), $L$ is the core length (m), $A$ is the cross sectional area of the core ($A = \pi r^2$; $r$ is the core radius in m) and $\Delta P$ is the differential pressure across the sample resulted from inducing a specific flowrate. $\frac{Q}{\Delta P}$ is taken from the slope of linear regression between flowrates and pressure differences during the SPM experiment (e.g. Figure C-1).

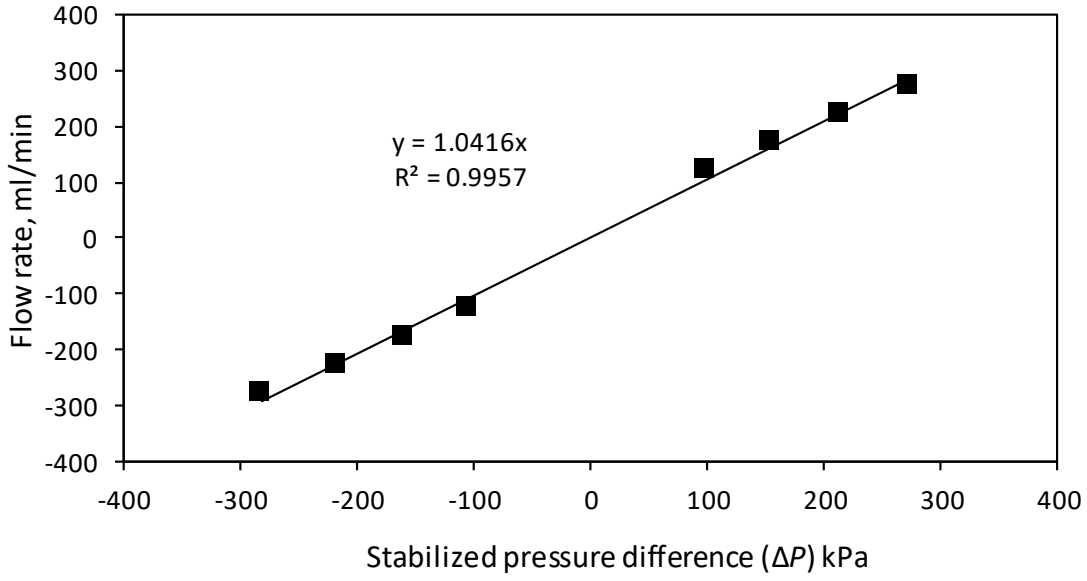



**Figure C-1: Example of flowrate vs. stabilized pressure difference in a Ketton sample during SPM experiment. The slope of linear regression is equal to Q/∆P (ml min-1 kPa). In this case, *k* = 1.159 D. given *r* = 0.0378m, *L*=0.076m and *μ*=0.00097Pa.s.**

## C.2 Rock Porosity

The rock porosity was measured using both helium porosimeter and fluid saturation method. The latter involves weight measurements of dry and saturated sample and the difference between the two masses divided by fluid density is equal to the pore volume (PV) of the tested sample.

$$PV = \pi r^2 L\phi, \tag{C.2}$$

where $PV$ is the core pore volume ($m^3$), $r$ is the core radius (m), $L$ is the core length (m), $\phi$ is the porosity of core.

## C.3 Fluid Saturations

C.3.1. Initial oil saturation:

$$S_{oi} = 1 - S_{wi} = \frac{V_{wp}}{PV}, \tag{C.2}$$

where $S_{oi}$ is the initial oil saturation, $S_{wi}$ is the initial oil saturation and $V_{wp}$ is volume of water displaced by oil during drainage process.

C.3.2. Oil Saturation after spontaneous imbibition (SI):

$$S_{osi} = 1 - S_{wsi} = \frac{V_{wp} - V_{osi}}{PV}, \tag{C.3}$$

where $S_{osi}$ is the oil saturation after SI and $V_{wsi}$ is the volume of oil displaced spontaneously by water during the SI process.

C.3.3. Residual oil saturation /Remaining oil saturation:

$$S_{or} = 1 - S_w = \frac{V_{wp} - V_{osi} - V_{owf}}{PV}, \tag{C.4}$$

where $S_{or}$ is the residual oil saturation after waterflooding process, $S_w$ is the water saturation in the core sample (connate) after waterflooding process and $V_{owf}$ is the volume of oil produced by waterflooding after 10 PVs.

# Appendix D: n-decane SPM experiments

Pure n-decane (Sigma Aldrich ≥99%) was used in the first set of multiphase experiments in Estaillades samples to represent the end-member of a non-wetting oil for comparison against single phase measurements reported in Figure 4-11.

We begin by reporting the zeta potential obtained when the sample is saturated FW and SW at the irreducible saturation after primary drainage using n-decane (Figure D-1). The zeta potential is positive when the core sample is partially saturated with FW, and negative when fully or partially saturated with SW. The magnitude of the zeta potential in core saturated with n-decane and irreducible saturation is the same within experimental error to that obtained in cores fully saturated with brine. It has been shown that n-decane cannot alter carbonate rock wettability towards a more oil-wet state (*Tanino and Blunt*, 2013), which explains why the presence of n-decane has no effect on the zeta potential.

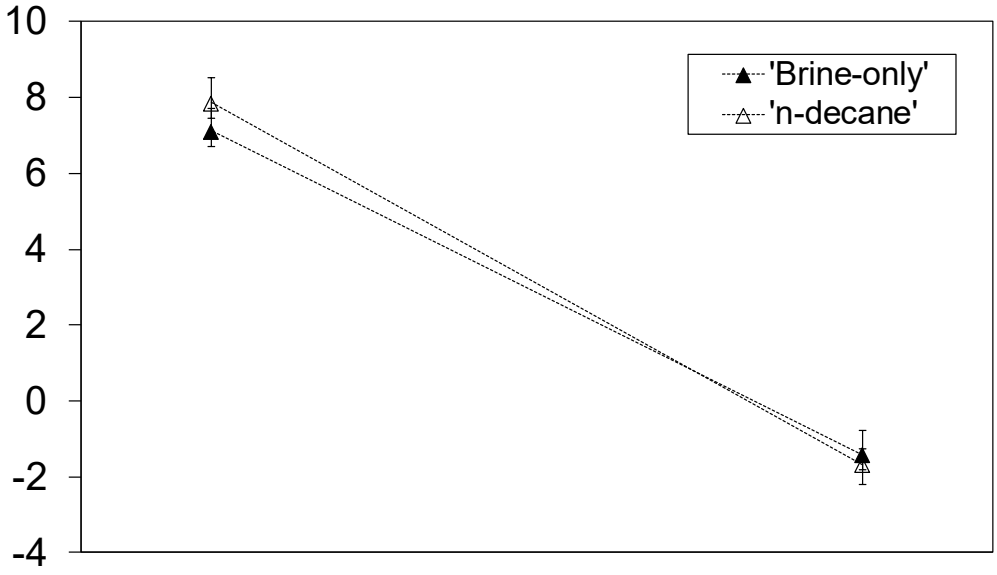



**Figure D-1: Zeta potential of Estaillades core when is fully brine saturated (filled triangles) and when is saturated with brine and residual n-decane (empty triangles) at FW and SW.**

Figure D-2 shows that modification of the SW composition by either lowering the ionic strength (bulk dilution) or increasing ionic strength (adding $SO_4^{2-}$) further increases the magnitude of the negative zeta potential. However, the rate of change of zeta potential with increasing ionic strength through addition of $SO_4^{2-}$

is less than that observed with decreasing ionic strength (by dilution), similar to results obtained for single phase in Figure 4-11b.

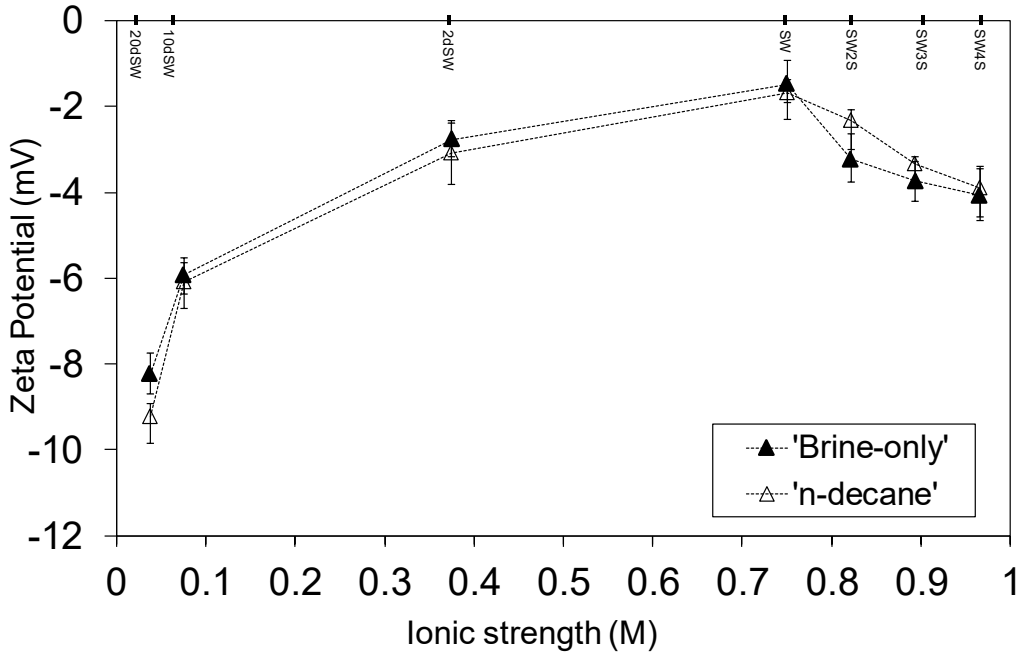



**Figure D-2: Zeta potential of Estaillades core when is fully brine saturated (filled triangles) and when is saturated with brine and residual n-decane (empty triangles) against ionic strength by either varying $SO_4^{2-}$ concentration in SW up to four times, or SW bulk dilution up to 20 times dilution.**

# Appendix E: Compilation of SPM and Coreflooding Results

**Table E-1: Compilation of SPM results from NaCl-EQ experiments**

| Plug # | Exp | NaCl, M | $C_{sp}$, V/Pa | $\sigma_{rf}$, S/m | $\sigma_f$, S/m | $F_a$ | $\varepsilon$, F/m | $\mu$, Pa.s | ζ, mV | $\zeta_{corrected}$, mV | k, D | Na, M | pCa | pMg | $pSO_4$ | pH |
|---|---|---|---|---|---|---|---|---|---|---|---|---|---|---|---|---|
| **K3** | NaCl-EQ | 0.01 | -8.406E-08 | 0.007 | 0.113 | 11.890 | 7.065E-10 | 9.468E-04 | -12.780 | -14.446 | 1.666 | 0.012 | 2.890 | 4.341 | 2.932 | 8.27 |
| **K3** | NaCl-EQ | 0.05 | -2.189E-08 | 0.034 | 0.452 | 13.224 | 7.033E-10 | 9.497E-04 | -13.365 | -13.584 | 1.315 | 0.050 | 2.846 | 4.589 | 2.959 | 8.37 |
| **K3** | NaCl-EQ | 0.1 | -1.043E-08 | 0.062 | 0.799 | 12.913 | 7.052E-10 | 9.529E-04 | -11.265 | -11.725 | 1.208 | 0.092 | 2.817 | 4.185 | 3.009 | 8.25 |
| **K3** | NaCl-EQ | 0.5 | -1.494E-09 | 0.261 | 3.468 | 13.286 | 7.052E-10 | 9.836E-04 | -7.225 | -7.309 | 1.138 | 0.430 | 2.697 | 3.953 | 2.867 | 8.43 |
| **K3** | NaCl-EQ | 1 | -4.206E-10 | 0.483 | 6.493 | 13.452 | 6.205E-10 | 1.019E-03 | -4.484 | -4.480 | 1.225 | 0.944 | 2.577 | 3.828 | 2.713 | 8.35 |
| **K3** | NaCl-EQ | 2 | -1.740E-10 | 0.818 | 10.740 | 13.130 | 5.584E-10 | 1.086E-03 | -3.635 | -3.721 | 1.158 | 1.705 | 2.484 | 3.662 | 2.706 | 8.24 |
| **K3** | NaCl-EQ | 3.5 | -7.252E-11 | 1.238 | 16.815 | 13.584 | 4.556E-10 | 1.266E-03 | -3.387 | -3.352 | 1.159 | 3.167 | 2.544 | 4.019 | 2.700 | 8.32 |
| **K3** | NaCl-EQ | 5 | -2.901E-11 | 1.138 | 19.835 | 17.432 | 6.945E-10 | 1.427E-03 | -1.182 | -0.911 | 1.089 | 4.946 | 2.437 | 4.205 | 3.138 | 8.23 |
| **E2** | NaCl-EQ | 0.01 | -6.074E-08 | 0.012 | 0.140 | 11.482 | 7.063E-10 | 9.469E-04 | -11.364 | -12.545 | 0.133 | 0.014 | 3.099 | 4.320 | 3.486 | 8.10 |
| **E2** | NaCl-EQ | 0.05 | -2.148E-08 | 0.034 | 0.408 | 11.895 | 7.037E-10 | 9.492E-04 | -11.811 | -12.585 | 0.139 | 0.045 | 3.255 | 4.417 | 3.600 | 8.11 |
| **E2** | NaCl-EQ | 0.1 | -8.049E-09 | 0.079 | 0.943 | 12.001 | 6.670E-10 | 9.543E-04 | -10.859 | -11.468 | 0.135 | 0.100 | 3.112 | 4.300 | 3.605 | 8.45 |
| **E2** | NaCl-EQ | 0.5 | -1.421E-09 | 0.261 | 3.158 | 12.117 | 6.670E-10 | 9.799E-04 | -6.594 | -6.897 | 0.135 | 0.403 | 3.147 | 4.231 | 3.611 | 8.49 |
| **E2** | NaCl-EQ | 1 | -3.916E-10 | 0.416 | 5.493 | 13.197 | 6.340E-10 | 1.007E-03 | -3.416 | -3.281 | 0.120 | 0.858 | 3.034 | 4.169 | 3.502 | 8.37 |
| **E2** | NaCl-EQ | 2 | -7.252E-11 | 0.953 | 11.345 | 11.909 | 5.474E-10 | 1.101E-03 | -1.654 | -1.761 | 0.145 | 1.674 | 3.008 | 4.342 | 3.649 | 8.19 |
| **E2** | NaCl-EQ | 3.5 | 1.740E-11 | 1.256 | 16.905 | 13.457 | 4.541E-10 | 1.227E-03 | 0.795 | 0.749 | 0.126 | 3.058 | 2.966 | 4.264 | 3.718 | 8.15 |
| **E1** | NaCl-EQ | 0.05 | -1.983E-08 | 0.040 | 0.445 | 11.060 | 7.034E-10 | 9.496E-04 | -11.900 | -13.638 | 0.109 | 0.044 | 3.265 | 4.292 | 3.752 | 8.39 |
| **E1** | NaCl-EQ | 0.5 | -1.247E-09 | 0.284 | 3.469 | 12.216 | 6.624E-10 | 9.836E-04 | -6.424 | -6.666 | 0.116 | 0.431 | 3.067 | 4.296 | 3.765 | 8.35 |
| **E1** | NaCl-EQ | 1 | -3.046E-10 | 0.557 | 6.685 | 12.011 | 6.179E-10 | 1.021E-03 | -3.365 | -3.551 | 0.113 | 0.922 | 3.191 | 4.344 | 3.671 | 8.44 |
| **E1** | NaCl-EQ | 2 | -2.175E-11 | 0.979 | 12.020 | 12.273 | 5.390E-10 | 1.113E-03 | -0.540 | -0.557 | 0.142 | 1.770 | 3.223 | 4.441 | 3.689 | 8.41 |
| **E1** | NaCl-EQ | 3.5 | 4.351E-11 | 1.205 | 16.000 | 13.280 | 4.667E-10 | 1.241E-03 | 1.851 | 1.767 | 0.138 | 3.416 | 3.104 | 4.331 | 3.734 | 8.27 |
| **E3** | NaCl-EQ | 0.05 | -1.675E-08 | 0.044 | 0.453 | 10.238 | 7.034E-10 | 9.496E-04 | -10.237 | -12.672 | 0.122 | 0.051 | 3.063 | 4.315 | 3.757 | 8.17 |
| **E3** | NaCl-EQ | 0.5 | -9.442E-10 | 0.343 | 3.652 | 10.644 | 6.598E-10 | 9.857E-04 | -5.151 | -6.134 | 0.125 | 0.515 | 2.995 | 4.255 | 3.769 | 8.41 |
| **E3** | NaCl-EQ | 1 | -1.595E-10 | 0.623 | 6.744 | 10.819 | 6.171E-10 | 1.022E-03 | -1.782 | -2.087 | 0.117 | 1.095 | 2.949 | 4.240 | 3.671 | 8.42 |
| **E3** | NaCl-EQ | 2 | 2.756E-11 | 0.997 | 12.060 | 12.100 | 5.364E-10 | 1.116E-03 | 0.692 | 0.724 | 0.117 | 1.985 | 3.011 | 4.207 | 3.693 | 8.34 |
| **E3** | NaCl-EQ | 3.5 | 5.801E-11 | 1.470 | 16.900 | 11.496 | 4.543E-10 | 1.268E-03 | 2.737 | 3.018 | 0.123 | 3.496 | 2.947 | 4.222 | 3.802 | 8.10 |

**Table E-2: Compilation of SPM results from Ca experiments**

| Plug # | Exp | NaCl, M | $C_{sp}$, V/Pa | $\sigma_{rf}$, S/m | $\sigma_f$, S/m | $F_a$ | $\varepsilon$, F/m | $\mu$, Pa.s | ζ, mV | $\zeta_{corrected}$, mV | k, D | IS, M | pCa | pMg | pSO4 | pH |
|---|---|---|---|---|---|---|---|---|---|---|---|---|---|---|---|---|
| K1 | NaCl-EQ | 0.5 | -1.378E-09 | 0.253 | 3.307 | 13.073 | 6.604E-10 | 9.852E-04 | -8.430 | -9.252 | 1.390 | 0.862 | 2.700 | 4.277 | 2.867 | 8.15 |
| K1 | 0.5CaSW | 0.5 | -1.059E-09 | 0.260 | 3.841 | 14.796 | 6.571E-10 | 9.879E-04 | -6.114 | -5.929 | 1.406 | 0.886 | 1.978 | 3.564 | 2.669 | 7.52 |
| K1 | CaSW | 0.5 | -9.369E-10 | 0.272 | 3.926 | 14.437 | 6.558E-10 | 9.889E-04 | -5.546 | -5.512 | 1.404 | 0.873 | 1.808 | 3.641 | 2.730 | 7.28 |
| K1 | 2xCaSW | 0.5 | -7.832E-10 | 0.282 | 4.074 | 14.428 | 6.537E-10 | 9.906E-04 | -4.835 | -4.808 | 1.367 | 0.895 | 1.555 | 3.626 | 2.732 | 7.06 |
| K1 | 4xCaSW | 0.5 | -5.801E-10 | 0.288 | 4.379 | 15.227 | 6.494E-10 | 9.941E-04 | -3.889 | -3.665 | 1.377 | 0.957 | 1.255 | 3.615 | 2.711 | 6.90 |
| K1 | 10xCaSW | 0.5 | -2.393E-10 | 0.357 | 5.321 | 14.911 | 6.363E-10 | 1.005E-03 | -2.011 | -1.935 | 1.394 | 1.221 | 0.887 | 3.613 | 2.747 | 6.58 |
| K1 | 15xCaSW | 0.5 | -1.073E-10 | 0.396 | 6.059 | 15.294 | 6.263E-10 | 1.014E-03 | -1.052 | -0.987 | 1.367 | 1.293 | 0.693 | 3.622 | 2.751 | 6.40 |
| K1 | 20xCaSW | 0.5 | -3.191E-11 | 0.451 | 6.749 | 14.967 | 6.170E-10 | 1.022E-03 | -0.357 | -0.342 | 1.354 | 1.468 | 0.557 | 3.608 | 2.757 | 6.36 |
| K1 | 30xCaSW | 0.5 | 6.091E-11 | 0.561 | 8.172 | 14.558 | 5.974E-10 | 1.041E-03 | 0.867 | 0.855 | 1.334 | 1.791 | 0.378 | 4.116 | 2.735 | 6.12 |
| K1 | FMBCaMgS | 0.5 | 7.397E-11 | 0.607 | 8.720 | 14.373 | 5.896E-10 | 1.049E-03 | 1.148 | 1.146 | 1.317 | 1.923 | 0.397 | 1.091 | 2.721 | 6.12 |
| K1 | NaCl-EQ | 2 | -2.030E-10 | 0.800 | 11.480 | 14.348 | 5.462E-10 | 1.102E-03 | -4.704 | -4.704 | 1.487 | 1.985 | 2.634 | 3.746 | 2.666 | 8.14 |
| K1 | 0.5CaSW | 2 | -1.740E-10 | 0.810 | 12.030 | 14.857 | 5.369E-10 | 1.115E-03 | -4.350 | -4.201 | 1.506 | 2.009 | 2.107 | 3.717 | 2.678 | 7.41 |
| K1 | CaSW | 2 | -1.595E-10 | 0.815 | 12.110 | 14.864 | 5.356E-10 | 1.117E-03 | -4.031 | -3.891 | 1.493 | 2.075 | 1.895 | 3.793 | 2.838 | 7.26 |
| K1 | 2xCaSW | 2 | -1.450E-10 | 0.849 | 12.290 | 14.475 | 5.325E-10 | 1.122E-03 | -3.756 | -3.723 | 1.474 | 2.444 | 1.602 | 3.792 | 2.814 | 7.02 |
| K1 | 4xCaSW | 2 | -1.160E-10 | 0.859 | 12.450 | 14.497 | 5.297E-10 | 1.126E-03 | -3.071 | -3.039 | 1.472 | 2.455 | 1.316 | 3.820 | 2.827 | 6.85 |
| K1 | 10xCaSW | 2 | -5.801E-11 | 0.863 | 12.750 | 14.774 | 5.246E-10 | 1.134E-03 | -1.599 | -1.553 | 1.419 | 2.413 | 0.859 | 3.733 | 2.681 | 6.57 |
| K1 | 20xCaSW | 2 | -4.351E-12 | 0.882 | 13.920 | 15.788 | 5.044E-10 | 1.168E-03 | -0.140 | -0.127 | 1.435 | 2.753 | 0.556 | 3.825 | 2.810 | 6.26 |
| K1 | 30xCaSW | 2 | 3.452E-11 | 0.961 | 14.710 | 15.304 | 4.909E-10 | 1.192E-03 | 1.233 | 1.156 | 1.384 | 3.200 | 0.353 | 3.864 | 2.811 | 6.20 |
| E3 | NaCl-EQ | 0.5 | -9.442E-10 | 0.343 | 3.652 | 10.644 | 6.598E-10 | 9.857E-04 | -5.151 | -5.636 | 0.117 | 0.473 | 3.109 | 4.240 | 3.769 | 8.38 |
| E3 | 0.5CaSW | 0.5 | -3.466E-10 | 0.333 | 3.957 | 11.889 | 6.554E-10 | 9.892E-04 | -2.070 | -2.028 | 0.114 | 0.541 | 2.200 | 4.168 | 3.696 | 7.46 |
| E3 | CaSW | 0.5 | -1.595E-10 | 0.359 | 3.970 | 11.054 | 6.552E-10 | 9.894E-04 | -0.956 | -1.008 | 0.114 | 0.556 | 1.829 | 4.119 | 3.737 | 7.49 |
| E3 | 2xCaSW | 0.5 | 5.366E-11 | 0.349 | 4.135 | 11.854 | 6.528E-10 | 9.913E-04 | 0.337 | 0.331 | 0.112 | 0.583 | 1.531 | 4.182 | 3.762 | 7.17 |
| E3 | 4xCaSW | 0.5 | 2.466E-10 | 0.397 | 4.452 | 11.207 | 6.484E-10 | 9.950E-04 | 1.684 | 1.750 | 0.113 | 0.643 | 1.241 | 4.182 | 3.808 | 6.91 |
| E3 | 10xCaSW | 0.5 | 4.453E-10 | 0.491 | 5.285 | 10.774 | 6.368E-10 | 1.005E-03 | 3.712 | 4.013 | 0.108 | 0.873 | 0.837 | 4.195 | 3.876 | 6.66 |
| E3 | 20xCaSW | 0.5 | 4.815E-10 | 0.615 | 6.763 | 11.004 | 6.168E-10 | 1.022E-03 | 5.397 | 5.711 | 0.107 | 1.199 | 0.577 | 4.085 | 3.812 | 6.41 |
| E3 | 30xCaSW | 0.5 | 4.496E-10 | 0.713 | 8.103 | 11.364 | 5.984E-10 | 1.040E-03 | 6.332 | 6.489 | 0.104 | 1.535 | 0.386 | 3.946 | 3.819 | 6.27 |
| E3 | FMBCaMgS | 0.5 | 4.206E-10 | 0.768 | 8.869 | 11.550 | 5.874E-10 | 1.052E-03 | 6.678 | 6.733 | 0.097 | 1.812 | 0.368 | 1.053 | 2.670 | 6.28 |
| E3 | NaCl-EQ | 2 | 2.756E-11 | 0.997 | 12.060 | 12.100 | 5.364E-10 | 1.116E-03 | 0.692 | 0.666 | 0.117 | 2.031 | 3.011 | 4.207 | 3.693 | 8.15 |
| E3 | 0.5CaSW | 2 | 3.771E-11 | 0.951 | 11.560 | 12.156 | 5.449E-10 | 1.104E-03 | 0.883 | 0.846 | 0.116 | 1.938 | 2.200 | 4.225 | 3.593 | 7.67 |
| E3 | CaSW | 2 | 5.221E-11 | 0.973 | 11.750 | 12.076 | 5.417E-10 | 1.109E-03 | 1.256 | 1.211 | 0.117 | 2.066 | 1.923 | 4.231 | 3.586 | 7.47 |
| E3 | 2xCaSW | 2 | 7.107E-11 | 1.012 | 11.970 | 11.830 | 5.379E-10 | 1.114E-03 | 1.762 | 1.734 | 0.115 | 2.102 | 1.623 | 4.227 | 3.533 | 7.08 |
| E3 | 4xCaSW | 2 | 1.044E-10 | 1.025 | 12.170 | 11.871 | 5.345E-10 | 1.119E-03 | 2.660 | 2.610 | 0.117 | 2.051 | 1.344 | 4.235 | 3.522 | 6.84 |
| E3 | 10xCaSW | 2 | 1.436E-10 | 1.078 | 12.710 | 11.787 | 5.253E-10 | 1.133E-03 | 3.937 | 3.889 | 0.115 | 2.322 | 0.873 | 4.222 | 3.586 | 6.61 |
| E3 | 20xCaSW | 2 | 1.698E-10 | 1.167 | 13.420 | 11.503 | 5.130E-10 | 1.153E-03 | 5.122 | 5.185 | 0.116 | 2.426 | 0.609 | 4.198 | 3.562 | 6.35 |
| E3 | 30xCaSW | 2 | 1.987E-10 | 1.219 | 14.280 | 11.719 | 4.982E-10 | 1.179E-03 | 6.711 | 6.670 | 0.114 | 3.008 | 0.387 | 4.193 | 3.524 | 6.17 |
| E3 | FMBCaMgS | 2 | 2.001E-10 | 1.281 | 14.690 | 11.471 | 4.912E-10 | 1.191E-03 | 7.131 | 7.239 | 0.113 | 3.114 | 0.385 | 1.206 | 2.633 | 6.10 |

**Table E-3: Compilation of SPM results from SO4 and Mg experiments**

| Plug # | Exp | NaCl, M | $C_{sp}$, V/Pa | $\sigma_{rf}$, S/m | $\sigma_f$, S/m | $F_a$ | $\varepsilon$, F/m | $\mu$, Pa.s | $\zeta$, mV | $\zeta_{corrected}$, mV | k, D | IS, M | pCa | pMg | pSO4 | pH |
|---|---|---|---|---|---|---|---|---|---|---|---|---|---|---|---|---|
| SO4-SPM experiments | | | | | | | | | | | | | | | | |
| E3 | NaCl-EQ | 0.5 | -8.735E-10 | 0.309 | 3.582 | 11.603 | 6.608E-10 | 9.849E-04 | -4.664 | -4.681 | 0.103 | 0.500 | 2.589 | 4.156 | 3.623 | 7.83 |
| E3 | SO4FMB | 0.5 | -9.398E-10 | 0.337 | 3.893 | 11.568 | 6.563E-10 | 9.885E-04 | -5.511 | -5.548 | 0.109 | 0.500 | 2.852 | 3.899 | 2.708 | 8.16 |
| E3 | 4xSO4FMB | 0.5 | -9.500E-10 | 0.357 | 3.945 | 11.055 | 6.556E-10 | 9.891E-04 | -5.654 | -5.956 | 0.113 | 0.500 | 2.938 | 4.080 | 2.121 | 8.29 |
| E3 | SO4FMB | 0.5 | -1.009E-09 | 0.348 | 4.083 | 11.738 | 6.536E-10 | 9.907E-04 | -6.247 | -6.198 | 0.115 | 0.500 | 2.938 | 4.098 | 1.637 | 8.32 |
| E3 | 2xSO4SW | 0.5 | -9.746E-10 | 0.364 | 4.258 | 11.714 | 6.511E-10 | 9.927E-04 | -6.327 | -6.290 | 0.112 | 0.501 | 2.924 | 4.097 | 1.326 | 8.29 |
| E3 | 4xSO4SW | 0.5 | -9.616E-10 | 0.416 | 4.623 | 11.124 | 6.460E-10 | 9.969E-04 | -6.861 | -7.182 | 0.106 | 0.504 | 2.957 | 4.190 | 1.063 | 8.33 |
| E3 | NaCl-EQ | 2 | 2.175E-11 | 0.948 | 11.480 | 12.111 | 5.467E-10 | 1.102E-03 | 0.503 | 0.484 | 0.093 | 2.000 | 2.751 | 4.468 | 3.693 | 7.96 |
| E3 | 1/2SO4FMB | 2 | 1.740E-11 | 1.013 | 11.920 | 11.768 | 5.396E-10 | 1.112E-03 | 0.427 | 0.423 | 0.097 | 2.000 | 3.053 | 4.599 | 2.852 | 8.33 |
| E3 | 4xSO4FMB | 2 | 1.305E-11 | 1.007 | 12.300 | 12.219 | 5.369E-10 | 1.115E-03 | 0.334 | 0.318 | 0.106 | 2.000 | 3.083 | 4.583 | 2.050 | 8.25 |
| E3 | SO4SW | 2 | 5.801E-12 | 0.923 | 12.080 | 13.086 | 5.369E-10 | 1.115E-03 | 0.146 | 0.130 | 0.100 | 2.000 | 3.083 | 4.456 | 1.595 | 7.86 |
| E3 | 2xSO4SW | 2 | -7.252E-12 | 1.001 | 12.080 | 12.063 | 5.369E-10 | 1.115E-03 | -0.182 | -0.176 | 0.100 | 2.001 | 3.083 | 4.580 | 1.285 | 8.34 |
| E3 | 4xSO4SW | 2 | -2.466E-11 | 0.836 | 12.320 | 14.740 | 5.369E-10 | 1.115E-03 | -0.631 | -0.499 | 0.100 | 2.005 | 3.092 | 4.575 | 1.019 | 8.34 |
| Mg-SPM experiments | | | | | | | | | | | | | | | | |
| E3 | NaCl-EQ | 0.5 | -8.735E-10 | 0.309 | 3.582 | 11.603 | 6.608E-10 | 9.849E-04 | -4.664 | -4.681 | 0.103 | 0.500 | 2.995 | 4.255 | 3.804 | 8.38 |
| E3 | 0.5MgSW | 0.5 | -1.073E-10 | 0.359 | 3.918 | 10.909 | 6.559E-10 | 9.888E-04 | -0.634 | -0.677 | 0.064 | 0.500 | 2.941 | 1.705 | 3.792 | 8.16 |
| E3 | MgSW | 0.5 | 3.481E-11 | 0.361 | 4.196 | 11.617 | 6.520E-10 | 9.920E-04 | 0.222 | 0.223 | 0.068 | 0.501 | 2.910 | 1.387 | 3.796 | 8.06 |
| E3 | 2xMgSW | 0.5 | 2.088E-10 | 0.397 | 4.631 | 11.658 | 6.459E-10 | 9.970E-04 | 1.493 | 1.491 | 0.074 | 0.504 | 2.926 | 1.037 | 3.737 | 7.74 |
| E3 | 4xMgSW | 0.5 | 3.278E-10 | 0.491 | 5.374 | 10.955 | 6.356E-10 | 1.006E-03 | 2.787 | 3.360 | 0.076 | 0.514 | 2.845 | 0.784 | 3.762 | 7.40 |
| E3 | 6xMgSW | 0.5 | 3.278E-10 | 0.615 | 6.337 | 10.311 | 6.199E-10 | 1.019E-03 | 3.416 | 4.360 | 0.071 | 0.531 | 2.845 | 0.602 | 3.808 | 7.32 |
| E3 | NaCl-EQ | 2 | 2.901E-11 | 0.948 | 11.850 | 12.502 | 5.467E-10 | 1.102E-03 | 0.693 | 0.645 | 0.096 | 2.000 | 2.936 | 4.207 | 3.693 | 8.30 |
| E3 | 0.5MgSW | 2 | 6.817E-11 | 1.012 | 12.200 | 12.057 | 5.417E-10 | 1.109E-03 | 1.702 | 2.000 | 0.097 | 2.000 | 2.883 | 1.648 | 3.593 | 8.29 |
| E3 | MgSW | 2 | 9.572E-11 | 1.025 | 12.040 | 11.745 | 5.345E-10 | 1.119E-03 | 2.413 | 2.392 | 0.101 | 2.001 | 2.960 | 1.347 | 3.586 | 8.17 |
| E3 | 2xMgSW | 2 | 1.305E-10 | 1.025 | 12.540 | 12.232 | 5.345E-10 | 1.119E-03 | 3.427 | 3.262 | 0.100 | 2.004 | 2.950 | 1.046 | 3.533 | 7.95 |
| E3 | 4xMgSW | 2 | 1.668E-10 | 1.078 | 12.940 | 12.001 | 5.213E-10 | 1.139E-03 | 4.717 | 4.577 | 0.100 | 2.016 | 2.904 | 0.745 | 3.522 | 7.75 |
| E3 | 6xMgSW | 2 | 1.856E-10 | 1.167 | 13.270 | 11.374 | 5.156E-10 | 1.149E-03 | 5.487 | 5.618 | 0.097 | 2.036 | 2.863 | 0.569 | 3.572 | 7.61 |
| E3 | 8xMgSW | 2 | 2.059E-10 | 1.167 | 13.530 | 11.597 | 5.111E-10 | 1.156E-03 | 6.302 | 6.328 | 0.094 | 2.065 | 2.825 | 0.444 | 3.562 | 7.42 |

**Table E-4: Compilation of SPM results from SW and modified SW composition experiments**

| Plug # | Exp | NaCl, M | $C_{sp}$, V/Pa | $\sigma_{rf}$, S/m | $\sigma_f$, S/m | $F_a$ | $\varepsilon$, F/m | $\mu$, Pa.s | ζ, mV | $\zeta_{corrected}$, mV | k, D | IS, M | pCa | pMg | $pSO_4$ | pH |
|---|---|---|---|---|---|---|---|---|---|---|---|---|---|---|---|---|
| K1 | NaCl-EQ | 0.5 | -1.278E-09 | 0.261 | 3.758 | 14.423 | 6.582E-10 | 9.869E-04 | -7.199 | -7.162 | 1.056 | 0.500 | 2.700 | 4.277 | 2.867 | 8.30 |
| K1 | SW | 0.5 | -6.759E-10 | 0.337 | 4.533 | 13.468 | 6.472E-10 | 9.959E-04 | -4.714 | -5.022 | 1.143 | 0.750 | 1.854 | 1.347 | 1.620 | 7.40 |
| K1 | 2dSW | 0.5 | -1.592E-09 | 0.177 | 2.529 | 14.286 | 6.761E-10 | 9.726E-04 | -5.794 | -5.819 | 1.159 | 0.375 | 2.155 | 1.648 | 1.921 | 7.90 |
| K1 | 10dSW | 0.5 | -9.829E-09 | 0.048 | 0.622 | 13.056 | 7.015E-10 | 9.512E-04 | -8.295 | -9.117 | 1.121 | 0.075 | 2.854 | 2.347 | 2.620 | 8.20 |
| K1 | 20dSW | 0.5 | -2.181E-08 | 0.026 | 0.320 | 12.485 | 7.046E-10 | 9.485E-04 | -9.389 | -10.790 | 1.117 | 0.038 | 3.155 | 2.648 | 2.921 | 8.20 |
| K1 | SW2S | 0.5 | -7.324E-10 | 0.360 | 4.723 | 13.126 | 6.446E-10 | 9.981E-04 | -5.356 | -5.855 | 1.139 | 0.822 | 1.854 | 1.347 | 1.319 | 7.50 |
| K1 | SW3S | 0.5 | -7.353E-10 | 0.360 | 4.802 | 13.345 | 6.435E-10 | 9.990E-04 | -5.482 | -5.894 | 1.052 | 0.894 | 1.854 | 1.347 | 1.143 | 7.50 |
| K1 | SW4S | 0.5 | -7.542E-10 | 0.360 | 4.985 | 13.854 | 6.409E-10 | 1.001E-03 | -5.872 | -6.082 | 1.071 | 0.966 | 1.854 | 1.347 | 1.018 | 7.50 |
| E1 | NaCl-EQ | 0.5 | -8.397E-10 | 0.278 | 3.786 | 13.612 | 6.591E-10 | 9.862E-04 | -4.757 | -4.704 | 0.118 | 0.473 | 3.109 | 4.240 | 3.769 | 8.38 |
| E1 | SW | 0.5 | -2.088E-10 | 0.343 | 4.515 | 13.164 | 6.475E-10 | 9.957E-04 | -1.450 | -1.483 | 0.123 | 0.750 | 1.854 | 1.347 | 1.620 | 7.40 |
| E1 | 2dSW | 0.5 | -6.976E-10 | 0.213 | 2.588 | 12.156 | 6.752E-10 | 9.733E-04 | -2.602 | -2.881 | 0.124 | 0.375 | 2.155 | 1.648 | 1.921 | 7.90 |
| E1 | 10dSW | 0.5 | -6.387E-09 | 0.053 | 0.685 | 12.930 | 7.008E-10 | 9.518E-04 | -5.939 | -6.182 | 0.121 | 0.075 | 2.854 | 2.347 | 2.620 | 8.20 |
| E1 | 20dSW | 0.5 | -1.556E-08 | 0.029 | 0.379 | 12.889 | 7.048E-10 | 9.483E-04 | -7.939 | -8.291 | 0.121 | 0.038 | 3.155 | 2.648 | 2.921 | 8.20 |
| E1 | SW2S | 0.5 | -4.119E-10 | 0.393 | 4.727 | 12.037 | 6.445E-10 | 9.981E-04 | -3.015 | -3.372 | 0.118 | 0.822 | 1.854 | 1.347 | 1.319 | 7.50 |
| E1 | SW3S | 0.5 | -4.728E-10 | 0.393 | 4.942 | 12.585 | 6.415E-10 | 1.001E-03 | -3.644 | -3.898 | 0.117 | 0.894 | 1.854 | 1.347 | 1.143 | 7.50 |
| E1 | SW4S | 0.5 | -5.120E-10 | 0.393 | 5.104 | 12.997 | 6.393E-10 | 1.002E-03 | -4.098 | -4.244 | 0.117 | 0.966 | 1.854 | 1.347 | 1.018 | 7.50 |

**Table E-5: Compilation of SPM results from NaCl-EQ experiments at elevated temperatures**

| Plug # | Exp | NaCl, M | Temp, C | $C_{sp}$, V/Pa | $\sigma_{rf}$, S/m | $\sigma_f$, S/m | $F_a$ | $F_0$ | $\varepsilon$, F/m | $\mu$, Pa.s | $\zeta$, mV | $\zeta_{corrected}$, mV | pCa | pMg | $pSO_4$ | pH |
|---|---|---|---|---|---|---|---|---|---|---|---|---|---|---|---|---|
| K1 | NaCl-EQ | 0.01 | 22 | -6.274E-08 | 0.010 | 0.136 | 13.120 | 13.870 | 7.063E-10 | 9.469E-04 | -11.456 | -12.111 | 2.666 | 4.024 | 2.782 | 8.05 |
| K1 | NaCl-EQ | 0.01 | 39 | -4.922E-08 | 0.013 | 0.165 | 12.489 | 13.870 | 6.493E-10 | 6.535E-04 | -8.190 | -9.096 | 2.482 | 4.026 | 2.788 | 7.93 |
| K1 | NaCl-EQ | 0.01 | 57 | -4.161E-08 | 0.017 | 0.214 | 12.504 | 13.870 | 5.970E-10 | 4.675E-04 | -6.970 | -7.731 | 2.457 | 4.059 | 2.795 | 7.81 |
| K1 | NaCl-EQ | 0.01 | 81 | -3.175E-08 | 0.022 | 0.283 | 12.891 | 13.870 | 5.591E-10 | 3.693E-04 | -5.934 | -6.384 | 2.444 | 4.043 | 2.831 | 7.80 |
| K1 | NaCl-EQ | 0.01 | 120 | -3.066E-08 | 0.032 | 0.369 | 11.511 | 13.870 | 4.903E-10 | 2.259E-04 | -5.210 | -6.277 | N/A | N/A | N/A | N/A |
| K1 | NaCl-EQ | 0.5 | 22 | -1.327E-09 | 0.252 | 3.615 | 14.333 | 13.870 | 6.599E-10 | 9.948E-04 | -7.233 | -6.999 | 2.906 | 4.196 | 2.967 | 7.99 |
| K1 | NaCl-EQ | 0.5 | 40 | -1.402E-09 | 0.331 | 4.735 | 14.318 | 13.870 | 6.485E-10 | 6.849E-04 | -7.014 | -6.794 | 2.905 | 4.196 | 2.959 | 7.95 |
| K1 | NaCl-EQ | 0.5 | 60 | -1.523E-09 | 0.409 | 6.055 | 14.808 | 13.870 | 5.962E-10 | 4.927E-04 | -7.620 | -7.137 | 2.909 | 4.193 | 2.964 | 7.87 |
| K1 | NaCl-EQ | 0.5 | 80 | -1.427E-09 | 0.497 | 7.216 | 14.521 | 13.870 | 5.524E-10 | 3.765E-04 | -7.018 | -6.703 | 2.914 | 4.210 | 2.975 | 7.85 |
| K1 | NaCl-EQ | 0.5 | 120 | -1.443E-09 | 0.639 | 9.837 | 16.981 | 13.870 | 4.926E-10 | 2.476E-04 | -7.135 | -6.431 | N/A | N/A | N/A | N/A |
| E2 | NaCl-EQ | 0.01 | 22 | -8.141E-08 | 0.008 | 0.125 | 14.947 | 12.920 | 7.031E-10 | 9.554E-04 | -13.839 | -11.962 | 3.132 | 4.045 | 3.550 | 8.02 |
| E2 | NaCl-EQ | 0.01 | 40 | -7.574E-08 | 0.011 | 0.167 | 14.929 | 12.920 | 6.521E-10 | 6.660E-04 | -12.886 | -11.152 | 3.083 | 4.044 | 3.556 | 7.95 |
| E2 | NaCl-EQ | 0.01 | 57 | -6.696E-08 | 0.016 | 0.215 | 13.369 | 12.920 | 6.043E-10 | 4.894E-04 | -11.670 | -11.278 | 3.033 | 4.042 | 3.590 | 7.86 |
| E2 | NaCl-EQ | 0.01 | 79 | -5.778E-08 | 0.022 | 0.292 | 13.431 | 12.920 | 5.571E-10 | 3.646E-04 | -11.023 | -10.604 | 3.001 | 4.087 | 3.565 | 7.82 |
| E2 | NaCl-EQ | 0.01 | 120 | -4.348E-08 | 0.032 | 0.391 | 12.213 | 12.920 | 4.903E-10 | 2.259E-04 | -7.839 | -8.293 | N/A | N/A | N/A | N/A |
| E2 | NaCl-EQ | 0.5 | 22 | -8.658E-10 | 0.276 | 3.647 | 13.227 | 12.920 | 6.599E-10 | 9.948E-04 | -4.761 | -4.650 | 3.146 | 4.311 | 3.700 | 8.00 |
| E2 | NaCl-EQ | 0.5 | 40 | -1.066E-09 | 0.331 | 4.642 | 14.009 | 12.920 | 6.429E-10 | 6.849E-04 | -5.272 | -4.862 | 3.166 | 4.315 | 3.708 | 8.03 |
| E2 | NaCl-EQ | 0.5 | 60 | -1.104E-09 | 0.409 | 6.063 | 14.827 | 12.920 | 5.962E-10 | 4.927E-04 | -5.530 | -4.819 | 3.182 | 4.312 | 3.703 | 7.97 |
| E2 | NaCl-EQ | 0.5 | 80 | -1.020E-09 | 0.497 | 7.080 | 14.233 | 12.920 | 5.524E-10 | 3.765E-04 | -4.919 | -4.465 | 3.176 | 4.298 | 3.700 | 7.82 |
| E2 | NaCl-EQ | 0.5 | 120 | -1.024E-09 | 0.549 | 9.537 | 17.387 | 12.920 | 4.926E-10 | 2.476E-04 | -4.908 | -3.647 | N/A | N/A | N/A | N/A |
| P1 | NaCl-EQ | 0.01 | 22 | -6.061E-08 | 0.009 | 0.167 | 18.288 | 22.040 | 7.061E-10 | 9.472E-04 | -13.537 | -16.315 | 3.508 | 4.417 | 3.745 | 8.11 |
| P1 | NaCl-EQ | 0.01 | 40 | -5.640E-08 | 0.014 | 0.262 | 18.624 | 22.040 | 6.549E-10 | 5.967E-04 | -13.475 | -15.946 | 3.443 | 4.408 | 3.749 | 7.97 |
| P1 | NaCl-EQ | 0.01 | 57 | -5.284E-08 | 0.017 | 0.309 | 18.187 | 22.040 | 5.898E-10 | 4.472E-04 | -12.373 | -14.994 | 3.357 | 4.430 | 3.740 | 7.88 |
| P1 | NaCl-EQ | 0.01 | 79 | -5.259E-08 | 0.018 | 0.349 | 18.881 | 22.040 | 5.591E-10 | 3.693E-04 | -12.118 | -14.146 | 3.342 | 4.445 | 3.744 | 7.89 |
| P1 | NaCl-EQ | 0.01 | 120 | -4.999E-08 | 0.024 | 0.432 | 18.186 | 22.040 | 4.903E-10 | 2.259E-04 | -9.949 | -12.057 | N/A | N/A | N/A | N/A |
| P2 | NaCl-EQ | 0.5 | 22 | -1.726E-09 | 0.161 | 3.546 | 22.037 | 22.040 | 6.599E-10 | 9.948E-04 | -9.227 | -9.228 | 3.498 | 4.431 | 3.622 | 8.08 |
| P2 | NaCl-EQ | 0.5 | 40 | -1.639E-09 | 0.256 | 5.050 | 19.713 | 22.040 | 6.485E-10 | 6.849E-04 | -8.741 | -9.773 | 3.507 | 4.473 | 3.659 | 7.90 |
| P2 | NaCl-EQ | 0.5 | 60 | -1.740E-09 | 0.312 | 6.180 | 19.806 | 22.040 | 5.962E-10 | 4.927E-04 | -8.888 | -9.891 | 3.500 | 4.463 | 3.590 | 7.80 |
| P2 | NaCl-EQ | 0.5 | 80 | -1.798E-09 | 0.357 | 7.525 | 21.049 | 22.040 | 5.524E-10 | 3.765E-04 | -9.222 | -9.656 | 3.511 | 4.472 | 3.597 | 7.78 |
| P2 | NaCl-EQ | 0.5 | 120 | -1.711E-09 | 0.477 | 10.125 | 21.235 | 22.040 | 4.926E-10 | 2.476E-04 | -8.709 | -9.040 | N/A | N/A | N/A | N/A |

**Table E-6: Compilation of SPM results from SW and modified SW composition experiments at 80°C**

| Plug # | Exp | IS, M | Temp, C | $C_{sp}$, V/Pa | $\sigma_{rf}$, S/m | $\sigma_f$, S/m | $F_a$ | $F_0$ | $\varepsilon$, F/m | $\mu$, Pa.s | ζ, mV | $\zeta_c$ (corrected), mV | pH |
|---|---|---|---|---|---|---|---|---|---|---|---|---|---|
| K1 | SW | 0.75 | 80 | -7.498E-10 | 0.605 | 8.233 | 13.601 | 13.870 | 5.524E-10 | 3.765E-04 | -4.207 | -4.290 | 7.15 |
| K1 | 20dSW | 0.0375 | 80 | -2.532E-08 | 0.037 | 0.575 | 15.573 | 13.870 | 5.531E-10 | 3.564E-04 | -9.375 | -8.350 | 8.11 |
| K1 | 10dSW | 0.075 | 80 | -1.011E-08 | 0.080 | 1.152 | 14.371 | 13.870 | 5.531E-10 | 3.572E-04 | -7.355 | -7.099 | 7.77 |
| K1 | 2dSW | 0.375 | 80 | -1.565E-09 | 0.327 | 4.620 | 14.128 | 13.870 | 5.528E-10 | 3.657E-04 | -4.783 | -4.695 | 7.38 |
| K1 | SWx4S | 0.966 | 80 | -1.007E-09 | 0.562 | 9.164 | 16.307 | 13.870 | 5.524E-10 | 3.765E-04 | -6.286 | -5.346 | 7.50 |
| E1 | SW | 0.75 | 80 | -4.801E-10 | 0.446 | 7.956 | 17.842 | 12.920 | 5.524E-10 | 3.765E-04 | -2.603 | -1.885 | 7.34 |
| E1 | 20dSW | 0.0375 | 80 | -1.833E-08 | 0.037 | 0.651 | 17.644 | 12.920 | 5.531E-10 | 3.564E-04 | -7.688 | -5.630 | 8.19 |
| E1 | 10dSW | 0.075 | 80 | -6.139E-09 | 0.080 | 1.324 | 16.517 | 12.920 | 5.531E-10 | 3.572E-04 | -5.250 | -4.107 | 7.84 |
| E1 | 2dSW | 0.375 | 80 | -8.223E-10 | 0.327 | 4.762 | 14.563 | 12.920 | 5.528E-10 | 3.657E-04 | -2.591 | -2.298 | 7.44 |
| E1 | SWx4S | 0.966 | 80 | -6.613E-10 | 0.613 | 9.440 | 15.404 | 12.920 | 5.524E-10 | 3.765E-04 | -4.255 | -3.568 | 7.29 |

**Table E-7: Compilation of Coreflooding and SPM results from multiphase experiments**

| Plug # | Oil phase | Initial Brine | Flooding Brine | $S_{wi}$ | 1-$S_{or}$ | $I_w$ | $C_{sp}$, V/Pa | $\sigma_{rf}$, S/m | $\sigma_f$, S/m | $F_a$ | $\varepsilon$, F/m | $\mu$, Pa.s | ζ, mV | ζcorrec, mV | k (D) | pH |
|---|---|---|---|---|---|---|---|---|---|---|---|---|---|---|---|---|
| En-d | n-decane | 2M NaCl | 2M NaCl | 0.220 | 0.370 | 0.870 | -5.366E-11 | 0.467 | 11.960 | 25.603 | 5.381E-10 | 1.114E-03 | -1.328 | -1.328 | 0.031 | 8.34 |
| En-d | n-decane | 2M NaCl | 0.5M NaCl | 0.220 | 0.370 | 0.870 | -1.027E-09 | 0.182 | 3.625 | 19.891 | 6.602E-10 | 9.854E-04 | -5.556 | -7.152 | 0.043 | 8.45 |
| En-d | n-decane | 2M NaCl | 0.5Mx20d | 0.220 | 0.370 | 0.870 | -3.849E-08 | 0.009 | 0.240 | 25.429 | 7.065E-10 | 9.468E-04 | -12.356 | -12.441 | 0.042 | 7.60 |
| En-d | n-decane | 2M NaCl | 20dSW | 0.220 | 0.370 | 0.870 | -1.752E-08 | 0.015 | 0.341 | 22.312 | 7.044E-10 | 9.486E-04 | -8.046 | -9.233 | 0.051 | 8.37 |
| En-d | n-decane | 2M NaCl | 10dSW | 0.220 | 0.370 | 0.870 | -5.307E-09 | 0.033 | 0.788 | 23.937 | 6.997E-10 | 9.528E-04 | -5.692 | -6.088 | 0.047 | 8.05 |
| En-d | n-decane | 2M NaCl | 10dSW | 0.220 | 0.370 | 0.870 | -6.730E-10 | 0.124 | 2.546 | 20.462 | 6.758E-10 | 9.728E-04 | -2.466 | -3.086 | 0.046 | 8.07 |
| En-d | n-decane | 2M NaCl | SW2S | 0.220 | 0.370 | 0.870 | -2.567E-10 | 0.230 | 4.608 | 20.013 | 6.462E-10 | 9.968E-04 | -1.825 | -2.334 | 0.046 | 7.66 |
| En-d | n-decane | 2M NaCl | SW3S | 0.220 | 0.370 | 0.870 | -3.655E-10 | 0.230 | 4.843 | 21.034 | 6.429E-10 | 9.995E-04 | -2.752 | -3.349 | 0.047 | 7.57 |
| En-d | n-decane | 2M NaCl | SW4S | 0.220 | 0.370 | 0.870 | -4.249E-10 | 0.230 | 4.944 | 21.474 | 6.415E-10 | 1.001E-03 | -3.277 | -3.907 | 0.048 | 7.53 |
| En-d | n-decane | 2M NaCl | SW | 0.220 | 0.370 | 0.870 | -1.856E-10 | 0.230 | 4.411 | 19.138 | 6.489E-10 | 9.945E-04 | -1.255 | -1.679 | 0.044 | 7.71 |
| En-d | n-decane | 2M NaCl | FMB | 0.220 | 0.370 | 0.870 | 1.943E-10 | 0.670 | 14.190 | 21.170 | 4.982E-10 | 1.179E-03 | 6.523 | 7.889 | 0.034 | 6.40 |
| Ec1 | oil B non aged | FMB | FMB | 0.570 | 0.800 | 0.640 | 2.292E-10 | 0.795 | 13.900 | 17.484 | 4.982E-10 | 1.179E-03 | 7.536 | 7.536 | 0.040 | 6.74 |
| Ec2 | oil B aged | FMB | FMB | 0.670 | 0.860 | 0.190 | 2.550E-10 | 0.505 | 14.400 | 28.540 | 4.962E-10 | 1.182E-03 | 8.748 | 8.748 | 0.012 | 6.51 |
| Ec3 | oil B aged | FMB | FMB | 0.710 | 0.920 | 0.140 | 2.660E-10 | 0.490 | 14.400 | 29.397 | 4.962E-10 | 1.182E-03 | 9.126 | 9.126 | 0.010 | 6.51 |
| Ec4 | oil B aged | FMB | FMB | 0.350 | 0.860 | 0.090 | 2.861E-10 | 0.183 | 14.440 | 79.067 | 4.962E-10 | 1.182E-03 | 9.611 | 9.611 | 0.022 | 6.51 |
| Ec5 | oil B aged | FMB | FMB | 0.000 | 0.500 | 0.030 | 3.128E-10 | 0.196 | 14.390 | 73.322 | 4.962E-10 | 1.182E-03 | 10.726 | 10.726 | 0.075 | 6.51 |
| Ec1 | oil B non aged | FMB | SW | 0.570 | 0.800 | 0.640 | -2.087E-10 | 0.146 | 4.580 | 31.329 | 6.522E-10 | 9.918E-04 | -1.454 | -1.454 | 0.025 | 7.84 |
| Ec2 | oil B aged | FMB | SW | 0.670 | 0.860 | 0.190 | 1.097E-10 | 0.215 | 4.437 | 20.682 | 6.489E-10 | 9.945E-04 | 0.746 | 0.746 | 0.032 | 7.40 |
| Ec3 | oil B aged | FMB | SW | 0.710 | 0.920 | 0.140 | 1.905E-10 | 0.097 | 4.533 | 46.930 | 6.472E-10 | 9.959E-04 | 1.329 | 1.329 | 0.038 | 7.50 |
| Ec4 | oil B aged | FMB | SW | 0.350 | 0.860 | 0.090 | 3.495E-10 | 0.097 | 4.533 | 46.930 | 6.472E-10 | 9.959E-04 | 2.438 | 2.438 | 0.038 | 7.60 |
| Ec5 | oil B aged | FMB | SW | 0.000 | 0.500 | 0.030 | 5.018E-10 | 0.055 | 4.636 | 84.493 | 6.522E-10 | 9.918E-04 | 3.538 | 3.538 | 0.061 | 7.84 |
| Ec1 | oil B non aged | FMB | 20dSW | 0.570 | 0.800 | 0.640 | -1.616E-08 | 0.013 | 0.363 | 28.975 | 7.042E-10 | 9.488E-04 | -7.910 | -7.910 | 0.025 | 7.65 |
| Ec2 | oil B aged | FMB | 20dSW | 0.670 | 0.860 | 0.190 | -9.578E-09 | 0.019 | 0.407 | 21.039 | 7.037E-10 | 9.492E-04 | -5.259 | -5.259 | 0.032 | 8.20 |
| Ec3 | oil B aged | FMB | 20dSW | 0.710 | 0.920 | 0.140 | -6.700E-09 | 0.010 | 0.428 | 43.034 | 7.035E-10 | 9.494E-04 | -3.873 | -3.873 | 0.052 | 8.31 |
| Ec4 | oil B aged | FMB | 20dSW | 0.350 | 0.860 | 0.090 | -4.637E-09 | 0.010 | 0.428 | 43.034 | 7.035E-10 | 9.494E-04 | -2.680 | -2.680 | 0.052 | 8.31 |
| Ec5 | oil B aged | FMB | 20dSW | 0 | 0.500 | 0.030 | -2.948E-09 | 0.006 | 0.471 | 76.014 | 7.037E-10 | 9.492E-04 | -1.871 | -1.871 | 0.059 | 8.20 |
| Ec6 | oil C aged | FMB | FMB | 0 | 0.471 | 0.032 | 2.565E-11 | 0.043 | 14.510 | 335.480 | 4.957E-10 | 1.183E-03 | 0.888 | 0.888 | 0.030 | 6.49 |
| Ec6 | oil C aged | FMB | SW | 0 | 0.503 | 0.030 | -8.064E-10 | 0.020 | 4.267 | 212.382 | 6.489E-10 | 9.945E-04 | -5.273 | -5.273 | 0.034 | 7.41 |
| Ec6 | oil C aged | FMB | 20dSW | 0 | 0.524 | 0.028 | -3.013E-08 | 0.004 | 0.328 | 86.326 | 7.045E-10 | 9.485E-04 | -13.286 | -13.286 | 0.048 | 8.31 |
| Ec7 | oil D aged | FMB | FMB | 0 | 0.492 | 0.053 | 7.020E-11 | 0.064 | 14.590 | 227.723 | 4.929E-10 | 1.188E-03 | 2.469 | 2.469 | 0.019 | 6.51 |
| Ec7 | oil D aged | FMB | SW | 0 | 0.539 | 0.048 | -7.246E-10 | 0.028 | 4.222 | 150.473 | 6.516E-10 | 9.923E-04 | -4.659 | -4.659 | 0.019 | 7.29 |
| Ec7 | oil D aged | FMB | 20dSW | 0 | 0.563 | 0.046 | -2.817E-08 | 0.002 | 0.339 | 142.851 | 7.045E-10 | 9.485E-04 | -12.850 | -12.850 | 0.017 | 8.31 |
| Ec8 | oil E aged | FMB | FMB | 0 | 0.518 | 0.042 | 5.236E-11 | 0.072 | 14.310 | 199.397 | 4.977E-10 | 1.179E-03 | 1.775 | 1.775 | 0.049 | 6.51 |

**Table E-7 (continued)**

| Plug # | Oil phase | Initial Brine | Flooding Brine | $S_{wi}$ | 1-$S_{or}$ | $I_w$ | $C_{sp}$, V/Pa | $\sigma_{rf}$, S/m | $\sigma_f$, S/m | $F_a$ | $\varepsilon$, F/m | $\mu$, Pa.s | ζ, mV | ζcorrect, mV | k (D) | pH |
|---|---|---|---|---|---|---|---|---|---|---|---|---|---|---|---|---|
| Ec8 | oil E aged | FMB | SW | 0 | 0.542 | 0.040 | -1.086E-09 | 0.035 | 4.321 | 123.018 | 6.502E-10 | 9.934E-04 | -7.171 | -7.171 | 0.054 | 7.31 |
| Ec8 | oil E aged | FMB | 20dSW | 0 | 0.557 | 0.039 | -4.220E-08 | 0.003 | 0.320 | 118.776 | 7.046E-10 | 9.485E-04 | -18.170 | -18.170 | 0.041 | 8.31 |
| Ec9 | oil B aged | 20dSW | 20dSW | 0.382 | 0.947 | 0.023 | -2.070E-08 | 0.002 | 0.345 | 193.981 | 7.037E-10 | 9.492E-04 | -9.624 | -9.624 | 0.031 | 8.41 |
| Ec9 | oil B aged | 20dSW | SW | 0.382 | 0.904 | 0.025 | -2.814E-10 | 0.041 | 4.455 | 108.977 | 6.483E-10 | 9.950E-04 | -1.924 | -1.924 | 0.030 | 7.30 |
| Ec9 | oil B aged | 20dSW | FMB | 0.382 | 0.870 | 0.026 | 1.703E-10 | 0.105 | 14.150 | 134.378 | 5.005E-10 | 1.175E-03 | 5.654 | 5.654 | 0.030 | 6.51 |
| Ec10 | oil E aged | 20dSW | 20dSW | 0.418 | 0.906 | 0.092 | -1.168E-08 | 0.007 | 0.490 | 65.677 | 7.029E-10 | 9.500E-04 | -7.728 | -7.728 | 0.018 | 8.41 |
| Ec10 | oil E aged | 20dSW | SW | 0.418 | 0.906 | 0.092 | -3.727E-10 | 0.090 | 4.479 | 49.495 | 6.480E-10 | 9.953E-04 | -2.569 | -2.569 | 0.019 | 7.30 |
| Ec10 | oil E aged | 20dSW | FMB | 0.418 | 0.906 | 0.092 | 1.014E-10 | 0.283 | 14.820 | 52.296 | 4.890E-10 | 1.196E-03 | 3.666 | 3.666 | 0.016 | 6.51 |
| Ec11 | oil B aged | 2M NaCl | 2M NaCl | 0.422 | 0.887 | 0.032 | 9.867E-11 | 0.232 | 12.000 | 51.759 | 5.374E-10 | 1.115E-03 | 2.455 | 2.455 | 0.043 | 8.41 |
| Ec11 | oil B aged | 2M NaCl | 2M NaCl+0.014Ca | 0.422 | 0.894 | 0.032 | 1.221E-10 | 0.228 | 11.430 | 50.178 | 5.470E-10 | 1.101E-03 | 2.810 | 2.810 | 0.041 | 8.20 |
| Ec11 | oil B aged | 2M NaCl | 2M NaCl+0.14Ca | 0.422 | 0.907 | 0.031 | 2.419E-10 | 0.175 | 11.210 | 63.995 | 5.507E-10 | 1.096E-03 | 5.398 | 5.398 | 0.045 | 7.30 |
| Ec11 | oil B aged | 2M NaCl | 2M NaCl+0.42Ca | 0.422 | 0.912 | 0.031 | 3.787E-10 | 0.178 | 9.856 | 55.326 | 5.725E-10 | 1.069E-03 | 6.966 | 6.966 | 0.043 | 6.30 |
| Ec12 | oil C aged | FMB | FMB | 0.423 | 0.871 | 0.059 | 9.949E-11 | 0.145 | 14.310 | 98.506 | 4.962E-10 | 1.182E-03 | 3.402 | 3.402 | 0.006 | 6.51 |
| Ec12 | oil C aged | FMB | FMB-0.0003Ca | 0.423 | 0.880 | 0.058 | 7.774E-11 | 0.249 | 15.530 | 62.249 | 4.769E-10 | 1.219E-03 | 3.093 | 3.093 | 0.008 | 6.51 |
| Ec12 | oil C aged | FMB | FMB-0.014Ca | 0.423 | 0.880 | 0.058 | 5.875E-11 | 0.249 | 15.970 | 64.012 | 4.697E-10 | 1.234E-03 | 2.471 | 2.471 | 0.010 | 6.80 |
| Ec12 | oil C aged | FMB | FMB-0.14Ca | 0.423 | 0.878 | 0.059 | 4.873E-11 | 0.293 | 16.010 | 54.607 | 4.697E-10 | 1.234E-03 | 2.054 | 2.054 | 0.011 | 7.30 |
| Ec13 | oil D aged | FMB | FMB | 0.459 | 0.840 | 0.095 | 1.069E-10 | 0.232 | 14.440 | 62.243 | 4.955E-10 | 1.183E-03 | 3.687 | 3.687 | 0.057 | 6.51 |
| Ec13 | oil Daged | FMB | FMB-0.0003Ca | 0.459 | 0.852 | 0.092 | 7.237E-11 | 0.312 | 15.920 | 50.978 | 4.705E-10 | 1.233E-03 | 3.018 | 3.018 | 0.066 | 6.51 |
| Ec13 | oil D aged | FMB | FMB-0.014Ca | 0.459 | 0.850 | 0.092 | 3.843E-11 | 0.337 | 15.050 | 44.720 | 4.853E-10 | 1.203E-03 | 1.434 | 1.434 | 0.073 | 6.80 |
| Ec13 | oil D aged | FMB | FMB-0.14Ca | 0.459 | 0.844 | 0.094 | 2.944E-11 | 0.210 | 16.420 | 78.077 | 4.622E-10 | 1.251E-03 | 1.340 | 1.340 | 0.070 | 7.30 |




‘And Say O my Lord increase me in knowledge’

(Quran, Ta-Ha, 20: 114)